Lorenzo Montanari

VIBRATION-BASED DAMAGE IDENTIFICATION IN BEAM STRUCTURES THROUGH WAVELET ANALYSIS

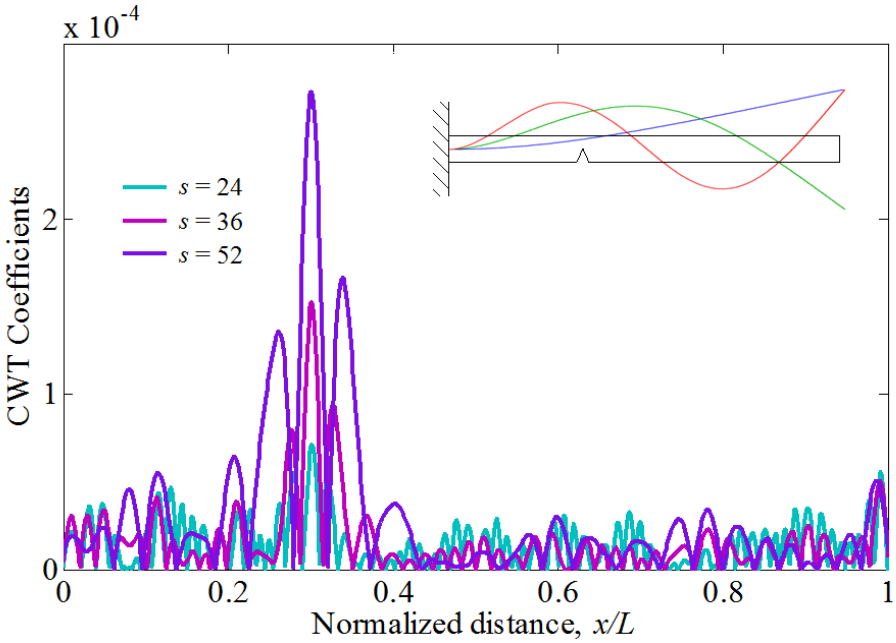

Tutor: Prof. Andrea Spagnoli

Doctorate Coordinator: Prof. Gianfranco Forlani

University of Parma
Research Doctorate in Civil Engineering ï XXVI Cycle

UNIVERSITY OF PARMA

RESEARCH DOCTORATE IN CIVIL ENGINEERING

XXVI Cycle

VIBRATION-BASED DAMAGE IDENTIFICATION IN BEAM STRUCTURES THROUGH WAVELET ANALYSIS

Doctorate Coordinator:
Prof. Gianfranco Forlani

Tutor:
Prof. Andrea Spagnoli

Doctoral Student:
Lorenzo Montanari

January *2014*

Research Doctorate in Civil Engineering ï XXVI Cycle
Curriculum: Structural Mechanics
University of Parma
Tutor: Prof. Andrea Spagnoli
Doctorate Coordinator: Prof. Gianfranco Forlani

To Lino, Gabriella and Agnese.

Acknowledgements

For these special years of Ph.D, firstly I would like to thank Prof. Andrea Spagnoli, an exquisite person of deep humanity who has introduced and guided me into the world of the structural mechanics. I would like to thank for their kindness and availability all the team of structural mechanics, Prof. Andrea Carpinteri, Prof. Roberto Brighenti and Prof. Sabrina Vantadori, all the other Professors, in particular Prof Gianfranco Forlani, and all the Staff of DICATeA, University of Parma. A particular thank to Prof. Biswajit Basu and Prof. Brian Broderick for having kindly hosted me in the Department of Civil, Structural and Environmental Engineering of Trinity College, Dublin, and for having introduced me into the subject of the structural damage identification. I would like to thank all my Ph.D student colleagues, Daniela, Nicholas, Camilla, Cristian, Nicola, Alessandro, Cecilia, Fulvio, Matteo, Laura, Annalisa, Simone, Andrea, Lin, Michael, William. Finally a great thank to my family and all my friends always next to me to help and support me.

Table of Contents

Abstract

Nowadays the topic of damage identification in structures is of primary interest in the field of civil, aerospace, mechanical engineering research. Indeed, due to the increasing use of advanced structural systems (e.g. airplanes, space shuttles, wind turbines, etc.) and to the aging of old structures (e.g. buildings, towers, bridges, etc.), the safety and reliability of structures have to be guaranteed to avoid catastrophic events and loss of human lives.

The present thesis is focused on vibration-based damage identification in beam structures through wavelet analysis. The dissertation is arranged in six chapters. Chapter 1 introduces the topic of the thesis through a broad presentation of the state of the art of damage identification methods for structural health monitoring and control, with particular attention to vibration-based structural damage identification methods. In Chapter 2, the time-frequency technique, named wavelet analysis, is firstly theoretically presented and its application, available in the literature particularly for beam-like structures, as a damage detection tool both in time and in space domains is discussed. In Chapter 3, the mechanical models of homogeneous and fiber-reinforced cracked beams are presented. The models are used to simulate the real static and dynamic responses of beam structures for successive damage detection through wavelet analysis. The last three chapters of the thesis are devoted to the original findings of the present research. Chapter 4 focuses on the issue of border distortions in damage detection by continuous wavelet transform. To tackle the problem, a new polynomial padding method is proposed and compared with the most effective padding methods commonly used in the literature. In Chapter 5 the effect of spatial sampling in damage detection of cracked beams by continuous wavelet transform is thoroughly investigated through a parametric study. From the outcomes, some general indications on the optimal number of sampling intervals for an effective damage detection are obtained. Finally in Chapter 6, a new health structural monitoring method based on time-spatial wavelet analysis is presented to control the static and dynamic, elastic-plastic behaviour of a cracked fiber-reinforced beam. The capability of the method is discussed particularly with respect to scale of the analysing wavelet, the noise level and the spatial sampling interval, considering a small crack.

Chapter 1

State of the Art of Vibration-based Structural Damage Identification

1.1 Structural monitoring and damage assessement

Nowadays, wherein the products cost-effectiveness conjoined to the life-safety is one of the main production goal, reliable systems of monitoring and damage assessment in structures are widely required by private and government subjects (Worden & Dulieu-Barton, 2004; Farrar & Worden, 2007).

Today several engineering structures are approaching or exceeding their initial design life. Nevertheless, for economic issues, they are still in use despite their aging and associated damage accumulation. For such structures, the assessment of their healthy becomes fundamental. Moreover, reliable Structural Health Monitoring (SHM) systems are of primary need at the occurrence of extraordinary strong events (earthquakes, explosions, hurricane, etc.) to assess, for example, if a building is safe for reoccupation. These systems can therefore significantly mitigate economic losses.

In the past, engineers used to design ideal ófree-damageô structures withstanding given operational loading by implementing very conservative factors of safety, but with the result of heavy and costly structures. Together with the need to reduce the material costs by building lightweight systems, the designers assumed a ódamage tolerantô based approach operating at the margin of safety. Particularly in such cases, reliable intelligent monitoring systems become essential in identifying the arise of damage and in avoiding collapses.

It is a current practice to apply time-based maintenance to several structural systems. For instance, missiles are retired after a given amount of captive-carry hours on the wing of an aircraft. A great breakthrough would be to replace the current time-based maintenance philosophy with the more cost-effective condition-based maintenance philosophy; that is, to monitor the structure state through a sensing system (constituted by a sophisticated monitoring hardware

and an effective measured data analysis procedure), so as to detect the damage occurrence at the earliest possible time and to intervene before the failure.

Worden and Dulieu-Barton (2004) identify four key multidisciplinary areas for which structural monitoring and damage assessment are of principal concern:

- Structural Health Monitoring (SHM);
- Condition Monitoring (CM);
- Non-Destructive Evaluation (NDE);
- Statistical Process Control (SPC).

Structural Health Monitoring (Farrar & Worden, 2007) pertains to aerospace, civil and mechanical engineering structures and implies a sensor network (e.g. optical fibres, strain gauges or acoustic devices) that monitors the on-line behaviour of the structure. Condition Monitoring (Bentley & Hatch, 2003) is analogous to SHM but is addressed to rotating and reciprocating machinery, such as used in manufacturing and power generation. Non-Destructive Evaluation (see Section 1.3.1) (Shull, 2002) is usually applied off-line to characterize and calibrate the severity of the damage after it has been located using on-line sensors. An exception to this rule is the use of NDE as a monitoring tool, for example for pressure vessels and rails. Statistical Process Control (Montgomery, 2001) is process-based rather than structure-based and uses a variety of sensors to monitor the process output. This monitoring tool is based on verifying if the process changes are due to its natural inherent variability (ópprocess in statistical controlô) or to a specific cause, such as a structural damage (ópprocess out of controlô).

The aforementioned areas of SHM, CM, NDE and SPC differ mainly for their application branches, but they exhibit common features. As an example, they all make use of a sensor system to acquire features of the structural response. Therefore, a general intelligent damage identification system for SHM, CM, NDE and SPC has to be designed.

1.2 Intelligent damage identification systems

As Worden and Dulieu-Barton (2004) highlight, a *holistic approach* has to be assumed for an intelligent damage identification: the structure and sensor network must be treated as one unique system at the design stage. Indeed, not only the structure should be monitored but also sensor failures have to be accounted for in such way that the whole system ópstructure-sensorsô will work correctly and safely. Some issues related to the design of intelligent damage identification systems are presented and discussed in the following.

1.2.1 Types of structural damage

Firstly, let us define three main typologies of structural damage: *defect*, *damage* and *fault*.

Due to the variability of composition and manufacturing process, all the materials have statistically different microstructures and varying numbers or shapes of inclusions, voids and other defects. These *defects* are inherent to the material and therefore are not considered as damage: the structure works in its design condition.

For in-service operational and environmental loadings (fatigue, creep, corrosion, temperature variations, extraordinary events, etc.), the defects of the microstructure grow and coalesce evolving in *damage*. When damage develops into a system its behavior is adversely modified. Note that damage is in this way defined on the basis of the comparison between two different states of the system, where the initial one is often the undamaged state.

In structural systems, damage is associated to changes of the material (crack, local plasticity, delamination or debonding in composite materials, etc.) and/or geometrical properties (e.g. changes to the boundary conditions). The structure operates no longer in its optimal manner but can still work satisfactorily in a sub-optimal manner. As the damage continues to grow, the system reaches a limit state when it is no longer acceptable to the user. In this state damage is called *fault.*

1.2.2 Damage identification

The monitoring system has the objective to detect the damage that will, if not corrected, lead to a fault. It needs to store the necessary information in order to take remedial actions to restore the system to high-quality operation or at least to ensure safety.

Damage identification can be regarded as a hierarchical process composed by five levels (Rytter, 1993; Worden and Dulieu-Barton, 2004):

1) **Detection**: verify the presence of damage in the structure;
2) **Localisation**: identify the position of damage;
3) **Classification**: characterize the type of damage;
4) **Assessment**: quantify the severity of the damage;
5) **Prediction**: evaluate the residual life of the structure.

Damage identification presents a pyramidal structure composed of different levels, so that each level requires the information related to the lower ones.

There are basically two complementary approaches for structural damage identification:

- damage identification is treated as an inverse problem;
- damage identification is treated as a pattern recognition problem.

The first approach usually adopts a model of the structure and tries to relate changes in measured data from the structure to changes in the model (Friswell, 2007). To simplify the analysis, sometimes locally linearised models are used. The correlation between the behavior of the real structure and that of the corresponding model is calculated through algorithms based on linear algebra or optimization theory (e.g. see model updating based methods in Section 1.3.2.7)

The second approach is based on the idea of Pattern Recognition (PR) problem (Schalkoff, 1992). In the following, the PR approach to design intelligent damage identification systems is discussed in details.

1.2.3 Pattern recognition approach

Patterns represent different damage conditions, damage type (e.g. crack, delamination, plastic deformation), damage location and severity, etc. The major task in PR problem is to distinguish between different classes of patterns representing these conditions. Therefore, data representing different normal or no damage conditions have to be acquired over a period of time to form a template and new sets of data are compared with the template to detect damage or to obtain information about damage advancement.

To detect and locate damage and to indicate the severity of damage, PR *supervised learning* scheme can be employed. From a large set of data pertaining to any conceivable damage condition, the algorithm defines correctly the pattern. However serious demands are associated with these data accessibility. Basically the two possible sources of such data are *modelling* and *experiment*. Modelling is problematic for structures geometrically or materially complex. For instance, Finite Element (FE) analysis of structures requiring a fine mesh can be extremely time-consuming; constitutive models of composite-cohesive or viscoelastic materials are hardly accurate; damage itself may be difficult to model, especially for nonlinear dynamics of structures (e.g. see an opening-closing fatigue crack). On the other hand, even from an experiment viewpoint the situation is not easier; in order to accumulate enough training data, it would be necessary to make copies of the system of interest and damage it in all the ways that might occur naturally (for high value structures like aircraft, this would simply not possible).

An alternative to supervised learning is the *unsupervised learning*. The drawback of this approach is that it can only be used for detecting the presence of damage. The techniques related to the unsupervised learning are often referred to as *novelty detection* or *anomaly detection* methods (Worden, 1997; Worden et al., 2000). The idea of novelty detection is that only training data from the normal operating condition of the structure is used for the diagnostics. A model in normal condition is created and data acquired during monitoring are compared with those of the model. If the system departs from normal condition (i.e. damage is develops), the algorithm detects significant deviations in the acquired data and

indicates novelty. Note that, from both modelling and experimental viewpoint, this approach is advantageous because only the training data related to the undamaged condition are required. However, since novelty detection method is only suitable for damage detection, it is applicable to safety critical systems, where any occurrence of damage would require to take the system out of service.

In line with the PR problem approach, an intelligent damage identification system, function of the case-situation, should be designed to: measure the appropriate data (*operational evaluation and sensor network design*), pre-process the data with the opportune algorithms (*data pre-processing*), magnify damage features eliminating redundancy-worthless data (*feature extraction and data reduction*) and operate on the extracted feature vectors to quantify the damage state of the structure (*pattern recognition*) (e.g. see Fig. 1.1). In the following sections, these steps are analysed in details.

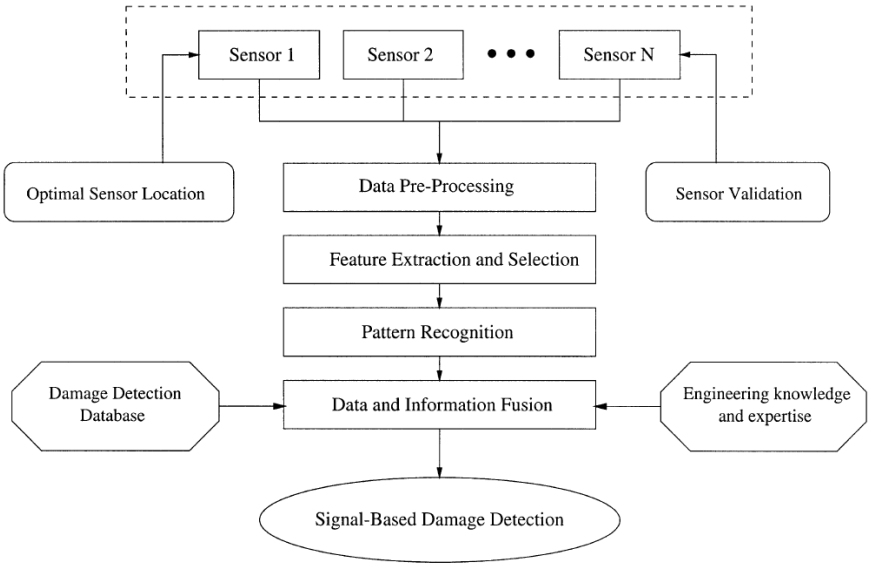

Fig. 1.1 ï Schematic of a multi-sensor intelligent damage identification system (after Staszewski, 2002).

1.2.3.1 Operational evaluation

The first aim of an intelligent damage detection system for SHM is to measure the appropriate data. In general, the design of the monitoring system should deal with queries such as following pointed out by Worden and Dulieu-Barton (2004) and Farrar and Wonder (2007):

(i) What are the life-safety and/or economic justification for performing the monitoring?

(ii) How is damage defined for the investigated system and, in case of multiple damage types, which type is of the most concern?
(iii) What are the conditions, both operational and environmental, under which the system should be monitored?
(iv) What are the limitations on acquiring data in the operational condition?
(v) Which is the appropriate level of monitoring as a function of the context-specific features?

Each of the abovementioned requirements needs to substantially support the design process. According to point (ii) for applying a supervised learning scheme for the diagnostics, training data are required. Hence, in order to build a model or design an experimental programme to generate training data, firstly the expected damage features (type, severity, location, etc.) has to be specified. Then, knowing the likely damage locations (the so-called ôhot spotsõ), one can choose whether to design a local or a global monitoring system or a hybrid one. For example, the supposed ôhot spotsõ can be inspected using a high-resolution local method, while the rest of the structure can be monitored using a less sensitive but global vibration-based method.

As highlighted in Section 1.2.2, care should be taken to point (iii) when designing a monitoring system. If the data used to characterize the normal operating condition does not span the whole range of conditions, the system will erroneously diagnose damage instead of an operational or environmental change. Some examples of systems where this occurs are: offshore structures changing their mass because of oil storage and/or marine fouling, aircrafts before and after dropping a load, bridges in desert areas undergoing substantial temperature changes from day to night.

1.2.3.2 Sensor network design

The decision of the appropriate sensor system for the structure is one of the most critical issue in the specifications of a monitoring system. Indeed there can be no monitoring without the appropriate sensor system. The choice of the optimal type and location of the sensors is a primary matter. The knowledge of the expected damage types and structure ôhot spotsõ can drive this choice. Also, the decision between local and global monitoring must be taken at this stage.

Given the so-called holistic approach to health monitoring, even the sensor network is deemed to be monitored. Indeed a fault in the sensor network will have undesirable consequences: a sensor failure that causes an unnecessary alarm may cause the system to be needlessly taken out of service; a sensor failure that causes a structural damage to go unnoticed may have severe costs or safety implications.

There are essentially two approaches in monitoring the sensors. The first approach consist of individual sensors that can be self-monitoring (e.g. Henry &

Clarke, 1993). This kind of sensors is capable of self-diagnostics and also returns the on-line uncertainty of the measurements. The alternative approach is to allow the sensors to monitor each other as shown by Kramers (1991 and 1992). This approach is suitable for sensors which cannot accommodate substantial electronics (e.g. accelerometers). Since the sensor outputs are correlated, there is a *redundancy* in the sensor network, so that, not only the identification of defective sensors is allowed, but also approximate values of what the defective sensors should read are generated.

Note that the redundancy feature for an intelligent monitoring system is crucial. If a sensor is diagnosed as defective, the information that would have been delivered by the sensor should be available elsewhere. During the design stage, the issue of sensor optimization is to be dealt with. The simplest approach is to collocate sensors at critical points, but to keep only one active at a given time: redundant sensors are switched in when damage occurs to an active sensor. Another approach is to overdesign the sensor network in such a way that damage to a single sensor still leaves a network which is optimised for monitoring in the desired manner (the fail-safe sensor optimization approach is discussed in Staszewski et al. (2000)).

The new technology of piezoelectric sensors, like piezoceramic or piezopolymer sensors, given their ability to act as both sensors and actuators, allows the possibility of active validation for monitoring. In turn, each sensor can act as a signal generator and the response of the other sensors can be compared with a template to verify their health accuracy.

Once the operational evaluation stage is fulfilled and the sensor network has been designed, system response data can be delivered. The choice and implementation of algorithms to process the data and carry out the identification is a most crucial ingredient of an intelligent damage identification strategy. All the actions, between the data acquisition by sensors and the ultimate decision about the system health, are collected in the Data to Decision (D2D) process (Lowe, 2000) which is based on the idea of *data fusion*. The concept of data fusion is to integrate multiple data and knowledge representing the same object into a consistent, accurate and useful representation. As an example, sensor fusion, also known as multi-sensor data fusion, is a subset of information fusion in which all the relevant information generated by the sensor network with different types of sensors are fused together. In general, information can be combined at any stage of the process. The objective is basically to reach the final decision with higher confidence than the on which could be reached using any of the information sources alone.

1.2.3.3 Data pre-processing

The *data pre-processing* has the purpose to elaborate the raw data acquired by the sensors and to prepare these for the feature extraction. The pre-processing stage encompass three tasks: *data normalization*, *data cleansing* and *data reduction*.

Data normalization helps to generalize amplitude levels for different types of data. It often identifies relationships between measurements and features. As it applies to SHM, data normalization process aids to separate changes in sensor reading caused by damage from those caused by varying operational and environmental conditions (Sohn, 2007). If measured inputs are available, the most common procedure is to normalize the measured responses with respect to them. On the other hand, when environmental or operational variability is an issue, it is opportune to normalize the data in some temporal manner to facilitate the comparison of data measured at similar times of an environmental or operational cycle.

Data cleansing is the process of selectively choosing data to pass on or to reject for the feature extraction process. Examples of cleansing processes are: noise and spike removal, reduction of outliers and treatment of missing data values. A large variety of signal processing procedures in smoothing and denoising is available, including mean averaging techniques, many low-pass filters, such as the Wiener filter and the Savitzky-Golay filter (Hamming, 1989) and wavelet-based denoising techniques (usually composed of three steps: orthogonal wavelet transform, thresholding of wavelet coefficients and inverse wavelet transform; Mallat, 2001). Data fitting is a further smoothing process which identifies unwanted, temporal relationships in the data. Outliers, on the other hand, are signals which are statistically far from the normal selection of observed signals. They can be eliminated using standard statistical analysis based on probability density or distribution estimation.

Another possible pre-processing process is the reduction of the dimensions of the data vectors with signal denoising. The aim would be to reduce the dimension of the data set from possibly many thousands to perhaps a hundred. For example, given a random time-series with many points, it is often useful to represent the data in frequency-domain by Fourier transform. If the signal is divided into contiguous blocks before transformation and the resulting spectra are averaged, the number of points in the spectrum can be much lower than in the original time-history and noise is averaged away. By treating the time signal in this way, another advantage is that the data vector obtained should be independent of time, and if, the original time-series is random, it makes little sense to compare measurements at different starting times.

Data pre-processing stage is a very delicate and case-dependent task and has to be carried out on the basis of engineering judgement and experience. Finally,

note that the pre-processing process should not be static: from the feature selection and the pattern recognition process insight can arise to improve the process.

1.2.3.4 Feature extraction and data reduction

Feature extraction process is fundamental in the damage identification problem and have received a great attention in the technical literature. Its task is to emphasize the characteristics of the various damage features and to suppress background effects. Once damage dominant features are isolated in the data, the problem of damage identification can be easily solved. However, in general, the components of the signal concerning the various damage features are hidden by those related to the normal operating conditions of the structure, particularly when the damage is not severe.

There exists a number of different types of procedures used for feature extraction. Simple methods are based on data reduction procedures in order to obtain scalar features, e.g. maximum amplitude. Advanced procedures leads to vectorial or pattern representations such as power spectrum.

Hereafter some common feature extraction methods are presented. As an example, suppose to have measured time-series data that has been pre-processed and converted into an averaged spectrum. In such a situation, the isolation of the harmonics sensitive to damage could be a strategy of feature extraction. More in general, a common method is based on correlating measured response quantities (e.g. vibration amplitudes or frequencies) with the first measurements of the degrading system. Another method is to apply engineered flaws, similar to ones expected in the actual operating conditions, to the system in order to understand the response to the expected damage. The flawed system can also be used to check if the diagnostic measurements are sensitive enough to distinguish features of damage. Furthermore, numerical tools, such as experimentally validated FE models with or without damage, can be used to perform numerical experiments in order to characterize the damage features in signals. Damage accumulation testing, (e.g. fatigue testing, corrosion growth, temperature cycling, etc.), during which structural components of the system are degraded by submitted them to real operational and environmental conditions, can also be used to identify appropriate damage features.

A data dimensionality reduction process can be advantageous and necessary for an effective pattern recognition when many feature sets, e.g. obtained over an extend period of measurements on the structure, must be compared. In order to achieve reduction of dimensionality, one can reduce a number of features, combine existing features into new features or select a subset of features. There exist two major categories of feature reduction procedures. The first one involves the process of reducing redundancies in the feature space. The second includes

linear (e.g. the principal component analysis) and nonlinear transforms, and mapping techniques. However, the data dimension reduction has to be carried out carefully in order not to discard information relevant for diagnosing the damage.

1.2.3.5 Pattern recognition

Once features related to damage are extracted into continuous, discrete or discrete-binary variables and arranged in vectors or matrices, damage detection can be regarded as a problem of pattern recognition. It needs to operate on the extracted features in order to quantify the damage state of the structure.

Three different methods, namely syntactic, neural and statistical, are mainly used in PR (Schalkoff, 1992). All these methods can applied to either the *supervised* or the *unsupervised* learning: it depends on which level of damage identification is required (see Section 1.2.1). Syntactic pattern recognition classifies data according to its structural description (Bunke & Sanfeliu, 1990). Neural networks have been established in recent years as a powerful tool for pattern recognition (Ripley, 2007). Artificial neural networks map the input data into selected output categories using artificial neurons and learning processes that simulate the biological nervous system. For satisfactory results a significant level of network training is required. Statistical methods use probabilistic models to form and estimation/decision theory to classify patterns (Jain et al., 2000). These algorithms can be divided mainly into three categories: n*ovelty detection*, *group classification* and r*egression analysis*. Statistical PR approach is appropriate for SHM since it can distinguish among statistical fluctuations in the data and real deviations due to changes of operating and environmental conditions or to anomalies (Worden & Dulieu-Barton, 2004 and Farrar & Worden, 2007).

The statistical and neural models are also used to minimize false indications of damage, such as: (i) *false-positive damage indication*, i.e. indication of damage when none is present, and (ii) *false-negative damage indication*, i.e. no indication of damage when damage is present. The first type of errors are undesirable, as they will cause unnecessary downtime and loss of profit and of confidence in the monitoring system. Instead, safety issues can be clearly provoked by the second type of false indication.

The presence of noise in signal limits strongly the damage identification system in all its stages. A trade-off between the diagnosis resolution and the de-noising capability of the algorithm is needed. As noise-free data present very little fluctuations in the measurements from normal operating condition, small damages cause detectable signal deviations. On the other hand, when some noise is present on the training data, it is difficult to distinguish between fluctuations due to noise and deviations due to damage unless the damage is severe.

1.3 Damage identification methods

Many damage identification methods have been developed to highlight, from the data obtained by the sensors, the damage characteristics (presence, location, extent, etc.) in comparison to those of the healthy structure in its operational conditions. Focusing on the non-destructive damage identification methods, these can be distinct primarily in classical nondestructive evaluation methods and vibration-based damage identification methods.

1.3.1 Classical nondestructive evaluation methods

Nondestructive evaluation (NDE) methods, sometimes referred to as nondestructive inspection (NDI), nondestructive testing (NDT) or nondestructive examination (NDEx), are the historically first damage identification methods developed by researchers. The most widely used techniques (American Society for Metals, 1989; Doherty, 1991; Malhotra, & Carino, 2004) are:

- visual inspection;
- liquid penetrant method;
- acoustic emission method;
- ultrasonic method;
- magnetic particle or field methods;
- radiography methods;
- electric or eddy current methods;
- thermal field methods.

These damage detection methods do not need any benchmark data or theoretical models of the undamaged structure and assess directly the damaged structure. Their application requires to know a priori the damaged portion of the structure to be inspected and to be readily accessible. The damage is analysed mainly on or near the surface of the structure and, consequently, the damage investigation is essentially local. The damage diagnostic turns out to be very effective for small and regular structures, such as pressure vessels, or some special components of a structure, whilst it is difficult to be applied for large and complex structures. The need to investigate the global behavior of these structures, such as multi-store buildings, bridges, or aerospace systems, has led to the development of methods that examine changes in the vibration characteristics of the structure.

1.3.2 Vibration-based damage detection methods

The basic idea of vibration-based damage detection is that damage alters the physical properties of the structural system (stiffness, damping and mass) and

consequently, its measured dynamic and static response. Often, damage detection methods investigate the change of the modal properties of the system (notably natural frequencies, damping ratios, modal shapes). However, despite its intuitively simple basic concept, several technical aspects make difficult the actual application of vibration-based damage detection technology, which is still nowadays an open research topic in many engineering fields.

Yan et al. (2007) highlight that a significant development has occurred in vibration-based structural damage detection techniques, so that they can be divided into traditional-type damage detection methods and modern-type damage detection methods, also called intelligent damage diagnosis.

The traditional-type vibration-based damage detection methods are mainly based on the structural natural vibration characteristics, such as natural frequencies, modal shapes, modal damping (Sections 1.3.2.2 ï 1.3.2.7). The damage location and severity can be determined through finding the difference of dynamic characteristics between the intact and damaged structural conditions. Generally the dynamic characteristics related to the undamaged state of the system are gathered from baseline data or from a baseline analytical/numerical model: the damaged state of the system is found out from the measured data of the natural frequencies or mode shapes. However, as it will be exposed in-depth in Sections 1.3.2.2 ï 1.3.2.7, these kinds of methods, due to some disadvantages, have lost research interest in the past decade. Experimental modal analysis or transfer function measures are required, which are expensive, time-consuming and very unsuitable for online in service detection of structures because of their instruments and manual operations. Moreover, it is difficult to model accurately the undamaged state of the structure and to establish a universal methodology for various structures. Finally, in general these methods are not sensitive to initial tiny damage.

The modern-type methods (Sections 1.3.2.8 - 1.3.2.11) refer to structural damage detection methods based on online measured response signal of structures in service. These methods mainly use modern signal-processing techniques and artificial intelligence to analyze the structural response and to extract useful characteristic information of the structural damaged status. Advantages of these techniques are to be less dependent on experiments and on the structural shape, more economical and feasible online, and to be able to detect small structural damage. Some of the open problems to be solved are as follows. Measured signals are usually contaminated by noise so information from tiny damage in structures may be masked; these methods have to rely on the environment excitation to the structures (output-only damage identification); the selection and construction of the sensitive feature index of structural damage are very flexible and variable. Representative methods among them are the time-frequency techniques (e.g. wavelet analysis, Hilbert-Huang transform), genetic algorithms and artificial neural networks.

The effects of damage on the structure can be classified as linear or nonlinear. Indeed, in consequence of a damage, the initially linear-elastic behavior of the structure can remain linear or can turn into nonlinear. A typical example of nonlinear damage is the formation of a mode I crack that, under operating dynamic loadings, opens and closes. Initially, researchers tackled this damage identification problem by assuming the damaged system behaves in a linear manner. Only in the past few years vibration-based damage identification has been tackled considering the nonlinear behavior of the system (Farrar et al., 2007). Traditional-type methods focus primarily on linear damage detection, while the modern-type methods consider both linear and nonlinear ones.

Before presenting traditional-type and modern-type vibration based damage identification methods, a brief summary of the first research applications of these techniques in various engineering braches is illustrated. An extended review of vibration based damage identification methods can be found in Doebling et al. (1996), Sohn et al. (2003), Carden and Fanning (2004) and Yan et al. (2007).

1.3.2.1 Brief historical background

As explained by Farrar et al. (2001), the development of vibration-based damage detection methods occurred concurrently with the evolution, miniaturization and cost reductions of Fast Fourier Transform (FFT) analyser hardware and computing hardware.

Until now, the monitoring of rotating machinery is the most successful application of vibration-based damage identification (Heng et al., 2009; Randall, 2004a,b). The damage detection is based almost exclusively on non-model based approach, which consists in analyzing the time histories or spectra generally measured on the housing of the machinery during its normal operating conditions. Thanks to wide databases, specific types of damage (as for example, loose or damaged bearings, misaligned shafts or chipped gear teeth) can be identified from particular features of the vibration signal. Moreover, for these systems, the approximate location of the damage is generally known through FFT. In the past decades, the application of CM has moved from a research topic to industrial practice, so that commercial software integrated with measurement hardware is marketed to help the user to apply systematically this technology to operating equipment. During the 1970s and 1980s, the oil industry made considerable efforts to apply vibration-based damage detection for offshore platforms. Since, in this case, the damage location is unknown and the majority of the structure is not readily accessible for measurement, a methodology attempted to correlate the changes in the resonant frequencies found in numerical models simulating various damage scenarios with those measured on the platform. After extended efforts, this technology was abandoned in the early 1980s since the hostile environmental context, the platform machine noise, the

changing mass caused by marine growth and varying fluid storage levels, and other causes were sources of many practical measurements problems.

During the late 1970s and early 1980s, in conjunction with the development of the space shuttle, even the aerospace community began to study the use of vibration-based damage identification. Hereafter the research continued for the National Aeronautics and Space Administrationôs space station and reusable launch vehicle. The Shuttle Modal Inspection System (SMIS) was developed to identify fatigue damage in components such as control surfaces, fuselage panels and lifting surfaces. The traditional local NDE methods could not be applied since the inaccessibility of those portions of the shuttle, covered with a thermal protection system. The SMIS resulted to be successful and since 1987 it has been used to test periodically all orbiter vehicles. Space station applications primarily consisted of damage-detection methods based on correlating analytical models of the undamaged structure with measured modal properties from both the undamaged and damaged structure. To locate and quantify the damage are used the changes in stiffness indices, as assessed from two model updates. The development of a composite fuel tank for a reusable launch vehicle at the mid-1990s motivated the study of damage identification methods for composite materials. For this kind of materials and their failure mechanisms, such as delamination, a SHM based on fibre optic sensing systems was considered more effective. Boller & Buderath (2007) discuss and emphasize the impact of SHM as a mean of possibly revolutionizing the current aircraft design and maintenance processes.

Since the early 1980s, the civil engineering community has studied vibration-based damage assessment of bridge structures and has observed that significant challenges are related to the environmental and operating condition variability and the physical size of these structures. Modal properties and quantities derived from these properties, such as mode-shape curvature and dynamic flexibility matrix indices, have been the main features used to identify damage in bridge structures. For instance, regulatory guidelines in Eastern Asia countries, which require the companies to periodically certify the structural health of the constructed bridges, have encouraged research and development of vibration-based bridge monitoring systems. To further examine the applications of SHM to civil engineering infrastructure one might refer to Brownjohn (2007) and Lynch (2007) are suggested.

1.3.2.2 Natural frequency based methods

The observation that changes in structural stiffness and mass properties cause changes in vibration frequencies prompted the use of modal methods for damage identification and health monitoring. The damage identification methods based on natural frequency changes are one of the first modal based methods

developed, given the ease to measure the natural frequencies (only a single sensor is required in many applications). A wide review of these damage detection techniques is found in Salawu (1997).

As shown by many researchers, natural frequency shifts for damage identification can successfully be used in small simple laboratory structures with only a single damage location. Adams et al. (1978) and Cawley and Adams (1979) analyse several laboratory bars and, through the ratio of the axial resonance frequency changes related to two modes, evaluate successfully the location of moderate damage levels. The authors demonstrate that the measurement of one pair of frequencies yields a locus of possible damage sites. By evaluating the loci of several pairs of modes, the actual damage site can be determined by the intersection of the curves. Narkis (1994) develops a closed-form solution for the inverse problem of determining in a simply supported beam the location of a single crack from the first two, either bending or axial, frequency shifts. The proposed method is confirmed by means of FE analysis and it results independent of crack size, shape and configuration. Lee and Chung (2000) present a method using the first four natural frequencies to locate and calibrate the size of a single crack in cantilever beams. The application and accuracy of the procedure is demonstrated through an experimental test. Nikolakopoulos et al. (1997) experimentally identify a single crack in a single storey frame from shifts in the first three natural frequencies. The location and depth of the crack is determined from the intersection of the contour plots for all variations of location and depth against change in the natural frequencies.

The use of frequency shifts appears not to be effective in identifying multiple damage scenarios, even for simple laboratory structures. As an example, Messina et al. (1996) propose a Multiple Damage Location Assurance Criterion (MDLAC), later extended in (Messina et al., 1998), by introducing a linearised sensitivity and statistically based method able to locate and size single or multiple damages. The method requires only the measurements of the changes in a few of the structural natural frequencies between the undamaged and damaged states. Its effectiveness is verified numerically on two truss structures and experimentally on a three-beam test structure with up to two damage locations.

In the light of the above, despite the large amount of research work related to this class of damage identification methods, successful algorithms are limited to the identification of a single or few damage locations in small simple laboratory structures. Since modal frequencies are a global property of the structure, generally frequency shift can be used only to detect the presence/absence of damage, while limitations arise for example to uniquely identify the damage position or distinguish its typology (Kessler et al., 2002). An exception to these limitations occurs at higher modal frequencies, where the modes are associated with local responses, but the excitation and the extraction of these local modes turn out to be difficult in practice. The rather low sensitivity of frequency shifts

to damage requires either very precise measurements or significant levels of damage to locate and quantify it (Farrar et al., 1994; Chen et al., 1995; Palacz & Krawczuk, 2002).

1.3.2.3 Mode shape based methods

Many modal analysis techniques are available for the extraction of mode shapes from the data measured in the time domain (Heylen et al., 1997; Ewins, 2000). Damage detection methods are developed for the identification of damage based directly on *measured mode shapes* or *mode shape curvatures*.

Two commonly used methods to compare two sets of mode shapes are the Modal Assurance Criterion, MAC (Allemang & Brown, 1982) and the Coordinate Modal Assurance Criterion, COMAC (Lieven & Ewins, 1988).The MAC value can be considered as a measure of the similarity of two mode shapes. A MAC value of 1 is a perfect match and a value of 0 means they are completely dissimilar. Therefore, the reduction of a MAC value may be an indication of damage. Salawu and Williams (1995) test a reinforced concrete bridge before and after repair and observed that the modeshape based MAC method is a more robust technique for damage detection than shifts in natural frequencies.

The COMAC is a parameter pointwise measuring of the difference between two sets of mode shapes and takes a value between 1 and 0. A low COMAC value would indicate discordance at a point and thus can be used as damage location indicator. Frýba & Pirner (2001) apply the COMAC method to check the quality of a repair to a prestressed concrete segment bridge. The analysis confirms that the repaired segment responses tend to be consistent with that of a undamaged segment.

A drawback of many mode shape based methods is the necessity of having measurements from a large number of locations. Khan et al. (2000) use a scanning Laser Doppler Vibrometer (LDV), allowing for a dense grid of measurements, to measure mode shapes in a steel cantilever beam, a steel cantilever plate and concrete beams, containing cracks. Since in thick metal structures defects are detectable only when their depths are more than half of the structure thickness, it may be concluded that, despite the potentiality of the scanning LDV, improvements in reducing the noise interference would be necessary for a successful application to actual field structures.

Araújo dos Santos et al. (2000) describe a damage identification algorithm based on the orthogonality conditions of the mode shape sensitivities. The algorithm is applied to a plate with reduced stiffness to simulate damage. The results are compared with those obtained by using the mode shape sensitivities and are found to be more accurate. The same orthogonality based technique is applied by Ren & De Roeck (2002a; 2002b) to a laboratory scale concrete beam. They conclude that, although mode shape based methods are effective with

simulated data, there are significant difficulties in the application to real structures, due to noise and measurement errors, mode shape expansion of incomplete measurements and accurate modelling of test structures.

Pandey et al. (1991) are the first through analytical and FEM beam models, to show that the curvature modeshape can be a successful parameter for identifying and locating damage. The curvature modeshapes are calculated using a central difference approximation from the simulated displacement modeshapes. Furthermore, the authors underline that the changes in the curvature mode shapes increase with increasing size of damage and this increase, more pronounced than that related to the changes in the displacements of the mode shapes, can be used to calibrate damage severity.

Modal curvature based methods are applied also on measured data to identify damage. Rathcliffe & Bagaria (1998) use a gapped smoothing method to successfully locate a delamination in an experimental composite beam. The curvature shape is calculated using Laplaceôs difference equations from the displacement mode shape and is then locally smoothed using a gapped polynomial at each point. Through the difference between the curvature and the polynomial at each point, the damage index is defined: the largest index indicates the location of the delamination. Wahab and De Roeck (1999) apply successfully a curvature-based method to the Z24 Bridge in Switzerland. They introduce a damage indicator named the curvature damage factor, equal to the difference in curvature before and after damage averaged over a number of modes. They conclude that the use of modal curvature to locate damage in civil engineering structures seems promising.

The number of modal curvatures useable in damage identification routines is, naturally, limited to the available number of displacement mode shapes. In an effort to increase the amount of data available for input into damage identification routines, Sampaio et al. (1999) extend the curvature approach to all frequencies in the measurement range by using FRF data. This method is tested with data related to an intentionally damaged bridge and it is found to have higher performance than the curvature method.

In conclusion, despite the weak points of measuring mode shapes (mode shapes measurement accuracy is lower than that of the natural frequencies, see Farrar et al., 1997 and Doebling et al., 1997, and measured vibration modes are often incomplete so that they have to be expanded with a consequent increase of measurements errors) mode shape based methods, since they contain more damage information, are more robust than natural frequency based methods to detect, locate and calibrate damage.

Researchers have investigated other methods, such as that using *operational deflection shapes* (Schwarz & Richardson, 1999; Pai & Young, 2001; Waldron et al., 2002), which are very similar to mode shapes, and other methods based on more complex formulations involving the use of natural frequencies and mode

shapes (*modal strain energy based methods*, see section 1.3.2.4, *dynamically measured flexibility based methods*, see section 1.3.2.5, and *model updating based methods*, see section 1.3.2.7).

1.3.2.4 Modal strain energy based methods

When a given vibration mode stores a large amount of strain energy for a particular structural load path, the frequency and shape of that mode are highly sensitive to changes in the load path. Consequently, changes in modal strain energy can be considered as indicator of the damage location. The strain energy, U_i, in a Euler-Bernoulli beam of length l associated with a particular mode shape, ϕ_i, may be calculated from:

$$U_i = \frac{1}{2}\int_0^l EI\left(\frac{\partial^2 \phi_i}{\partial x^2}\right)^2 dx \qquad 1.1$$

where EI = bending stiffness, x = axial coordinate. The curvature required for this calculation is commonly extracted from the measured displacement mode shapes using a central difference approximation.

Kim and Stubbs (1995) apply a damage identification algorithm to locate and calibrate a single crack in an experimental plate girder. The method locates up to two damage sites in a simulated plate girder and quantifies the damage on the basis of the ratio of the modal strain energy of elements before and after the damage. Cubic spline functions are used to interpolate the incomplete mode shapes and produce a curvature function to calculate the modal strain energy. It is found that false-positive and false-negative damage indications are strongly influenced by the quality and amount of available modal information. Later, Kim and Stubbs (2002) derive a new damage index in a simulated two span beam, enhancing the accuracy of damage localization in comparison with the method proposed in their previous work (Kim & Stubbs, 1995).

Law et al. (1998) introduce the Elemental Energy Quotient (EEQ), defined as the ratio of the modal strain energy of an element to its kinetic energy. The difference in the EEQ before and after damage is normalised and averaged over several modes and used as a damage location indicator. The method is first demonstrated on a simulated space frame and is shown to be successful when 10% random noise is added. The method is also successfully applied to an experimental two-storey plane frame with up to two joints loosened to simulate damage. Based on the intuitive concept that mode shapes are more sensitive to local changes in stiffness in the damaged ports than in the undamaged ones , Shi et al. (2000) present an algorithm focused on the largest changes in modal strain energy in the damaged area. The change in modal strain energy before and after damage is used successfully to locate the damage in an experimental steel frame. The quantification of damage is based on the calculated sensitivities of the modal

strain energy. In an effort to compare methods, Kim et al. (2003) apply both a frequency based and a modal strain energy based method to identify a single damage location and size in a simulated beam using two modes. It is found that the modal strain energy method gives a more accurate prediction of damage location than the frequency based method.

1.3.2.5 Dynamically measured flexibility based methods

The flexibility matrix is defined as the inverse of the stiffness matrix and, therefore, relates the applied static forces to the resulting structural displacements. Each column of the flexibility matrix represents the displacements associated with a unit force applied to a given Degree Of Freedom (DOF).

The dynamically measured flexibility matrix, $\mathbf{F}$, is generally estimated from

$$\mathbf{F} = \bar{\mathbf{u}}\, \Ş^{-1} \bar{\mathbf{u}}^{T} \qquad 1.2$$

where $\bar{\mathbf{u}}$ is the matrix of measured mode shapes and $\Ş$ is the associated diagonal matrix of squared measured modal frequencies.

As shown by Pandey and Biswas (1994), the flexibility matrix can easily and accurately be estimated from a few lower frequency modes of vibration of the structure, which are the easiest to be measured. Indeed the effect of high-frequency components in the flexibility matrix rapidly decrease with the increase of natural frequency. Using both simple analytical beam models and experimental data related to a wide-flange steel beam, the authors demonstrate the effectiveness of the changes in the flexibility matrix in detecting the presence of damage and in localising it.

Yan and Golinval (2005) present a damage diagnosis technique based on changes in both dynamically measured flexibility and stiffness of structures. A subspace identification technique is applied for the identification of modal parameters, from which the measured flexibility matrix can be constructed. The corresponding stiffness matrix is obtained by a pseudo-inversion of the flexibility matrix. Damage localisation is achieved by analyzing the changes in these two measured matrices in moving from the reference state to the damaged state. Note that the combined consideration of both the two matrices provides more reliable information on damage location. Furthermore, since the location of damage is connected directly with the position of sensors, no geometrical measurements and FE models are needed. Simple numerical and experimental applications are presented to show the efficiency the limitations of the method. Simple numerical and experimental applications of the method show that its efficiency requires a sufficient number of well distributed sensors but, if the damage is too small, it may be masked by numerical errors.

In a review study of modal parameter based methods, Zhao and DeWolf (1999) examine the sensitivity to damage of the modal flexibility based method with respect to the natural frequency and the mode shape based methods. By

applying the methods to a simulated five DOFs spring-mass system, the modal flexibility method results to be the most sensible to damage. On the other hand, Farrar and Doebling (1999) compare the strain energy, the mode shape curvature and the changes in flexibility based methods in locating damage on an I-40 bridge over the Rio Grande in America. Four controlled damage states are investigated and the strain energy based method, followed by the mode shape curvature based method, is found to be the most successful one.

In conclusion, at the occurrence of damage in a structure, changes in the stiffness matrix generally provide more information than those in the mass matrix. However, if the damage is small, this method is not effective.

1.3.2.6 Frequency response function based methods

Some authors investigate the use of Frequency Response Function (FRF) measurements, as an alternative to the modal data extracted from the FRF measurements. According to Lee and Shin (2002) there are two main advantages of using FRF data. Firstly, modal data are derived data and hence can be contaminated by modal extraction errors in addition to measurement errors. Secondly, a complete set of modal data can be measured only in simple structures. In addition, FRF data can provide much more information on damage in a desired frequency range in comparison to modal data that are extracted from a very limited range around resonances. The drawback of FRF methods is that the accuracy of structural damage detection is strongly dependent on the amount and position of measurement points.

Wang et al. (1997), considering an original analytical model and FRF data measured before and after damage, formulate an algorithm based on nonlinear perturbation equations of FRF data, to locate and quantify the structural damage. The proposed algorithm is also extended to cases of incomplete measurement in terms of coordinates by means of an iterative procedure. The validity and applicability of the method is demonstrated through numerical and experimental studies on a 3-bay plane framed structure.

Fanning and Carden (2003) propose a damage detection methodology which requires a single measured FRF of the damaged system sampled at several frequencies and a correlated numerical model of the structure in its initial state. The method is successful in detecting stiffness changes in a numerically simulated 2-D frame structure and is shown experimentally to be able to detect additional lumped masses in a lattice steel tower (Fanning & Carden, 2004). Park and Park (2005), using only measured frequency-response functions without a baseline model, develop a method which reduces the experimental load by detecting damage within a substructure.

Since measurements are always contaminated by noise and sufficient measurement data are often difficult to obtain, Furukawa et al. (2006) present a

damage identification method for uncertain FRFs. The structural damage is detected according to the changes in FRFs from the original intact state. The method iteratively zooms into the damaged elements by excluding the elements which are labelled as undamaged from the damage candidates.

1.3.2.7 Model updating based methods

Many damage identification methods are based on updating the physical parameters (e.g. mass, damping and stiffness matrices) of the numerical model of the structure (generally a finite element model) in order to reproduce as closely as possible the measured static or dynamic response data. This technique is essentially an optimization problem based usually on the structural equations of motion, a baseline model of the undamaged configuration of the structure and the measured data (e.g. natural frequencies, mode shapes, FRFs). Once the updated numerical model reproduces the measured data to a sufficient degree of accuracy, the identification of the damage location and extent is achieved by comparing the model updated parameters to the corresponding parameters of the baseline model. Reviews of model updating based damage identification methods can be found in Mottershead and Friswell (1993), Hemez (1993), Friswell and Mottershead (1995) and Marwala (2010).

Primarily, these methods are based on the equations of motion and differ basically in the objective function to be minimized, in the imposed constraints and in the numerical scheme used to implement the optimization. The main developed methods are: the *matrix-update methods*, the *optimal matrix methods*, the *sensitivity based methods*, the *eigenstructure assignment methods* and the more recent *computational intelligence methods* (Marwala, 2010).

Consider the eigenvalue equations of the *i*th mode of a damaged n-DOFs system:

$$(-\omega_{d_i}^2 \mathbf{M}_d + \omega_{d_i} \mathbf{C}_d + \mathbf{K}_d)\tilde{\mathbf{u}}_{d_i} = 0, \tag{1.3}$$

where ω_{d_i} and $\tilde{\mathbf{u}}_{d_i}$ are, respectively, the measured natural frequency and mode shape of the *i*th mode and $\mathbf{M}_d$, $\mathbf{C}_d$ and $\mathbf{K}_d$ the mass, damping and stiffness matrices of the damaged model. Assuming that these matrices can be defines as following,

$$\begin{aligned} \mathbf{M}_d &= \mathbf{M}_u - \Delta\mathbf{M} \\ \mathbf{C}_d &= \mathbf{C}_u - \Delta\mathbf{C} \\ \mathbf{K}_d &= \mathbf{K}_u - \Delta\mathbf{K} \end{aligned}, \tag{1.4}$$

being $\mathbf{M}_u$, $\mathbf{C}_u$ and $\mathbf{K}_u$ the matrices related to the undamaged model and $\Delta\mathbf{M}$, $\Delta\mathbf{C}$ and $\Delta\mathbf{K}$ the óperturbationô matrices representative of the occurred damage.

Substituting Eq. 1.4 into Eq. 1.3, yields to the identity:

$$(-\omega_{d_i}^2 \mathbf{M}_u + \omega_{d_i} \mathbf{C}_u + \mathbf{K}_u)\tilde{\mathbf{u}}_{d_i} = (-\omega_{d_i}^2 \Delta\mathbf{M} + \omega_{d_i} \Delta\mathbf{C} + \Delta\mathbf{K})\tilde{\mathbf{u}}_{d_i} . \quad 1.5$$

With the availability of the measured mode shapes and natural frequencies and the undamaged baseline model of the faulty structure, the left side of Eq. 1.5 consists of known quantities and can be regarded as equivalent to a Residual Force Vector (RFV), $\mathbf{r}_i$, related to the *i*th mode:

$$\mathbf{r}_i = (-\omega_{d_i}^2 \Delta\mathbf{M} + \omega_{d_i} \Delta\mathbf{C} + \Delta\mathbf{K})\tilde{\mathbf{u}}_{d_i} . \quad 1.6$$

The RFV may physically be interpreted as the harmonic excitation that if it is applied at the frequency ω_{d_i} to the undamaged structure, expressed by $\mathbf{K}_u$, $\mathbf{C}_u$ and $\mathbf{M}_u$, it would produce a structural response described by the mode shape $\tilde{\mathbf{u}}_{d_i}$.

Equation 1.6 is fundamental in the model updating based methods and it is often used as both objective function and constraint. Other constraints used in several methods are the preservation for each matrix of symmetry,

$$\begin{aligned} \Delta\mathbf{M} &= \Delta\mathbf{M}^T \\ \Delta\mathbf{C} &= \Delta\mathbf{C}^T \\ \Delta\mathbf{K} &= \Delta\mathbf{K}^T \end{aligned} , \quad 1.7$$

of sparsity (i.e. the zero/non zero pattern of the matrix),

$$\begin{aligned} sparse(\mathbf{M}_u) &= sparse(\mathbf{M}_d) \\ sparse(\mathbf{C}_u) &= sparse(\mathbf{C}_d) \\ sparse(\mathbf{K}_u) &= sparse(\mathbf{K}_d) \end{aligned} , \quad 1.8$$

and of positivity,

$$\begin{aligned} \mathbf{x}^T \Delta\mathbf{M}\, \mathbf{x} &\geq 0 \\ \mathbf{x}^T \Delta\mathbf{C}\, \mathbf{x} &\geq 0 \\ \mathbf{x}^T \Delta\mathbf{K}\, \mathbf{x} &\geq 0 \end{aligned} , \quad 1.9$$

where $\mathbf{x}$ is an arbitrary vector.

The *matrix-update techniques* are based on the modification of structural model matrices, for example the mass, stiffness and damping matrices, to identify damage in structures (Baruch, 1978). The method aims in minimizing the norm of the RFV by updating physical parameters $\mathbf{M}_u$, $\mathbf{C}_u$ and $\mathbf{K}_u$ of the model appearing in Eq. 1.6. The difference between updated matrices and original matrices identifies the damage. These techniques are classified as iterative since they are employed by iteratively changing the relevant parameters until the error function (RFV) is minimized.

DôAmbrogio and Zobel (1994) developed a matrix-update method by minimizing the Euclidean norm of the RFV in the frequency domain. This

methodology is computationally expensive and in addition, it is difficult to find a global minimum through the optimization technique, due to the presence of multiple stationary points (Janter & Sas, 1990). Techniques such as the use of genetic algorithms and multiple starting design variables have been applied to increase the probability of finding the global minimum (Larson and Zimmerman, 1993; Mares and Surace 1996; Levin and Lieven, 1998; Dunn, 1998).

The *optimal matrix methods* use a closed-form, direct solution to compute the damaged model matrices or the perturbation matrices. The problem is generally formulated as a Lagrange multiplier or penalty-based optimization, which can formally be written as

$$\min_{\Delta\mathbf{M},\Delta\mathbf{C},\Delta\mathbf{K}} \{J(\Delta\mathbf{M},\Delta\mathbf{C},\Delta\mathbf{K}) + \lambda R(\Delta\mathbf{M},\Delta\mathbf{C},\Delta\mathbf{K})\}, \qquad 1.10$$

where J is the objective function, R is the constraint functions and λ is the Lagrange multiplier or penalty constant.

Chen and Garba (1988) present a method for minimizing the norm of the property perturbations with a constraint on the RFV. The updates are obtained at the element parameter level rather than at the matrix one. This method is applied to a truss structure. Brock (1968) and Kammer (1988) propose the minimization of the RFV with a property matrix symmetry constraint which preserves the reciprocity condition in the updated structural model. Smith and Beattie (1991) formulate the problem imposing the minimization of both the perturbation matrix norm and the RFV norm subject to the symmetry and sparsity constraints. Liu (1995) apply the minimization of the square of the RFV to locate and quantify the damage in a simulated plane truss structure. In the presence of noise, multiple modes are needed to be considered for a proper identification.

Another approach to the optimal matrix problem involves the minimization of the rank of the perturbation matrix, rather than its norm. The idea behind this approach is that the perturbation matrices tend to be of small rank since damage is generally concentrated in a few structural members. Zimmerman and Kaouk first present this approach (1994) and later develop the Minimum Rank Perturbation Theory (MRPT) algorithm (Kaouk & Zimmerman, 1995; Kaouk & Zimmerman, 1994; Zimmerman, 1995). For example, in (Kaouk & Zimmerman, 1994), the MRPT algorithm is extended to estimate mass, stiffness and damping perturbation matrices simultaneously. The computation is accomplished by exploiting the cross-orthogonality conditions of the measured mode shapes with respect to the damaged property matrices. Doebling (1996) presents a method to compute a minimum-rank update for the element parameter vector rather than for global or element stiffness matrices. The method uses the same basic formulation as that of MRPT, but it constrains the global stiffness matrix perturbation to be a function of the diagonal element stiffness parameter perturbation matrix. The author shows that this method performs better than a minimum-norm parameter update technique on the experimental data related to a truss damaged structure. A

limitation of this method, similarly to that of all minimum-rank procedures, is that the rank of the perturbation is always equal to the number of modes used in the computation of RFV. Considering incomplete measured modal data, Carvalho et al. (2007) successfully apply a direct technique for model updating. However, one limitation of this technique is that the updated model is not always physically realistic.

The *sensitivity based methods* exploit refined techniques which are based on the assumption that experimental data are perturbations of design data about the baseline numerical model. These methods aim at evaluating a modified parameter vector,

$$\mathbf{p}^{(n+1)} = \mathbf{p}^{(n)} + \delta\mathbf{p}^{(n+1)}, \tag{1.11}$$

where the perturbation parameter vector $\delta\mathbf{p}^{(n+1)}$ is computed by minimizing the objective function through a Newton-Raphson iteration,

$$J\left(\mathbf{p}^{(n)} + \delta\mathbf{p}^{(n+1)}\right) \approx J\left(\mathbf{p}^{(n)}\right) + \left[\frac{\partial J}{\partial \mathbf{p}}\mathbf{p}^{(n)}\right] \otimes \delta\mathbf{p}^{(n+1)} = 0, \tag{1.12}$$

where $J(\mathbf{p})$ is the objective function. Typically this function is selected to be the RFV, as defined in Eq. 1.5.

The various sensitivity-based update methods differ in the scheme used to estimate the sensitivity matrix. Basically, either the experimental or the analytical modal properties or frequency-response functions are used in the differentiation. Some relevant sensitivity-based update methods are presented in the following.

Ricles and Kosmatka (1992) present a methodology using RFVs to potentially locate the damaged regions and a weighted sensitivity analysis to assess the mass and/or stiffness variations. Measured modal test data and a correlated analytical structural model are used. A wide variety of numerical examples are analysed to show that the current method works successfully even if reduced models are considered. Farhat and Hemez (1993) minimize the norm of the RFV by updating both stiffness and mass matrices in a sensitivity based procedure. The minimization of the RFV is used also to expand the incomplete mode shapes. The effectiveness of the method is applied to a simulated cantilever and plane truss structures. Modes storing sufficient strain energy in the damaged elements are found to be critical for the identification.

Ben-Haim and Prells (1993) propose selective frequency-response function sensitivity to uncouple the finite-element-updating problem, while Lin et al. (1995) improve the modal sensitivity technique by ensuring that it can be applicable to large magnitude damages.

Kosmatka and Ricles (1999) use measured modes and frequencies in conjunction with vibratory residual forces and a weighted sensitivity analysis to locate and calibrate single damage events (stiffness loss, connection loosening,

lumped mass addition) in a laboratory space truss structure. RFVs are estimated by means of analytical models differently correlated to the undamaged configuration of the truss structure. As expected, as the correlation between the analytical model and the baseline test data increases, the prediction improves. However, reasonable results can also be obtained using an uncorrelated analytical model.

In the study of Yang and Liu (2007) the RFV based method is developed in order to successfully detect structural damages when the measured modal parameters are incomplete and have noises. To expand the incomplete measured mode shapes the best technique presented by Lim and Kashangaki (1994) is applied, where three techniques for damage quantification are studied: the algebraic solution of the residual force equation (Chen & Garba, 1988), the minimum-rank element update technique (Zimmerman & Kaouk, 1994) and the natural frequency sensitivity method (Lin et al., 1993). These damage detection methods are compared for a numerical plane truss structure with measurement noise and the authors recommend the third one as the most appropriate in the actual engineering practices.

Eigenstructure assignment methods are based on control-system theory. The structure under investigation is forced to respond in a predetermined manner. During damage detection, the desired eigenstructure is the one that is measured in the test. Lim (1995) illustrates clearly the eigenstructure assignment technique and applies a constrained eigenstructure technique experimentally to a twenty-bay plane truss structure. His approach identifies element-level damage directly, rather than finding perturbations to the stiffness matrix. The technique is shown to work well even with limited instrumentation. Zimmerman and Kaouk (1992) apply an eigenstructure assignment technique to the identification of the elastic modulus of a cantilevered beam. They include algorithms to improve the assignability of the mode shapes and preserve sparsity in the updated model. Schultz et al. (1996) improve this approach through using measured frequency-response functions. Lim and Kashangaki (1994) introduce the use of the best achievable eigenvectors for the location of damage and apply the technique to the detection of damage in an cantilevered truss structure.

Computational intelligence methods (Marwala, 2010) use modern optimization methods in order to minimize the distance between the finite-element predicted data and the measured data. Some of these methods are the Nelderï Mead simplex methods, a nongradient-based technique (Bürmen et al., 2006; Jung & Kim, 2009), the artificial neural networks (see Section 1.3.2.10), the genetic algorithms (see Section 1.3.2.11), the particle-swarm optimization methods, inspired by algorithms that model the ñflocking behaviorò seen in birds (Kennedy, 2010; Marwala, 2005) and the simulated annealing methods (Paya-Zaforteza, 2009).

In the literature many damage identification methods concerned with model updating have been proposed. However, several issues arise when creating a well-correlated numerical model of undamaged structure (Carden & Fanning, 2004):

- accuracy of the initial model;
- size and complexity of the model;
- non-uniqueness of resultant model in matching the measured data;
- number of updating parameters;
- measured data chosen to be matched by the model.

As found by Fritzen et al. (1998), the *accuracy of the initial model* of the structure is essential. The authors use a sensitivity based algorithm to locate and detect damage but, even using a Euler-Bernoulli beam model instead of a Timoshenko beam model, no reasonable results are obtainable in relation to the change of the higher eigenfrequencies.

Despite the constantly increasing of the available computing power which allows us to deal with larger and more complex models than before, the *size and the complexity of the model* to be updated is of concern and can be computationally infeasible. Möller and Friberg (1998) propose a computational time saving method that projects the problem onto a subspace spanned by a few eigenvectors of the initial model. Law et al. (2001), to reduce the number of DOFs, formulate super-elements while the modal sensitivities to small physical changes are maintained in a sensitivity based updating algorithm.

The *non-uniqueness of updated models* is an important concern in damage identification as well as model updating. Berman (1979), argues that as a real structure has an infinite number of DOFs, there exist an infinite number of physically reasonable models with finite DOFs, which adequately predict the behaviour of the structure over an adequate frequency range. Therefore there can be no uniquely corrected dynamic model of the structure. He concludes that the identification of the true changes in the physical characteristics due to the damage is far more demanding than the prediction of model. Baruch (1997) shows that damage affecting both mass and stiffness properties is not uniquely identified when using modal measurements alone. He notices that methods using mode shapes as a reference basis may identify matrices quite different from the actual stiffness and mass matrices. Engineering judgement is hence fundamental in the success of any model updating technique.

The issue of the *number of parameters identifiable* in sensitivity based updating methods is tackled by Gola et al. (2001). The theoretical number of parameters achieved by the matching of eigenvalues is equal to the number of measured resonant frequencies. When mode shapes are used, the number of parameters has an upper limit depending on the number of measured degrees of freedom. This limit is further reduced as a function of the mode derivatives.

In the study of Casas and Aparicio (1994), a model updating technique is used for damage identification in laboratory concrete beams and the *effect of damping* is investigated. It is found that damping does not vary significantly in the cracked beams compared to the uncracked ones and further there is no clear relation between crack growth and increase in damping. The authors conclude that damping can be neglected as a model updating parameter. Indeed, generally, the damping matrix is neglected in model updating methods also due to the difficulty in modelling it accurately.

Some authors propose damage detection with a model updating technique using only measured natural frequencies (e.g. Morassi & Rovere, 1997; Messina et al., 1998; Yang & Liu, 2007). However, even though the measurement of natural frequencies alone is faster and more economical than measurement of mode shapes, using only natural frequencies reduces the number of possible updating parameters and therefore the type, number and location of damage that may be identified. For this reason, most of the model updating methods uses measured natural frequencies together with measured mode shapes to be matched by the model (e.g. Farhat & Hemez, 1993; Kaouk & Zimmerman, 1994; Kosmatka & Ricles, 1999). Model updating using FRF measurements directly instead of modal data has the obvious advantage that it avoids the need to identify the modal parameters from measurements. A further advantage is that FRF data can provide much more information in a desired frequency range than modal data (Lin & Ewins, 1990). In his PhD dissertation, Grafe (1998) points out that by using FRFs much more data points are available. Systems of updating equations can easily be turned into over-determined sets of equations taking care of avoiding ill-conditioned matrices.

In summary, in damage identification many techniques have been developed for model updating. Despite their intrinsic limitations exposed above, the recent methods based on computational intelligence seem to be promising. The main drawback is that these methods are strongly structure-dependent.

1.3.2.8 Nonlinear damage identification methods

An initially linear structural system, consequently to damage occurrence, can respond to its operational and environmental loads in a nonlinear manner. Typical examples are cracks that open and close under operational loading, yielded structural components that, due to cyclic stresses, have hysteretic behaviour and delamination in composite materials (introduced for example by impact loading). In all these cases, damage identification methods for SHM, based on the hypothesis of linear behaviour of the system (e.g. the modal parameters-based methods, the model updating-based methods and the FRF-based methods; Doebling et al., 1996), are poor and therefore not suitable for

most real-world applications. Therefore nonlinear damage identification methods are developed (Worden et al., 2008).

Numerical analyses and experimental investigations on the forced vibrations of beams with a breathing crack show the appearance of sub- and super-harmonic resonances and demonstrate that their nonlinearity features of the beam vibrations are much more affected by the presence of a crack than the changes of natural frequencies and modeshapes. Some authors (Tsyfansky & Beresnevich, 2000; Andreaus & Baragatti, 2011-2012; Giannini et al., 2013) propose these nonlinear vibration features as indicators of the presence of a crack at a very early stage of its nucleation and to quantify damage parameters (type, size and location). As far as practical applications are concerned, Bovsunovsky and Surace (2005) highlight three essential obstacles to be considered. Firstly, the aforementioned nonlinear features may arise in the presence of any type of nonlinearity of a vibrating system (e.g. material nonlinearity, geometrical nonlinearity, nonlinear contact. Then, it is difficult to ensure the application of precise harmonic excitations, and the manifestation of nonlinear features depends not only on the crack parameters but also on the level of damping in the vibrating system.

The recent concept introduced by Lang and Billings (1996, 2005), named Nonlinear Output Frequency Response Functions (NOFRFs), which allows the analysis of nonlinear systems to be handle in a manner similar to that of linear systems, appears to be a good approach in structural defect diagnosis. Peng et al. (2008) use the NOFRF concept to analyze the nonlinear response of a beam with a closing crack. The high order NOFRFs result to be extremely sensitive to the appearance of a crack in the beam, and hence they seem to be useful as crack damage indicator in terms of crack existence and size. Later, Peng et al. (2011) demonstrate through experimental test in a damaged aluminium plate the potential and effectiveness of a new damage detection technique based on the well-known Nonlinear Auto-Regressive Moving Average with eXogenous Inputs (NARMAX) modelling method and the NOFRFs-based analyses. Firstly, the NARMAX modelling method is applied to establish a NARX model from a testing input and output data of an inspected structural system. The NOFRFs and the associated index for the inspected structure are determined from the established NARX model. Finally, structural damage detection is conducted by comparing the values of the NOFRF index of the inspected structure and the values of the index for a damage-free structure. Lang et al. (2011) introduce the concept of *transmissibility* related to the NOFRFs and develop a technique aimed to detect and locate both linear and non-linear damage in MDOF structural systems. Numerical simulation results and experimental studies on a three-storey building structure verify the effectiveness of the new technique.

The output only vibration-based damage detection methods (Yan et al., 2007), which consider only operational structural response conveniently recorded

in one or more points are strongly investigated in the last decade. These methods do not require analytical or numerical models and the knowledge of the undamaged structure response. Moreover, these methods are made attractive by the nowadays availability of measurement techniques which may capture with high precision the dynamic deflection shapes of large areas (plates and shells) or lengths (beams) in a point-by-point spatial field at high time frequency. Wang et al. (2006) utilize the auto-correlation and the cross-correlation functions of the output data recorded in different zones of the structure to define a Local Damage Factor (LDF) which is capable of determining the presence, severity, and location of structural damage at the same time. Analysing the dynamic characteristics of the intact structure, the influence of structural nonlinearity, imperfections, and system noise are efficaciously taken in account by the LDF method. A Modified LDF (MLDF) method is also proposed in order to detect damage without requiring benchmark data for the intact structure. The effectiveness of the proposed LDF and MLDF methods are verified experimentally by detecting the damage in a 3D steel framed structure with a cracked pillar. Finally it should be recalled that Time-Frequency Techniques (TFT), such as the Short Time Fourier Transform (STFT), the Empirical Mode Decomposition (EMD), the Hilbert Transform (HT) and the Wavelet Analysis (WA), are widely used to deal with the damage detection in nonlinear system (see Section 1.3.2.9).

1.3.2.9 Time-frequency techniques

Time-frequency techniques have been shown to be great analysis tools for damage identification due to their multitasking capability in data pre-processing, feature extraction and selection, pattern recognition and data/information fusion. Among these techniques wavelet analysis and Hilbert-Huang Transform (HHT) are the most powerful in damage detection. In comparison with the Fast Fourier Transform (FFT), which analyses globally a signal as it would be stationary and find out its frequency components from an average over its whole length, these techniques can deal with non-stationary signals (e.g. impulse responses, structural vibrations due to earthquake or to wind storms, etc.) and uncover their local contents (Staszewski & Robertson, 2007; Nagarajaiah, & Basu, 2009).

STFT is used by Fitzgerald et al. (2010) to monitor the stiffness reduction in time due to cumulative fatigue damage of a general wind turbine blade. The time history of the blade displacement is analyzed by STFT and the decreasing of the local dominant frequency due to the system stiffness change is evaluated.

Wavelet analysis (Mallat, 2001), thanks to its multi-resolution properties, works as a signal microscope identifying the details of non-stationary signals conversely to the traditional analysis tools, such as FFT. A depth exposition of

wavelet analysis theory and its application in vibration based damage identification is presented in Sections 2.3.

The Hilbert-Huang transform (Huang & Shen, 2005) is a recent time-frequency technique obtained by the combination of the Empirical Mode Decomposition (EMD) (Huang et al., 1998) and the Hilbert Transform (HT) (King, 2009). The key part of the method is the decomposition of the original signal into the óIntrinsic Mode Functionsô (IMFs) through the EMD. These functions, as explained below, are ideal for to be used with the HT and, therefore, to obtain a full energy-frequency-time distribution of the data (i.e. the Hilbert spectrum and the instantaneous frequency for each IMFs). Since the HHT is adaptive and based on the local characteristic time scale of the data, it is highly efficient to analyse nonlinear and non-stationary processes. In the following, the theory of the HT and of the EMD are introduced. Then some relevant structural damage identification methods based on the HHT are presented.

The Hilbert transform is an integral transform that, thanks to its properties, has been applied for more than 25 years to analysis non-stationary vibration signal. During the last decade, HT has shown a growing use, often in conjunction with EMD, in nonlinear mechanical system identification and structural damage identification (Feldman, 2011). HT is strictly related to the ñanalyticò signal $s_a(t)$ of a general non-stationary signal $s(t)$ and, as shown below, its application to a general signal provides some additional information about amplitude, instantaneous phase and frequency of vibrations.

The HT of the function $s(t)$ is defined by an integral transform (King, 2009):

$$¢\left[s(t)\right] = \frac{1}{\pi}\int_{-\infty}^{+\infty} s(\tau)/(t-\tau)\,d\tau\,, \tag{1.13}$$

where t is the fixed time variable and τ is the running time variable.

Signals in nature are real valued but for analysis, but it is often more convenient to treat them as complex variables. A complex signal $s_a(t)$ can be written as sum of the real part $s(t)$ and the imaginary part $\bar{s}(t)$, that is $s_a(t)$

$$s_a(t) = s(t) + \mathrm{j}\bar{s}(t)\,, \tag{1.14}$$

where $\mathrm{j} = \sqrt{-1}$. By knowing the real part $s(t)$, the complex signal $s_a(t)$ can be determined by taking the positive part of the spectrum of the real signal, $s(\omega)$, multiplying it by a factor of 2 and then performing Fourier inversion, namely

$$s_a(t) = 2\frac{1}{\sqrt{2\pi}}\int_0^{\infty} s(\omega)e^{j\omega t}d\omega\,. \tag{1.15}$$

Therefore, substituting the definition of $s(\omega)$ in Eq. 1.15, we have

$$s_a(t) = \frac{1}{\pi}\int_0^{\infty}\int_{-\infty}^{+\infty} s(\tau)e^{-j\omega\tau}e^{j\omega t}d\tau\,d\omega\,. \tag{1.16}$$

By considering that,

$$\int_0^{\infty} e^{j\omega x} d\omega = \pi\delta(x) + \frac{\mathrm{j}}{x}, \tag{1.17}$$

where $x = t - \tau$ and $\delta(x)$ is Dirac function , Eq. 1.16 becomes,

$$s_a(t) = s(t) + \frac{\mathrm{j}}{\pi}\int_{-\infty}^{+\infty} s(\tau)/(t-\tau)\, d\tau\,. \tag{1.18}$$

Comparing Eq. 1.13 with Eq. 1.18, finally, the imaginary part $\bar{s}(t)$ turns out to be the Hilbert transform of $s(t)$:

$$\bar{s}(t) = \frac{1}{\pi}\int_{-\infty}^{+\infty} s(\tau)/(t-\tau)\, d\tau = \mathrm{H}[s(t)]\,. \tag{1.19}$$

Note that, by definition, complex signals $s_a(t)$, called ñanalyticò signals, are signals whose spectrum consist only of positive frequencies.

The analytic signal $s_a(t)$ can also be expressed as

$$s_a(t) = A(t)e^{j\varphi(t)}, \tag{1.20}$$

where $A(t)$ and $\varphi(t)$ are, respectively, the instantaneous amplitude (or envelope), equal to $A(t) = \sqrt{s^2(t) + \bar{s}^2(t)}$, and phase, equal to $\varphi(t) = \arctan\left(\bar{s}(t)/s(t)\right)$, of the analytic signal.

The Instantaneous Frequency (IF) $\omega_i(t)$ is given by

$$\omega_i(t) = \dot{\varphi}(t) = \frac{\mathrm{d}}{\mathrm{d}t}\left(\arctan\left(\frac{\bar{s}(t)}{s(t)}\right)\right). \tag{1.21}$$

Through the derivative properties, $\omega_i(t)$ is obtained by

$$\omega_i(t) = \frac{(s(t)\bar{s}(t) - \bar{s}(t)\dot{s}(t))}{s^2(t) + \bar{s}^2(t)}\,. \tag{1.22}$$

Figure 1.2 shows the representation in a complex plain of a general analytic signal and its parts: the real signal, the imaginary part, obtained by the Hibert transform of the real component and the phase.

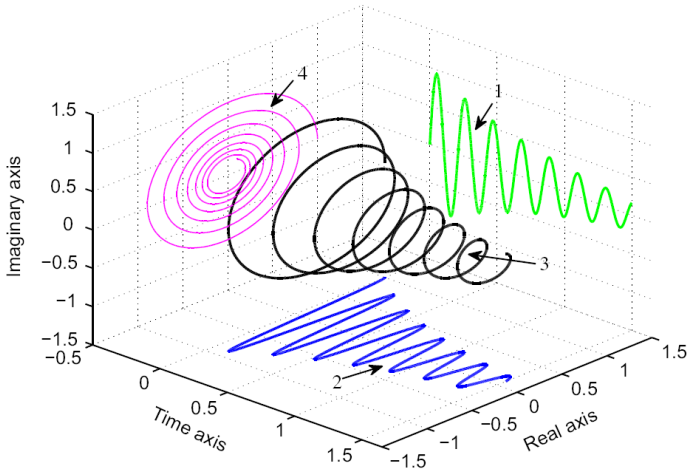

Fig. 1.2 - Representation of a general analytic signal (3) and its components: the real signal (2), the imaginary part (1) and the phase (4) (after Feldman, 2011).

The empirical mode decomposition allows any complicated data set to be decomposed into a finite and, often small number of óIntrinsic Mode Functions' (IMFs) through a particular ósifting processô. The name óintrinsic mode functionsô is adopted because they represent the oscillation modes embedded in the data. The IMFs are ómonocomponentô functions satisfying the following two conditions: (1) in the whole data set, the number of extrema and the number of zero crossings must either equal or differ at most by one; (2) at any point, the mean value of the envelope defined by the local maxima and of that defined by the local minima, is zero. The first condition is similar to the narrow-band requirement for a stationary Gaussian process. The second condition modifies a global requirement to a local one, and it is necessary to ensure meaningful instantaneous frequency without unwanted fluctuations as induced by asymmetric waveforms (Cohen, 1995; Huang et al., 1998).

A general signal $s(t)$ can be decomposed as follows,

$$s(t) = \sum_{i=1}^{n} \mathrm{imf}_i(t) + r_n(t), \qquad 1.23$$

where $\mathrm{imf}_i(t)$ are the IMFs and $r_n(t)$ is the residue of the decomposition. In Fig. 1.3 an example of empirical mode decomposition of a general signal, $s(t)$, is shown.

The intrinsic mode functions of $s(t)$ are obtained iteratively (Huang et al., 1998) using the following algorithm:

1. inizialize $r_0(t) = s(t)$ and $i = 1$;
2. extract the $\mathrm{imf}_i(t)$ as follows:

(a) initialize: $h_0(t) = r_{i-1}(t)$ and $j = 1$;

(b) identify all the local maxima and minima of $h_{j-1}(t)$;

(c) interpolate the local maxima by a spline to form the upper envelope $e_{max}(t)$ and execute the same with the local minima to form the lower envelope $e_{min}(t)$;

(d) calculate the mean $m_{j-1}(t) = (e_{min}(t) + e_{max}(t)) / 2$;

(e) compute $h_j(t) = h_{j-1}(t)$ **ï** $m_{j-1}(t)$;

(f) if the stopping criterion (expose below in Eq. 1.24) is satisfied then set $imf_i(t) = h_j(t)$; else return to (b) with $j = j + 1$;

3. $r_i(t) = r_{i-1}(t) - imf_i(t)$;

4. if $r_i(t)$ still has at least 2 extrema then go to 2 with $i = i + 1$; else the decomposition is finished and $r_i(t) = r_n(t)$ is the residue.

A satisfactory stopping criterion for the sifting process is defined to ensure that the IMFs retain the amplitude and frequency modulations of the actual signal. Huang *et al*. (1998) propose to accomplish the stopping criterion by limiting the Standard Deviation (SD) of $h(t)$ obtained from consecutive sifting,

$$SD = \sum_{k=0}^{N} \left[\frac{\left| h_{j-1}(kdt) - h_j(kdt) \right|^2}{h_{j-1}^2(kdt)} \right], \qquad 1.24$$

where $N = T / dt$ and T is the total time and dt is the time sampling interval. A typical value for SD is set between 0.2 and 0.3.

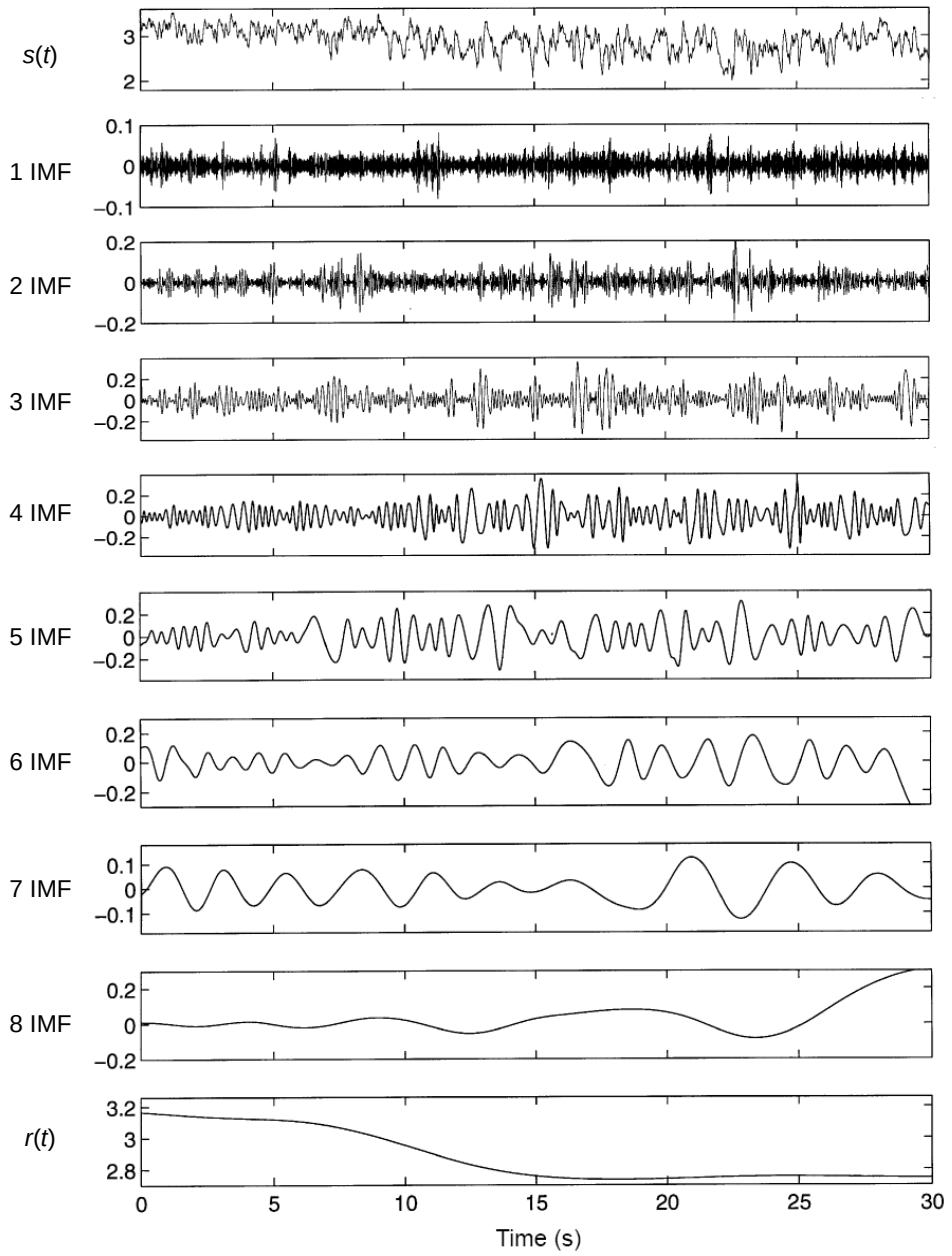

Fig. 1.3 - Example of empirical mode decomposition of a general signal, $s(t)$ in its 8 intrinsic mode functions and the residual function, $r(t)$ (after Huang et al., 1998).

Rilling *et al*. (2003) present an improvement of this criterion based on two thresholds, δ_1 and δ_2, aimed at reducing globally small fluctuations and in the mean while attacking into account locally large excursions. The mode amplitude $a(t) = (e_{\max}(t) - e_{\min}(t))/2$ and an evaluation function $\sigma(t) = |m(t)/a(t)|$ are computed and the sifting process is iterated until $\sigma(t) < \theta_1$ for a fraction of the total duration while $\sigma(t) < \theta_2$ for the remaining fraction. Usually, $\theta_1 \approx 0.05$ and $\theta_2 \approx 10\theta_1$.Once extracted the IMFs are extracted from *s*(*t*), the analytic signal $s_a(t)$ and the instantaneous frequencies $\gamma_i(t)$, associated with each $\text{imf}_i(t)$ component, can be obtained using Eqs 1.13-1.22 by letting $s(t) = \text{imf}_i(t)$ for each IMFs.

In the following, some essential works regarding the application of the HHT technique for structural damage identification are presented.

Yang et al. (2003) introduce two methods to detect the structural damage analyzing measured acceleration data. The first method, based on the EMD, performs the detection of the damage time instants and damage locations if the noise level is very small and only if the change of the system stiffness is abrupt and not gradual. On the other hand, the second method, based on the EMD, the Random Decrement Technique (RDT) and the HT, is capable of accurately determining the time instant of the damage occurrence regardless of the noise level and identifying the natural frequencies and damping ratios of the structure before and after damage quite accurately even if the system stiffness variation is gradual.

Douka and Hadjileontiadis (2005) analyze theoretically and experimentally through the EMD and the HT the free vibration response of a beam with a breathing crack. The authors show that IF oscillates between frequencies corresponding to the open and closed states, revealing the breathing behavior of the crack the mean variation of it increases with crack depth following a second order polynomial law: IF demonstrates to be an efficient tool for the description of the nonlinearities caused by the presence of a closing crack. However, the calculation of the mean variation of IF using experimental data from free vibration tests appears to be difficult since relatively high vibration amplitudes are needed to ensure proper opening and closing of the crack. Later, Loutridis et al. (2005) theoretically and experimentally investigate a cantilever beam with a breathing crack under harmonic excitation. In this case, it is shown that the mean variation range of IF and even the mean harmonic distortion obtained by the IMFs are efficient indicators of crack size and descriptors of system nonlinearity.

Tang et al. (2011) propose a damage detection index, called the ratio of the equivalent damping (RED), estimated from the smoothed HHT spectra, for detecting structural damage in steel structures due to strong earthquakes. Shaking table test data obtained for benchmark models based upon the Kobe and El

Centro earthquakes are analysed. Since the RED continuously increases with increasing PGA values as the structure experiences nonlinear behaviour, the authors conclude that RED is an effective and sensitive index for damage detection and can be used in on-line structural health monitoring of steel structures experiencing intense ground motions. In the work of Hsu et al. (2013), another damage detection index evaluated from the HHT acceleration spectra, called the ratio of bandwidth (RB), is adopted to detect initial damage in steel structures subjected to ground motion. Both numerical and experimental data highlight the index effectiveness: the change in RB is sensitive to stiffness reduction of the system, even when only a 10% decrement occurs.

1.3.2.10 Artificial neural network methods

The brain is capable of high performance in natural information processing tasks, such as perception, language understanding, motor control, etc., given the suitability of the neuronal system, consisting of billions of neurons that are interconnected with a fan-in and fan-out, to elaborate simultaneously a large number of pieces of information and constraints (Rumelhart et al., 1986). The Artificial Neural Networks (ANNs) algorithm has been inspired exactly by the neuronal architecture and the operation of brain (Anderson & Davis, 1995; Adeli & Park, 1998; Haykin, 1999).

The basic model of an individual neuron was developed in 1943, by Warren McCulloch and Walter Pitts and it is still considered the heart of most neural networks (McCulloch & Pitts, 1943). Later, Rosenblatt (1962) extended their model providing to networks the capability of self-organization and learning. His models, characterized by only two-layered networks so unsuitable of learning certain types of functions, paved the way to modern multilayer networks, such as the Back Propagation Neural Networks (BP NNs).

ANNs are a modern and powerful artificial intelligence technique which operates as blackbox, model-free and adaptive tool to capture and learn significant structures in data. They are suitable particularly for problems too complex to be modeled and solved by classical mathematics and traditional procedures. Their computing abilities have been proven in many fields, such as prediction, estimation, pattern recognition and optimization (Zhang et al., 1998; Bishop, 1995; Cochocki & Unbehauen, 1993; Adeli, 2001). The development of the error Back Propagation (BP) training algorithm (Rumelhart et al., 1986; Hecht-Nielsen, 1989), which is based on a gradient-descent optimization technique, launches the use of the neural networks. The BP NN is usually constructed by three layers, an input layer, a hidden layer and an output layer and due to its strong non-linear mapping ability and simplicity it is the most commonly used NNs algorithm (Werbos, 1990; Hegazy et al., 1994; Paola & Schowengerdt, 1995).

The basic strategy for developing a NN-based approach to damage identification of a structural system is to train a BP NN algorithm to recognize the structural damage conditions from the measured response of the structure (Wu et al. 1992). The first step is to provide a data set to train an appropriate NN. Ideally, this data set should contain the response of the undamaged structure as well as the responses of the structure in various damaged states. This data can be generated through measurements of structural response, model test results, numerical simulations or a combination of them. Therefore, once a network architecture is defined and a training algorithm is selected, the NN is trained with the training data set. The trained network is then tested to verify its performance and its generalization capability. In this step, different data with respect to those used to train the network have to be used for testing. Note that how well a trained network is able to work is strongly dependent on the adequacy of the selected network architecture and the richness of the training data set. Often, changes in the network architecture and/or additions to training data set are needed. Such changes are followed by the repetition of the whole training and testing process. This quasi iterative fine tuning is repeated until satisfactory performance of the NN is obtained. Finally, the experimentally measured real structural damage data are inserted into the trained NN and the output of the NN will be able to provide the effective location and severity of the structural damage.

Numerous research papers on structural damage detection using NN techniques are available in the literature; in the following the most important works are reviewed. Pandey and Barai (1995) apply the multilayer perceptron in the damage detection of truss steel bridge structures. The training patterns are generated for multiple damaged zones in the structure and the performance of the NNs with one and two hidden layers are examined. The network architecture with two hidden layers appears to be better than that with a single layer. Furthermore, the authors underline the fact that measured input at only a few locations in the structure is needed in the identification process using ANNs. In the work of Yun and Bahng (2000) a BP NN-based substructural identification for estimating the stiffness parameters of a complex structural system, in the case of noisy and incomplete measurement of the modal data, is presented. The substructural technique and the concept of the submatrix scaling factor are employed to reduce the relevant number of unknown stiffness parameters to be estimated. The natural frequencies and mode shapes are used as input patterns to the NN, and the Latin hypercube sampling and the component mode synthesis methods are used to efficiently generate such training data. Two numerical examples on truss and frame structures demonstrate the satisfactory performance of the method. Chen et al. (2003) study by a NN-based approach the problem of damage identification in engineering structures when excitation signals are unavailable or inaccessible. BP NNs are trained by output only response data and

transmissibility functions, which demonstrate to be effective features in training NN for structural damage identification.

Some authors realize online damage detection and health monitoring combining wavelet-based damage feature extraction and ANN-based identification. Yam et al. (2003) apply a combined technique to identify effectively crack damage in PVC sandwich plates, both through numerical and experimental analysis. Piezoelectric smart structure technology is used for the generation of excitation and structural response measurement. In the work of Paya et al. (1997), single and multiple faults in rotating machinery are successfully detected and classified using multilayer ANNs on the sets of preprocessed data by wavelet transforms.

1.3.2.11 Genetic algorithm methods

Genetic Algorithm (GA) is a powerful universal optimization method based on Darwinôs theory of evolution and survival of the fittest. Analogous to genes in genetics, GA represents the parameters in a given problem by encoding them in a string. Differently from the conventional optimization methods which finds the optimum from a single point, the GA uses a set of points, i.e. a population of coded strings, to search for the optimum solution.

Simple GA (Goldberg, 1989) consists of three basic operators: reproduction, crossover and mutation. In genetics, genes, which consist of alleles, constitute a chromosome. Similarly, in simple GA, encoded strings are composed of bits. In damage identification problems, the parameters of structural elements to be encoded are the ratios of the damaged value to the undamaged value of one or more specified variables (e.g. Youngôs modulus, cross-sectional area, etc.). Hence, the values of the specified variables pertaining to the structure elements to be identified are equal to the above ratio times their baseline values from the original undamaged structure. The values of the variables calculated from the above procedure are to be used in FE analysis to compute the structural response, which has to be compared with the corresponding measured response in identifying structural damage.

Some benchmark papers based on the application of GA in damage identification are presented. Mares and Surace (1996) use GA to adjust the structural parameters to minimizing the RFV, to locate and identify structural damage from measured natural frequencies and mode shapes. The initial population is not random but defined heuristically to represent the undamaged structure. The robustness of the GA method towards the noise influence on measured data is also shown in comparison with the conventional application of RFV method. Chou and Ghaboussi (2001) compare two GA-based methods of structural damage detection assuming different string representation schemes: the first scheme is the usual string representation used in simple GA; the second one

is that proposed by Raich and Ghaboussi (1997), called the Implicit Redundant Representation (IRR). A small number of simulated static displacements of a truss structure are considered and it has been demonstrated that the IRR GA works more successfully than the simple GA in detecting the location and magnitude of the most severe damage scenario. Furthermore, from the analysis of an additional structure, it has been shown that IRR GA, for its ability of active search, can find the optimum solution for both the material properties and the unmeasured displacements simultaneously, without the availability of complete FE analysis or other numerical simulations. In the work of Hao and Xia (2002) a genetic algorithm with real number encoding is applied to identify the structural damage by minimizing the objective function, which directly compares the changes in the measurements before and after damage. Three different criteria are considered: the frequency changes, the mode shape changes and a combination of the two. A laboratory tested cantilever beam and a frame are used to demonstrate the proposed technique. Numerical results show that the damaged elements can be detected by genetic algorithm, even when the analytical model is not effective.

Chapter 2

Wavelet Analysis and Damage Identification Methods

2.1 Introduction

Due to the lack of time-frequency techniques to properly analyse non-stationary signals, in the past decades the modern wavelet theory has been developed. The Continuous Wavelet Transform (CWT), the Discrete Wavelet Transform (DWT), the Stationary Wavelet Transform (SWT) and the discrete wavelet packet transform are the most well-known wavelet analysis tools, used nowadays in very diverse application fields, as image compression, speech processing, chemistry, neurophysiology, nondestructive evaluation, fractals and economics.

This chapter starts with an historical overview (Polikar, 1999) and introduces the theoretical basics of wavelet analysis, focusing on the CWT used throughout this study. Then, an in depth review of the state of the art of the wavelet-based methods for structural damage identification is exposed.

2.2 Wavelet analysis

2.2.1 Brief historical overview

To introduce wavelet functions and wavelet transform, we can start from the original idea of Fourier, where a complex function is approximated by weighted sum of simpler functions, which themselves are obtained from one simple basis function. The basis function can then be thought as a building block, and the original function can be approximated, or under certain conditions be fully represented, by using similar building blocks. There are significant advantages by

means of such an approximation as complicated functions can be described by a few of these building blocks with a good approximation.

Fourier used sinusoids of varying frequencies as building blocks, and this representation provides the frequency content of the original function (Bracewell, 1968). Fourier transform is used in a variety of fields, but it has one major drawback: sinusoids have perfect compact support in frequency domain, but not in time domain. In other words, sinusoids stretch out to infinity in time and, therefore, they cannot be used to approximate non-stationary signals, whose spectral content change in time. Since Fourier representation provides only spectral content with no indication about the time localization of the spectral components, Time-Frequency Representations (TFR) are required to analyse non-stationary signals.

The Short Time Fourier Transform (STFT) was the first modification to the Fourier transform in order to analyse non-stationary signals (Cohen, 1995). The idea behind the STFT was to segment the signal by using a time-localized window (e.g. Hanning, Hamming, cosine, Kaiser or Gaussian) and performing the analysis for each segment. Since the Fourier transform was computed for every windowed time localized segment of the signal, STFT provides a real time-frequency representation. In 1946 was Gabor the first one who modified the Fourier transform into STFT using a Gaussian window. Shortly after, in 1947, Jean Ville developed a similar TFR, named the Wigner-Ville transform, for representing the energy of a signal in the time-frequency plane. Between late 1940s and early 1970s, many other TFRs have been proposed each of which differed from the other ones only by the selected windowing function. A fundamental drawback limit of these TFRs is that, since the entire signal is analysed by means of a windowing function of fixed length, the time-frequency resolution of these TFRs is fixed (Fig. 2.1a). Therefore broad window results in better frequency resolution but poor time resolution and narrow window results in good time resolution but poor frequency resolution, due to the time-bandwidth relation (uncertainty principle; see Cohen, 1995).

At the end of 1970s, Morlet, a geophysical engineer, faced the problem of analyzing signals which had very high frequency components with short time lengths and low frequency components with long time lengths. Noticing that the STFT is inappropriate to analyze both high frequency components and low frequency components using the same window, he had the ingenious idea of using a different window function for analyzing different frequency bands. He generated window functions by dilation or compression of a prototype Gaussian which had compact support (its meaning is explained below) both in time and in frequency. Due to the ósmall and oscillatoryô feature of these window functions, Morlet named his basis functions as *wavelets of constant shape.*

Facing strong criticisms from his colleagues, at the beginning of the 1980s Morlet, helped by the theoretical physicist Grossman, arrived to formalize

mathematically what now is known as the continuous wavelet transform and its inverse transformation. Since both the STFT and the CWT are convolutions of the signal with a function that varies in both time and frequency, both transforms are confined by the uncertainty principle, which limits the area of a time-frequency atom in the overall time-frequency map (see Fig. 2.1). However, while the STFT atoms are of constant shape, the CWT atoms vary. The fatter atoms in the lower frequencies provide a better resolution in frequency and worse resolution in time, whereas the taller atoms in the upper frequencies provide better time resolution and worse frequency resolution (Fig. 2.1b). This variable resolution in general result advantageous in the analysis of non-stationary signals than a fixed one.

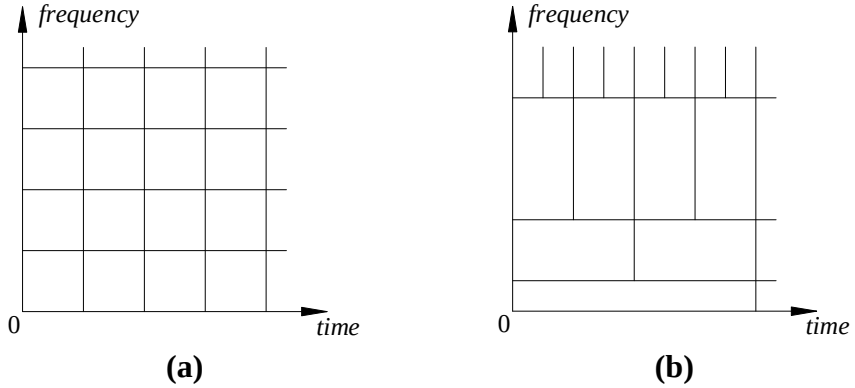

Fig. 2.1 ï Comparing STFT and wavelet transform resolution in time and frequency domain: (a) STFT fixed resolution; (b) CWT multi-resolution.

The French mathematician Meyer, who in 1984 noticed the similarity between Morletôs and Calderónôs 1964 work, was fascinated by the elegant non-stationary function analysis scheme and continued to study wavelets. Noticing the great deal of redundancy in Morletôs choice of basis functions, he worked on developing wavelets with better localization properties. In 1985, he constructed *orthogonal wavelet* basis functions with very good time and frequency localization. However, it turned out that another harmonic analyst, Strömberg, had already discovered the very same wavelets about five years before. Nevertheless, it should be underlined that the honor of the discovery of orthonormal wavelet basis functions goes to the German mathematician Haar (1909). Haar wavelets, the first and simplest orthonormal wavelets, are of little practical use due to their poor frequency localization. In 1930s Levey, studying random signals of Brownian motion, and independently Littlewood and Paley, working on localizing the contributing energies of a function, expanded Haarôs work on developing orthonormal basis functions.

Meanwhile, a former graduate student of Grossman, developed wavelet frames to discretize time and scale parameters of the wavelet transform, allowing a broad choice of basis functions. Along with Mallat, Daubechies is considered the developer of the transition from continuous to discrete signal analysis. In 1986 Mallat with Meyer developed the idea of MultiResolution Analysis (MRA) for discrete wavelet transform, which later in 1988 became his Ph.D. dissertation. The idea was to decompose a discrete signal into its dyadic frequency bands by a series of lowpass and highpass filters to compute its DWT from the approximations at these various scales. However, Mallatôs work constituted a natural extension of time localization to the well-established frequency localization idea of quadrature mirror filters and subband filtering, which were developed by Croisier, Esteban and Galand around 1976. In 1988, with the development of Daubechiesô orthonormal bases of compactly supported wavelets, the foundations of the *modern wavelet theory* were laid.

In the following years until nowadays, researchers focused on developing other wavelet basis functions with different properties and modifications of the MRA algorithms. For instance, Cohen, Feauveau and Daubechies constructed the compactly supported biorthogonal wavelets, whereas Coifman, Meyer and Wickerhauser developed wavelet packets, a natural extension of MRA.

2.2.2 Wavelet functions

A wavelet function $\psi(x)$ is a zero mean local wave-like function which decays rapidly and must satisfy the following mathematical conditions (Mallat, 2001):

(i) have *finite energy*, i.e.

$$E_{\psi} = \int_{-\infty}^{+\infty} |\psi(x)|^2 dx < \infty , \qquad 2.1$$

where usually the wavelet function is normalized in order to have $E_{\psi} = 1$;

(ii) satisfy the weak *admissibility condition* (see the Calderon-Grossman Morlet theorem; Mallat, 2001) to ensure the completeness of the wavelet transform and to maintain energy balance, i.e.

$$C_g = \int_0^{+\infty} \frac{|\hat{\psi}(\omega)|^2}{\omega} d\omega < \infty , \qquad 2.2$$

where $\hat{\psi}(\omega)$ is the Fourier transform of $\psi(x)$ and C_g is called *admissibility constant*, function of the chosen wavelet. This condition is necessary for executing the inverse continuous wavelet transform;

(iii) the Fourier transform of a complex wavelet must be real and null for negative frequencies.

Many wavelet functions have been developed during the years (Daubechies, 1992). Figure 2.2 shows the mother wavelets of some common wavelet families:

- *Haar* wavelet or (the 1st order *Daubechies* wavelet) (Fig. 2.2a) and the 15th order *Daubechies* wavelet (Fig. 2.2b), which are orthogonal and biorthogonal wavelets characterized by compact support (i.e. the region where the mother wavelet is not equal to zero is finite);
- the 2nd and the 8th order *Symlet* wavelets (Figs 2.2 (c-d)), and the 1st and the 4th order *Coiflet* wavelets (Figs 2.2(e-f)), which are nearly symmetric, orthogonal and biorthogonal wavelets with compact support;
- the 2nd order *Gaussian* wavelet (or *Mexican hat* wavelet) (Fig. 2.2g), the 4th order *Gaussian* wavelet (Fig. 2.2h) and the real *Morlet* wavelet (Fig. 2.2i), which are symmetric wavelets with infinite support, but not orthogonal and biorthogonal;
- *Meyer* wavelet (Fig. 2.2j), which is regular (i.e. indefinitely derivable), symmetric, orthogonal and biorthogonal wavelet with infinite support.

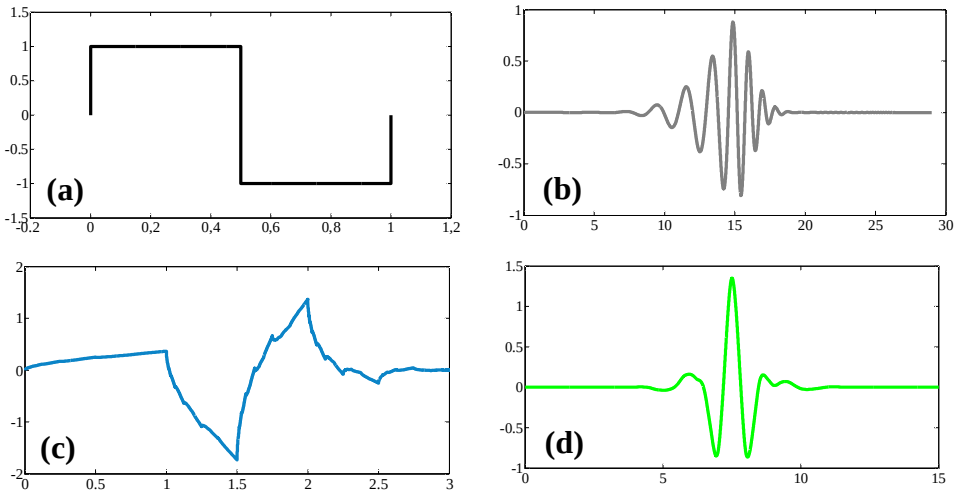

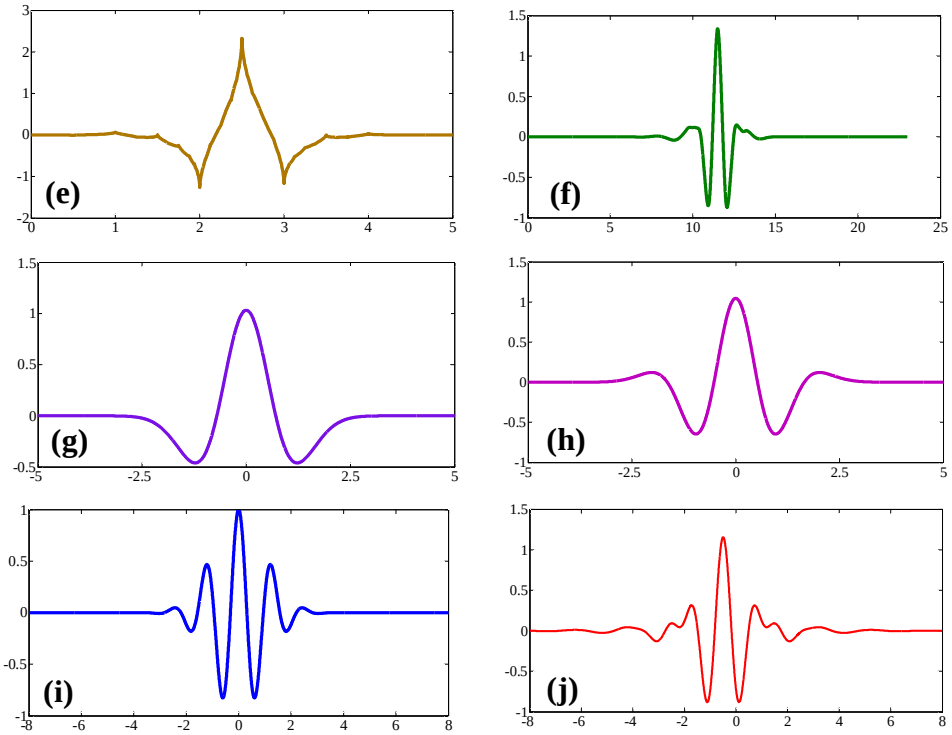

Fig. 2.2 ï Example of wavelet functions: (a) Haar wavelet (or 1st order Daubechies wavelet); (b) 15th order Daubechies wavelet; (c) 2nd order Symlet wavelet; (d) 8th order Symlet wavelet; (e) 1st order Coiflet wavelet; (f) 4th order Coiflet wavelet; (g) 2nd order Gaussian wavelet (Mexican hat wavelet); (h) 4th order Gaussian wavelet; (i) real Morlet wavelet (or Gabor wavelet); (j) Meyer wavelet.

In this study the 4th order Coiflets wavelet (óCoif4ô), the 2nd order Daubechies wavelet (óDb2ô), the 4th order Gaussian wavelet (óGaus4ô) and the real Morlet wavelet (ôMorlô) are used in the wavelet transform.

A wavelet family of functions is obtained by scaling and translating the mother wavelet:

$$\psi_{t,s}(x) = \frac{1}{\sqrt{s}}\psi\left(\frac{x-t}{s}\right) \qquad 2.3$$

where s and t are, respectively, the scale and the translation parameters. As an example, Fig. 2.3 displays in blue Mexican hat mother wavelet (s = 1, t = 0) and in green and in red the wavelet, respectively, scaled by 2 (s = 2) and centred at x = 2 (t = 2), and scaled by 3 (s = 3) and centred at x = 5 (t = 5).

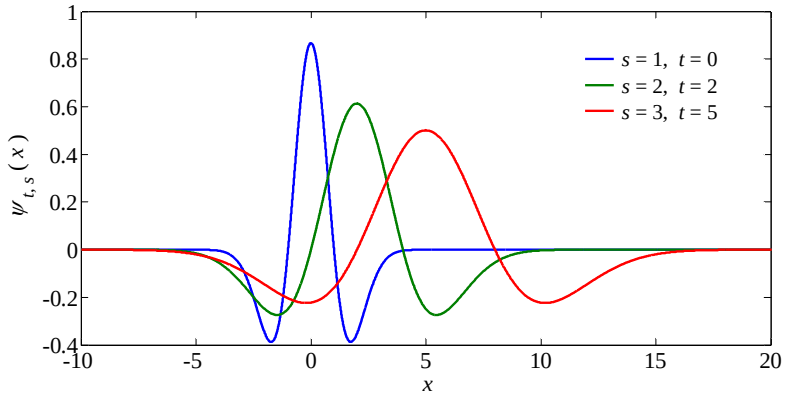

Fig. 2.3 ï In blue Mexican hat mother wavelet (s = 1, t = 0); in green and in red the wavelet, respectively, scaled by 2 (s = 2) and centred at x = 2 (t = 2), and scaled by 3 (s = 3) and centred at x = 5 (t = 5).

Figure 2.4 shows the frequency contents, obtained through Fourier transform, of Mexican hat mother wavelet and of its scaled wavelets (s = 2, 3). Since the scaled wavelet functions are simply stretched mother wavelets, their spectral energy is located in narrower bands centered at lower frequencies with respect to that of the mother wavelet.

The center frequency f_c is defined as the frequency maximizing the Fourier transform of the mother wavelet modulus. Thus, the center frequency associates a given mother wavelet with a periodic signal of frequency f_c, as shown in Fig. 2.5 for óCoif4ô(f_c = 0.6957), óDb2ô (f_c = 0.6667), óGaus4ô (f_c = 0.3180) and ôMorlô (f_c = 0.8125).

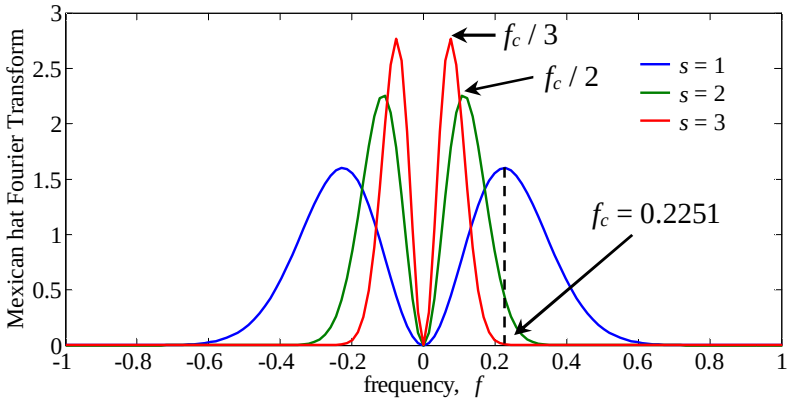

Fig. 2.4 ï Fourier transform of Mexican hat mother wavelet (s = 1) and its scaled wavelets (s = 2, 3). The center frequency of Mexican hat mother wavelet is f_c = 0.2251.

By stretching to the scale *s* the mother wavelet, the center frequency of the scaled wavelet results to be inversely proportional to the scale *s* (Fig. 2.4). Thus, at any scale, a wavelet can be associated to a periodic signal containing a single frequency f_a, known as pseudo-frequency:

$$f_a = \frac{f_c}{dx\, s} \qquad 2.4$$

where *dx* is the sampling interval of the wavelet function. Therefore, the pseudo-frequency f_a of a generic wavelet function captures its main oscillations and can be regarded as the dominant frequency analysing the signal in the wavelet transform.

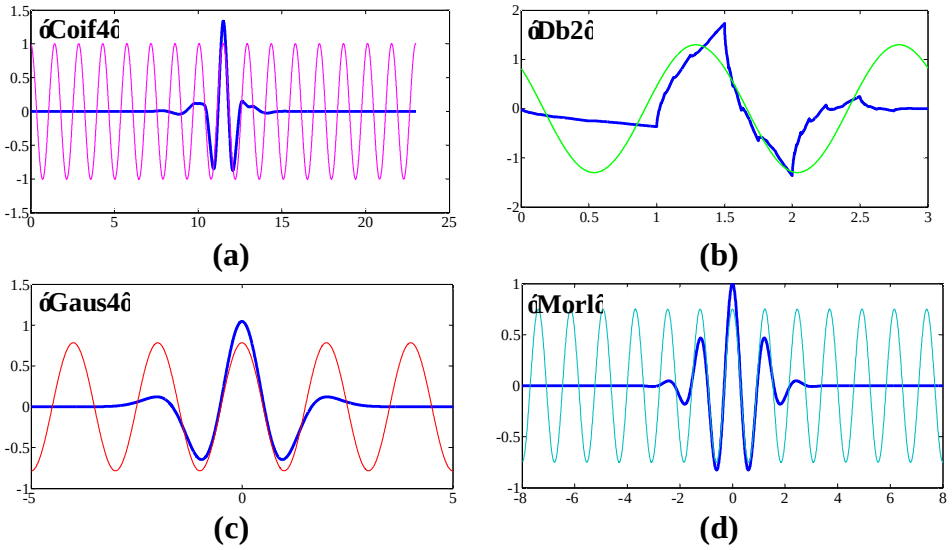

Fig. 2.5 ï Some mother wavelets plotted with the periodic signals of frequency equal to their center frequency f_c: (a) óCoif4ô, f_c = 0.6957; (b) óDb2ô, f_c = 0.6667; (c) óGaus4ô, f_c = 0.3180; (d) óMorlô, f_c = 0.8125.

Another fundamental property of wavelets is to have vanishing moments μ_α, where

$$\mu_\alpha = \int_{-\infty}^{+\infty} x^\alpha \psi(x) dx = 0 \quad \text{with} \quad \alpha = 0,1,2,\ldots,m-1 \qquad 2.5$$

and *m* depends on the mother wavelet. For instance, Daubechies and Symlet wavelets of order N have *m* = N vanishing moments; Coiflets wavelet of order N has *m* = 2N vanishing moments (Daubechies, 1992). Hence, óDb2ô and óCoif4ô have, respectively, 2 and 8 vanishing moments. óGaus4ô has 4 vanishing

moments, whilst ôMorlô has vanishing moments for even values of α (i.e. $\alpha = 0,2,4,\ldots$).

Since $\psi(x)$ is a zero mean function, a wavelet function has at least one vanishing moment, i.e.

$$\mu_0 = \int_{-\infty}^{+\infty} \psi(x)dx = 0 \,. \tag{2.6}$$

In general, the greater is the vanishing moment order, the higher is the frequency contents of the mother wavelet, and the more powerful is the related wavelet transform to process the high frequency components of a signal. As highlighted in the following, this property is fundamental in damage detection through CWT, as damage is represented by high frequencies in the signal.

2.2.3 The Continuous Wavelet Transform

This study exploits the continuous wavelet transform as basic analysis tool to deal with the problems of localization (Chapters 4-5) and characterization (Chapter 6) of damage in beam deflections.

The CWT, in the square integrable space, can be defined by the convolution of the input signal $\eta(x)$ with a wavelet function generated from the mother wavelet $\psi(x)$ by scaling and translating it:

$$W(t,s) = \int_{-\infty}^{+\infty} \eta(x) \frac{1}{\sqrt{s}} \psi^* \left(\frac{x-t}{s} \right) dx \,, \tag{2.7}$$

where ψ^* is the complex conjugate of ψ.

Considering a wavelet function $\psi(x)$ with m vanishing moments, it can be demonstrated that, for very small values of the scale s in the domain of interest, the CWT of a signal $\eta(x)$ can be related to its mth derivative, that is

$$\lim_{s \to 0} \frac{W(k,s)}{s^{m+1/2}} = K \frac{d^m \eta(x)}{dx^m} \,, \tag{2.8}$$

where K is a non-zero parameter equal to

$$K = \int_{-\infty}^{+\infty} \zeta(x)dx \tag{2.9}$$

and $\zeta(x)$ is fast decaying function satisfying

$$\psi(x) = (-1)^m \frac{d^m \zeta(x)}{dx^m} \,. \tag{2.10}$$

In the light of Eq. 2.8, it is possible for a wavelet transform to detect singularities in a signal or its derivatives by choosing an appropriate wavelet function $\psi(x)$ (Mallat & Hwang, 1992).

A remarkable property of the wavelet transform is its ability to characterize the local regularity of functions. In mathematics, the measure of the local regularity of a function in the neighbourhood of a point can be related to the local

Lipschitz exponent around that point. According to Mallat & Hwang (1992), a function $\eta(x)$ in the square integrable space presents a Lipschitz exponent $\kappa \geq 0$ at a point ν, if there exists a $\breve{K} > 0$ and a polynomial p_ν of degree $\breve{m}$ such that

$$\left|\eta(x) - p_\nu(x)\right| \leq \breve{K}\left|x - \nu\right|^{\kappa}, \ \forall x \in \mathrm{R} \qquad 2.11$$

The term κ provides the degree of singularity in the neighbourhood of the point x. If the function $\eta(x)$ presents a uniform Lipschitz condition of order κ over an interval $\left[\breve{a}, \breve{b}\right]$, then there exists a constant $\breve{A} > 0$ such that

$$\left|W(t,s)\right| \leq \breve{A} s^{\kappa+\frac{1}{2}}\left(a + \left|\frac{t-\nu}{s}\right|\right)^{\kappa}, \ \forall (t,s) \in \left[\breve{a}, \breve{b}\right] \times \mathrm{R} \qquad 2.12$$

The magnitude of the wavelet coefficients of a function around a point can be related to the local Lipschitz exponent, and hence to the pointwise degree of the function. This in turn indicates that the magnitude of a local extremum of the CWT coefficients formed at the location of damage can be a descriptor of the extent of damage present at that point (Hong et al., 2002).

Considering a beam with a crack which may introduce discontinuities or singularities in the derivatives of the deflection shape, wavelet transform is deemed to be a powerful tool to locate the damage. Due to the presence of the singularity, a transformed deflection shape yields a local variation or extremum of the wavelet coefficient at the damage location throughout the different scales, and hence it allows damage detection. As an example, in Fig. 2.6 the absolute value of the CWT coefficients of a generic noisy deflection shape sampled at dx/L = 0.001 and with crack at x/L = 0.4 is shown. The CWT is executed using ócoif4ô wavelet at the scales 24, 36 and 52 and the polynomial padding method (see Section 4.3). At each scale the wavelet coefficients allow the proper localization of the crack, as their maximum value is at the crack position.

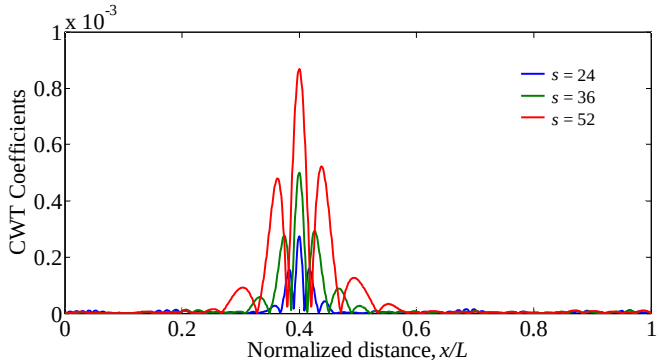

Fig. 2.6 ï Absolute value of the CWT coefficients of a generic noisy deflection shape sampled at dx/L = 0.001 and with crack at x/L = 0.4. The CWT is executed using ócoif4ô wavelet at the scales 24, 36 and 52 and the polynomial padding method.

Figure 2.7a presents the contour plot of the absolute values of the CWT (from scale 1 to scale 60) of the same cracked beam deflection analysed to obtain in Fig. 2.6. In the contour plot, the lighter colors represent high coefficient values, whilst darker colors correspond to low coefficient values (see the color bar on the right of Fig. 2.7a). Since a wavelet with more than one vanishing moment (in this case óCoif4ô) associates high coefficient values to the signal discontinuities and since high wavelet scales are able to detect a discontinuity even if the wavelet is not centered on it, the contour plot displays a pattern characterized by a central bright cone and a number of adjacent less bright cones, all pointing to the singularity location. In Fig. 2.7a the bright cones point correctly towards the crack location. Moreover, since the wavelet window at higher scales is larger and consequently bigger values of the CWT coefficients are attained, the cone color blends moving to smaller scales, respectively, from lighter to darker tones.

Figure 2.7b presents the same results in Fig. 2.7a, but as a function of the pseudo-frequencies f_a. Since f_a is inversely proportional to s, in Fig. 2.7b the contour plot of the CWT coefficients is characterized by bright cones pointing to the top.

(a)

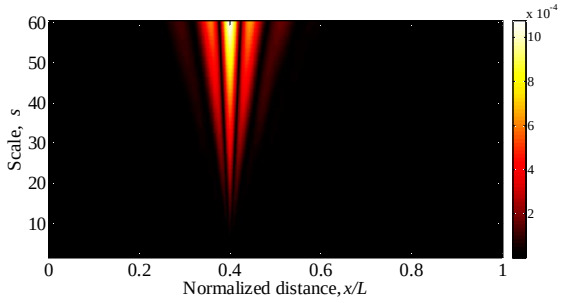

(b)

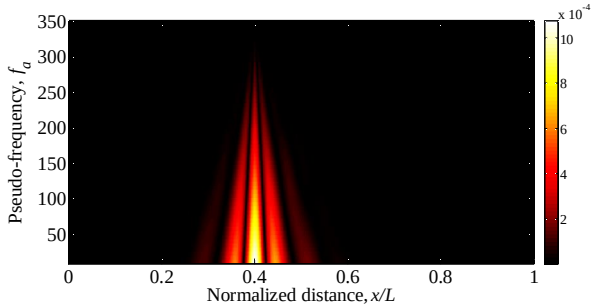

Fig. 2.7 ï Contour plots of the absolute values of the CWT (óCoif4ô is used) of the same cracked beam deflection analysed in Fig. 2.6. In (a) the contour plot is displayed as a function of the scales, while in (b) as a function of the corresponding pseudo-frequencies.

2.2.3.1 CWT implementation

A MATLAB routine to perform the CWT has been implemented to improve the accuracy of the existing built-in one. While the original routine approximates the signal roughly through a piecewise constant function, the implemented one considers a piecewise linear trend.

Assume $\boldsymbol{q}(x)$ as the discrete original signal defined in the domain $x = 0, \Delta x, 2\Delta x, \ldots, N\Delta x$, being Δx and N, respectively, the sampling interval and number of sampling points of $\boldsymbol{q}(x)$. In order to properly execute the CWT by avoiding edge effects (for more details see Chapter 4), $\boldsymbol{q}(x)$ is extended at the beginning and at the end by means of the padding functions $f_1(x)$ and $f_2(x)$. Defining the padded signal as $\overline{\eta}(x) = f_1(x) \cup \eta(x) \cup f_2(x)$ (Fig. 2.8), Eq. 2.7 can be rewritten as follows

$$W(t,s) = \int_{-\infty}^{+\infty} \overline{\eta}(x) \frac{1}{\sqrt{s}} \psi^* \left(\frac{x-t}{s} \right) dx \,. \qquad 2.13$$

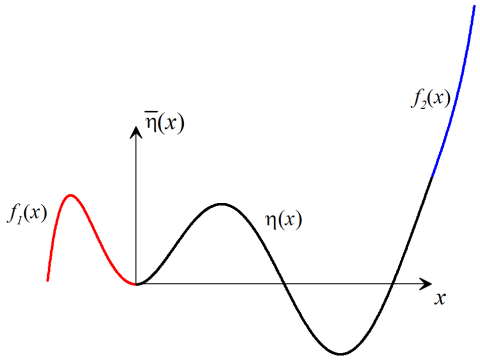

Fig. 2.8 ï Sketch of padded signal $\overline{\eta}(x)$ constituted by the original signal $\boldsymbol{q}(x)$ extended by the padding functions $f_1(x)$ and $f_2(x)$.

Considering the integer number Λ as the distance from the center of the mother wavelet to the position where the wavelet attains negligible values (e.g. for ócoif4ô $\Lambda = 11$), Eq. 2.13 may be simplified in

$$W(t,s) = \frac{1}{\sqrt{s}} \int_{-s\Lambda\Delta x+t}^{+s\Lambda\Delta x+t} \overline{\eta}(x) \psi^* \left(\frac{x-t}{s} \right) dx \,. \qquad 2.14$$

Treating $\overline{\eta}(x)$ as a piecewise linear function of values $\overline{\eta}_i$ with $i = -N_1, \ldots, -1, 0, \ldots, N-1, N, \ldots, N+N_2-1$, being $\overline{\eta}(x = -\Delta x) = \overline{\eta}_{-1}$, $\overline{\eta}(x = 0) = \overline{\eta}_0$, $\overline{\eta}(x = \Delta x) = \overline{\eta}_1$, etc., and N_1 and N_2, respectively, the number of

sampling points of $f_1(x)$ and $f_2(x)$ (note that $N_1 = N_2 \geq s\Lambda$), the integral of Eq. 2.14 can discretized as

$$W(j,s) = \frac{\Delta x}{\sqrt{s}} \sum_{i=-s\Lambda+j}^{+s\Lambda-1+j} \left[\overline{\eta}_i \int_{i-j}^{i+1-j} \psi^* \left(\frac{x'}{s} \right) dx' + \left(\overline{\eta}_{i+1} - \overline{\eta}_i \right) \int_{i-j}^{i+1-j} x' \psi^* \left(\frac{x'}{s} \right) dx' \right], \quad 2.15$$

where $j = 0,1,2,\ldots,N-1$ and the dimensionless variable x', upon which the mother wavelet is defined, is equal to $x/\Delta x$. Note that in Eq. 2.15 the index j is used as translation parameter since $t = j\,\Delta x$.

Note that, knowing the of the mother wavelet complex function ψ^* analytically (e.g. Gaussian wavelets) or pointwise through an iterative procedure (e.g. Coiflet wavelets), for each scale s the values of the two integrals in Eq. 2.15 can numerically be calculated (for example by means of composite Simpsonôs rule until convergence; Atkinson, 1989) as follows

$$Q_i(s) = \int_i^{i+1} \psi^* \left(\frac{x'}{s} \right) dx' \quad 2.16$$

and

$$U_i(s) = \int_i^{i+1} x' \psi^* \left(\frac{x'}{s} \right) dx \quad 2.17$$

with $i = -s\Lambda,\ldots,s\Lambda-1$.

Once the values of the integrals of Eq. 2.16 and Eq. 2.17 are calculated and stored for the wavelet function of interest and for every s, the CWT can easily be calculated every time with low computational cost by summation

$$W(j,s) = \frac{\Delta x}{\sqrt{s}} \sum_{i=-s\Lambda+j}^{+s\Lambda-1+j} \left[\overline{\eta}_i\, Q_{i-j}(s) + \left(\overline{\eta}_{i+1} - \overline{\eta}_i \right) U_{i-j}(s) \right]. \quad 2.18$$

Moreover, since $\gamma(x)$ is a zero mean function, for every scale s the following relation has to be satisfied

$$\sum_{i=-s\Lambda}^{+s\Lambda-1} Q_i(s) \to 0 \quad 2.19$$

To reduce as much as possible the absolute value of the summation in Eq. 2.19 a numerical trick is used in order to perform accurately the CWT. Assuming $\overline{Q}_s = \sum_{i=-s\Lambda}^{+s\Lambda-1} Q_i(s)$ and considering, if $\overline{Q}_s < 0$, $\overline{Q}_s = \left| \overline{Q}_s \right|$, in case of symmetric wavelets (for example óMorlô and óGaus4ô) it can be imposed that

$$Q_{-1}(s) = Q_{-1}(s) - \overline{Q}_s / 2 \quad \text{and} \quad Q_0(s) = Q_0(s) - \overline{Q}_s / 2, \quad 2.20$$

On the other hand, for non symmetric wavelet functions (for example óCoif4ô or óDb2ô) it can be imposed that

$$Q_0(s) = Q_0(s) - \overline{Q}_s. \quad 2.21$$

2.3 Wavelet-based Damage Identification Methods

Among the modern vibration-based damage identification methods (Yan et al., 2007), thanks to its ability to process non-stationary signals, wavelet analysis is well known to be a strong technique. Hereafter an in depth review of the state of the art of wavelet-based damage identification methods in time and in space domains is presented.

2.3.1 Wavelet-based damage identification methods in time domain

In processing time histories of structural response data, wavelet analysis is widely recognised to be an efficacious tool to identify the sudden or gradual system stiffness degradation and to localize temporally and spatially the damage occurrence. The work of Surace and Ruotolo (1994) is one of the first study in which wavelet analysis is applied in detecting damage in beam structures. The authors consider a FE model to simulate the dynamic response of a cantilever with a single crack subjected to sinusoidal or impulsive loadings. The crack opening-closing behaviour is taken into account, yielding a nonlinear beam response. By analysing through CWT the time-history of the displacement at the free-end, the presence of the crack and the variation of the dynamic behaviour which occurs when the crack changes state are identified.

Hou et al. (2000) present a wavelet-based approach for SHM on a simple structural model with breakage springs and on actual recorded data of the building response during an earthquake event. They show that the time instant of the damage occurrence or of the change in system stiffness is detected by spikes in the details of the discrete wavelet transform decomposition of the response data. Melhem and Kim (2003) analysis the response of two full-scale concrete structures, a pavement slab on foundation and a simply supported prestressed beam. The effectiveness of using wavelet transform as a tool for damage detection and health monitoring over traditional Fourier transform is highlighted both in identifying the frequency components which exist in the signal and in detecting the variation between the initial and damaged states. In order to identify the time more sharply and effectively at which structural damage occurs than by using the wavelet transform method alone, Li et al. (2007), firstly adopt the EMD technique to decompose the response signal of structure vibration into several mono-component signals (IMFs) and then, via wavelet transform, they detect the exact time location and severity of damage. The numerical simulation and the analysis of the response signal data from a shear building show the accuracy of the method.

In the work of Hera and Hou (2004) the discrete wavelet analysis is applied to process the simulated acceleration response data at some representative points

of a four-story building when one or more sudden damages occur. Depending on the noise level and the damage severity, the spikes of the wavelet details and their distribution in the structure are used to detect the instant of damage occurrence and the damage location. Moreover, the authors highlight that the analysis of acceleration response data is more efficacious than that of displacement data and that this online SHM method is in general not suitable for cumulative damages over relatively long period such as those caused by fatigue and corrosion.

Basu et al. (2008) propose a technique based on wavelet analysis for online identification of variation of stiffness in structural systems. Using the modified Littlewoodï Paley wavelet (Basu & Gupta, 1998), characterized by non-overlapping frequency bands for different scale parameter values, the online variation in natural frequency of a SDOF system and in natural frequencies and mode shapes of a MDOF system, arising out of change in stiffness, is tracked accurately. The method is versatile as it has the ability to detect abrupt changes over a short time scale (due to a sudden event/failure) in addition to track changes due to long-term phenomena.

Sun and Chang (2004) propose a SHM method based on the Wavelet Packet Transform (WPT) technique and the statistical process control concept. First the recorded acceleration time-histories of the structural response are decomposed into wavelet packet components, then only dominant wavelet packet components of dominant energy are retained and two damage indicators, quantifying the change of these components (without the requirement of baseline data), are calculated. To monitor the change of these damage indicators, control charts are constructed based on the statistical properties of the damage indicators. Experimental tests demonstrate the effectiveness of both the two damage indicators for monitoring structural health condition, since they are sensitive to damage and yet insensitive to measurement noise. Han et al. (2005) propose a WPT-based energy rate index for identification of structural damage location. Although the proposed methodology shows great potential in simulated and laboratory tested beams, its application has two important limitations: a reliable reference structural model for undamaged conditions is required and the algorithm can detect damage only when a sensor is placed at a damaged location. A wavelet entropy-based structural damage identification method is presented and demonstrated by Ren and Sun (2008). Wavelet entropy, relative wavelet entropy and wavelet-time entropy are investigated and compared in terms of numerically simulated results and laboratory test results. Wavelet-time entropy is found to be powerful in detecting abnormal features in vibration signals collected from an on-line structural health monitoring system. Relative wavelet entropy, instead, is a sensitive damage feature to locate damage, with the advantage that if the undamaged location of the structure is known and simultaneously measured, an additional intact structure is not required.

Finally, as witnessed by the review paper of Peng and Chu (2004) and by the works of Kim and Melhem (2004) and Peng et al. (2007), wavelet analysis is a strong technique even in machine condition monitoring and fault diagnostics, due to its abilities in fault feature extraction, singularity detection, denoising and compression of vibration signals and system identification.

2.3.2 Wavelet-based damage identification methods in space domain

Liew and Wang (1998) and Wang and Deng (1999) use for the first time wavelet transform to analyse numerical and experimental, static and dynamic, space domain structural responses of simple cracked beams, and to identify damage. They highlight that WA is capable of identifying the abrupt variation in beam deflection due to damage through a local abnormality of the wavelet coefficients at that position. Subsequently many authors studied and showed the effectiveness and versatility of wavelet analysis as tool to detect, localize and quantify damage in generic structural deflections. Hereafter some of the most interesting works in terms of methodology, results and applications are presented.

Focusing on the Gaussian wavelets, Gentile and Messina (2003) discuss in a numerical-theoretical way the CWT features of derivation, convolution and smoothing of noisy data. Due to CWT limitation in the presence of noise (in fact CWT behaves as a high-pass filter at the fine scales and looses details at the large scales), they highlight the need of a trade-off for the scales in detecting damage. Moreover, due to CWT redundancy regarding the free choice of scales, the authors recommend the use of continuous WT rather than discrete WT. By analysing different cracked beam modeshapes, the authors notice that the sensitivity in damage detection with respect to crack location depends on the modeshape local curvature in the damaged area. Furthermore, Messina (2004), dealing with transversal beam vibrations in both the non-transformed and Fourier transformed domains, discuss the ability of CWT in conjunction with differential operators to act as frequency filter and therefore to reduce undesired high frequency noise.

Loutridis et al. (2004) analyse through CWT both the analytical and the experimental fundamental vibration mode of a double-cracked cantilever beam by using the 4th order Symlet wavelet. In addition to the task of locating the crack positions, they propose an intensity factor as indicator of crack size. Through a numerical and an experimental study, Wang and Wu (2011) detect the location of a delamination in a beam structure under static loading with a spatial wavelet transform using Gabor wavelet. A barely invisible perturbation in the deflection profile of the delaminated beam at the two delamination edges owing to the curvature discontinuity is discerned through the WA.

Pakrashi et al. (2007) present a detailed numerical and experimental study regarding the issue of efficient and robust calibration of position and extent of

damage in structures. It is observed that wavelet analysis on the mode or the static deflected shape of a structure can successfully identify the presence and the location of the damage even at significant noise levels using the 4th order Coiflet wavelet. Partial windowing of the deflected shapes and consequent wavelet analysis of the segments is found to improve the localization. As far as the damage quantification is concerned, while a wavelet based calibration of damage is found to be inconsistent and unstable due to noise, the authors propose a wavelet-kurtosis based calibration technique which is more robust and consistent. Montanari et al. (2013) consider a FE model of a cracked fiber-reinforced beam in order to analyse its static deflection. The fiber effect in the crack opening response is taken into account through a bridged crack model. Damage detection and calibration are studied in the presence of synthetic noise by varying the crack depth and the fiber yielding condition. When a large proportion of the fibers have yielded, even with constant crack depth, the damage location becomes easier through wavelet analysis. The kurtosis and wavelet-kurtosis techniques for damage severity calibration, exposed in (Pakrashi et al., 2007), are compared. While the kurtosis index seems to well describe damage severity when most of the fibers are yielded, the wavelet-kurtosis technique is seen to be insensitive to damage severity both when few fibers have yielded and when most of them have yielded. Again Pakrashi et al. (2009) statistically deal with the identification of the existence, location, and extent of an open crack from the first fundamental modeshape of a simply supported beam by using CWT with the 4th order Coiflet wavelet. The problem of false alarm and its significant reduction by the use of multiple measurements are illustrated.

Rucka and Wilde (2006b) analyse numerically and experimentally the first modeshape of a plexiglass cracked cantilever by the one-dimensional CWT and the first modeshape of a clamped steel plate with a central defect by the two-dimensional CWT. The 4th order Gaussian wavelet and the reverse biorthogonal 5.5 wavelet, having both four vanishing moments, are used to analyse the beam and the plate, respectively. The problem of damage detection in plates is tackle also by Huang et al. (2009) which develop a 2D CWT algorithm for SHM. The feasible and accuracy of the method in locating the damage positions and in qualitatively assessing the damage severity for both dense and sparse sensor networks is numerically demonstrated.

Zhong and Oyadiji (2011a) compare Stationary Wavelet Transform (SWT) and the Discrete Wavelet Transform (DWT) as tools for small crack detection in beam-like structures. The first four mode shapes of damaged simply supported beams, obtained numerically and experimentally, are analysed. Although crack information can be obtained from the detail coefficients of the SWT or of the DWT of mode shapes, due to the fact that DWT is a down-sampling algorithm whereas SWT is an up-sampling one, the SWT provides better crack identification than DWT, especially when the crack is relatively small and noise

is relevant. Cao and Qiao (2008) propose and validate numerically and experimentally, under relatively high noise environment, a novel methodology, so-called Integrated Wavelet Transform (IWT), for damage detection in structural vibration mode shapes. The IWT algorithm has the merit of integrating the SWT, to extract pure damage information by eliminating random noise and regular interferences, and the CWT to reveal abnormality from the extracted damage. Moreover, a guideline for rationally choosing the optimal mother wavelet for effective damage identification is provided. Reverse biorthogonal 2.2 wavelet is chosen as the optimal mother wavelet for both the wavelet transforms. Gökdaĵ and Kopmaz (2009) develop a new wavelet-based damage detection approach based on the assumption that a damaged mode shape of a beam is approximately composed of an undamaged mode and other contributors such as variations induced by measurement and local damage. Through DWT, assuming a suitable wavelet function and decomposition level, a proper approximation function to be used as undamaged mode is extracted from the damaged one. In this way, a reliable damage index is defined taking the difference of the CWT coefficients of the damaged mode and those of the approximation function. The method is tested and validate numerically and experimentally.

Rucka (2011) investigates both experimentally and numerically the behavior of the CWT damage detection technique in analyzing the first eight mode shapes of a cantilever beam with damage in the form of notch of depth 20%, 10% and 5% of the beam height. The analysis is performed using the Gaussian wavelets of 4th, 6th and 8th order, having respectively 4, 6 and 8 vanishing moments. The experimental results highlight that damage detection by the wavelet analysis is more effective on higher measured mode shapes and using wavelets with smaller numbers of vanishing moments. Since higher modes contain more regions in which the curvature is null and consequently there is less sensitivity to damage, a reliable damage localization needs at least two modes. In the work of Gianniccaro et al. (2009), based on Gaussian continuous wavelet transforms which behave as differentiator filters with easily controlled lowpass cutting frequencies, a new global index, aimed at identifying damaged places through wavelet analysis of dynamical shapes, is introduced. The appeal of the new damage index is to overcome the need of the undamaged condition of the structure and to bring in an unique formulation the information related to several dynamical shapes. In this way the method makes the analyst free from choosing a specific mode, thus allowing a straightforward multimodal analysis. Moreover, the global index also provides the possibility of reducing the long wave signals which, to a certain extent, can hide damaged places.

Umesha et al. (2009) present a method for crack detection and quantification in beams based on Symlet wavelet analysis. The static deflection is measured at a particular point for various locations of a point load along the beam. This deflection profile is used as the input signal for wavelet analysis. Due to variation

in deflection at some points, compared to their adjacent points, peaks in the wavelet coefficients are observed. Since these peak points can be related to damage, sensor points or supports, to locate the real damage position, the false indicators of damage are eliminated by performing wavelet analysis of the deflection profile measured at another point. A generalized curve, considering the variations of damage size and location, intensity of load, flexural rigidity and beam length, is proposed to quantify the damage.

Chapter 3

Damage modelling

3.1 Introduction

In the present thesis numerical and analytical models of damaged beam-structures are developed to perform damage identification through wavelet analysis. More specifically, the damage identification is related to the identification of discontinuities due to damage in the beam deflection. Two different beam types with constant cross-section are considered: a linear type constituted by a homogeneous isotropic elastic material and a nonlinear one constituted by Fiber-Reinforced (FR) composite material. In the beams a through-thickness edge crack of Mode I (ó*opening mode*ô) is present: the linear beam has an open edge crack, while the nonlinear beam presents a breathing crack bridged by fiber reinforcements. In the following, sectional crack models and the analytical and numerical beam models are presented.

3.2 Sectional crack models

3.2.1 Open crack model

In presence of cracked linear elastic, Linear Elastic Fracture Mechanics (LEFM) theory (e.g. Broek, 1986) allows the quantification of the effects of the cracks (e.g. in terms of Stress Intensity Factor (SIF), local stiffness, displacements, etc.), depending on the geometry and loading configuration, through analytical or numerical solutions (Tada et al., 2000).

In this work, a homogeneous isotropic linear elastic beam contains a through-thickness open edge crack of Mode I (Fig. 3.1a). The cracked beam element is modelled by connecting the two uncracked beam portions through a rotational spring which represents the local stiffness k_c of the cracked cross-section of the beam (Fig. 3.1b). Considering a rectangular cross-section of height h and width b

(*a* the crack depth and *E* Youngôs modulus of the material), according to the LEFM concepts, the local stiffness k_c can be evaluated through the following polynomial expression (Tada et al., 2000):

$$k_c = \frac{bh^2E}{24\left(\delta/(1-\delta)\right)^2(5.93-19.69\delta+37.14\delta^2-35.84\delta^3+13.12\delta^4)}, \qquad 3.1$$

where $\delta = a/h$ is the relative crack depth.

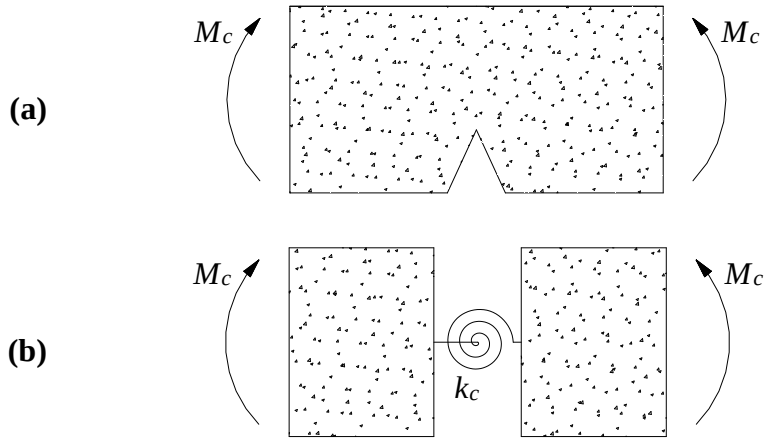

Fig. 3.1 ï (a) Beam element with a through-thickness open edge crack; (b) corresponding model where the rotational spring represents the bending behaviour due to the crack.

3.2.2 Breathing bridged crack model

A nonlinear mechanical model is adopted to describe the behaviour of an edge crack in a beam portion constituted by a fiber reinforced material. In fact, fibrous composites in general are characterized by a bridging or reinforcing action exerted by the fibers. This action affects the global structural response of the composite material mainly in the post-cracking phase, enhancing mechanical properties, such as strength, stiffness, toughness, ductility and fatigue strength. Two fracture mechanics-based approaches are commonly used for modeling the behavior of cracked fibrous composites: the *bridged crack* model and the *cohesive crack* model (Carpinteri Al. & Massabò, 1996). Here the sectional bridged crack model proposed in (Carpinteri An. et al., 2004; Spagnoli et al., 2014) is adopted.

Conversely to the linear assumption of the model of Section 3.2.1, where the crack is fully open, in general, cracks open and close during vibrations and, consequently, it exhibits a nonlinear behaviour because of the variation in the

rotational stiffness. Are Carlson (1974) and Gudmunston (1983), among the firsts, who study experimentally and numerically the effects of closing cracks on the dynamical characteristics. Later on, several researchers propose models of beam with one or more breathing cracks in order to take properly into account the nonlinear behavior and to allow vibration-based identification methods to correctly detect the features of the damaged system (e.g. sub- and super-harmonics in the forced dynamic response of the beam; Andreaus & Baragatti, 2012).

The most simple model of a breathing crack is a bilinear one wherein the crack opens or closes instantaneously, i.e. it is either completely open or completely closed (e.g. Zastrau, 1985; Qian et al., 1990; Friswell & Penny, 1992; Ruotolo et al., 1996). However, as demonstrated experimentally (e.g. Clark et al., 1987), the transition from closed to open crack and *vice versa* happens in a smooth way. Accordingly Krawczuk and Ostachowicz (1994), Abraham and Brandon (1995), Cheng et al. (1999), Pugno et al. (2000), Kisa and Brandon (2000) develop breathing crack models which consider the varying stiffness of the crack in its partially open and closed situations.

In the present thesis the smooth opening-closure behaviour of the crack is considered into the bridged crack model by imposing that the relative crack rotation and the crack opening displacements at the fiber levels cannot be negative so as, when either the rotation or all the displacements are null, the beam section is assumed to be intact.

Consider the through-thickness edge crack in the fiber-reinforced composite beam element with a rectangular cross-section. The crack is located in the tensile part of the element and is subjected to Mode I loading due to the cross-section bending moment $M_c(t)$, in equilibrium with the applied forces, and to the fiber bridging forces (Fig. 3.2). Note that the time t represents the ordering variable of the events in a static problem.

Unidirectional fibers are discretely distributed across the crack and oriented parallel to the longitudinal axis of the element. The position of the i-th fiber $(i = 1,\ldots,n)$ is described by the distance c_i with respect to the bottom of the beam cross-section. Further, the relative crack depth $\delta = a/h$ and the normalized coordinate $\zeta_i = c_i/h$ are defined (Fig. 3.2).

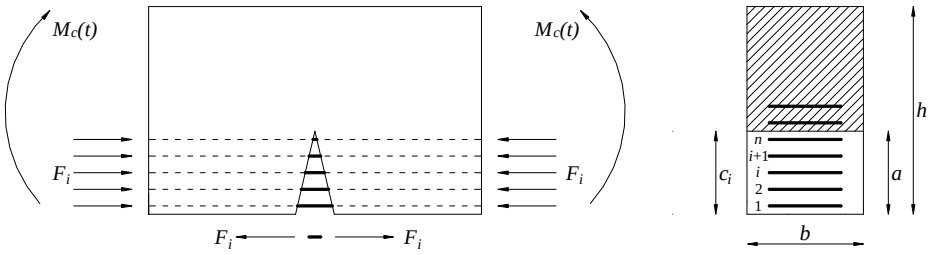

Fig. 3.2 - Schematic of the bridged crack model.

The matrix of the beam is assumed to present a linear elastic behaviour, whereas the fibers act as rigid-perfectly plastic bridging elements which connect together the two surfaces of the crack. Hence, the plastic bridging law for the generic *i*-th fiber is characterized by an ultimate force $F_{P,i}$ (and $-F_{P,i}$ in compression). Note that during the general loading process, brittle catastrophic fracture or compressive crushing of the matrix are disregarded. Further, no edge crack is assumed to develop in the upper part of the beam. Similarly, fatigue propagation of the initial crack due to loading is also beyond the scope of the present investigation.

The successive cross-sectional configurations during the loading process must satisfy equilibrium and compatibility conditions (Carpinteri An. et al., 2004). Since the problem being examined is statically indeterminate, the unknown fiber reactions F_i, positive if the fiber is under tensile loading, on the matrix can be deduced from *n* kinematic conditions related to the crack opening displacements u_i at the different fiber levels. If $|F_i|$ is equal to $F_{P,i}$, the force of the *i*-th fiber becomes known, and the crack opening displacements are hereafter shown to depend on such a value. Since the matrix is assumed to behave in a linear elastic manner, the crack opening displacement u_i at the *i*-th fiber level is computed through the superposition principle (Einsteinôs summation rule for repeated indices holds):

$$u_i = \lambda_{iM} M_c - \lambda_{ij} F_j \quad \text{with} \quad i = 1,...,n, \tag{3.2}$$

where λ_{iM} and λ_{ij} are the crack opening compliances induced by the bending moment and the crack bridging forces, respectively. Equation 3.2 can be written in matrix form as follows:

$$\mathbf{u} = \boldsymbol{\lambda}_{\mathbf{M}} M_c + \boldsymbol{\lambda} \mathbf{F}, \tag{3.3}$$

where $\mathbf{u} = \{u_1,...,u_n\}^T$ is the vector of the crack opening displacements at the different fiber levels, and $\mathbf{F} = \{F_1,...,F_n\}^T$ is the vector of the crack bridging forces. Further, $\boldsymbol{\lambda}_{\mathbf{M}} = \{\lambda_{1M},...,w_{nM}\}^T$ is the vector of the compliances related to the bending moment M_c, whereas $\boldsymbol{\lambda}$ is a symmetric square matrix of order *n*,

whose generic element *ij* represents the compliance λ_{ij} related to the *i*-th crack opening displacement and the *j*-th fiber force.

The relative rotation $\Delta\vartheta_c$ due to the crack only (i.e. excluding the elastic deformation of the matrix) of the two extreme cross-sections of the beam portion in Fig. 3.2 is given by:

$$\Delta\vartheta_c = \lambda_{MM}\, M_c - \boldsymbol{\lambda}_{\mathbf{M}}^T \mathbf{F}\,, \tag{3.4}$$

where λ_{MM} is the rotational compliance due to the bending moment.

Within the framework of LEFM, the compliances can be determined from energy balance considerations as follows (Carpinteri Al. & Massabò, 1997):

$$\begin{aligned}
&\lambda_{iM} = \frac{2}{hbE_m}\int_{\zeta_i}^{\delta} Y_M(\delta')Y_F(\delta',\zeta_i)d\delta'\,,\quad \lambda_{MM} = \frac{2}{h^2 bE_m}\int_0^{\delta} Y_M^2(\delta')d\delta'\,,\\
&\lambda_{ij} = \lambda_{ji} = \frac{2}{bE_m}\int_{\max\{\zeta_i,\zeta_j\}}^{\delta} Y_F(\delta',\zeta_i)Y_F(\delta',\zeta_j)d\delta'\,,
\end{aligned} \tag{3.5}$$

where E_m is the Young modulus of the matrix.

The dimensionless functions Y_M and Y_F are based on the analytical expressions of the SIFs for, respectively, bending moment and point load acting on the crack surfaces (Tada et al., 2000):

$$\begin{aligned}
Y_M(\delta) &= \begin{cases} 6(1.99\delta^{0.5} - 2.47\delta^{1.5} + 12.97\delta^{2.5} - 23.17\delta^{3.5} + 24.8\delta^{4.5}) & \delta \le 0.6 \\ \dfrac{3.99}{(1-\delta)^{1.5}} & \delta > 0.6 \end{cases}\\
Y_F(\delta,\zeta_i) &= \frac{2}{\sqrt{\pi\delta}}\frac{1}{(1-\delta)^{1.5}\sqrt{1-\left(\dfrac{\zeta_i}{\delta}\right)^2}}Q(\delta,\zeta_i) \qquad \text{for} \quad \delta \ge \zeta_i\,,
\end{aligned} \tag{3.6}$$

where

$$\begin{aligned}
Q(\delta,\zeta_i) &= q_1(\delta) + q_2(\delta)\frac{\zeta_i}{\delta} + q_3(\delta)\left(\frac{\zeta_i}{\delta}\right)^2 + q_4(\delta)\left(\frac{\zeta_i}{\delta}\right)^3\\
q_1(\delta) &= 0.46 + 3.06\delta + 0.84(1-\delta)^5 + 0.66\delta^2(1-\delta)^2\\
q_2(\delta) &= -3.52\delta^2\\
q_3(\delta) &= 6.17 - 28.22\delta + 34.54\delta^2 - 14.39\delta^3 - (1-\delta)^{1.5} - 5.88(1-\delta)^5 +\\
&\quad - 2.64\delta^2(1-\delta)^2\\
q_4(\delta) &= -6.63 + 25.16\delta - 31.04\delta^2 + 14.41\delta^3 + 2(1-\delta)^{1.5} + 5.04(1-\delta)^5 +\\
&\quad + 1.98\delta^2(1-\delta)^2.
\end{aligned} \tag{3.7}$$

The unknown crack bridging forces $\mathbf{F}$ can be determined from compatibility conditions. In other words, because of the rigid-plastic crack bridging law for the fibers, compatibility requires that

$$\mathbf{u} = \mathbf{A}\,, \tag{3.8}$$

where the vector $\mathbf{A}$ contains the (plastic) crack opening displacements. Since the vector $\mathbf{A}$ is a function of the load history, no one-to-one relationship can be constructed between the load and the opening displacements. Therefore, Eq. 3.8 must be solved according to an incremental procedure of the complete loading process which accounts for the loading-unloading alternative corresponding to elastic-to-plastic transitions and to plastic-to-elastic returns. The governing Eq. 3.2 can be solved in the following incremental form:

$$\dot{u}_i = \lambda_{iM}\,\dot{M}_c - \lambda_{ij}\,\dot{F}_j \quad \text{with} \quad i = 1,...,n\,, \tag{3.9}$$

where dot symbol indicates time derivatives, being time the ordering variable, and $F_i = \int \dot{F}_i\,dt$ and $u_i = \int \dot{u}_i\,dt$. If the general *i*-th fiber is in the elastic domain, the corresponding increment $\dot{u}_i$ of crack opening displacement is null, namely if $|F_i| < F_{P,i} \Rightarrow \dot{u}_i = 0$. On the other hand, if the general *i*-th fiber is yielded, i.e. $|F_i| = F_{P,i}$, the following two alternatives are possible: $\dot{F}_i = 0 \Rightarrow F_i\,\dot{u}_i > 0$ or $F_i\,\dot{F}_i < 0 \Rightarrow \dot{u}_i = 0$ (plastic-to-elastic return). In other words, we have:

$$F_i\,\dot{u}_i > 0 \ \text{ if } |F_i| = F_{P,i} \text{ and } \dot{F}_i = 0\,; \qquad \dot{u}_i = 0 \ \text{ otherwise.} \tag{3.10}$$

Instead of time derivatives of crack opening displacements and fiber forces, one could use $\mathrm{d}u_i$ and $\mathrm{d}F_i$, i.e. their incremental values, and the above incremental procedure could be implemented using finite length holonomic steps.

Once the incremental crack bridging forces are evaluated, the incremental relative rotation $\Delta\dot{\vartheta}_c$ of the cracked section is given by:

$$\Delta\dot{\vartheta}_c = \lambda_{MM}\,\dot{M}_c - \lambda_{iM}\,\dot{F}_i\,. \tag{3.11}$$

Moreover, since during dynamic vibrations the crack opens and closes, as previously explained, the breathing bridged crack model assumes no material compenetration along the crack surfaces and consequently $u_i \geq 0$ and $\Delta\vartheta_c \geq 0$ is imposed. When the crack is closing and the crack surfaces at the *i*-th fiber level touch each other ($u_i = 0$), the force F_i is not any more related to the rigid-perfectly plastic *i*-th fiber but to a pointwise contact of the linear-elastic matrix along the crack surface. Therefore, the solution of the Eq. 3.9 is obtained assuming that, at every *i*-th fiber level where $u_i = 0$, $F_i = \int \dot{F}_i\,dt$ can be inferior than $-F_{P,i}$.When, the closed crack stars opening again, Eq. 3.9 is solved considering the rigid-perfectly plastic law of the fibers where for every *i*-th fiber with $u_i = 0$, $F_i = \int \dot{F}_i\,dt$ is evaluated assuming that at the beginning of its crack opening time step $F_i = -F_{P,i}$.

3.3 Cracked beam models

The open crack model and the breathing bridged crack model are included, respectively, in a cracked Euler-Bernoulli beam model and in a FE beam model to simulated damage identification under static and dynamic responses.

3.3.1 Analytical linear cracked beam model

3.3.1.1 Static equilibrium

The static equilibrium equation of a beam portion, neglecting shear deformation, is given by:

$$\frac{d^2\eta(x)}{dx^2} = \frac{M(x)}{EI}, \qquad 3.12$$

where x represents the longitudinal x-axis of beam, $\eta(x)$ the transversal deflection of the beam, $M(x)$ the bending moment along the beam and I the inertia moment of the beam cross-section.

Consider that V cracks of rotational stiffness k_{cv} are present in the beam, located at x_{cv}, where $v = 1,2,\ldots,V$, and other Z sources of deflection discontinuities (e.g. internal constrains or point load) are positioned along the beam length. Therefore, $J\ (=V+Z)$ total sources of deflection discontinuity are present along the beam length. The counting parameter j is used to number the beam elements ($j = 1,2,\ldots,V+Z+1$).

By integrating Eq. 3.12 twice, the static deflection η_r of the generic j-th element of the beam is as follows:

$$\eta_j(x) = \int_{x_{j-1}}^{x}\int_{x_{j-1}}^{x} M(x)/EI\ d^2x + C_{1j}x + C_{2j} \qquad x_{j-1} \le x < x_j \qquad 3.13$$

where $C_{(.)}$ terms are the integration constants and x_{j-1} and x_j are, respectively, the initial and final points of the j-th beam element. Note that if $j=1$, $x_{j-1}=0$ and if $j=V+Z+1$, $x_j = L$, where L is the total length of the beam.

By imposing the boundary conditions for every j-th element of the beam (e.g. due to constrains, crack presence, external force, etc.), $\eta(x)$ of the whole beam is analytically evaluated.

Considering the open crack model (Section 3.2.1), the boundary conditions due the v-th crack located at $x = x_{cv}$ are related to the following condition of continuity of displacement

$$\eta_j(x_{cv}) = \eta_{j+1}(x_{cv})\,. \qquad 3.14$$

The rotational spring of stiffness k_{cv} at the cracked section introduces a discontinuity of the rotation, which can be written as:

$$\eta'_{j+1}(x_{cv}) - \eta'_j(x_{cv}) = \frac{EI}{k_{cv}} \eta''_{j+1}(x_{cv}) . \qquad 3.15$$

In the case of the other Z sources of deflection discontinuity, kinematic boundary conditions related to the relative transversal displacements and rotations are to be imposed.

3.3.1.2 Dynamic equilibrium

The flexural free vibration response of a beam can be written as:

$$EI \frac{\partial^4 y(x,t)}{\partial x^4} + \rho A \frac{\partial^2 y(x,t)}{\partial t^2} = 0 , \qquad 3.16$$

where $y(x, t)$ is the transversal displacement of the beam from its static equilibrium position at the position x and at the time t, and ρ and A are, respectively, the material density and the cross-sectional area.

Consider that V cracks of rotational stiffness k_{cv} are present in the beam, located at x_{cv}, where $v = 1, 2, \ldots, V$, and Z internal constrains are positioned along the beam length. The counting parameter j is used to number the beam elements ($j = 1, 2, \ldots, V + Z + 1$).

By separating the variables in Eq. 3.16 as $y(x,t) = \eta(x) g(t)$ and solving the differential equation function of x, the modeshapes η_j of the j-th element of the beam become:

$$\eta_j(x) = C_{1j} \sin(\alpha x) + C_{2j} \cos(\alpha x) + C_{3j} \sinh(\alpha x) + C_{4j} \cosh(\alpha x) \qquad 3.17$$

with $x_{j-1} \le x < x_j$,

where $\alpha = \left(\frac{\rho A \omega^2}{EI} \right)^{1/4}$, ω is the natural frequency of the cracked beam. Note that if $j = 1$, $x_{j-1} = 0$ and if $j = V + Z + 1$, $x_j = L$, where L is the total length of the beam.

The $C_{(.)}$ terms are the integration constants arising from the solution of a fourth order differential equation in space. A system of $4(V + Z + 1)$ linear equations is formed by imposing the static and kinematic boundary conditions along each element of the beam. The kinematic boundary conditions due the v-th crack located at $x = x_{cv}$ are expressed by Eq. 3.14, while the static ones are

$$\eta''_j(x_{cv}) = \eta''_{j+1}(x_{cv}) , \quad \eta'''_j(x_{cv}) = \eta'''_{j+1}(x_{cv}) . \qquad 3.18$$

The modeshapes and, hence, the natural frequencies of the cracked beam are found by setting the determinant of the coefficient matrix of the linear system to zero, and solving it numerically for the roots of ω. The coefficient C_{1L} is imposed to be equal to unity.

3.3.1.3 The case of cantilever and simply-supported beams

The vibration-based damage identification by wavelet analysis presented in Chapters 4 and 5 is carried out by applying the analytical cracked beam model to the case of cantilever and simply supported beams with a single open edge crack. Free vibration and static deflection responses are evaluated for both the beam types (Fig. 3.3).

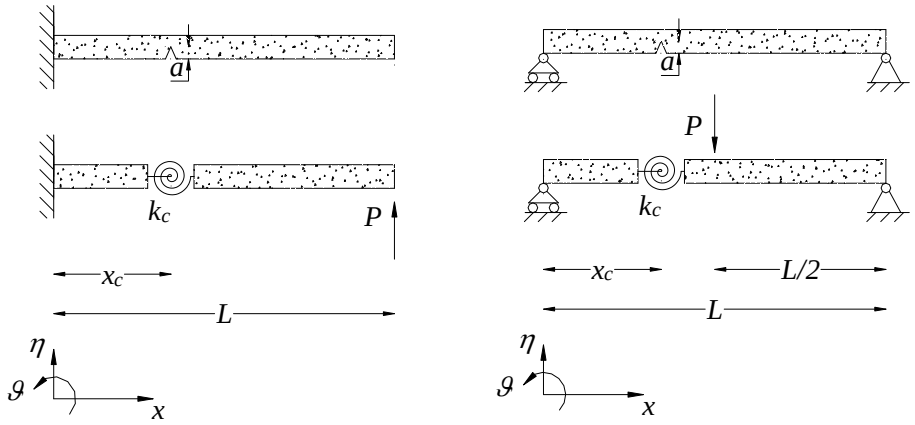

Fig. 3.3 - Cracked cantilever and simply-supported beam models.

To obtain the solutions of the problem of Eq. 3.13 for the cantilever and the simply supported beam, the boundary conditions due to the crack (Eqs 3.14 and 3.15) and to the constraints are imposed.

For the cantilever beam, since the bending moment $M(x)$ along the beam due to the force P is $M(x) = P(L - x)$, the boundary conditions are:

$$\eta_1(0) = 0 \quad \text{and} \quad \eta_1'(0) = 0, \tag{3.19}$$

$$\eta_1(x_c) = \eta_2(x_c) \quad \text{and} \quad \eta_2'(x_c) - \eta_1'(x_c) = P(L - x_c)/k_c, \tag{3.20}$$

where $\eta_1(x)$ is related to the beam portion of $0 \le x < x_c$, while $\eta_2(x)$ that of $x_c \le x \le L$. The resulting static deflection of the cantilever is given by:

$$\eta_1(x) = \frac{P}{2EI}\left(Lx^2 - \frac{x^3}{3}\right) \quad 0 \le x < x_c \tag{3.21}$$

and

$$\eta_2(x) = \frac{P}{2EI}\left(Lx^2 - \frac{x^3}{3}\right) + \frac{P(L - x_c)}{k_c}(x - x_c) \quad x_c \le x \le L. \tag{3.22}$$

The bending moment $M(x)$ acting on the simply supported beam is $M(x) = Px/2$ of $0 \le x < L/2$ and $M(x) = P(L-x)/2$ of $L/2 \le x \le L$ and the boundary conditions are:

$$\eta_1(0) = 0, \quad \eta_3(L) = 0, \tag{3.23}$$

$$\eta_1(x_c) = \eta_2(x_c), \quad \eta_2'(x_c) - \eta_1'(x_c) = Px_c/(2k_c), \tag{3.24}$$

$$\eta_2(L/2) = \eta_3(L/2) \quad \text{and} \quad \eta_2'(L/2) = \eta_3'(L/2), \tag{3.25}$$

where $\eta_1(x)$ represents the beam portion of $0 \le x < x_c$ (assuming $x_c < L/2$), $\eta_2(x)$ that of $x_c \le x < L/2$ and $\eta_3(x)$ that of $L/2 \le x \le L$. The resulting static deflection of the simply supported beam is given by:

$$\eta_1(x) = \frac{Px}{4EI}\left(\frac{x^2}{3} - \frac{L^2}{4}\right) + \frac{Px_c}{2k_c}\left(\frac{x_c}{L} - 1\right)x, \quad 0 \le x < x_c \tag{3.26}$$

$$\eta_2(x) = \frac{Px}{4EI}\left(\frac{x^2}{3} - \frac{L^2}{4}\right) + \frac{Px_c^2}{2k_c}\left(\frac{x}{L} - 1\right), \quad x_c \le x < L/2 \tag{3.27}$$

and

$$\eta_3(x) = \frac{P}{4EI}\left(-\frac{x^3}{3} + Lx^2 - \frac{L^2x}{4} + \frac{L^3}{12}\right) + \frac{Px_c^2}{2k_c}\left(\frac{x}{L} - 1\right) \quad L/2 \le x \le L. \tag{3.28}$$

In the case of the free vibration response, the boundary conditions due to the crack (Eqs 3.14, 3.15 and 3.18) and to the end constraints, have to be imposed to Eq. 3.17 so as to evaluate numerically the roots of $\breve{\boldsymbol{U}}$ (i.e. the modeshapes and, hence, the natural frequencies). For the cantilever beam the boundary conditions at the clamped end and at the free end are, respectively:

$$\eta_1(0) = 0 \quad \text{and} \quad \eta_1'(0) = 0, \tag{3.29}$$

$$\eta_2''(L) = 0 \quad \text{and} \quad \eta_2'''(L) = 0. \tag{3.30}$$

For the simply supported beam, the boundary conditions at the hinged ends are:

$$\eta_1(0) = 0 \quad \text{and} \quad \eta_1''(0) = 0, \tag{3.31}$$

$$\eta_2(L) = 0 \quad \text{and} \quad \eta_2''(L) = 0. \tag{3.32}$$

3.3.2 Numerical nonlinear cracked beam model

A Finite Element (FE) model is used to simulate the nonlinear static and dynamic response due to external loading of a generic rectangular fiber-reinforced beam with edge cracks. The composite matrix presents a linear-elastic behaviour, while the breathing bridged crack model (Section 3.2.2) is used to

describe the nonlinear elastic-plastic and the opening-closuring responses of the cracked sections.

Two-node Timoshenko beam finite elements with 4 degrees of freedom, coupled transversal displacements and rotations, are employed in the FE model. The portions of the uncracked beam are modelled through finite elements with linear-elastic bending and shear behaviour (Friedman & Kosmatka, 1993). On the other hand, the breathing bridged crack model is accommodated within the Timoshenko beam element (Viola et al., 2002).

3.3.2.1 Finite element formulation

The cracked finite element is constituted by two solid portions of beam connected at mid-length by a lumped rotational spring of stiffness $k_c(t)$, representing the nonlinear crack (Fig. 3.4Fig. 3.4). The stiffness $k_c(t)$ is calculated using the breathing bridged crack model at every time t through the relation:

$$k_c(t) = \dot{M}_c(t) / \Delta\dot{\vartheta}_c(t) . \qquad 3.33$$

Note that, if the crack is close ($\Delta\vartheta_c = 0$ and/or $\mathbf{u} = 0$), until a reversal of the bending moment at the crack section does not occurs (i.e. $M_c(t)\cdot\dot{M}_c(t) < 0$), the stiffness of the spring is assumed to be perfectly-rigid ($|k_c(t)| = \infty$), i.e. the cracked finite element behaves like a uncracked linear-elastic element.

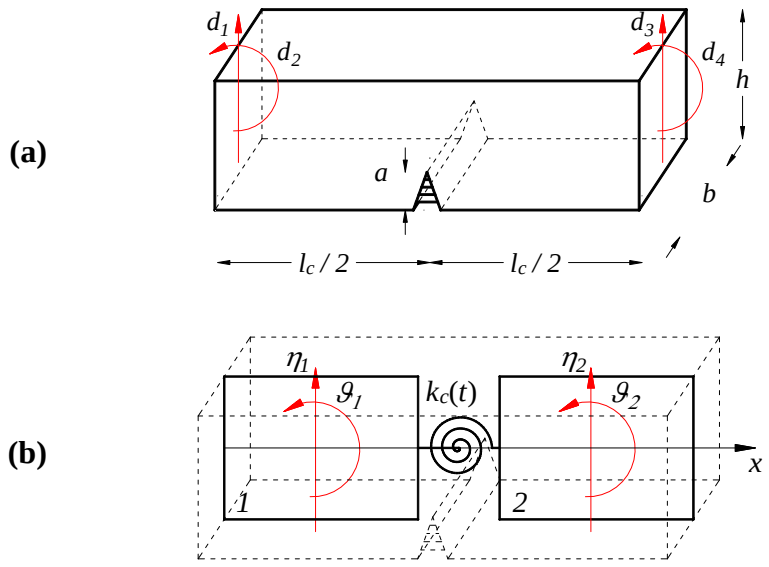

Fig. 3.4 ï (a) Beam element with breathing bridged edge crack; (b) sketch of the corresponding cracked finite element with nonlinear rotational spring.

In line with Timoshenkoôs beam theory and considering the coupling of transversal displacements and rotations, the shape functions of the two portions of the cracked finite element can be obtained. The shape functions, N_{1i} and N_{2i}, pertaining to the transversal displacement field, are equal to (see Fig. 3.4):

$$N_{11}(x)=\frac{(l_c-x)(l_c^2\tilde{u}\ +\ l_c^2\ +l_cx\ -\ 2x^2)}{l_c^3(\tilde{u}+\ 1)}$$

$$N_{12}(x,t)=\frac{x(\Gamma+2)}{2(\Gamma+1)}-\frac{x^2}{2(Z(t)+l_c)}-\frac{3x^2}{2l_c(\Gamma+1)}+\frac{x^3}{l_c^2(\Gamma+1)}$$

$$N_{13}(x)=\frac{x(l_c^2\tilde{u}+3l_cx\ -\ 2x^2)}{l_c^3(\tilde{u}+\ 1)} \qquad 0\le x<\frac{l_c}{2} \qquad 3.34$$

$$N_{14}(x,t)=-\frac{x\Gamma}{2(\Gamma+1)}+\frac{x^2}{2(Z(t)+l_c)}-\frac{3x^2}{2l_c(\Gamma+1)}+\frac{x^3}{l_c^2(\Gamma+1)}$$

and

$$N_{21}(x)=\frac{(l_c-x)(l_cx\ +\ l_c^2\tilde{u}\ +\ l_c^2\ -\ 2x^2)}{l_c^3(\tilde{u}+\ 1)}$$

$$N_{22}(x,t)=\frac{(Z(t)+x)(l_c-x)}{2(Z(t)+l_c)}+\frac{x(l_c^2-3l_cx+2x^2)}{2l_c^2(\Gamma+1)} \qquad \frac{l_c}{2}\le x\le l_c \qquad 3.35$$

$$N_{23}(x,t)=\frac{x(l_c^2\tilde{u}+3l_cx\ -\ 2x^2)}{l_c^3(\tilde{u}+\ 1)}$$

$$N_{24}(x,t)=-\frac{(Z(t)+x)(l_c-x)}{2(Z(t)+l_c)}+\frac{x(l_c^2-3l_cx+2x^2)}{2l_c^2(\Gamma+1)}$$

where l_c is the length of the cracked finite element, $\Gamma=12E_{eq}I\chi/(G_mAl_c^2)$ is the shear deformation parameter of the beam, $Z(t)=E_{eq}I/k_c(t)$, E_{eq} is the equivalent Youngôs modulus of the composite material, A and I area the area and the moment of inertia of the cross-section, respectively, χ is the shear coefficient (equal to 1.2 for a rectangular cross-section), G_m the shear elastic modulus of the matrix. Note that, being E_m and E_f, respectively, the Youngôs modulus of the matrix and of the fibers and ν_f the volume fraction of the fibers, through the classical rule of mixture so the equivalent Youngôs modulus is equal to $E_{eq}=(1-\nu_f)E_m+\nu_fE_f$.

The shape functions, R_{1i} and R_{2i}, pertaining to the rotation field, are (see Fig. 3.4):

$$R_{11}(x) = -\frac{6x(l_c - x)}{l_c^3(\tilde{u} + 1)}$$

$$R_{12}(x,t) = \frac{(l_c + Z(t) - x)}{(Z(t) + l_c)} + \frac{3(-l_c^2 x + l_c x^2 + Z(t)(x^2 - l_c x))}{l_c^2(\Gamma + 1)(Z(t) + l_c)} \qquad 0 \le x < \frac{l_c}{2} \qquad 3.36$$

$$R_{13}(x) = \frac{6x(l_c - x)}{l_c^3(\tilde{u} + 1)}$$

$$R_{14}(x,t) = \frac{x}{Z(t) + l_c} - \frac{3x(l_c - x)}{l_c^2(\Gamma + 1)}$$

and

$$R_{21}(x) = -\frac{6x(l_c - x)}{l_c^3(\tilde{u} + 1)}$$

$$R_{22}(x,t) = \frac{l_c - x}{Z(t) + l_c} + \frac{3x(l_c - x)}{l_c^2(\Gamma + 1)} \qquad \frac{l_c}{2} \le x \le l_c \qquad 3.37$$

$$R_{23}(x) = \frac{6x(l_c - x)}{l_c^3(\tilde{u} + 1)}$$

$$R_{24}(x,t) = \frac{Z(t) + x}{Z(t) + l_c} - \frac{3x}{l_c(\Gamma + 1)} + \frac{3x^2}{l_c^2(\Gamma + 1)} \ .$$

According to the standard definition of the stiffness matrix $\mathbf{K_c}(t)$, its related terms can be evaluated by differentiating the shape functions related to the rotations along the finite element, that is:

$$\mathbf{K_c}(t) = E_{eq} I \begin{bmatrix} R_{11}''(x=0) & R_{12}''(x=0) & R_{13}''(x=0) & R_{14}''(x=0) \\ -R_{11}'(x=0) & -R_{12}'(x=0) & -R_{13}'(x=0) & -R_{14}'(x=0) \\ -R_{21}''(x=l_c) & -R_{22}''(x=l_c) & -R_{23}''(x=l_c) & -R_{24}''(x=l_c) \\ R_{21}'(x=l_c) & R_{22}'(x=l_c) & R_{23}'(x=l_c) & R_{24}'(x=l_c) \end{bmatrix} \qquad 3.38$$

where the apex symbol indicates a derivative with respect to *x*.

The resulting stiffness matrix $\mathbf{K_c}(t)$ of the cracked beam element takes the form:

$$\mathbf{K_c}(t)=\frac{E_{eq}I}{(1+\Gamma)}\begin{bmatrix} \frac{12}{l_c^3} & \frac{6}{l_c^2} & -\frac{12}{l_c^3} & \frac{6}{l_c^2} \\ \frac{6}{l_c^2} & \left(\frac{3}{l_c}+\frac{(1+\Gamma)}{Z(t)+l_c}\right) & -\frac{6}{l_c^2} & \left(\frac{3}{l_c}-\frac{(1+\Gamma)}{Z(t)+l_c}\right) \\ -\frac{12}{l_c^3} & -\frac{6}{l_c^2} & \frac{12}{l_c^3} & -\frac{6}{l_c^2} \\ \frac{6}{l_c^2} & \left(\frac{3}{l_c}-\frac{(1+\Gamma)}{Z(t)+l_c}\right) & -\frac{6}{l_c^2} & \left(\frac{3}{l_c}+\frac{(1+\Gamma)}{Z(t)+l_c}\right) \end{bmatrix}. \quad 3.39$$

The translational, $\mathbf{M_c^t}(t)$, and the rotational, $\mathbf{M_c^r}(t)$, mass matrices can be obtained by the kinetic energy of the cracked finite element, as follows:

$$\mathbf{M_c^t}(t)=\int_0^{l_2/2}\mathbf{N}_1^T\rho_{eq}A\mathbf{N}_1dx+\int_{l_2/2}^{l_2}\mathbf{N}_2^T\rho_{eq}A\mathbf{N}_2dx, \quad 3.40$$

and

$$\mathbf{M_c^r}(t)=\int_0^{l_2/2}\mathbf{R}_1^T\rho_{eq}I\mathbf{R}_1dx+\int_{l_2/2}^{l_2}\mathbf{R}_2\rho_{eq}I\mathbf{R}_2dx, \quad 3.41$$

where ρ_{eq} is the density of the composite material, $\mathbf{N}_1=\{N_{11},N_{12},N_{13},N_{14}\}$, $\mathbf{N}_2=\{N_{21},N_{22},N_{23},N_{24}\}$, $\mathbf{R}_1=\{R_{11},R_{12},R_{13},R_{14}\}$ and $\mathbf{R}_2=\{R_{21},R_{22},R_{23},R_{24}\}$. Note that, being ρ_m and ρ_f respectively the density of the matrix and of the fibers, $\rho_{eq}=(1-\nu_f)\rho_m+\nu_f\rho_f$.

The translational mass matrix $\mathbf{M_c^t}(t)$ takes the form:

$$\mathbf{M_c^t}(t)=\frac{Al_c\rho_{eq}}{1680(1+\Gamma)^2}\begin{bmatrix} 8m_1 & l_cm_2-m_5 & 8m_3 & l_cm_2-m_5 \\ & 2l_c^2+m_4m_6 & l_cm_2-35l_c^2m_5 & 2l_c^2-m_4m_6 \\ & & 8m_1 & -l_cm_2+m_5 \\ sym & & & 2l_c^2+m_4m_6 \end{bmatrix} \quad 3.42$$

where $m_1=70\Gamma^2+147\Gamma+78$, $m_2=105\Gamma^2+224\Gamma+123$, $m_3=35\Gamma^2+63\Gamma+27$, $m_4=20Z^2(t)+25Z(t)l_c+8l_c^2$, $m_5=\frac{35l_c^2(1+\Gamma)^2}{(Z(t)+l_c)}$ and $m_6=\frac{1.75l_c^2(1+\Gamma)^2}{(Z(t)+l_c)^2}$.

The rotational mass matrix $\mathbf{M_c^r}(t)$ takes the form:

$$\mathbf{M_c^r}(t)=\frac{I\rho_{eq}}{(1+\Gamma)^2}\begin{bmatrix} \frac{6}{5l_c} & -\frac{5\Gamma-1}{10} & -\frac{6}{5l_c} & -\frac{5\Gamma-1}{10} \\ & -\frac{l_c m_7}{20(1+\Gamma)}+l_c m_8 m_{10} & \frac{5\Gamma-1}{10} & -\frac{l_c m_7}{20(1+\Gamma)}+l_c^2 m_9 m_{10} \\ & & \frac{6}{5l_c} & \frac{5\Gamma-1}{10} \\ sym & & & -\frac{l_c m_7}{20(1+\Gamma)}+l_c m_8 m_{10} \end{bmatrix} \quad 3.43$$

where $m_7=10\Gamma^2+14\Gamma+4$, $m_8=6Z^2(t)+9Z(t)l_c+4l_c^2$, $m_9=3Z(t)+2l_c$ and $m_{10}=\frac{(1+\Gamma)^2}{12(Z(t)+l_c)^2}$.

3.3.2.2 Static and dynamic equilibrium

According to the adopted FE model, the nonlinear static and dynamic equilibrium of the fiber-reinforced cracked beam can be written, respectively, in the following discretized forms

$$\mathbf{K}(t)\,\mathbf{q}=\mathbf{P}(t) \quad 3.44$$

and

$$\mathbf{M}(t)\,\ddot{\mathbf{q}}+\mathbf{C}(t)\,\dot{\mathbf{q}}+\mathbf{K}(t)\,\mathbf{q}=\mathbf{P}(t), \quad 3.45$$

where $\mathbf{M}(t)$, $\mathbf{C}(t)$ and $\mathbf{K}(t)$ are, respectively, the mass matrix, the damping matrix and the stiffness matrix of the beam. The vectors $\ddot{\mathbf{q}}$, $\dot{\mathbf{q}}$ and $\mathbf{q}$ represent the translational and rotational nodal accelerations, velocities and displacements and $\mathbf{P}(t)$ is the vector of the nodal forces acting on the beam.

The global matrices $\mathbf{M^t}(t)$, $\mathbf{M^r}(t)$ and $\mathbf{K}(t)$ are formed by assembling the translational mass matrices, the rotational mass matrices and the stiffness matrices of each uncracked and cracked finite element. Then, the mass matrix $\mathbf{M}(t)$ is obtained by the sum of $\mathbf{M^t}(t)$ and $\mathbf{M^r}(t)$. The classical Rayleigh method (Chopra, 1995) is employed to build the damping matrix $\mathbf{C}(t)$ as a linear combination of the mass matrix $\mathbf{M}(t)$ and the stiffness matrix $\mathbf{K}(t)$. The coefficients of the Rayleigh mass matrix are calculated on the basis of the damping ratio at the first two natural frequencies of the beam.

Due to the nonlinearity of the static and dynamic problems, related to the nonlinear elastic-plastic behaviour of the breathing bridged crack, Eqs 3.44 and 3.45 are solved in incremental form. The explicit Wilson step-by-step method is used to solve the dynamic equilibrium (Chopra, 1995). Furthermore, in both the static and dynamic problems, at every time step *dt*, the possible variation of k_c is

checked. If such a variation occurs, *dt* is subdivided in two sub-intervals and the proper value of k_c to be used at the second sub-interval is calculated, as explained in more detail below. At the first time step, if the bending moment M_c opens the crack, the elastic value of k_c (obtained by assuming all the fibers rigid) is assumed. Otherwise if the crack is kept closed, k_c is imposed to be equal to infinite. At a generic time step, the system of Eq. 3.9 is solved and it is checked if at least a inequality condition of the breathing bridged crack model (related to $\Delta\vartheta_c$ and to F_i and w_i and for every *i*-th fiber, see Section 3.2.2) is not satisfied. If the control is negative (i.e. all the inequality conditions of the crack model are fulfilled) in the following time step the same k_c is used. Otherwise if the control is positive, using the Newton-Raphsonôs method, the first instant within the time interval *dt*, wherein a limit constraint is reached, is identified. Consequently, *dt* is subdivided in two sub-intervals and, by updating the state of the crack and of the fibers, the proper value of k_c to be used at second sub-interval is calculated through Eq. 3.33. Furthermore, the algorithm checks the occurrence of a load reversal within *dt*, namely a plastic-to-elastic return or an elastic-to-elastic return. Through a nonlinear optimization procedure, the time instant, wherein the reversal takes place by looking for the $\max\{|M_c|\}$ in *dt*, is evaluated.

3.3.2.3 The case of a cantilever beam

The FE model of the cracked fiber reinforced beam is used to simulated the nonlinear static and dynamic behavior of a cantilever beam with a single crack subjected to a point load $P(t)$ at the free end (Fig. 3.5). The static and dynamic responses are studied by wavelet analysis to assess the nonlinear damage in Chapter 6.

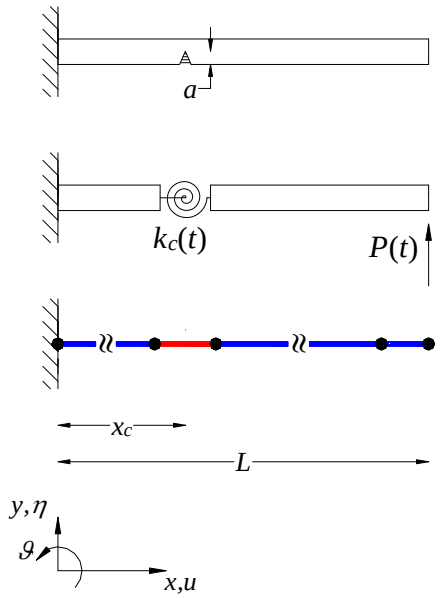

Fig. 3.5 ī Sketch of the FE model of a generic FR cantilever beam with a breathing bridged crack.

Chapter 4

Edge effects in damage detection using spatial CWT

4.1 Introduction

As exposed in Chapters 1 and 2, wavelet analysis is widely recognized to be an effective and robust damage identification tool, in analysing static or dynamic deflection shapes of structures. Nevertheless a reliable detection of tiny damages is still an open challenge because they can be masked by measurement noise and/or border distortions (edge effects) of the wavelet transform. While the damage identification technology is progressing in the development of modern techniques for precise and dense spatially distributed measurements (e.g. computer vision, laser scanning techniques and optical fibers) (Rastogi, 1997; Casciati, & Wu, 2010; Stanbridge & Ewins, 1999; Yang & Allen, 2011; Francis et al.), the issue of edge effects in continuous wavelet transforms remains poorly addressed in the literature (Rucka & Wilde, 2006a-2006b; Spanos et al., 2006; Messina, 2008).

It is well known that border effects are very common in many finite-length non-stationary signal analysis and processing approaches, e.g. WT (Mallat, 2001; Mertins 1999) and HHT (Deng et al., 2001; Cheng et al., 2007). In wavelet transform, near the signal ends the convoluting window extends partially on the signal domain and consequently abnormal coefficients arise and taint the transform. To handle boundary effects two approaches are usually used: the first is to impose some extra constraints on the signal (e.g. extension method) while the second is to construct a specific wavelet. For its simplicity the signal boundary constraint approach is usually preferred. Traditional extending methods as zero padding, periodic padding, symmetric padding and linear padding (see MATLAB Wavelet Toolbox; Misiti et al., 2000) are usually employed in WA but often case-dependent models are needed to conveniently alleviate the border effects for the specific application. Kijewski and Kareem (2002) and Su et al.

(2011) discuss extensively the edge effect problem in analysing oscillatory signals by Morlet wavelet. They suggest, respectively, a simple extension method to preserve the local spectral content of the signal and a smooth extension scheme using a Fourier-based method to preserve the signal time-varying characteristics. Williams and Amaratunga (1997) develop an extrapolated discrete wavelet transform, applicable to Daubechies and biorthogonal wavelet bases, which does not exhibit edge effects in image compression and other signal processing applications. A non-linear extension model for CWT, named the Leap-Step Time Series Analysis (LSTSA) model, is proposed by Zheng et al. (2000) to enhance the detection of low-frequency signals in the observed Length-Of-Day (LOD) series.

As mentioned above, few researchers have examined in depth the border distortion issue in structural damage detection through WT of deflection shapes. In fact, since the damage tends to nucleate and propagate in the most highly stressed zone of the structure which is often near the boundary (e.g. the zone close to the clamped end of a cantilever), the maximum WT coefficients due to the edge effects tend to mask the damage, leading to situations of false indication or even of false alarm. Spanos et al. (2006) consider multi-damaged Euler-Bernoulli beams subjected to static loads and show numerically that applying the WT on the difference between the damaged and the undamaged beam responses, boundary effects are eliminated and damage related to local maxima is clearly identified. However, the drawback of this method is the need of the availability of the undamaged response of the beam. Rucka and Wilde, imposing the local continuity of the first and second derivatives at the ends, extend the signal outside its original support through a simple cubic spline extrapolation based on three (Rucka & Wilde, 2006a) or four (Rucka & Wilde, 2006b) neighbouring points. On the other hand, Messina (2008) discuss extensively the border distortion in CWT dealing with the first four Gaussian wavelets and propose two methods. The first method consists of padding the signal through isomorphisms (called ñRotationò - corresponding to a polar-like symmetry - and ñTurnoverò - corresponding to a mirror symmetry) of the original signal. The author examine their quality in limiting the border distortions with respect to the beam boundary conditions and the derivative order. The second method (called ñSelf-minimizationò) aims at correcting a first approximated extension, for instance obtained by a fitting polynomial, by minimizing an objective function which depends on the wavelet convolution results.

In the present chapter the problem of the damage masked by CWT border distortions is discussed and a new signal extension polynomial method to reduce edge effects for enhanced damage detection by spatial CWT is proposed. Taking advantage of the slight oscillation of the structural deflection shapes, the method is based on high-order polynomial functions that fit the original signal and its first derivative so as to extend smoothly the signal and its derivatives. To

illustrate the effectiveness and the versatility of the method with respect to different boundary conditions and beam deflections (described by either trigonometric or polynomial functions), the free vibration and the static deflection responses of a cracked cantilever and a cracked simple supported beam are analytically simulated (see Section 3.3.1.3). A synthetic Gaussian white noise is added to the signal to represent real measured data. The fourth order Coiflet basis function (ócoif4ô) is used in wavelet analysis. The method is compared with the traditional linear padding method and with Messinaôs isomorphism methods (Messina, 2008).

4.2 Edge effects issue in damage detection by spatial CWT

As exposed in Section 2.2.3, the continuous wavelet transform is defined by the convolution of the input signal, $d(x)$, with a wavelet function generated from the mother wavelet, $\psi(x)$, by scaling and translating it. For a finite-length signal, when the convolution operation is executed close to the signal ends, the wavelet window extents into a region with no available data (Fig. 4.1a). Therefore the transform of the signal close to the borders is tainted by the non-existing data: in these regions the values of the CWT coefficients arise abnormally (*border distortions* or *edge effects*) and the real signal features are consequently corrupted by the transform (Fig. 4.1b). Edge effects can provoke the masking of the damage and yield situations of false indicators or false alarm.

Among the different approaches to handle edge effects, the most commonly used one is to preprocess the signal through extrema extension (Mallat, 2001; Mertins 1999). Traditional extension techniques include extension by zero padding, periodicity, symmetry and linearization (Misiti et al., 2000). These methods make simple assumptions about the signal characteristics outside the borders but they prove unsatisfactory for many applications (e.g. analysis of strong oscillating signals, imagine compression, coding applications, etc.), including damage detection (Rucka & Wilde, 2006a-2006b; Messina, 2008).

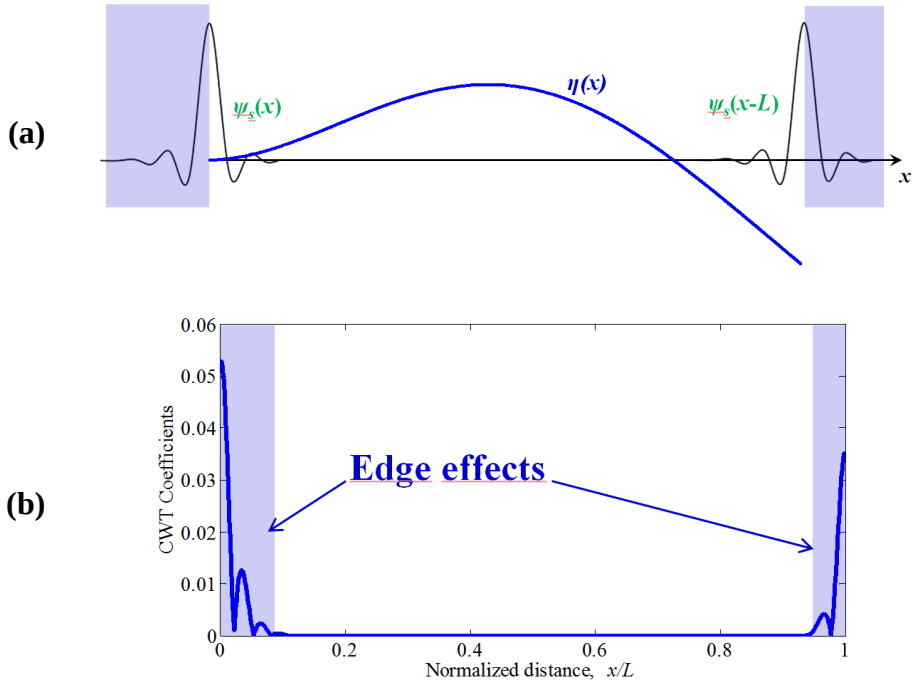

Fig. 4.1 ï (a) In the CWT convolution, the wavelet window, close to the signal ends, extents into a region with no available data; (b) edge effects occurs close to the signal extrema, corrupting the transform.

In this study the free vibrations and the static deflection of a cracked cantilever (Fig. 4.2) and of a cracked simple supported beam (Fig. 4.3) are considered as baseline signals $d(x)$ to be analysed by WA using ócoif4ô wavelet (see Chapter 2).

The cracked beam responses are described by means of the analytical model introduced in Section 3.3.1 and in accordance with the open crack model (see Section 3.2.1) the damage introduces a discontinuity in the rotation, $\eta'(x)$, of the structural response and consequently a singularity in the curvature, $\eta''(x)$, and singularities in the subsequent derivatives. As well-known (Section 2.2.3), a wavelet with *m* vanishing moments detects the local discontinuities of the signal and of its derivatives up to the *m*-th order. Therefore, suitable padding functions, to be added at both the ends in the original signal, need to have specific smoothness features to avoid the introduction of edge discontinuities into the padded signal and its derivatives up to the *m*-th order. The traditional padding methods cited above introduce discontinuities at the ends of the signal and/or in

its 1st or 2nd derivatives, so that small damages close to the beam extrema are masked by CWT border distortions. In the following, an ad-hoc extension method that minimizes edge effects is developed for a more effective damage detection through wavelet analysis.

(a)

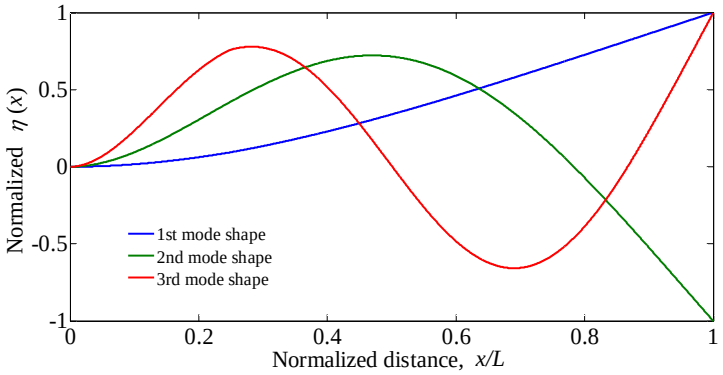

(b)

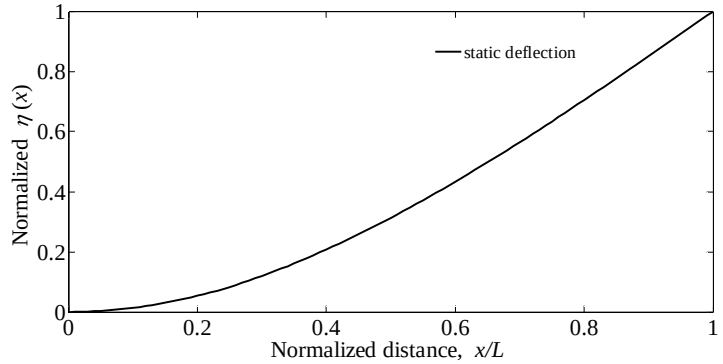

Fig. 4.2 ï (a) Normalized 1st, 2nd and 3rd mode shapes of a generic cantilever beam with an open edge crack at x/L = 0.25; (b) Normalized static deflection of a generic cantilever with an open edge crack at x/L = 0.25 subjected to a transversal load at $x = L$.

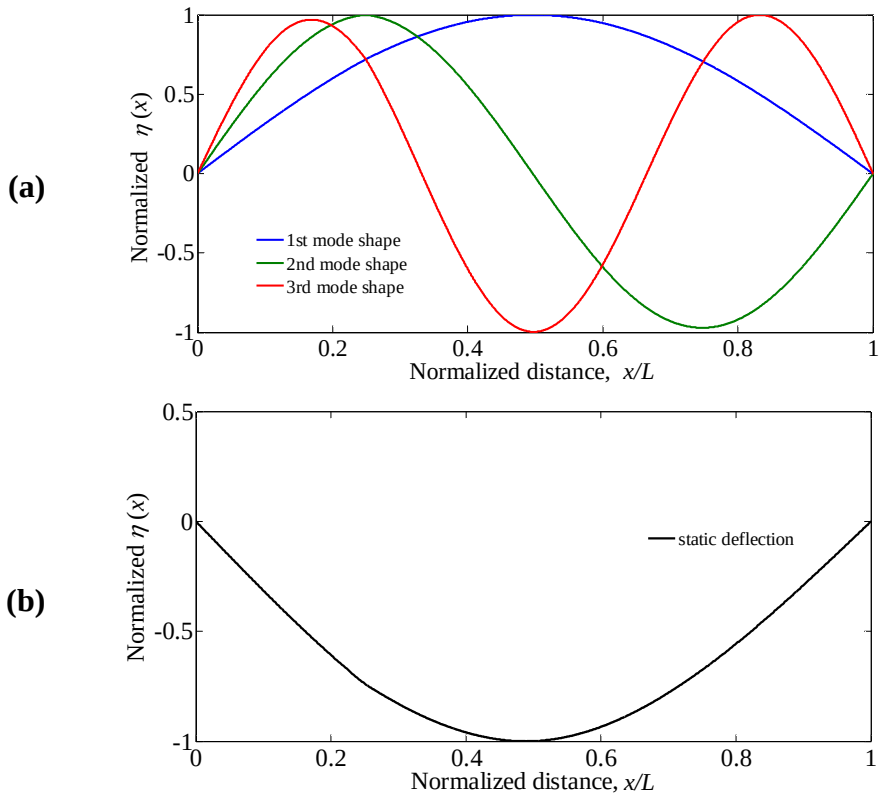

Fig. 4.3 ï (a) Normalized 1st, 2nd and 3rd mode shapes of a generic simply supported beam with an open edge crack at x/L = 0.25; (b) Normalized static deflection of a generic simply supported beam with an open edge crack at x/L = 0.25 subjected to a transversal load at $x = L/2$.

In order to consider realistic measured data, noise is superimposed on the simulated deflection shapes $\boldsymbol{d}(x)$. As a matter of fact, the ideal situation in the absence of noise would produce a trivial damage identification by extending the signal $\boldsymbol{d}(x)$ through its interpolating spline or fitting spline (Rucka & Wilde, 2006a-2006b). The border distortions would be suppressed and the location of very tiny damages close to the edges would easily be identified by WT. On the other hand numerical experiments prove this approach not to be effective in extending noisy signals. Note also that in the absence of noise WA would not be necessary to detect the damage position since, by numerically calculating the second derivative of the original signal, the damage location can readily be identified (Pandey et al., 1991).

The presence of noise is introduced by adding a synthetic Gaussian white noise to ***d***(*x*). To quantify the noise level, the signal to noise ratio (SNR) is considered. The SNR, expressed in decibels, is defined as:

$$\mathrm{SNR} = 10\log_{10}\left(\frac{P_{signal}}{P_{noise}}\right). \qquad 4.1$$

The term *P* with the subscripts in Eq. 4.1 denotes power and is computed as

$$P_{(.)} = \frac{1}{N_z}\sum_{i=0}^{N_z-1}\left|z(x_i)\right|^2, \qquad 4.2$$

where N_z denotes the number of discrete points of a generic sampled function $z(x)$.

4.3 The proposed padding method

A simple and computationally efficient method based on using two polynomial functions $f_1(x_1)$ and $f_2(x_2)$ to extend, in the range $x \le 0$ and $x \ge L$, respectively, the signal ***d***(*x*) is proposed (Fig. 4.4).

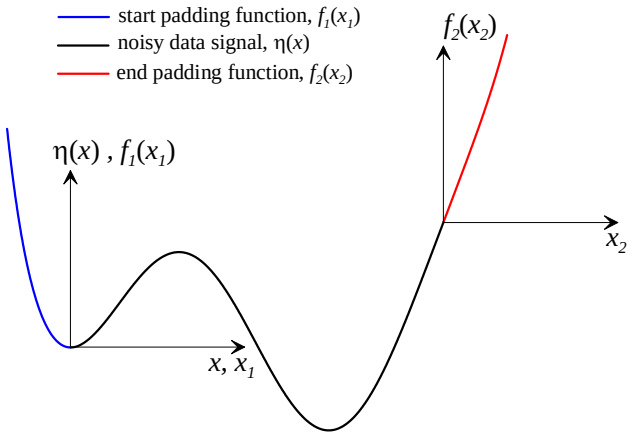

Fig. 4.4 - A generic noisy data signal, ***d***(*x*), is extended smoothly before the start by $f_1(x_1)$ and after the end by $f_2(x_2)$.

These functions are obtained by a fitting procedure in order to:
(i) describe correctly ***d***(*x*) in such a way to extend smoothly the trend of the signal and of its derivatives up to the order equal to the *m*-th vanishing moment of the adopted wavelet;
(ii) ensure continuity at the boundaries up to *m*-th derivative order.

Since the original signal is corrupted by noise, conditions (i) and (ii) may only be satisfied in an average sense.

This method assumes that the extension polynomials functions $f_1(x_1)$ and $f_2(x_2)$ have the same degree of the fitting functions $\bar{f}_1(x_1)$ and $\bar{f}_2(x_2)$ defined below. When adopting the óCoif4ô wavelet with 8 vanishing moments, boundary continuities up to the 8th derivative of $d(x)$ have to be satisfied. Hence, polynomial functions of degree 8 are generated for $f_1(x_1)$ and $f_2(x_2)$. However, even though a wavelet function with fewer vanishing moments is used, to extrapolate accurately the noisy signal trend, numerical analysis show that polynomial functions of degree 8 are recommended.

To define the extension functions, firstly $d(x)$ is fitted in a least squares sense through the two polynomial functions $\bar{f}_1(x_1)$ and $\bar{f}_2(x_2)$ as

$$\bar{f}_1(x_1) = \overline{A}_1 x_1^8 + \overline{B}_1 x_1^7 + \overline{C}_1 x_1^6 + \overline{D}_1 x_1^5 + \overline{E}_1 x_1^4 + \overline{F}_1 x_1^3 + \overline{G}_1 x_1^2 + \overline{H}_1 x_1 + \bar{I}_1 \quad 4.3$$

with $0 \le x_1 \le \beta_1 L$

and

$$\bar{f}_2(x_2) = \overline{A}_2 x_2^8 + \overline{B}_2 x_2^7 + \overline{C}_2 x_2^6 + \overline{D}_2 x_2^5 + \overline{E}_2 x_2^4 + \overline{F}_2 x_2^3 + \overline{G}_2 x_2^2 + \overline{H}_2 x_2 + \bar{I}_2 \quad 4.4$$

with $-L(1-\beta_2) \le x_2 \le 0$

where $\overline{A}_1, \overline{B}_1, \ldots, \bar{I}_1$ and $\overline{A}_2, \overline{B}_2, \ldots, \bar{I}_2$ are the coefficients of the fitting polynomial functions, $\bar{f}_1(x_1)$ and $\bar{f}_2(x_2)$, respectively. The function $\bar{f}_1(x_1)$ fits $d(x)$ from $x = 0$ to $x = \beta_1 L$; while $\bar{f}_2(x_2)$ fits $d(x)$ from $x = L(1-\beta_2)$ to $x = L$, where the parameters β_1 and β_2 can vary in the range $0.1-1$. There are no optimal value for these parameters, as they depend on the trend of the signal and the noise level. For instance in the case of signals characterized by no sign change, values in the range of $0.7-1$ work well while for oscillating signals values in the range $0.1-0.4$ are suggested; moreover the latter values are in general to be preferred in the presence of low noise content.

The extension polynomials $f_1(x_1)$ and $f_2(x_2)$ have the expressions:

$$f_1(x_1) = A_1 x_1^8 + B_1 x_1^7 + C_1 x_1^6 + D_1 x_1^5 + E_1 x_1^4 + F_1 x_1^3 + G_1 x_1^2 + H_1 x_1 + I_1 \quad 4.5$$

with $-\Lambda s \le x_1 \le 0$

and

$$f_2(x_2) = A_2 x_2^8 + B_2 x_2^7 + C_2 x_2^6 + D_2 x_2^5 + E_2 x_2^4 + F_2 x_2^3 + G_2 x_2^2 + H_2 x_2 + I_2 \quad 4.6$$

with $0 \le x_2 \le \Lambda s$

where s is the scale parameter considered in the WA, Λ represents the distance from the mother wavelet center to the position where the wavelet attains negligible values (for óCoif4ô, $\Lambda = 11\,dx$ is assumed, where dx is the sampling

step). The polynomial coefficients $A_1, B_1, \ldots, I_1$ and $A_2, B_2, \ldots, I_2$ are obtained as follows:

$$A_1 = \overline{A}_1;\ B_1 = \overline{B}_1;\ C_1 = \overline{C}_1;\ D_1 = \overline{D}_1;\ E_1 = \overline{E}_1;\ F_1 = \overline{F}_1;\ G_1 = \overline{G}_1;\ H_1 = \overline{H}_1;\ I_1 = \eta(x=0) \quad (4.7)$$

and

$$A_2 = \overline{A}_2;\ B_2 = \overline{B}_2;\ C_2 = \overline{C}_2;\ D_2 = \overline{D}_2;\ E_2 = \overline{E}_2;\ F_2 = \overline{F}_2;\ G_2 = \overline{G}_2;\ H_2 = \overline{H}_2;\ I_2 = \eta(x=L). \quad (4.8)$$

Then, the coefficients H_1 and H_2 are fitted through an iterative procedure to the first derivative $\gamma(x)$ of the noisy data $\boldsymbol{d}(x)$, being $0 \le x \le L$. Starting from the padded signal $f_1(x_1) \cup \eta(x) \cup f_2(x_2)$, where $x_1 \le 0$ and $x_2 \ge L$, $\gamma(x)$ is numerically calculated through Richardsonôs extrapolation (Atkinson, 1989), which allows a high-order approximation (e.g. $O(dx^8)$, $O(dx^{10})$ or $O(dx^{12})$) of the derivative.

The iterative procedure consists of the following steps:

(1) $\boldsymbol{\chi}(x)$ is fitted in a least squares sense through two polynomial functions $\tilde{f}_1(x_1)$ and $\tilde{f}_2(x_2)$, of one smaller degree with respect to that of $f_1(x_1)$ and $f_2(x_2)$, such as:

$$\tilde{f}_1(x_1) = \tilde{A}_1 x_1^7 + \tilde{B}_1 x_1^6 + \tilde{C}_1 x_1^5 + \tilde{D}_1 x_1^4 + \tilde{E}_1 x_1^3 + \tilde{F}_1 x_1^2 + \tilde{G}_1 x_1 + \tilde{H}_1 \quad (4.9)$$

with $0 \le x_1 \le \tilde{\beta}_1 L$

and

$$\tilde{f}_2(x_2) = \tilde{A}_2 x_2^7 + \tilde{B}_2 x_2^6 + \tilde{C}_2 x_2^5 + \tilde{D}_2 x_2^4 + \tilde{E}_2 x_2^3 + \tilde{F}_2 x_2^2 + \tilde{G}_2 x_2 + \tilde{H}_2 \quad (4.10)$$

with $-L(1-\tilde{\beta}_2) \le x_2 \le 0$

where $\tilde{A}_1, \tilde{B}_1, \ldots, \tilde{H}_1$ and $\tilde{A}_2, \tilde{B}_2, \ldots, \tilde{H}_2$ are the coefficients of the fitting polynomial functions, $\tilde{f}_1(x_1)$ and $\tilde{f}_2(x_2)$, respectively. The function $\tilde{f}_1(x_1)$ fits $\boldsymbol{\chi}(x)$ from $x=0$ to $x=\tilde{\beta}_1 L$; while $\tilde{f}_2(x_2)$ fits $\boldsymbol{\chi}(x)$ from $x = L(1-\tilde{\beta}_2)$ to $x = L$, where $\tilde{\beta}_1$ and $\tilde{\beta}_2$ can vary in the range $0.1-1$. In the following, unless not otherwise specified, $\tilde{\beta}_1 = \beta_1$ and $\tilde{\beta}_2 = \beta_2$.

(2) $\gamma(x)$ is recalculated through Richardsonôs extrapolation starting from the modified padded signal $f_1(x_1) \cup \eta(x) \cup f_2(x_2)$, where in $f_1(x_1)$ H_1 is replaced with $\tilde{H}_2$ and in $f_2(x_2)$ H_2 is replaced with $\tilde{H}_2$.

The steps (1) and (2) are repeated until the values of H_1 and H_2 converge.

Since differentiating the original signal increases the amount of noise, the above described optimization approach is not effective for the other polynomial

coefficients, $A_1,\ldots,G_1$ and $A_2,\ldots,G_2$. Note that the last two equalities of Eqs 4.7 and 4.8 impose the fundamental condition of signal continuity at the two extrema. Furthermore, it has to be underlined that good results can be achieved without performing the optimization procedure related to the first derivative (i.e. by assuming $H_1 = \overline{H}_1$ and $H_2 = \overline{H}_2$) and, in fact, better results could be obtained in some cases, e.g., when the noise level is high. Figures 4.4, 4.5 and 4.6 show respectively a generic noisy data signal and its 1st and 2nd derivatives extended through the proposed polynomial functions $f_1(x_1)$ and $f_2(x_2)$, and their corresponding derivatives. These figures point out that the conditions (i) and (ii), explained above, are satisfied.

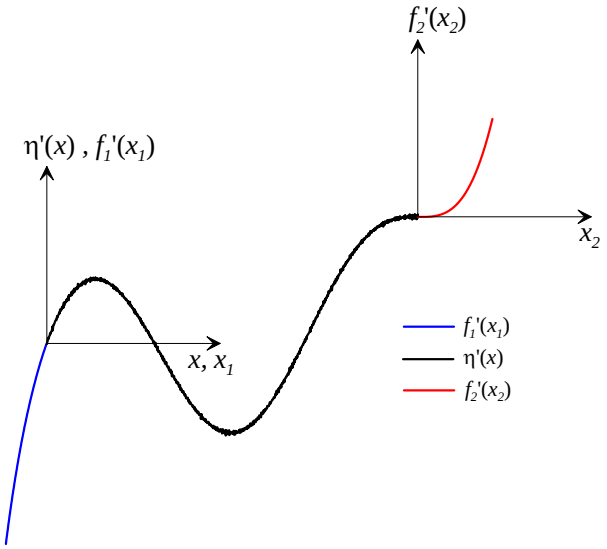

Fig. 4.5 - The 1st derivative of the padded noisy signal is shown. The functions $f_1'(x_1)$ and $f_2'(x_2)$ extend $\eta'(x)$ smoothly.

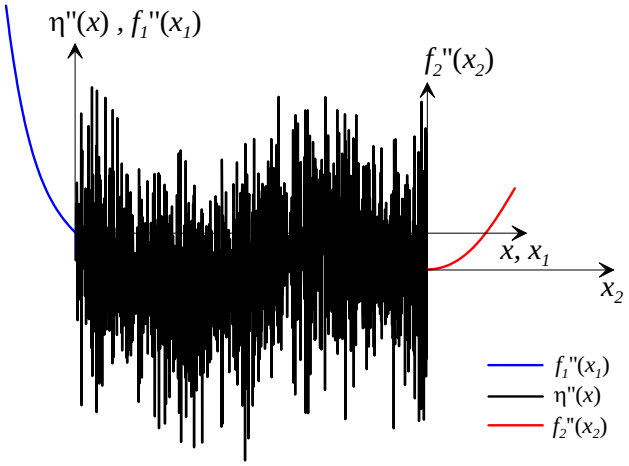

Fig. 4.6 - The 2nd derivative of the padded noisy signal is shown. Increasing the derivative order of ***d***(*x*) leads to an increase of noise. However $f_1''(x_1)$ and $f_2''(x_2)$ follow the average trend of $\eta''(x)$.

4.4 Illustrative examples

The effectiveness and the versatility of the proposed polynomial padding method in minimizing the CWT border distortions are investigated by considering the simulated noisy free vibrations and the static deflection of a cantilever and a simple supported cracked beam. The method is assessed by analyzing structural responses having different features (trigonometric function for the modeshapes and cubic polynomial for the static responses) and various constraint conditions (clamped, simple supported and free). Moreover, the CWT results are compared to those obtained by the application of the traditional linear padding method (Misiti et al., 2000) and Messinaôs isomorphism method (Messina, 2008), which is considered to be the most effective padding method available in the literature. Conversely to the linear padding method, which applies a linear extension of ***d***(*x*) interpolating the first two and the last two values of the sampled beam deflection (Fig. 4.7a), the isomorphism padding methods proposed by Messina extend the signal end parts either through mirror symmetry (called ñTurnoverò) when the signalôs first derivative tends to zero or through a polar-like symmetry (called ñRotationò), when the signalôs second derivative tends to zero (Fig. 4.7b).

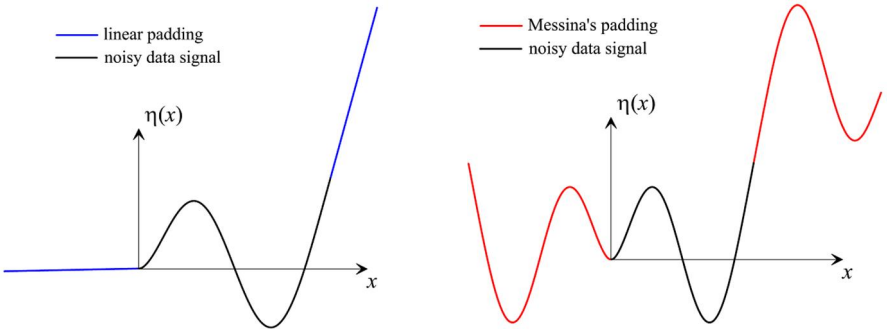

Fig. 4.7 ï (a) linear padding method; (b) Messinaçs padding method, where the initial part of $\boldsymbol{d}(x)$ is extended through the óTurnoverô, and its final part through the óRotationô

A cracked beam of length L = 1m and a rectangular cross-section of height h = 0.05L and width b = 0.5h, constituted by an elastic linear isotropic material with Young modulus, E = 200 GPa, and density, ρ = 7850 kg/m^3, is considered. The free vibration responses and the static deflections of the beams are sampled at dx = 0.001L intervals and analyzed through CWT using the óCoif4ô mother wavelet. The crack location, x_c, and the noise level (synthetic Gaussian white noise is used) are varied and, unless otherwise specified, the relative crack depth ratio, $\breve{\boldsymbol{u}}$ ($\breve{\boldsymbol{u}}$ = a/h), is fixed to 2%.

4.4.1 Free vibration response of a cantilever beam

The normalized first modeshape (maximum deflection equal to unity) of the damaged cantilever beam is analysed using the linear padding method, Messinaçs method (with the ñTurnoverò method at the clamped end and the ñRotationò method at the free end (see Giannoccaro et al., 2009) and the proposed polynomial method (with the fitting parameters, β_1 and β_2 assumed equal to 1). The crack is located at x_c/L = 0.02 from the clamped end. A noise level SNR = 120 dB is assumed.

In Fig. 4.8a, where the linear padding method is used, a jump in the curvature is evident at x = 0. In Fig. 4.8b, where the ñTurnoverò method is applied to the clamped end, the continuity of the second derivative at x = 0 is fulfilled while a jump of the third derivative is expected. On the other hand, in Fig. 4.8c, thanks to the proposed polynomial padding, no discontinuities are present in the boundaries and the extending functions are in agreement with the average trend in the curvature $\eta''(x)$. Incidentally, it is worth noticing that, for the selected combination of noise level and damage severity and location, it is not possible to

locate the crack by analyzing the curvature plot, and hence a wavelet transform technique is necessary to detect such damage.

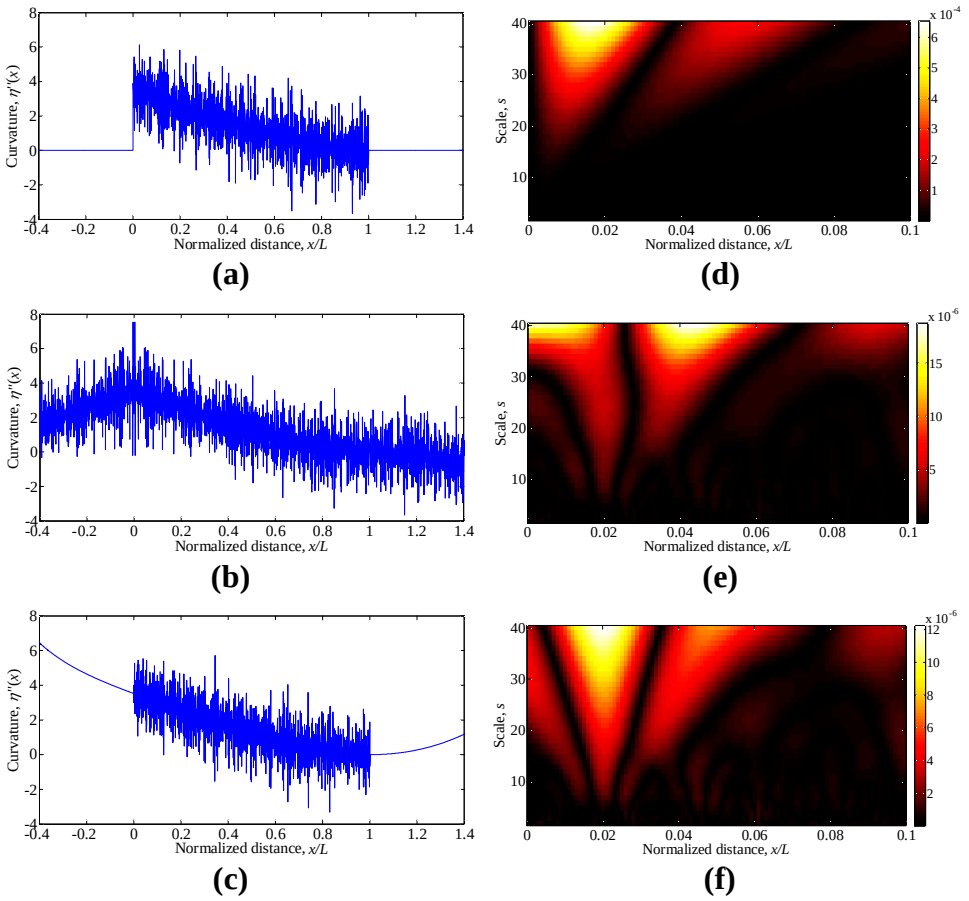

Fig. 4.8 ï Curvature and contour plots of the CWT absolute values of the normalized first modeshape of a cracked cantilever beam with ***ǔ*** = 2% and x_c = 0.02*L*, and SNR=120 dB: (a,d) linear padding method; (b,e) Messinaôs method; (c,f) proposed polynomial padding method.

Figures 4.8(d-f) present zoomed contour plots of the absolute values of the CWT (from scale 1 to scale 40) related to the normalized first modeshape padded using the three methods presented previously.

Since the linear padding method introduces a discontinuity in the second derivative at x = 0 (Fig. 4.8a), high coefficient values arise around that region and the bright cone points towards x = 0 (Fig. 4.8d). The damage location is consequently masked because of the edge effects. Furthermore if only the CWT

coefficients related to a given scale were considered (e.g. scale 24 in Fig. 4.8d), the analysis would locate erroneously the damage at about $x = 0.01L$.

When Messinaôs method is applied, even if a jump in the third derivative occurs at $x = 0$, crack discontinuity at finer and medium scales can be detected as the contour cones point correctly towards the crack location at $x = 0.02L$ (Fig. 4.8). On the other hand, at coarser scales, characterized by narrower bands of lower frequencies, the CWT detects the jump of the third derivative and hence it is unable to locate the damage.

Figure 4.8f shows that, when the proposed polynomial extension method is used, the central bright cone is characterized by an axis centered to the correct damage location. Therefore crack position can be detected at all CWT scales, leading to unambiguous and more reliable damage identification.

The contour plots of the absolute values of the CWT related to the normalized third modeshape of the cracked cantilever beam, obtained using Messinaôs method and the proposed polynomial method, are presented in Fig. 4.9 (the crack is located close to the free end at $x = 0.98L$ and a noise level SNR = 140 dB is imposed). Given the oscillating feature of the modeshape, β_1 and β_2 are assumed to be equal to 0.2 and 0.333, respectively.

Figures 4.9a and 4.9b demonstrate that wavelet analysis fails to detect the damage near the free end when Messinaôs method is applied. This is a consequence of the fact that the curvature near the free end tends to be null and therefore damage identification is more difficult. The jump in the modeshape third derivative at $x = 0$ due to the use of the ñTurnoverò padding method is the main discontinuity that óCoif4ô wavelet detects in analyzing the padded signal.

On the other hand, using the proposed polynomial padding method, no discontinuity is present at the extrema of the signal or its derivatives, and no border distortion is generated by the wavelet transform. The bright cones point properly to the damage position (see Figs 4.9(c-d)).

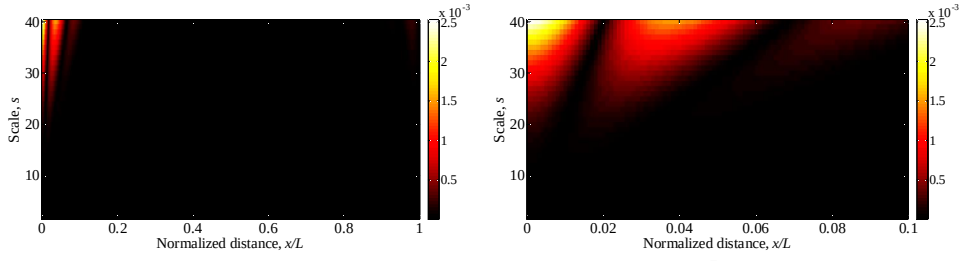

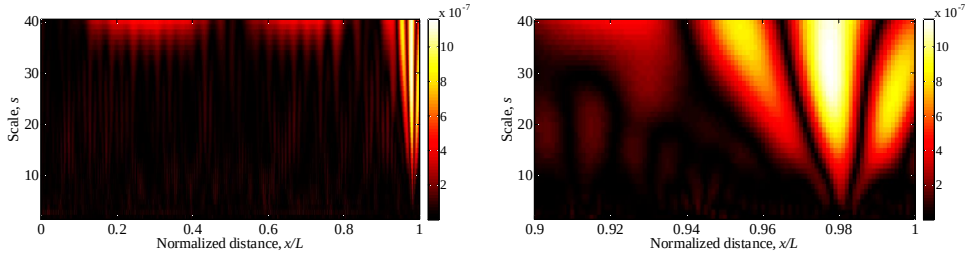

Fig. 4.9 ï Contour plots of the CWT absolute values of the normalized third modeshape of the cracked cantilever beam with $\breve{u}$ = 2% and x_c = 0.98*L*, and SNR=140 dB: (a) Messinaôs method; (b) zoom of (a); (c) proposed polynomial extension method; (d) zoom of (c).

4.4.2 Free vibration response of a simply supported beam

Figure 4.10 shows the effectiveness of Messinaôs method (the ñRotationò method is applied at both extrema) and of the polynomial method (β_1 and β_2 are equal to 1) in the case of the first modeshape of a cracked simply supported beam corrupted by noise (SNR = 140 dB). The crack, close to the left support at x = 0.02*L*, is correctly identified through both methods. Note that since the beam modeshape is sinusoidal, Messinaôs method does not introduce a discontinuity in the signal or its derivatives, and hence no border distortion occurs. Note also that the brightest cone of Fig. 4.10a is shifted at coarser scales to the left with respect to the damage location due to the presence of the mirrored damage at $x = -x_c$.

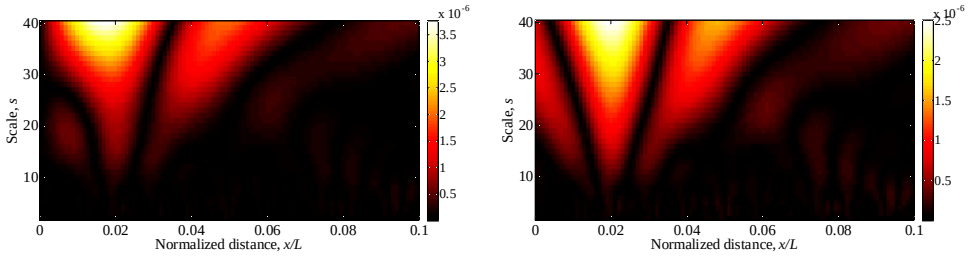

Fig. 4.10 ï Zoomed contour plot of the CWT absolute values of the normalized first modeshape of the cracked simply supported beam with $\breve{u}$ = 2% and x_c = 0.02*L*, and SNR=140 dB: (a) Messinaôs method; (b) proposed polynomial extension method.

4.4.3 Static deflection of a cantilever beam

The normalized noisy static deflections of the cantilever beam subjected to the point load *P* of Fig. 3.3, with an open crack of relative depth $\breve{\alpha}$ = 2%, located at 0.02*L* or at 0.98*L*, are analysed by CWT. The polynomial extension method is applied assuming β_1 and β_2 equal to 1 and compared with Messinaôs method. It can be observed that even if $\eta(x)$ is a cubic function and the continuity of $\eta(x)$ and its derivatives at the boundaries can be satisfied by polynomial functions of degree three, the presence of noise requires extending polynomial functions of eighth or higher order to overcome edge effects.

Both padding methods prove to be effective in analyzing static deflection when the crack is close to the clamped end (Fig. 4.11) or when it is near the free end (Fig. 4.12).

Considering a noise level of SNR = 100 dB, since finer scales are more sensible to noise than coarser ones, the lower parts (from scale 1 to 20) of the CWT contour plots in Figs 4.11a and 4.11c provide somewhat ambiguous damage detection for both the padding methods. On the other hand, by considering the upper parts of these contour plots (from scale 20 to 40) the damage location can clearly be identified (Figs 4.11Fig. 4.11b and 4.11d).

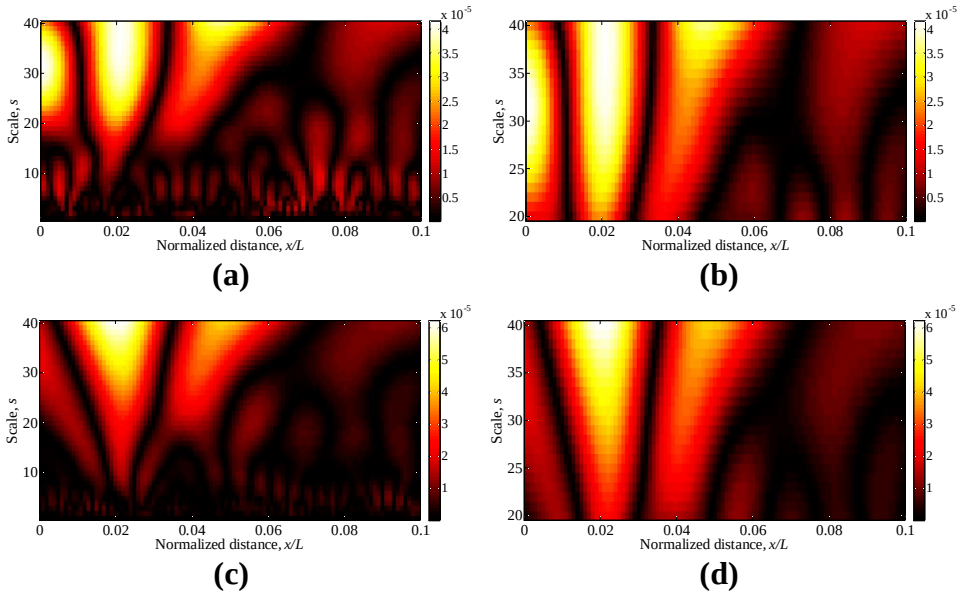

Fig. 4.11 ï Zoomed contour plots of the CWT absolute values of the normalized static deflection of the cracked cantilever beam with $\breve{\alpha}$ = 2% and x_c = 0.02*L*, and SNR=100 dB: (a,b) Messinaôs method; (c,d) proposed polynomial extension method.

Figure 4.12 compares the effectiveness of the two methods in removing edge effects as the noise level increases. When noise level is at SNR = 100 dB, the damage is clearly located by both methods. Increasing the noise level to SNR = 90 dB the damage is partially masked, while at SNR = 80 dB, the noise completely masks the damage. This behavioral trend demonstrates that CWT border distortions are effectively suppressed by both methods, but damage is masked when a certain level of noise (which is dependent on the specific beam features, and damage location and severity) is present.

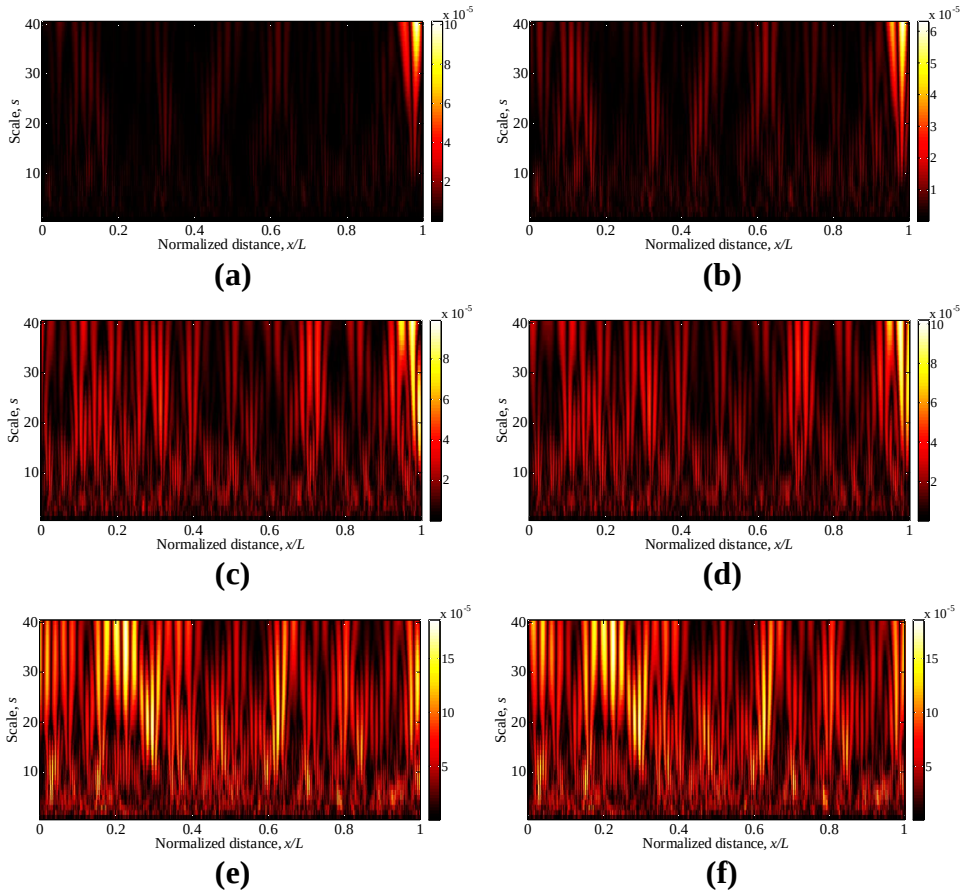

Fig. 4.12 ï Contour plots of the CWT absolute values of the normalized static deflection of the cracked cantilever beam with $\breve{\boldsymbol{u}} = 2\%$ and $x_c = 0.98L$, for varying noise levels: (a,b) SNR=100 dB; (c,d) SNR=90 dB; (e,f) SNR=80 dB. The contours (a,c,e) and (b,d,f) are obtained using Messinaôs method and proposed polynomial extension method, respectively.

At this point, one might ask the reason why using Messinaôs padding method, a crack of α = 2% at $x_c = 0.98L$ in the 3rd modeshape of the cantilever beam, with SNR = 140 dB, cannot be identified by CWT while the same damage in the same location can properly be detected through CWT of the static deflection of the same cantilever, assuming a higher amount of noise (SNR = 100 dB). In fact one would expect that the jump in the third derivative of the static deflection at $x = 0$ due to the use of the ñTurnoverò method would be more severe for the WA than the discontinuity due to the crack at $x/L = 0.98$.

The above can be understand by observing Figs 4.13a and 4.13b where the curvature of the normalized, respectively, first modeshape and static deflection of the cracked cantilever beam with α = 2% and $x_c = 0.98L$ are shown. In Fig. 4.13 the signals are extended at the start part by the ñTurnoverò and at the end part by the ñRotationò and the noise level is equal to SNR = 140 dB. Even though the beam and the crack features are the same, the trend of the static deflection, unlike that of the modeshape, magnifies the singularity due to the crack. Therefore, when the crack is close to the free end of the cantilever, the damage detection through CWT in combination with Messinaôs padding method is more effective in analyzing static deflections than the modeshapes. Finally, in Section 4.4.5 it is shown that the damage identification is more performing in analyzing static deflections than modeshapes of the cantilever irrespectively of the used padding method and the crack location (see Fig. 4.17 below).

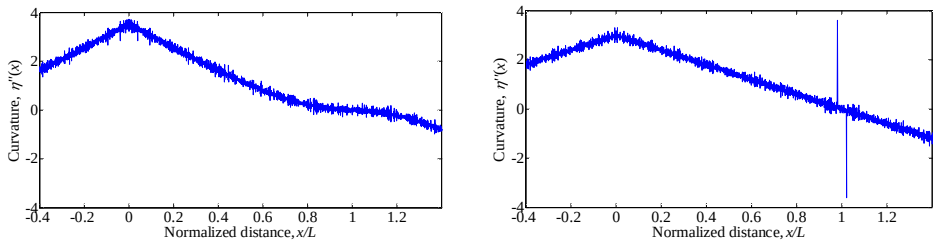

(a) **(b)**

Fig. 4.13 ï Curvature of the normalized first modeshape (a) and static deflection (b) of the cracked cantilever beam with α = 2% and $x_c = 0.98L$, and SNR = 140 dB. The signals $\eta(x)$ are extended at the start part by the ñTurnoverò and at the end part by the ñRotationò.

4.4.4 Static deflection of a simply supported beam

The normalized noisy static deflections of the cracked simply supported beam subjected to the point load P, applied at its middle length (Fig. 3.3), are analysed by CWT using ócoif4ô and the polynomial padding method (β_1 and β_2 are equal to 0.5). Since the point load P is applied at $x/L = 0.5$, the noisy

curvature trend is about triangular (Fig. 4.14a) and the wavelet analysis identifies, in presence of a small crack (***ŭ*** = 2% and x_c = 0.02L), primarily the jump of the deflection third derivative due to P (Fig. 4.14b).

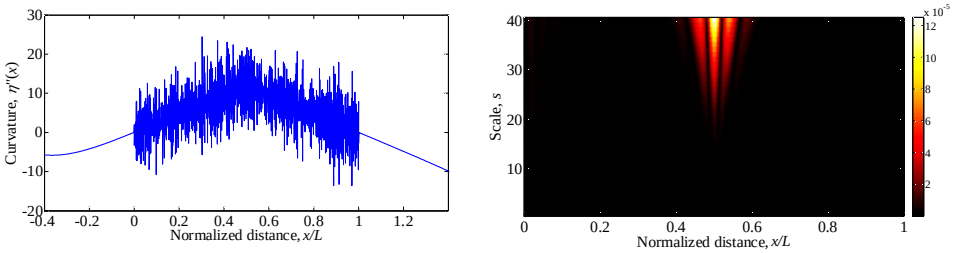

(a) **(b)**

Fig. 4.14 ï Curvature (a) and contour plot of the CWT absolute values (b) of the normalized static deflection of the cracked simply supported beam with ***ŭ*** = 2% and x_c = 0.02L, and SNR = 120 dB. The signal $\eta(x)$ is extended through the polynomial padding method.

To overcome the problem of deflection third order singularity due to P and localize correctly the damage, in the following the two beam portions $(0 \le x/L \le 0.5$ and $0.5 \le x/L \le 1)$ are analysed separately by CWT. Since in the following the crack of ***ŭ*** = 2% is assumed at x_c = 0.02L (SNR = 140 dB) or at x_c = 0.48L (SNR = 140), only the left portion of the beam static deflection $(0 \le x/L \le 0.5)$ is analysed (Fig 4.15). Note that the presence of damage at x_c = 0.5L could be checked by analyzing the beam static deflection due to the load P applied in $x \neq 0.5L$ (e.g. x = 0.7L).

The CWT contour plots of Figs 4.15(a-c) highlight that applying Messinaôs padding method (the ñRotationò is used at the hinged end and the ñTurnoverò at x/L = 0.5), the point load P on the beam deflection still affects the CWT damage detection. It can be observed that the crack at x_c/L = 0.48, where the curvature is considerable, can be identified (Fig. 4.15c), but the same crack at x_c/L = 0.02, where the curvature tends to be null, cannot be detected (Fig. 4.15a). On the other hand, the polynomial padding method (β_1 and β_2 are equal to 1, $\tilde{\beta}_1$ and $\tilde{\beta}_2$ are equal to 0.5), extending differently the deflection signal, allows an effective and clear performance of the CWT damage detection in both the cases (Figs 4.15b and 4.15d).

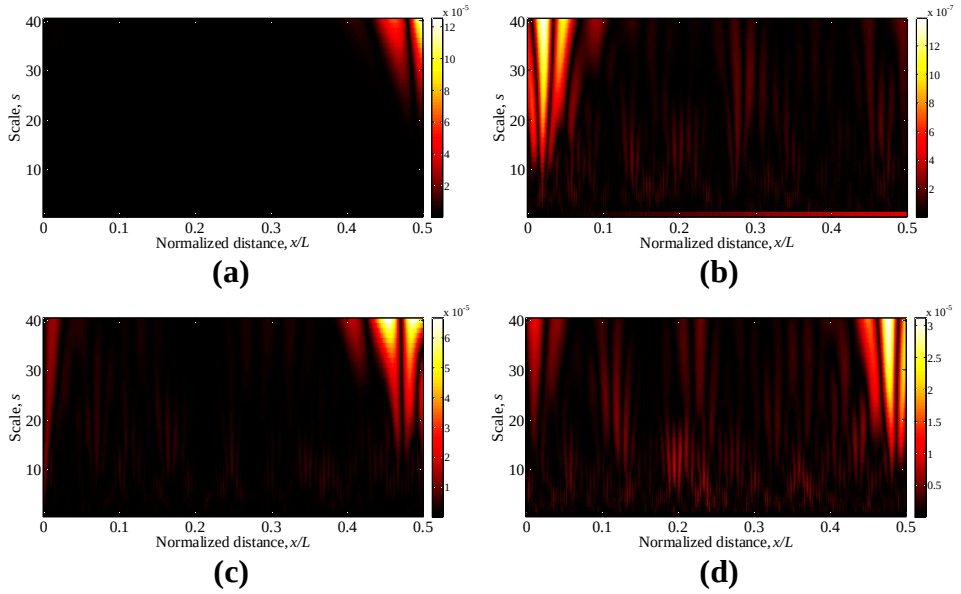

Fig. 4.15 ï Contour plots of the CWT absolute values of the normalized static deflection of the cracked simply supported beam with **ǔ** = 2%: (a,b) x_c = 0.02*L* and SNR = 140 dB where Messinaôs method and the polynomial extension method are respectively used; (c,d) x_c = 0.48*L* and SNR = 110 dB where Messinaôs method and the polynomial extension method are respectively used.

4.4.5 Summary of padding method comparison

The linear padding method, Messinaôs isomorphism method and the proposed polynomial extension method are quantitatively compared in Fig. 4.16 for a range of modeshapes and static deflections obtained by varying the crack depth ($\delta = 0.0001 - 0.9$) and its location (x = 0.02*L*, x = 0.48*L* or x = 0.98*L*). Crack depth is incremented by $d\delta = 10^{-j-2}$ throughout the range $10^{-j-1} < \delta \le 10^{-j}$ where $j = 0,1,2,3$. For a given noise level, the identification criterion considers arbitrarily that the damage is correctly detected if the highest absolute value of the CWT at the scale 24 falls either at the crack location or in the two nearest points (i.e. the preceding and the following point) for 25 different noise random distributions. Figure 4.16 identifies the minimum crack depth sizes correctly identified by each method for a given SNR. In these analyses, the fitting parameters β_1 and β_2 are equal to 1, except in the analysis of the second modeshape of the cantilever beam, where $\beta_1 = 0.15$ and $\beta_2 = 0.125$, and of the first modeshape of the simply supported beam, where $\beta_1 = \beta_2 = 0.1667$. On the other hand, the fitting parameters $\tilde{\beta}_1$ and $\tilde{\beta}_2$ of **ɔ**(*x*) are always equal,

respectively, to β_1 and β_2, except in the analysis of the static deflections of the simply supported beam, wherein they are assumed to be equal to 0.4. For the second modeshape of the cantilever beam, the values $H_1 = \overline{H}_1$ and $H_2 = \overline{H}_2$ are employed as coefficients of the extension polynomial function.

Figure 4.16 clearly shows, for all the conditions being analysed, the weakness of the linear padding method in tackling border distortions. For instance, when the first modeshape of the cantilever beam with x_c = 0.98*L* is analysed, even cracks of about $\delta = 0.9$ are masked by edge effects. Moreover, at a given noise level, the minimum crack size that can be identified using the linear padding method is larger than those detectable using the other methods. For both the linear padding method and Messinaôs method, the plots in Fig. 4.16 display a plateau representing the minimum crack size that can be detected irrespective of SNR. In the linear padding method this plateau occurs because óCoif4ô recognizes the dominance of the discontinuity in the second derivative at *x* = 0 over the discontinuity introduced to the first derivative by the crack. As expected, at higher noise levels, the minimum damage that can be detected increases.

Using Messinaôs method, the observed plateau in the $\delta-$ SNR curves is dependent on the discontinuity in the third derivative at *x* = 0 related to the ñTurnoverò method. Since a jump in the third derivative has less influence on the CWT than one in the second derivative, the minimum detectable crack using Messinaôs method at a given SNR is smaller than that detectable using the linear padding method. When Messinaôs method is applied to the modeshapes of the simply supported beam, the minimum detectable δ decreases monotonically with increasing SNR (Fig. 4.16d). As mentioned above, this is due to the fact that, extending a sinusoidal signal through the ñRotationò method, no edge discontinuities arise in all its derivatives. On the other hand, in analyzing half of the static deflection of the simply supported beam, Messinaôs method results to be weak (Figs 4.16 (g-h)) and, when the crack is close to the application point of the load *P*, it is not robust with respect to different noise distributions (Fig. 4.16h).

The proposed polynomial padding method is observed to be the most effective and versatile method in analyzing different structural responses corrupted by different noise levels. At severe noise levels, the proposed polynomial method and Messinaôs method succeed in identifying very similar minimum detectable damage levels. However, at medium-to-low noise levels, the polynomial method is more successful in removing CWT border distortions, and it is capable of identifying smaller cracks than either of the other two methods.

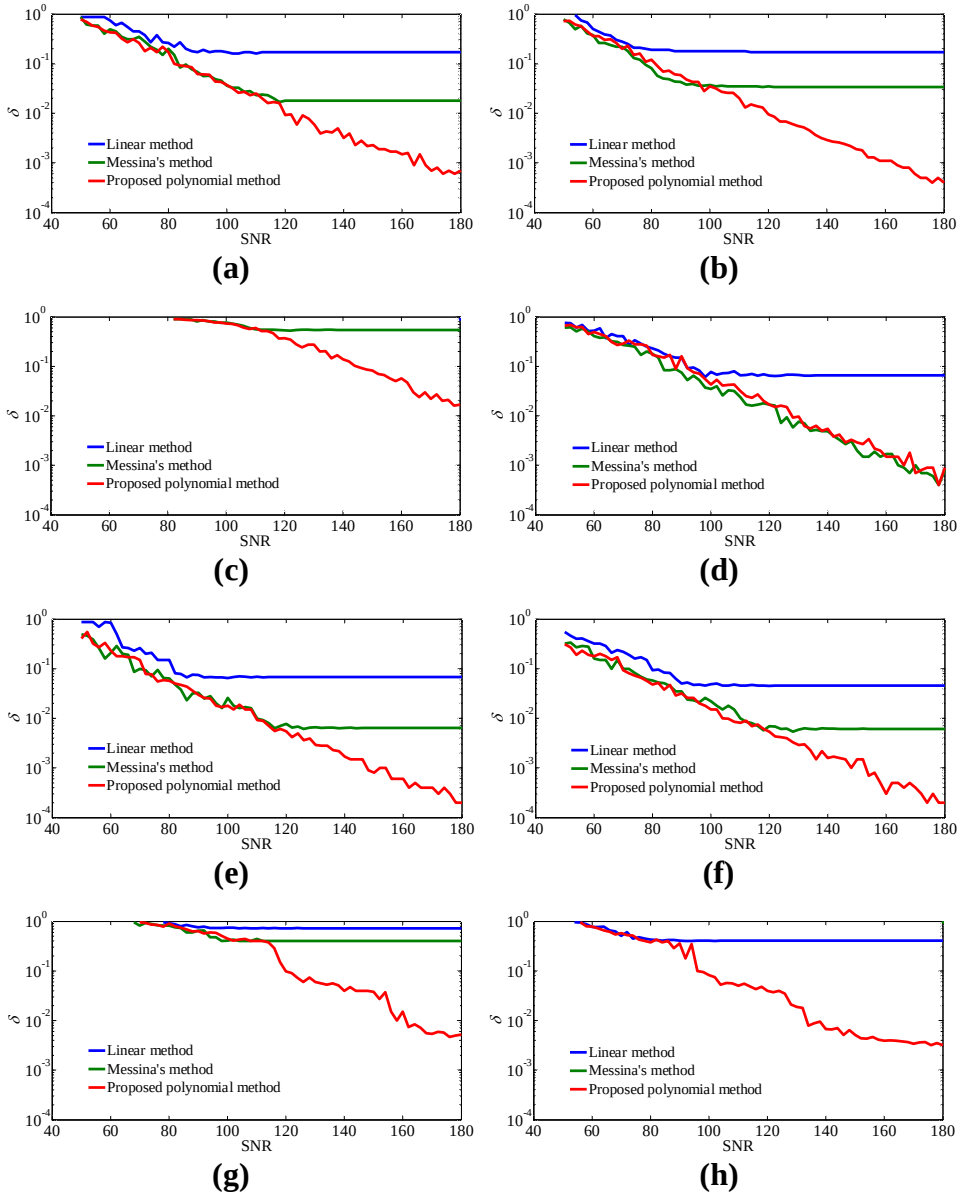

Fig. 4.16 ï Minimum detectable relative crack depth ***ǔ*** against noise level SNR for different padding methods. The following cases are analysed: (a,b) cantilever first and second modeshapes, respectively, with $x_c = 0.02L$; (c) cantilever first modeshape with $x_c = 0.98L$; (d) simply supported beam first modeshape with $x_c = 0.02L$; (e,f) cantilever static deflection with $x_c = 0.02L$ and $x_c = 0.98L$, respectively; (g,h) simply supported beam static deflection with $x_c = 0.02L$ and $x_c = 0.48L$, respectively.

Figure 4.17 shows the comparison of the performance in identifying damage by CWT (at scale 24) applied to the first modeshape and the static deflection of the cantilever beam, using Messinaôs padding method (Figs 4.17(a-b)) and the polynomial padding method (Figs 4.17(c-d)). It can be noted that, regardless of the padding method, the damage identification is more effective when applied to the static deflection than to the modeshapes. This behavior, which is more evident when the crack is located close to the free end (Figs 4.17b and 4.17d), is attributed to the different impact of cracks, at the same size, as the beam shape is made to vary.

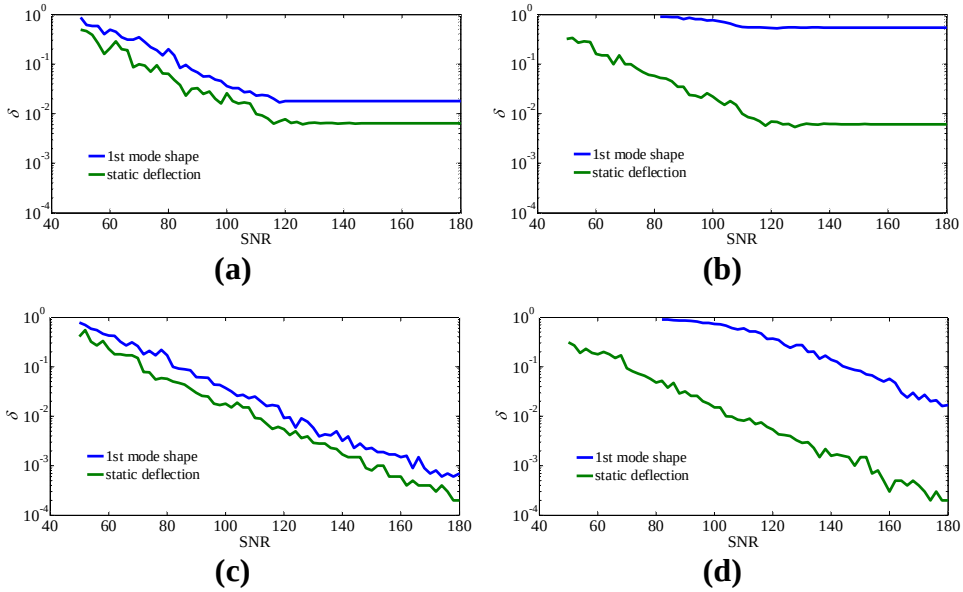

Fig. 4.17 ï Minimum detectable relative crack depth ***ǔ*** against noise level SNR for the first modeshape and the static deflection of the cantilever beam. The padding method and the crack position are varied: (a,b) Messinaôs padding method is used and the crack is located, respectively, at $x_c = 0.02L$ and $x_c = 0.98L$; (c,d) the polynomial padding method is used and the crack is located, respectively, at $x_c = 0.02L$ and $x_c = 0.98L$.

Chapter 5

Sampling effect in damage detection using spatial CWT

5.1 Introduction

In the last decades the researchers have made a great deal of effort in replacing traditional sensors (e.g. accelerometers, strain gages, load cells), which have the limitation of measuring the relevant parameters at a single location and of requiring cumbersome wiring. The modern measurement techniques, instead, can capture the spatial field of the relevant parameters with high precision and in a quasi-continuous manner, even for large civil engineering structures. Such techniques include the Digital Imagine Correlation (DIC) and the digital imagine stereo-correlation (3D-DIC) (Rastogi, 1997; Orteu, 2009; Ozbek et al., 2010), the Global Positioning Systems (GPS) (Nickitopoulou et al., 2006; Casciati & Fuggini, 2009), the Local Positioning Systems (LPS) (Casciati & Wu, 2010; Casciati & Wu, 2012), the scanning laser vibrometers (Stanbridge & Ewins, 1999; Khan et al., 2000; Yang, & Allen, 2011) and the optic fiber sensors (Zhou & Sim, 2002; Li et al., 2004; Adewuyi et al., 2009).

In order to fully exploit the potentiality and versatility of the spatial wavelet analysis when quasi-continuous spatial measurement data are available, the present chapter is centered on the impact of the spatial sampling of beam vibrating shapes in detecting the damage.

The state of the art highlights that in vibration-based damage detection methods the issue of the sampling interval to discretize operational deflection shapes is well known but few authors investigated in depth its effect. Sazonov and Klinkhachorn (2005) provide analytical and numerical arguments to select the optimal sampling interval on curvature or strain energy of modeshapes to maximize sensitivity to damage and accuracy of damage localization. They highlight that the effects of measurement noise invalid the intuitively reasonable idea that smaller sampling intervals mean higher precision in damage localization. Guan and Karbhari (2008), noticing that modal curvature methods

exhibit problems related to large sampling intervals and measurement noise increase by numerical differentiation procedures, propose a new damage identification method based on the concept of element modal strain damage index able to correctly locate a damage region even using sparse measurements of noisy data. Zhong and Oyadiji (2013) analyze the sampling interval sensitivity for damage detection in simply supported cracked beams using three different methods based on the stationary wavelet transform. They search for the proper sampling distance as a function of depth, width and location of the crack as well as of the amount of noise. The proposed methods are shown to be robust if higher modeshapes are considered and to be accurate if the sampling interval with respect to the beam length is equal or less than 0.01. In (Surace et al., 2012; Surace et al., 2013), the authors deal with the problem of crack localization in post-damage operational beam shapes through a method based on a polynomial annihilation technique. Through numerical simulations, they quantify the number of sampling points (19 to 100 sampling points were considered) needed for damage detection. Whilst in absence of noise, even with few measurements points (e.g. 25 data points), a small-medium crack can be located, increasing the noise level cracks can be identified only by using smaller sampling intervals. Many authors (Douka et al., 2003; Rucka & Wilde, 2006b; Zhong & Oyadiji, 2011b) notice that in the presence of course sampling intervals, damage detection may encounter difficulties when CWT is used. To overcome the problem, they adopt the technique of over-sampling the measured data through a cubic spline interpolation.

The present chapter aims at studying in depth the spatial CWT damage identification in beam structures with the goal of answering to the following key questions:

(i) can the cost of damage detection be reduced by down-sampling ?
(ii) what is the minimum number of sampling intervals performing the optimal damage detection ?

The beam structures of Section 3.3.1.3 with constant cross-section and characterized by homogeneous isotropic material with linear elastic behavior are considered in the following.

5.2 Parametric study

A thorough investigation of the effect of the spatial sampling of the beam shapes in identifying the damage through spatial CWT is numerically carried out varying the relevant features of the problem, that is:

(i) the normalized sampling interval dx/L: dx/L is considered equal to 0.025, 0.01, 0.005, 0.0025, 0.001, 0.0005 and 0.00025);

(ii) the noise level: SNR value is assumed equal to 130 dB, 100 dB or 70 dB (see Section 4.2);
(iii) the padding method: the linear padding (Misiti et al., 2000), Messinaôs isomorphism methods (Messina, 2008) and the polynomial padding method (Montanari et al., 2014) are considered (see Sections 4.3 and 4.4);
(iv) the wavelet function: the 4th order Coiflets wavelet (ôCoif4ô), the 2nd order Daubechies wavelet (ôDb2ô), the 4th order Gaussian wavelet (ôGaus4ô) and the real Morlet wavelet (ôMorlô) (Daubechies, 1992) are considered (see Section 2.2.2);
(v) the vibrating shape of the beam: the first three modeshapes of the cantilever and the simply supported beam are considered (see Section 3.3.1.3). Note that in the following the beam shapes are considered normalized with respect to the maximum value of the deflection;
(vi) the relative crack position x_c/L along the beam: x_c/L is considered to be equal to 0.1, 0.3, 0.5, 0.7, 0.9;

In Sections 5.2 and 5.3 cracked beams of length L = 1 m with a rectangular cross-section of height $h = 0.05L$ and width $b = 0.5h$, constituted by an elastic linear isotropic material of Young modulus E = 200 GPa and density ρ = 7850 kg/m^3, are considered. Then, in Section 5.4, the results found in Sections 5.2 and 5.3 are generalized by varying the beam parameters ρ, E, L, h, b.

5.2.1 Criterion for minimum detectable crack size

In order to investigate the effect of sampling interval in CWT damage detection, the minimum detectable (threshold) crack size for a given spatial sampling interval is obtained according to the following criterion based on an iterative procedure.

By increasing gradually the relative crack depth $\breve{\alpha}$ from a value of 0.0001 to 0.95, the wavelet transform is executed at fixed values of the scale s ($s = 2, 4, 6, \ldots, 200$) and the maximum absolute value of the transform is determined for each scale. If at a given relative crack depth such a maximum is always attained for all the scales at the crack position by considering an arbitrary number of 20 different random Gaussian white noise distributions, such a relative crack depth $\breve{\alpha}$ can be regarded to be detectable, otherwise a larger value of $\breve{\alpha}$ has to be assessed. Because of the numerical approximation of the CWT, it is assumed that, according to the aforementioned criterion, the crack depth can be regarded as detectable even if the CWT absolute maximum is attained in either of the two nearest points (i.e. the preceding and the following point) to the actual damage location. For very small sampling intervals ($dx/L < 0.005$), the criterion is relaxed to any of the four nearest points to the damage location.

The results pertaining the effect of sampling interval on the minimum detectable crack size are presented in the following Sections (see the bilogarithmic graphs in Figs 5.1 to 5.7) as a function of the pseudo-frequency f_a (see Section 2.2.2).

5.2.2 Sampling effect varying the padding method

Firstly the present study deals with the effect of sampling distance on CWT near-edge crack detection (x_c/L = 0.1 is considered) using three different padding methods (i.e. linear, Messinaôs and polynomial padding methods). The first modeshape of the cantilever beam is investigated and ócoif4ô wavelet is used.

Figures 5.1(a-c), 5.3(a-c) and 5.4(a-c) represent, for different noise levels and padding method, the minimum detectable relative crack depth $\breve{u}$ as a function of the data relative sampling distance dx/L and of the pseudo-frequency f_a. More in details, graphs (a) refer to ólowô noise (SNR = 130 dB), graphs (b) to óintermediateô noise (SNR = 100 dB) and graphs (c) to óighô noise (SNR = 70). Figures 5.1d, 5.3d and 5.4d summarize the results reported in the graphs (a-c), that is to say, they report the results for the three noise levels being considered as a function of the pseudo-frequency, irrespectively of the sampling interval. Note that the curves in Figs 5.1, 5.3 and 5.4 are plotted by considering an upper limit of $\breve{u}$ equal to 0.95.

By juxtaposing the results reported in Figs 5.1, 5.3 and 5.4, it can be observed that the padding method significantly influences the relation between minimum detectable crack size and pseudo-frequency. When the linear padding method is used, considering $f_a \geq 12$ m^{-1}, at low noise level (SNR = 130 dB) the damage identification results to be a function of the pseudo-frequency only and not of the sampling interval (Fig. 5.1a). Increasing the noise level, instead, at a given value of pseudo-frequency larger sampling intervals result to be more effective in damage detection in comparison to smaller ones (see Figs 5.1(b,c)). This occurrence is deemed to be due to the linear extension method whose performance in reducing edge effects might decrease substantially in the presence of high noise level and very small sampling step.

Moreover, considering $f_a \geq 12$ m^{-1}, the curves in Figs 5.1(a-c) present a positive curvature with a minimum value, regardless of the sampling distance, at about the same pseudo-frequency equal to around 330, 60 and 12 m^{-1} for SNR equal to 130, 100 and 70 dB, respectively (note that in Figs 5.1(b-c) for very low values of dx/L the positive curvature is not evident). This behavioral trend is caused by two reasons: the noise influence and the edge effects due to the linear padding. Moving from the high to low values of f_a, since high values of f_a are very sensible to noise, and smaller cracks can be detected until a minimum detectable crack size for certain level of noise is reached (the part of the curves

with respect to their minimum value is ruled by the *presence of noise*). The smallest detectable crack is obtained because when decreasing beyond a certain value f_a, the wavelet detects only edge discontinuity due to the padding method (the part of the curves on the left with respect to their minimum value is ruled by the *edge effects*).

Finally, as expected, the minimum detectable crack size tends to decrease with decreasing noise level (see Fig. 5.1d).

(a)

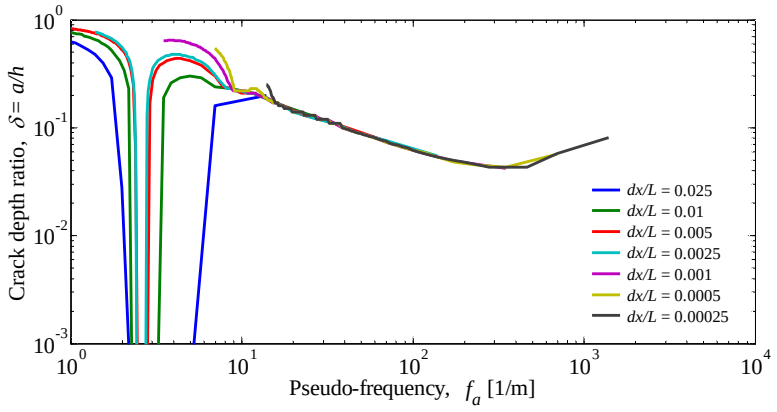

(b)

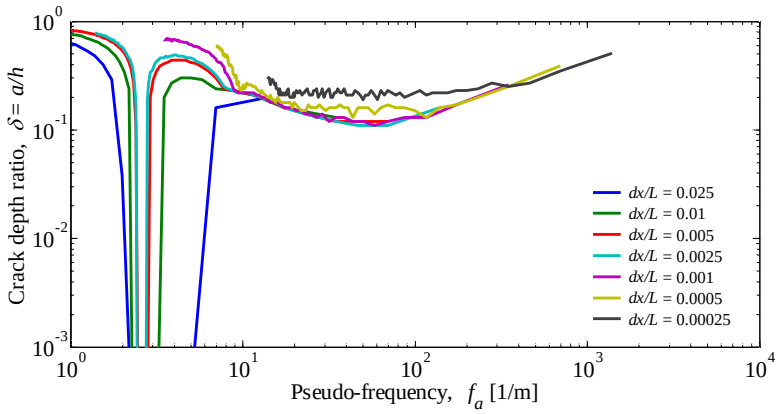

(c)

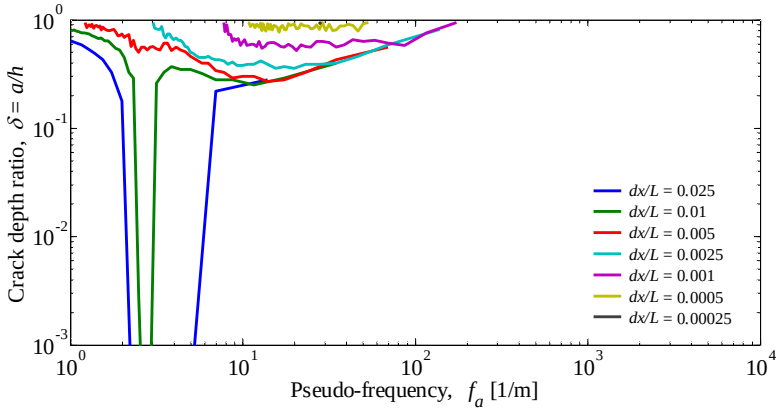

(d)

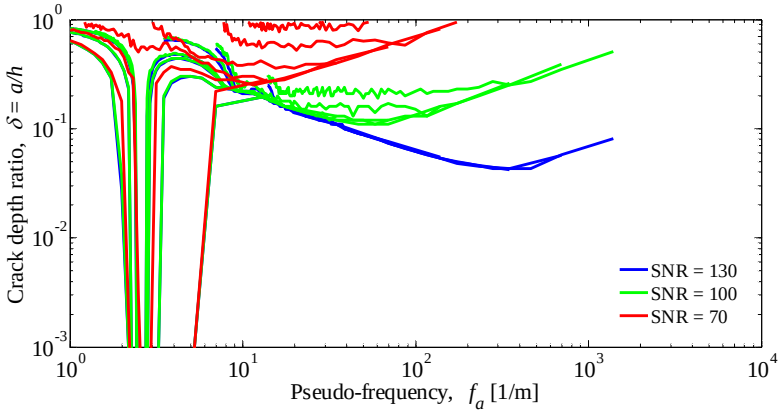

Fig. 5.1 ï Impact of the sampling interval in damage detection by spatial CWT with óCoif4ô. The linear padding method is used. The first modeshape of the cantilever beam with crack at $x_c/L = 0.1$ is analysed. (a) SNR = 130 dB; (b) SNR = 100 dB; (c) SNR = 70 dB; (d) summary of the results plotted in (a), (b) and (c).

At this point it might be worth explaining the reasons why for $f_a < 12$ m^{-1} the curves of Fig. 5.1 deviate from the behavioral trend described above, showing a vertical asymptote corresponding to about $f_a = 2.4$ m^{-1}. These reasons are related to the edge effect at $x = 0$ due to the linear padding method and the crack location close to that beam end ($x_c/L = 0.1$), as it is discussed at the following.

As shown in Fig. 4.8a, when the linear padding is applied to a signal end with curvature different from zero (at $x = 0$ in the case of the cantilever 1st modeshape), the second derivative of the padded signal presents a severe discontinuity at that position. Consequently, as shown in Fig. 5.2, the CWT analysis of the padded beam shape exhibits, when ***ŭ*** is smaller than a certain value, the highest coefficients close to the clamped end of the beam. More in

details, using s = 8, corresponding to f_a = 17.4 m^{-1}, the highest value of the wavelet coefficients is at $x/L \cong 0.02$ when $\delta \le 0.05$, while using s = 52, corresponding to f_a = 2.7 m^{-1}, it is at $x/L = 0.1$, regardless of the value of $\breve{\boldsymbol{u}}$ (the blue curves related to $\breve{\boldsymbol{u}}$ = 0 are overlapped by the green and red ones). This means that, around the pseudo-frequency range $f_a = [2-4]$ m^{-1}, the CWT analysis does not detect the presence of tiny cracks but the discontinuity due to the linear padded method at x = 0 (Fig. 5.2b) and the vertical asymptotic trend of Fig. 5.1 takes place. On the other hand, as shown in Fig. 5.2a, by analyzing the signal by means of high pseudo-frequencies (f_a = 17.4 m^{-1} is used), for small crack size the wavelet analysis is more sensitive to the discontinuity due to the padding method, while for large crack size, the wavelet analysis is more sensitive to the crack discontinuity and the damage identification is satisfied. Analogous reasoning can be made for f_a smaller than about 1.3 m^{-1}.

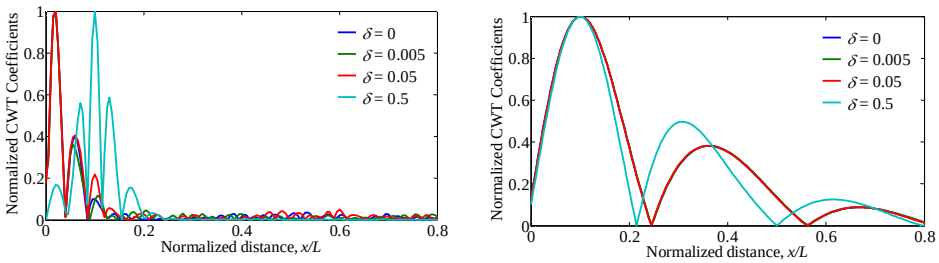

Fig. 5.2 ï Zoom of the normalized absolute values of the CWT coefficients obtained by analyzing the normalized first modeshape of the cantilever beam with crack at x_c/L = 0.1 varying the relative crack depth $\breve{\boldsymbol{u}}$. The signals are sampled at dx/L = 0.005, considering SNR = 100 dB. Two different scales are considered: (a) s = 8, corresponding to f_a = 17.4 m^{-1} in Fig. 5.1; (a) s = 52, corresponding to f_a = 2.7 m^{-1} in Fig. 5.1b.

Conversely to the results pertaining to the linear padding, by applying Messinaôs padding method, regardless of the noise level, the CWT- f_a curves for different values of dx/L tend to overlap and the damage identification becomes, with a good approximation, function of the pseudo-frequency only (see Fig. 5.3). This implies that, since the scale can be made to vary as desired, large sampling intervals can be as effective as small ones. As for linear padding with decreasing noise level, smaller cracks can be detected (Fig. 5.3d).

As in Fig. 5.1, the curves of Fig. 5.3 present a positive curvature with a minimum value, but now, given the smaller influence of border discontinuities on the CWT introduced by Messinaôs padding method (see Section 4.4.1), the curves of Figs 5.3(a-c) attain their minimum value at a lower pseudo-frequency with respect to that of Figs 5.1(a-c). The values of pseudo-frequencies offering

the optimal damage detection are equal to around 45, 16 and 5 m^{-1} for SNR values equal to 130, 100 and 70 dB, respectively.

(a)

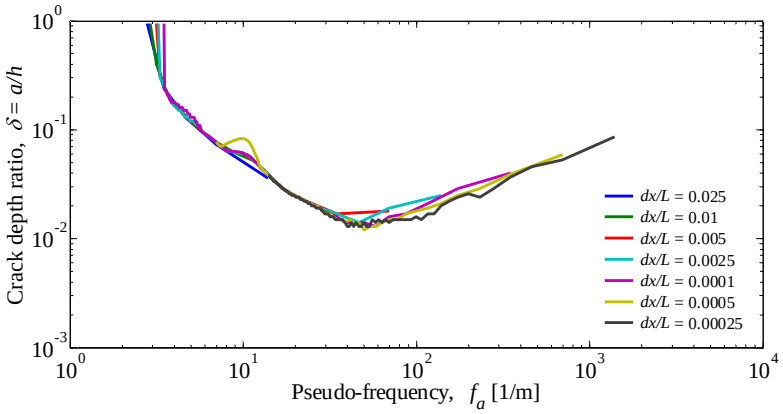

(b)

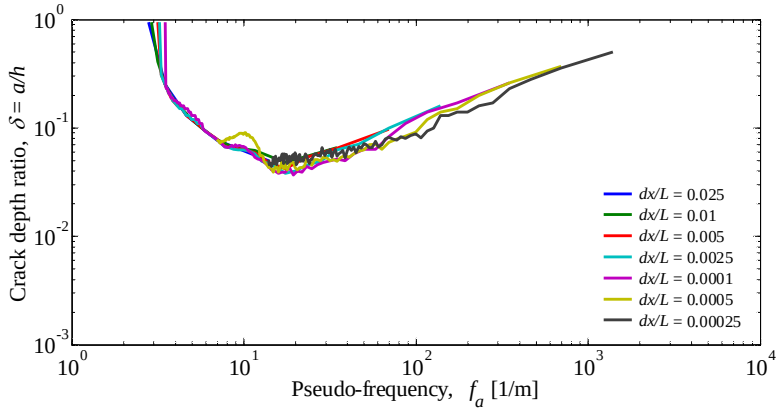

(c)

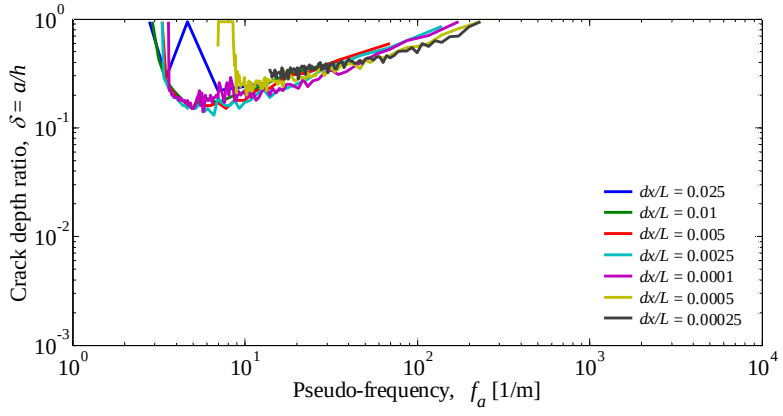

(d)

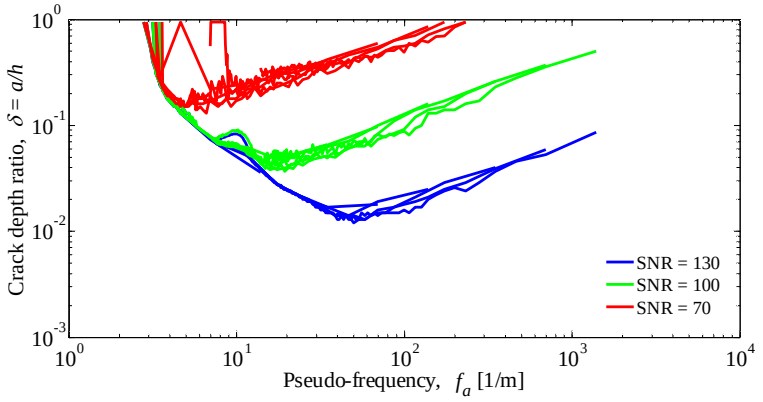

Fig. 5.3 ï Impact of the sampling interval in damage detection by spatial CWT with óCoif4ô. Messinaôs padding method is used. The first modeshape of the cantilever beam with crack at x_c/L = 0.1 is analysed. (a) SNR = 130 dB; (b) SNR = 100 dB; (c) SNR = 70 dB; (d) summary of the results plotted in (a), (b) and (c).

By using the polynomial padding method (see Section 4.3), (the following parameters are assumed, $\beta_1 = \beta_2 = 1$, $H_1 = \overline{H}_1$, $H_2 = \overline{H}_2$) the damage identification turns out to be, with a good approximation, function of the pseudo-frequency only (Fig. 5.4). However the of Fig. 5.4 curves exhibit a different trend than that, characterized by a of positive curvature, of the curves related to the linear and Messinaôs padding methods. They decrease monotonically from high to low pseudo-frequencies until, in correspondence to a specific frequency, a sudden jump occurs toward the upper limit of ***ǔ*** (say, equal to 0.95). Such a specific value of pseudo-frequency corresponds at the same time, with good approximation, to the *lowest* and *optimal* value of pseudo-frequency for damage identification (the optimal value is that allowing the minimum crack size to be detected as the pseudo-frequency is made to vary). It needs to be underlined that this lowest/optimal value of f_a is the same independently by the noise amount (Fig. 5.4). As shown further in Section 5.2.3, this result appears to occur when the polynomial padding method is used together with wavelet functions characterized by many vanishing moments.

The jump in the curves of Fig. 5.4 at the lowest/optimal value of f_a occurs because, by analyzing the cracked beam shape with wavelet functions characterized by lower pseudo-frequencies, even large cracks cannot be localized due to the influence of the edge effects. In Section 5.2.5 it will be illustrated that lower pseudo-frequencies can detect cracks located more far away from the beam end, but in any case below a certain value of f_a, damage detection fails due to the edge effects even in the presence of large cracks.

Figures 5.4(a-c) show that the curves related to dx/L = 0.00025 exhibit jumps to the upper limit of ***ŭ*** at higher values of pseudo-frequency in comparison to those related to larger sampling intervals. This trend is due to the fact that, when the crack is near the signal extremum, the wavelet analysis is tainted by edge distortions, and, particularly for very low sampling intervals, the maximum CWT coefficient value falls not exactly at the crack location (or at its two four nearest points, as permitted by the detection criterion), but at sampling points other from that of the crack location. In Section 5.2.5, it will be shown that when the crack is located far away from the beam ends, regardless of the value of the sampling interval, the lower bound of pseudo-frequency is the same.

Hereafter, since its effectiveness and versatility in handling general shapes of beam deflection (see Chapther 4), the polynomial padding method is used. Note that, in order to reduce the computational cost, $H_1 = \overline{H}_1$ and $H_2 = \overline{H}_2$ is always imposed, but this assumption does not affect the results of this investigation. The $f_{a,opt}$ is used to indicate the optimal value of pseudo-frequency f_a giving the minimum detectable crack size ($f_{a,opt}$ is equal to about 12 m^{-1} in Fig. 5.4). The value $f_{a,opt}$ of pseudo-frequency coincides, as shown above, approximately with the lowest pseudo-frequency for performing damage detection.

(a)

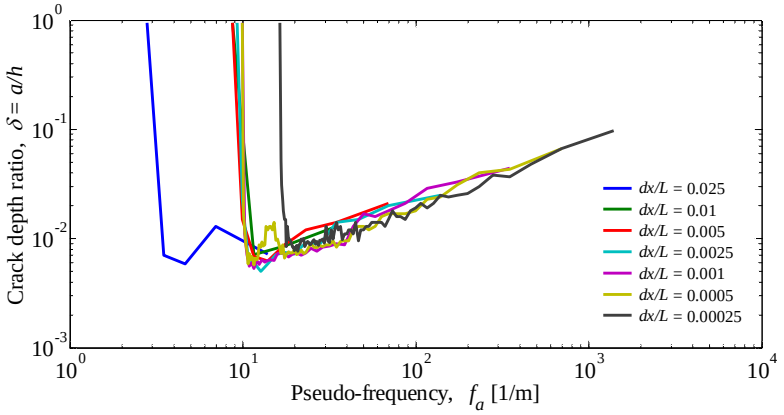

(b)

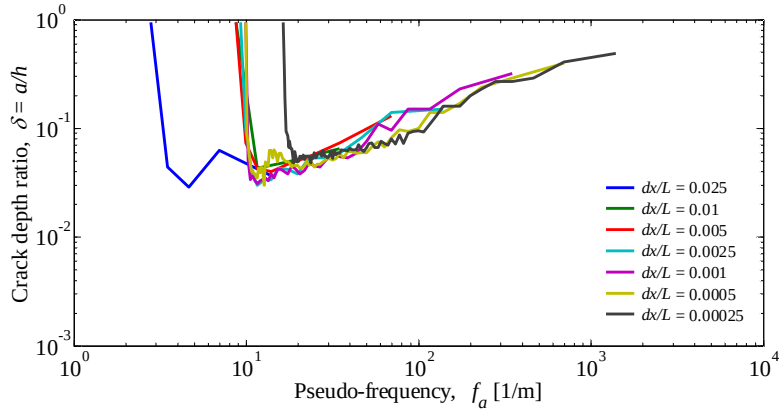

(c)

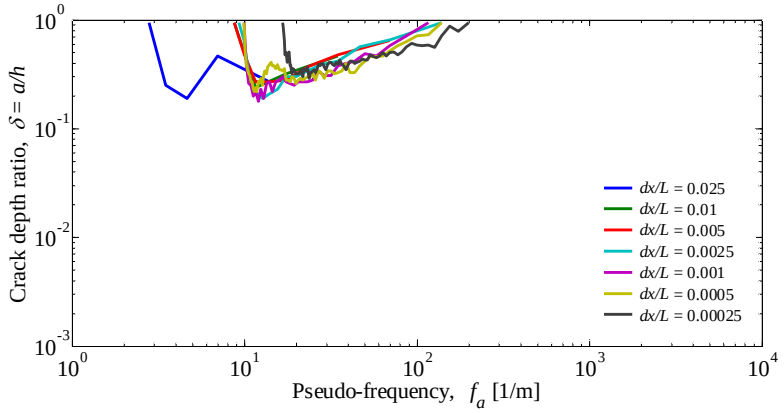

(d)

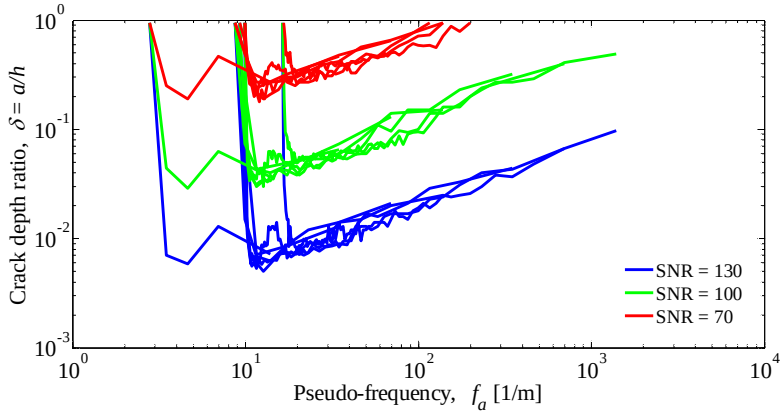

Fig. 5.4 ï Impact of the sampling interval in damage detection by spatial CWT with óCoif4ô. The polynomial padding method is used. The first modeshape of the cantilever beam with crack at x_c/L = 0.1 is analysed. (a) SNR = 130 dB; (b) SNR = 100 dB; (c) SNR = 70 dB; (d) summary of the results plotted in (a), (b) and (c).

5.2.3 Sampling effect varying the wavelet function

Figure 5.5 displays the results of the sampling step impact in the CWT damage detection using the 2nd order Daubechies (óDb2ô), the 4th order Gaussian (óGaus4ô) and the real Morlet (óMorlô) wavelet functions. The first modeshape of the cantilever beam with crack at $x_c/L = 0.1$ is analysed.

Figure 5.5a shows that CWT damage identification by óDb2ô, conversely to that by the other wavelet functions, depends on both ó*dx/L*ô and f_a. In addition, óDb2ô exhibits a poor damage identification performance due to its characteristic of having two vanishing moments only (see Section 2.2.2). Similarly to óCoif4ô, using óGaus4ô and óMorlô, the damage detection is, with good approximation, only pseudo-frequency dependent in the medium-high f_a range. Moreover, using óMorlô $f_{a,opt}$ is function of the sampling interval *dx/L* (Fig. 5.5c). The behavioral trend of results shown in Fig. 5.5 seems to be similar for the different SNR values being considered.

The comparison with the results for óCoif4ô (see Fig. 5.4d) demonstrates that óCoif4ô exhibits the best performances in damage detection in comparison to the other wavelet functions, and hence it is adopted in the following.

(a)

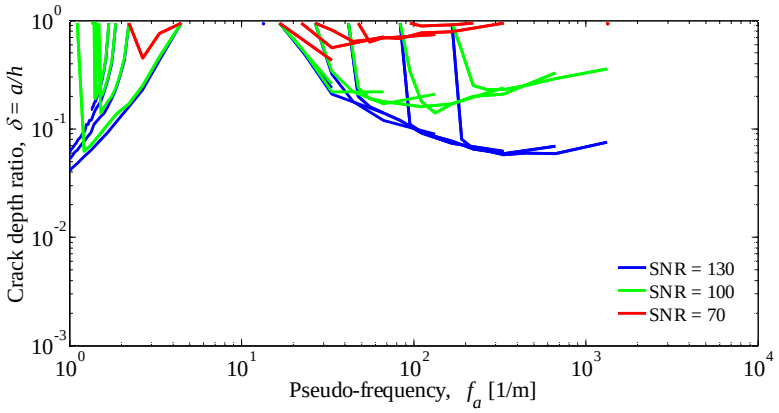

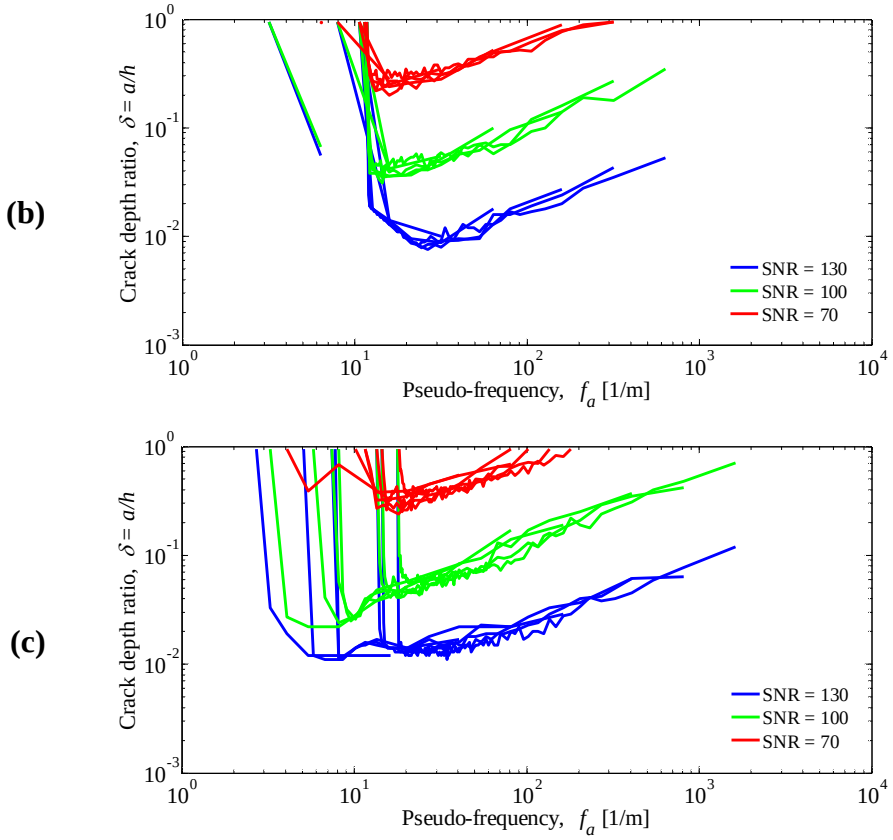

Fig. 5.5 ï Impact of the sampling interval in damage detection by spatial CWT varying the wavelet function. The polynomial padding method is used and the first modeshape of the cantilever beam with crack at x_c/L = 0.1 is analysed. (a) óDb2ô; (b) óGaus4ô; (c) óMorlô.

5.2.4 Sampling effect varying the modeshape

The second and the third modeshapes of the cantilever beam and the first three modeshapes of the simply supported beam are analysed. The crack is located at x_c/L = 0.1. Figure 5.6 illustrates the effect of sampling interval in CWT damage detection using óCoif4ô and the polynomial padding method ($\beta_1 = \beta_2 = 1$ is used in Figs 5.6(a,c), $\beta_1 = 0.25$ and $\beta_2 = 0.33$ in Fig. 5.6b, $\beta_1 = \beta_2 = 0.5$ in Fig. 5.6d and $\beta_1 = \beta_2 = 0.3$ in Fig. 5.6e). The jumps of the curves are dependent on the analysed modeshape and, neglecting the disturbance due to the edge effects at low frequencies, the damage identification appears to be clearly

function of f_a only. In Figs 5.6(a-e) the optimal pseudo-frequency $f_{a,opt}$ is, respectively, equal to about 11 m^{-1}, 18 m^{-1}, 12 m^{-1}, 16 m^{-1} and 21 m^{-1}.

(a)

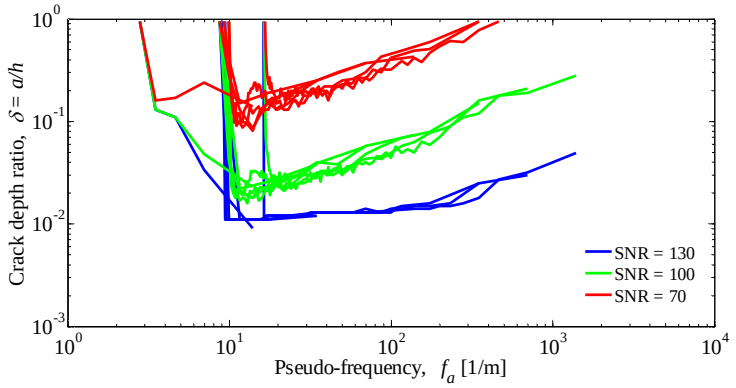

(b)

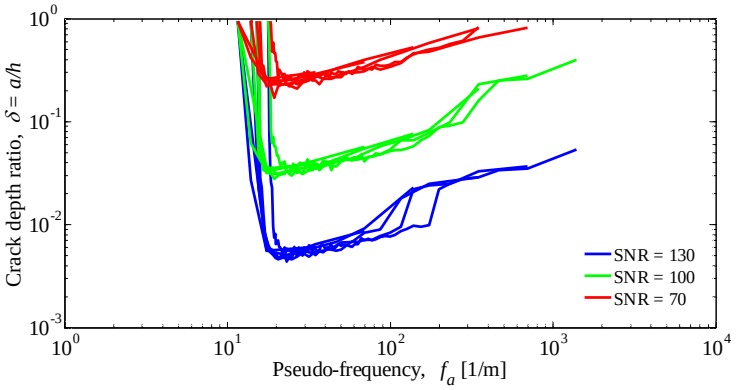

(c)

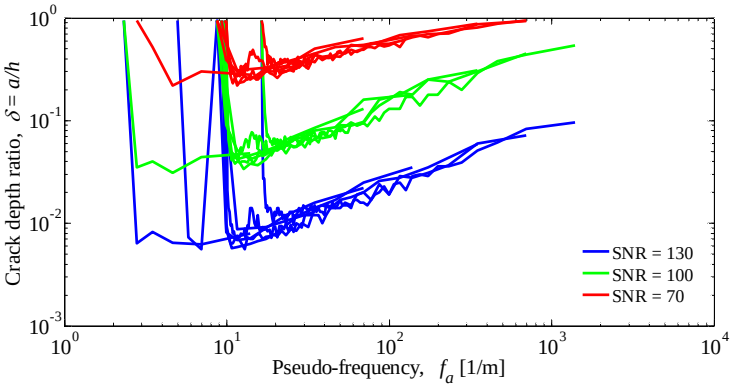

(d)

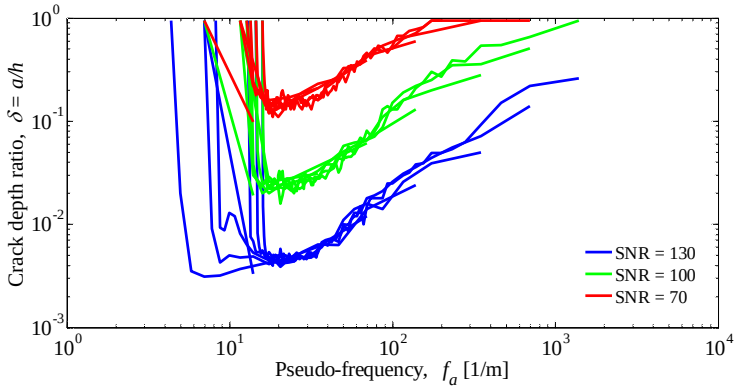

(e)

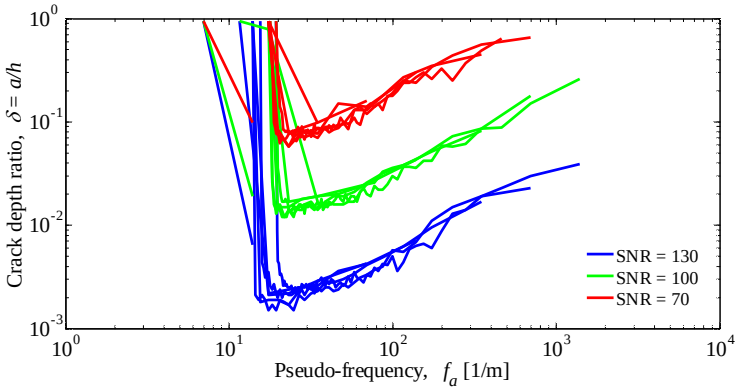

Fig. 5.6 ï Impact of the sampling interval in damage detection by spatial CWT with óCoif4ô. The polynomial padding method is used and different beam modeshapes with the crack at x_c/L = 0.1 are analysed. (a,b) second and third modeshape of the cantilever beam, respectively; (c,d,e) first, second and third modeshape of the simply supported beam, respectively.

5.2.5 Sampling effect varying the crack position

The effect of the sampling interval in the CWT damage detection is investigated varying the crack location: x_c/L = 0.3, 0.5, 0.7 and 0.9 are considered. The first modeshape of the cracked cantilever beam is analysed. By juxtaposing the results of Fig. 5.7 with those reported in Figs 5.1 to 5.6, the influence of border distortions in dictating the optimal value $f_{a,opt}$ of pseudo-frequency of the curves is clearly manifested. The more the crack location is far from either beam end, the lower is the optimal pseudo-frequency $f_{a,opt}$. This means that damage detection can be achieved considering a reduced number of sampling points. Furthermore, Figs 5.7(a-c) show that, since the crack is far away from the beam ends, the $f_{a,opt}$ is the same for every curves. In Fig. 5.7d, instead,

since the crack is close to the beam end (i.e. x_c/L = 0.9), a similar trend to that of Fig. 5.4d is shown. In Figs 5.7(a-d) the optimal pseudo-frequency $f_{a,opt}$ is, respectively, equal about 6 m^{-1}, 2.5 m^{-1}, 6 m^{-1} and 12 m^{-1}.

(a)

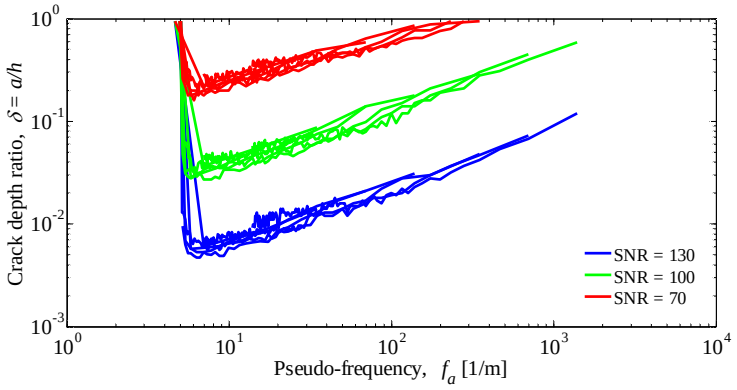

(b)

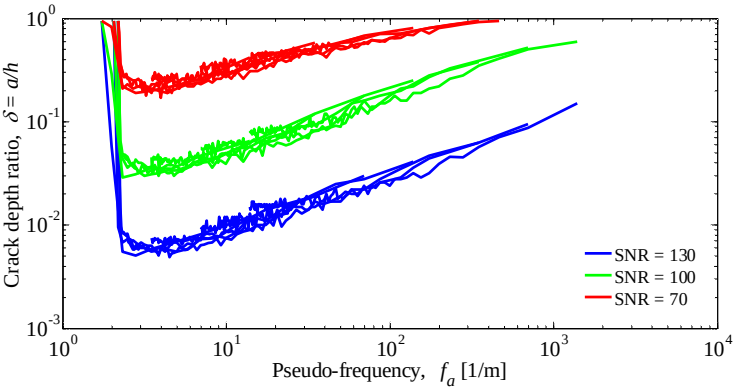

(c)

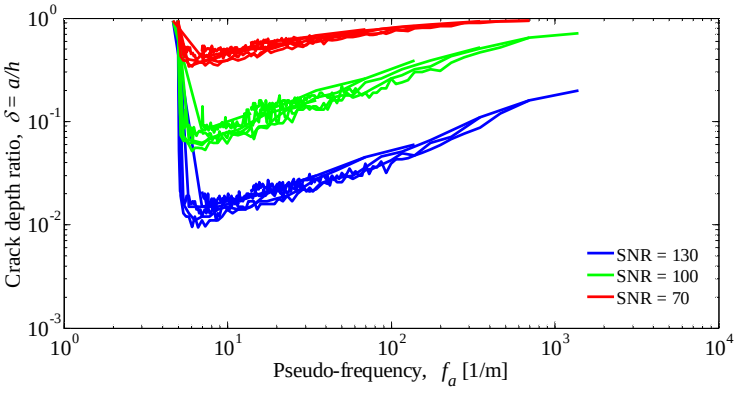

(d)

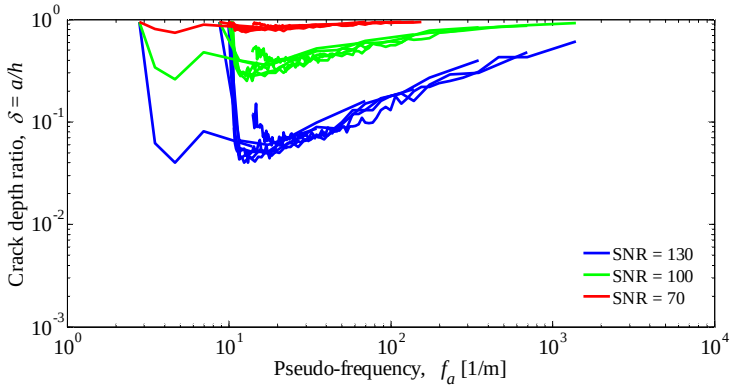

Fig. 5.7 ï Impact of the sampling interval in damage detection by spatial CWT with óCoif4ô. The polynomial padding method is used. The first modeshape of the cantilever beam with crack at different locations is analysed. (a) x_c/L=0.3; (b) x_c/L=0.5; (c) x_c/L=0.7; (d) x_c/L=0.9.

5.3 Discussion of the results

From the results of Section 5.2, pertaining to polynomial padding method and óCoif4ô wavelet, the following conclusion can be drawn:

(i) there is an optimal value of pseudo-frequency, independent on the noise level, which maximizes the performance of the damage detection for a given beam deflection shape and crack position;

(ii) by adjusting the wavelet scale, damage detection performances can be similar for small and large sampling intervals.

Being the CWT damage detection with good approximation function of the pseudo-frequency only, it is numerically illustrated how the choice of the proper scale range is essential in detecting the damage when different sampling intervals are considered.

Firstly, the first modeshape of the cantilever beam, defined in Section 5.2, with a crack of $\boldsymbol{\delta} = 0.2$ at $x_c/L = 0.1$ is analysed. The noise level is assumed to be equal to 70 dB. The same modeshape is sampled at $dx/L = 0.01$ and $dx/L = 0.0004$.

Figs 5.8(a,b) report the contour plots of the CWT (óCoif4ô and the polynomial padding method with $\beta_1 = \beta_2 = 1$ are used) when the signal is sampled at $dx/L = 0.01$, and the scale ranges $s = [4-24]$ (i.e. $s = 4,5,6\ldots, 24$) and $s = [4-6]$ are respectively used. The CWT coefficients, considering the broad scale range, completely mask the crack location (Fig. 5.8a), which on the contrary can be identified using the narrow scale range (Fig. 5.8b).

Figures 5.8(c-d) highlight that even if the signal is sampled at an extremely small sampling interval (dx/L = 0.0004), the CWT damage detection can be achieved only considering a proper scale range. The damage localization at the scale range $s = [2-40]$ fails (Fig. 5.8c), while it succeeds for $s = [96-158]$ (Fig. 5.8d).

The results reported in Fig. 5.8 are in agreement with those of Fig. 5.4c, which deal with the same beam deflection. Indeed Fig. 5.4c highlights that the optimal pseudo-frequency is in the range $f_a = [11-18]$ m^{-1}, which corresponds for dx/L = 0.01 to the scale range $s = [4-6]$, and for dx/L = 0.0004 to $s = [96-158]$.

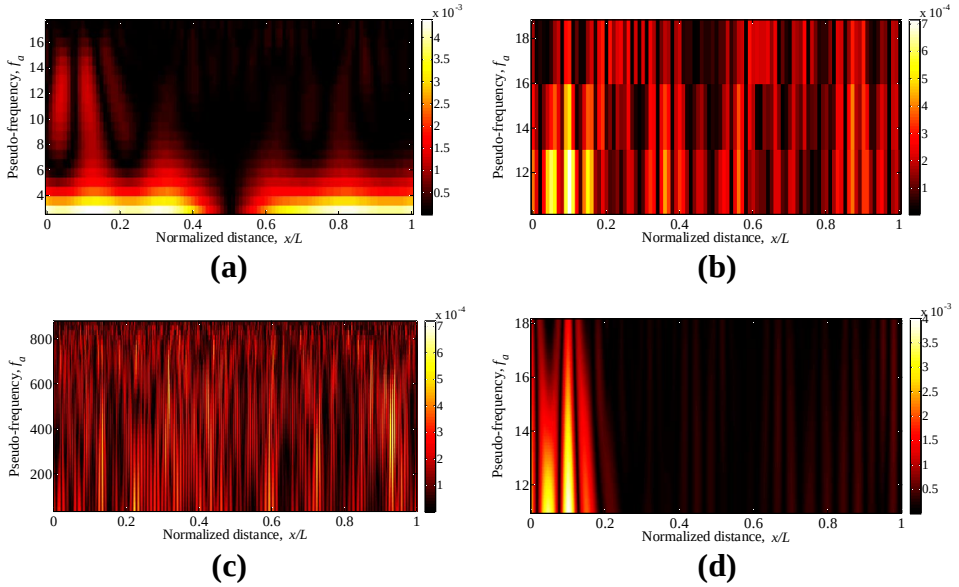

Fig. 5.8 ï Contour plots of the spatial CWT using óCoif4ô and the polynomial padding method (SNR = 70 dB). The first modeshape of the cantilever beam with crack of ***ǔ*** = 0.2 at x_c/L = 0.1 is analysed. Sampling interval dx/L and scale range are varied: (a) dx/L = 0.01, $s = [4-24]$; (b) dx/L = 0.01, $s = [4-6]$; (c) dx/L = 0.0004, $s = [2-40]$; (d) dx/L = 0.0004, $s = [96-158]$.

Then, the third modeshape of the simply supported beam with a crack of ***ǔ*** = 0.01 at x_c/L = 0.1 is analysed. The modeshape is sampled at dx/L = 0.005 and the noise level is assumed to be equal to 100 dB.

Figures 5.9(a-c) report the contour plots of the CWT (óCoif4ô and the polynomial padding method with $\beta_1 = \beta_2 = 0.33$ are used) when the scale ranges $s = [2-4]$, $s = [6-8]$ and $s = [10-12]$ are respectively considered to analyse

the same modeshape. The CWT coefficients at $s=[2-4]$ (Fig. 5.9a) and at $s=[10-12]$ (Fig. 5.9c) completely mask the crack location and hence damage detection fails. On the other hand, using the scale range $s=[6-8]$, the crack is properly localized (Fig. 5.9b). It can be noted that the results of Fig. 5.9 are in agreement with those reported in Fig. 5.6e, where the same beam deflection is considered. In fact, using the scale range $s=[6-8]$ when *dx*/*L* is equal to 0.005 corresponds to analyse the beam shape at a pseudo-frequency range $f_a=[17-23]$ m^{-1} centered to the optimal pseudo-frequency, and to be able to detect cracks with $\delta \geq 0.01$ (Fig. 5.6e).

(a)

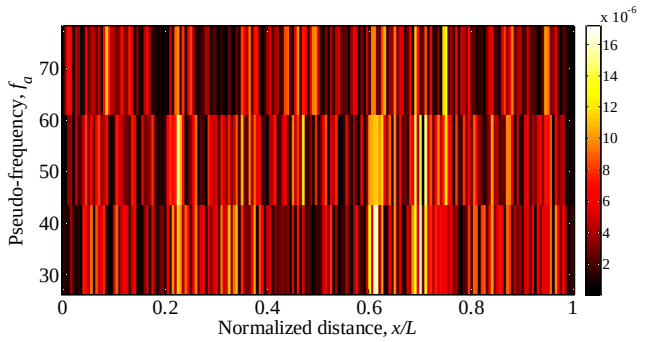

(b)

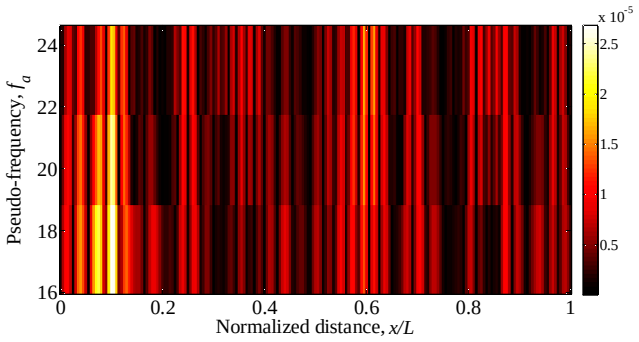

(c)

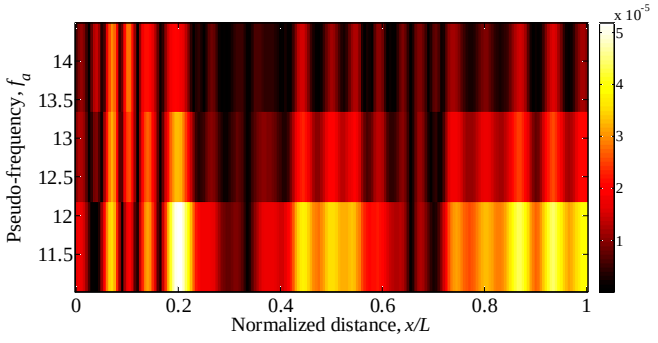

Fig. 5.9 ï Contour plots of the spatial CWT using óCoif4ô and the polynomial padding method (SNR = 100 dB). The third modeshape of the simply supported beam with crack of $\breve{u}$ = 0.01 at x_c = 0.1m is analysed. The modeshape is sampled at dx/L = 0.005 and the scale range is varied: (a) $s = [2-4]$; (b) $s = [6-8]$; (c) $s = [10-12]$.

5.4 Generalization of the parametric study

The results reported in Figs 5.4 to 5.7 in terms of minimum detectable crack size are related to beams characterized by particular values of the parameters ρ, h, b, L and E. In this Section, the influence of these beam parameters on the effect of sampling interval and on the optimal pseudo-frequency in the CWT damage identification is analysed.

Since the material density ρ affects the natural frequencies of the cracked beam but not its modeshapes, this beam parameter is not considered in the generalization of the parametric study. Then, by substituting the LEFM expression of the local rotational stiffness k_c due to the crack (Eq. 3.1) in the boundary condition representing the rotation discontinuity at the crack section (Eq. 3.15), we can write:

$$\eta_2'(x_c) - \eta_1'(x_c) = 2h\,\tilde{f}(\delta)\,\eta_2''(x_c). \qquad 5.1$$

where $\tilde{f}(\delta) = \left(\delta/(1-\delta)\right)^2 (5.93 - 19.69\delta + 37.14\delta^2 - 35.84\delta^3 + 13.12\delta^4)$ is a function of the relative crack depth $\breve{u}$ only.

Equation 5.1 demonstrates that the rotation discontinuity due to the crack is a function of h and $\breve{u}$, but not of the other beam parameters b and E. Therefore, at equal values of h and $\breve{u}$, keeping L constant, the beam deflection shape and, consequently, the CWT damage detection do not vary. In summary, similarly to the density ρ, the beam parameters b and E are not considered in the generalization of the parametric study.

Figure 5.10 presents the results, at different noise levels, of the CWT damage detection in terms of minimum detectable crack size, when the first modeshapes of cantilever beams with different height values h, crack at x_c/L = 0.1 and L = 1 m are analysed. Three different values of h are assumed (0.5m, 0.05m and 0.005m) in order to vary substantially the stiffness of the beam. As expected, Fig. 5.10 highlights that increasing the height h of the beam, and hence its stiffness, smaller cracks can be detected at equal values of pseudo-frequency. Moreover, Fig. 5.10 points out that, varying h, the performance of the CWT damage detection remains independent on dx/L and that h has no influence on the optimal pseudo-frequency value.

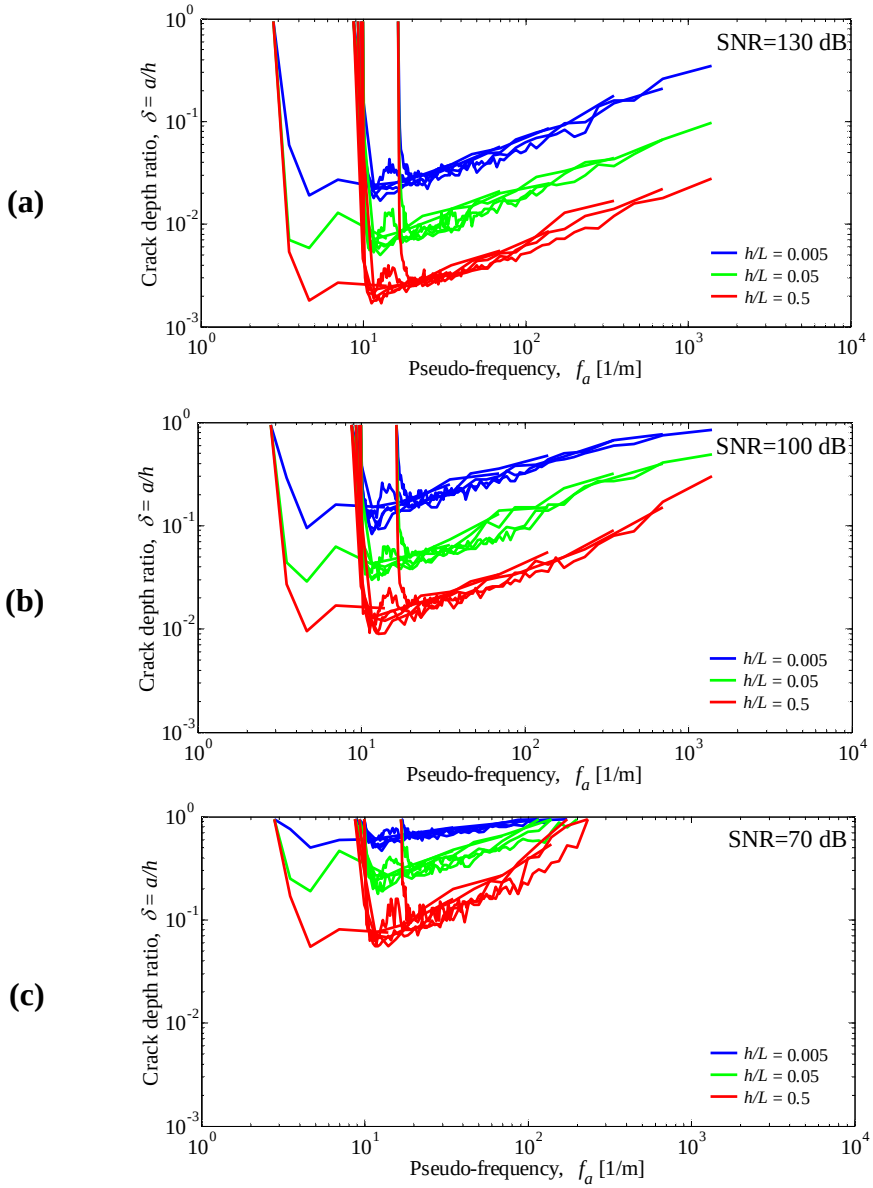

Fig. 5.10 ï CWT damage detection results in terms of minimum detectable crack size when the first modeshapes of cantilever beams with three different h values, crack at x_c/L = 0.1 and L = 1 m are analysed. Different noise levels are considered: (a) SNR = 130 dB; (b) SNR = 100 dB; (c) SNR = 70 dB.

The results obtained so far demonstrate that the optimal pseudo-frequency $f_{a,opt}$ is independent of the beam parameters b, h, E and ρ and hence it is function

of the padding method, the wavelet function, the beam shape and the relative crack position x_c/L. It remains to be discussed the relationship between $f_{a,opt}$ and the beam length L.

Consider a deflection shape of a beam long $L = L_1 = 1$ m and discretized by $dx = dx_1$. The beam has a crack at $x_{c,1}/L_1$. In addition, consider the same deflection shape for a beam of length $L = L_2$ Í 1 m, with crack at $x_{c,2}/L_2 = x_{c,1}/L_1$ and discretized by $dx = dx_2$. Executing the CWT with óCoif4ô and the polynomial padding method, the optimal pseudo-frequency of the beam of unit length can be express as:

$$f_{a,opt,1} = \frac{f_{c,Coif4}}{dx_1 s_1} = \text{f (beam deflection } x_{c,1}/L_1, L_1 = 1), \tag{5.2}$$

where f(Ã) express the dependence of $f_{a,opt}$ on same beam parameters and $f_{c,Coif4}$ indicates the center frequency of óCoif4ô.

The optimal pseudo-frequency of the beam with length L_2 is given by:

$$f_{a,opt,2} = \frac{f_{c,Coif4}}{dx_2 s_2} = \text{f (beam deflection}, x_{c,2}/L_2, L_2 \neq 1). \tag{5.3}$$

Let us now introduce the following normalized optimal pseudo-frequency for the beam of length L_2:

$$f^*_{a,opt,2} = \frac{f_{c,Coif4}}{\frac{dx_2}{L_2} s_2}. \tag{5.4}$$

Such a normalized quantity can be regarded as the optimal pseudo-frequency of a beam with spatial parameters normalized with respect to L_2, that is $dx_2^* = dx_2/L_2$, $L_2^* = L_2/L_2 = 1$. Given the dependence of the optimal pseudo-frequency on beam deflection, x_c/L and L, it follows that, since $x_{c,1}/L_1 = x_{c,2}/L_2$ by hypothesis,

$$f^*_{a,opt,2} = f_{a,opt,1} \tag{5.5}$$

and, thus

$$\frac{f_{c,Coif4}}{\frac{dx_2}{L_2} s_2} = f_{a,opt,1}. \tag{5.6}$$

Finally, combining Eqs 5.6 and 5.3, the relationship between $f_{a,opt,2}$ and $f_{a,opt,1}$ becomes:

$$f_{a,opt,2} = f_{a,opt,1} L_2. \tag{5.7}$$

Equation 5.7 shows that, at equal beam deflection shape and relative crack location x_c/L, the optimal pseudo-frequency of a beam is equal to the product of its length by the optimal pseudo-frequency of a beam of unit length. Note that Eq. 5.7 could be also easily be derived through the Buckingam theorem of dimensional analysis.

The relation expressed by Eq. 5.7 is numerically verified by considering the first modeshapes of cantilever beams of different length L, with h = 0.05 m, crack at x_c/L = 0.1, and different noise levels (Fig. 5.11). The beam lengths are assumed to be equal to L = 1 m (Fig. 5.11a), L = 2 m (Fig. 5.11b) and L = 3 m (Fig. 5.11c), while different sampling intervals are considered for discretizing the beam deflections (Tab. 5.1).

Tab. 5.1 ï Sampling intervals considered to discretize the beam deflections of different lengths.

***L* = 1 m**		***L* = 2 m**		***L* = 3 m**	
dx	***dx/L***	***dx***	***dx/L***	***dx***	***dx/L***
0.01	0.01	0.01	0.005	0.05	0.01667
0.0025	0.0025	0.004	0.002	0.01	0.00333
0.0005	0.0005	0.0008	0.0004	0.003	0.001

(a)

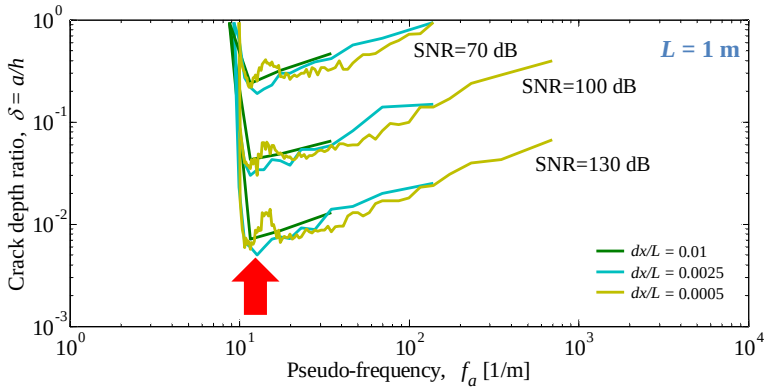

(b)

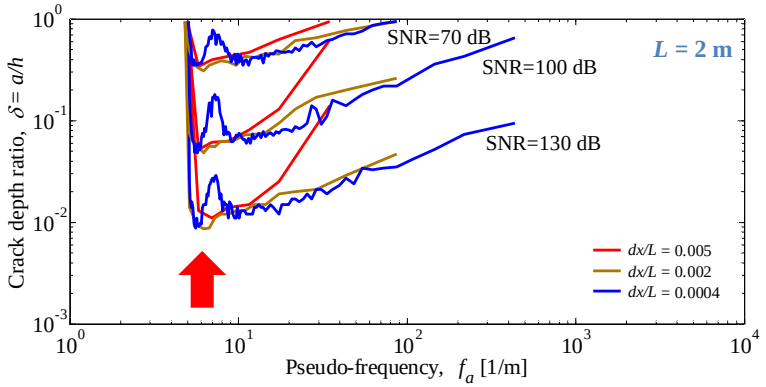

(c)

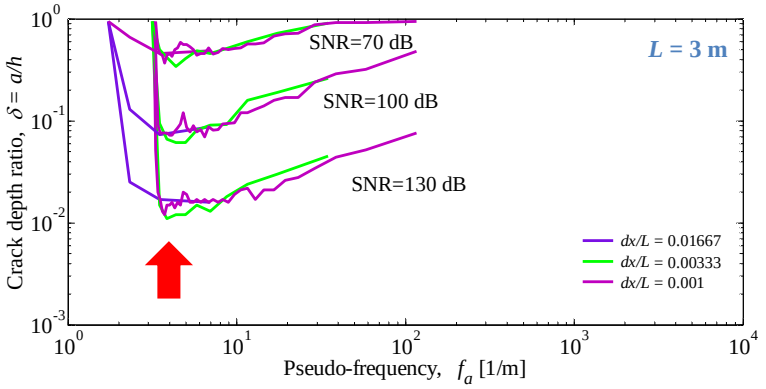

Fig. 5.11 ï CWT damage detection results in terms of minimum detectable crack size when the first modeshapes of cantilever beams of three different lengths with h = 0.05 m and crack at x_c/L = 0.1 are analysed. Different SNR values are considered: 130 dB, 100 dB and SNR = 70 dB. The beam lengths are equal to: (a) L = 1 m; (b) L = 2 m; (c) L = 3 m.

The results of Fig. 5.11 point out that, regardless of the noise amount, there is a specific value of optimal pseudo-frequency which depends on the beam length. This value is equal to about 11 m^{-1}, 5.7m^{-1} and 3.5 m^{-1} for L = 1 m, L = 2 m and L =3 m, respectively.

As shown in Fig. 5.12, by plotting the minimum detectable crack size against a normalized pseudo-frequency (equal to the pseudo-frequency times the beam length), the curves of Fig. 5.11 tend to converge together and to exhibit the same normalized optimal pseudo-frequency.

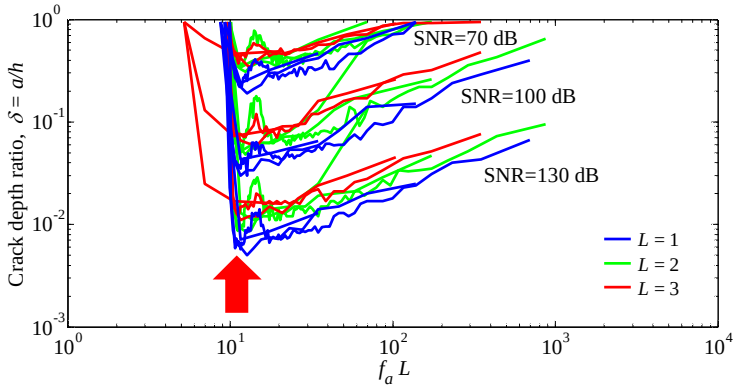

Fig. 5.12 ï Collection of the CWT damage detection results of Fig. 5.11 plotted versus the pseudo-frequency multiplied by the beam length.

5.5 Concluding remarks

The key parameter of the CWT damage detection, executed using the polynomial padding method and a wavelet function with a significant number of vanishing moments (e.g. óCoif4ô), is the optimal pseudo-frequency, representing the pseudo-frequency of the wavelet which allows the detection of the minimum crack depth. The optimal pseudo-frequency value is dependent on the beam deflection shape, the relative crack location x_c/L, the length L of the beam, while it is not influenced by the noise level and the parameters ρ, E, h and b.

The above dependence can be formally written as:

$$f_{a,opt} = \text{f (beam deflection}, x_c/L) \qquad 5.8$$

Using the normalized pseudo-frequency $f_a^* = f_a L$ (note that f_a^* is proportional to n/s, where n is the number of sampling intervals along the beam), Eq. 5.8 can be generalized as follows:

$$f_{a,opt}^* = f_{a,opt} L = \text{f (beam deflection}, x_c/L) \qquad 5.9$$

Figure 5.13 illustrates the $f_{a,opt}^*$ against x_c/L curves pertaining to the first three modeshapes of cantilever and simply supported beams. It can be noted that, mainly due to the edge effects, $f_{a,opt}^*$ turns out to be higher near the beam ends, especially for the third modeshapes.

(a)

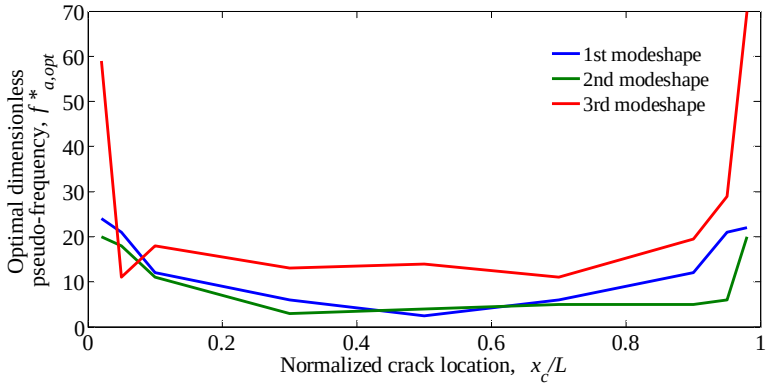

(b)

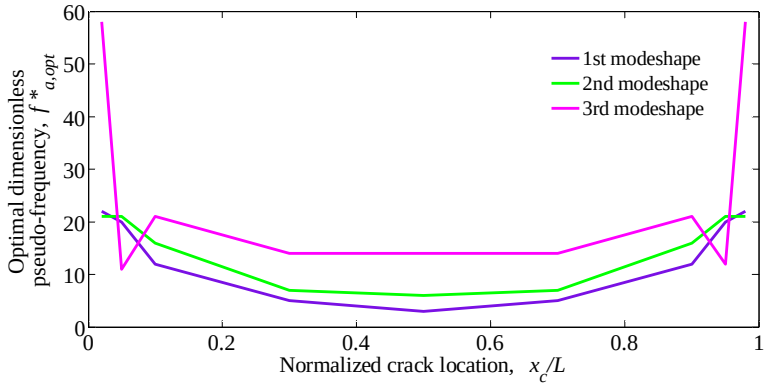

Fig. 5.13 - The optimal dimensionless pseudo-frequency $f^*_{a,opt}$ for the CWT damage detection is plotted against the normalized crack location for the first three modeshapes of: (a) cantilever beams; (b) simply supported beams.

The results of Fig. 5.13 can be understood also in the following manner. For a given wavelet scale, it is possible to know the optimal number of sampling intervals needed to detect the smallest crack located at x_c/L from a beam vibration modeshape. For example, suppose to monitor the service state of a wind turbine blade of L = 50 m through the spatial CWT using the polynomial padding method and óCoif4ô wavelet. By analyzing its first modeshape or its operational shapes similar to it, the optimum sampling interval capable of detecting the smallest crack at at least 1 m distant from the beam ends, e.g. using s = 2, is

$$dx = \frac{f_c\, L}{f^*_{a,opt}\, s} = \frac{0.6957 \cdot 50}{24 \cdot 2} \cong 0.72 \text{ m}.$$

Finally, from the definition of $f^*_{a,opt}$, the optimal number L/dx of sampling intervals to obtain the best CWT damage detection at the scale s for a given crack location x_c/L, is equal to $f^*_{a,opt}\, s / f_c$. As an example, in Fig. 5.14 the minimum of

such an optimal number of sampling intervals is considered by taking $s = 2$ (the value of $s = 1$ is discarded in the present study) and it is plotted as a function of x_c/L.

(a)

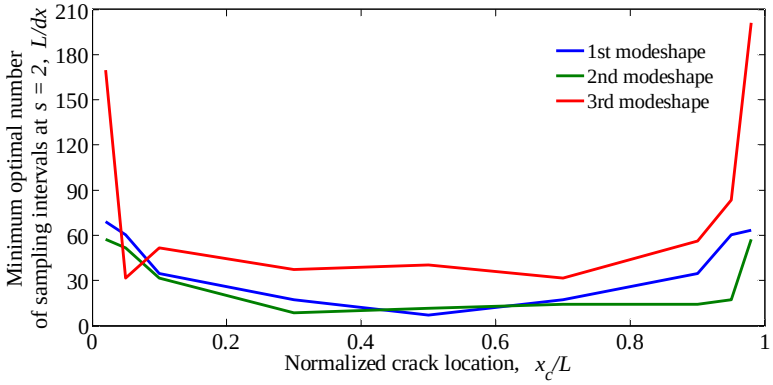

(b)

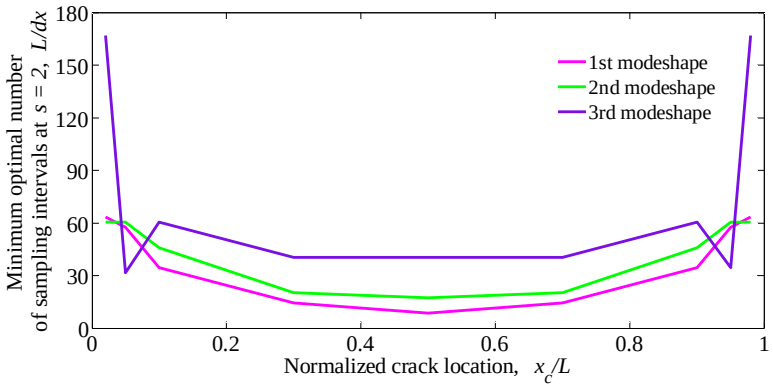

Fig. 5.14 - The minimum optimal number of beam sampling intervals, L/dx, to perform the optimum CWT damage detection at scale $s = 2$ is plotted against the normalized crack location for the first three modeshapes of: (a) cantilever beams; (b) simply supported beams.

Chapter 6

Nonlinear damage identification in cracked beams through time-space wavelet analysis

6.1 Introduction

In this chapter the problem of the quantification of damage severity for SHM is discussed. It is well-known that wavelet analysis is, in the space domain, an efficient way to determinate the damage location (Section 2.3.2), while, in the time domain, it is an efficient tool to identify the system stiffness variation (Section 2.3.1). Based on the idea of combining the information of the structural response in both space and time domains, a new time-space wavelet-based technique aimed at identifying the nonlinear behaviour of damage is developed.

The FE model of a fiber-reinforced cantilever beam, with rectangular cross-section and breathing crack, exposed in Section 3.3.2, is used to simulate the nonlinear, static and dynamic, structural response. On the basis of particular conditions related to the beam deflection CWT and of the features of ócoif4ô (the results of this chapter pertain to ócoif4ô only, even though other wavelet functions, such as the 8th order of Symlets, ómorlô and the 5th order of Coiflets, could be used), a linear relation between the values of the relative rotation due to the crack and the normalized wavelet coefficients at the crack position is ruled out. By analysing through CWT the time sequence of the beam response in the space domain through the aforementioned linear relation, the nonlinear structural behaviour due to damage is identified. The effectiveness of the method in calibrate a small crack is discussed with respect to the wavelet scale, the noise level and the spatial sampling interval.

6.2 Normalized CWT coefficients and crack relative rotation

In the following, on the basis of numerical findings, a linear relation between the values of the relative rotation due to the crack and the normalized CWT coefficients at the crack location, function of the wavelet scale, is determined.

Consider two linear elastic cantilever beams, modelled as in Section 3.3.1.3, of length L = 1 m and having very different values of flexural stiffness EI/L equal to 0.0015 and 0.15 Nm. Through CWT, using óCoif4ô at s = 8 and the polynomial padding method ($\beta_1 = \beta_2 = 0.2$), the static *non-normalized* deflections of the beams due to a point load P = 10 kN at the free end (see Fig. 3.3) are analysed. The both cases of intact structure and damaged structure with crack of rotational stiffness k_c = 8000 kNm at x_c/L = 0.2 (note that, according to Eqs 3.15 and 3.12, the relative rotation φ_c for P = 10 kN is equal to 0.001 rad) are considered. No noise is added to the deflections which are sampled at dx/L = 0.001. The results are shown in Fig. 6.1, where the wavelet coefficients $\overline{W}(t,s)$, normalized with respect to dx^2, are considered so that the values of the coefficients become independent of the signal sampling interval.

Observing the results pertaining to the first beam with lower stiffness and thus larger curvature, the wavelet transform of the undamaged beam deflection attains normalized values of the coefficients along the beam (Fig. 6.1a), of the same order of magnitude than those obtained by analyzing the damaged beam deflection (Fig. 6.1b). Note that in Fig. 6.1b the coefficient at the crack position x_c of value $h_{d,1} = 1.89 \cdot 10^{-3}$ can be read as the sum of two contributions: that due to deflection of the undamaged structure, $h_{u,1} = 2.56 \cdot 10^{-4}$ (see Fig. 6.1a), and that due to the crack discontinuity, $h_{c,1}$ (see Fig. 6.1b). Consequently we have $h_{d,1} \approx h_{u,1} + h_{c,1}$, and hence, $h_{c,1} \approx h_{d,1} - h_{u,1} \approx 1.63 \cdot 10^{-3}$.

The results related to the second beam with higher stiffness and thus lower curvature (Figs 6.1(c-d)) show that, for undamaged structure the wavelet coefficients have the same trend as that of Fig. 6.1a, but with values about two orders of magnitude smaller, i.e. $h_{u,2} = 2.56 \cdot 10^{-6} << h_{u,1} = 2.56 \cdot 10^{-4}$. The normalized wavelet coefficients of Fig. 6.1d, instead, attain a peak at the crack position, $h_{d,2} = 1.63 \cdot 10^{-3}$, while tend to negligible values at the other positions along the beam. As discussed before, we have $h_{d,2} \approx h_{u,2} + h_{c,2}$, but being $h_{u,2} << h_{d,2}$, thus $h_{d,2} \approx h_{c,2}$. Finally, comparing Fig. 6.1d and 6.1b it is noticeable that $h_{d,2} \approx h_{c,2} \approx h_{c,1} = 1.63 \cdot 10^{-3}$, that is to say that the value of the normalized wavelet coefficient at the crack location due to the crack discontinuity appears to be a function of the relative rotation.

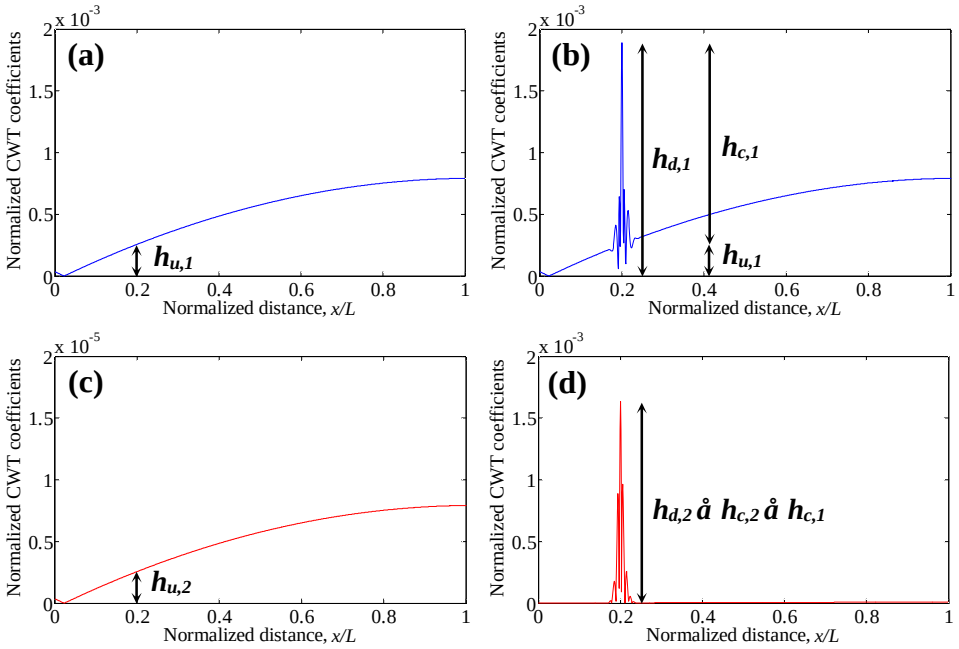

Fig. 6.1 ï Absolute value of the normalized CWT coefficients at s = 8 obtained by analyzing the static *non-normalized* deflection of cantilever beams of length L = 1 m with different flexural stiffness EI/L, both in the case of intact structure and damaged structure with crack of rotational stiffness k_c = 8000 kNm at x_c/L = 0.2. The signals are sampled at dx/L = 0.001 and no noise is added. (a,b) EI/L = 0.0015 Nm, respectively without and with crack; (c,d) EI/L = 0.15 Nm, respectively without and with crack.

Similar observation can be made in the presence of noisy signals. Assume again two cantilever beams of length L = 1 m modelled as in Section 3.3.1.3, but now with flexural stiffness EI/L equal to $5Ã10^3$ and $5Ã10^5$ Nm. Through CWT, using óCoif4ô at s = 8 and the polynomial padding method ($\beta_1 = \beta_2 = 0.2$), the static *non-normalized* deflections of the beams due to the point load P = 10 kN at the free end (see Fig. 3.3) are analysed. The both cases of intact structure and damaged structure with crack of rotational stiffness k_c = 8000 kNm at x_c/L = 0.2 (note that the relative rotation φ_c for P = 10 kN is equal to 0.001 rad) are considered. The beam deflections are sampled at dx/L = 0.001 and synthetic noise of 120 dB is added. The results are displayed in Fig. 6.2.

Considering the first beam with larger curvature, it appears that the normalized wavelet coefficients obtained by analysing the noisy undamaged beam deflection (Fig. 6.2a) attain values of the same order of magnitude of those obtained by analysing the noisy damaged beam deflection (Fig. 6.2b). In this case, even though the coefficient peak in Fig. 6.2b is clearly at the crack location

($h_{nd,1}$ = 1.94Ã10^{-3}), the contribution of the crack discontinuity, $h_{nc,1}$, can not be distinguished from the value of $h_{nd,1}$ due to the presence of noise.

On the other hand, when the wavelet coefficients detect more clearly the crack discontinuity than the noisy curvature trend (the normalized CWT coefficients of Fig. 6.2c are around two orders of magnitude smaller than those of Fig. 6.2d, i.e. $h_{nu,2} << h_{nd,2}$), the normalized CWT value at the crack location (i.e. $h_{nd,2}$ = 1.63Ã10^{-3}), obtained by analyzing the damaged beam deflection, can be assumed to be roughly equal to the contribution due to the crack relative rotation (i.e. $h_{nd,2}$ å $h_{nc,2}$ = 1.63Ã10^{-3}). Note further that, analyzing the beam with the same crack relative rotation, qr$_c$ = 0.001 rad, both in absence and in presence of noise, when the CWT attains negligible values of its coefficients in the undamaged parts of the beam with respect to those close to the crack location, the peak value at x_c is the same, i.e. $h_{c,2} = h_{nc,2}$ = 1.63Ã10^{-3}.

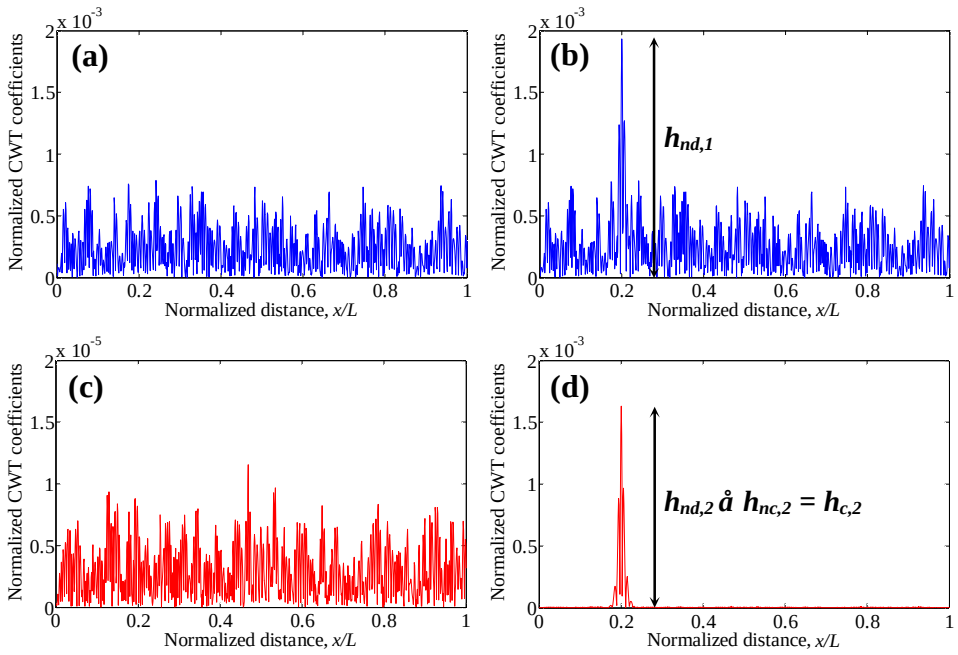

Fig. 6.2 ï Absolute value of the normalized CWT coefficients at s = 8 obtained by analyzing the static *non-normalized* deflections of cantilever beams of length L = 1 m with different flexural stiffness EI/L, both in the case of intact structure and damaged structure with crack of rotational stiffness k_c = 8000 kN at x_c/L = 0.2. The signals are sampled at dx/L = 0.001 and SNR = 120 dB. (a,b) EI/L = 5Ã10^3 Nm, respectively without and with crack; (c,d) EI/L = 5Ã10^5 Nm, respectively without and with crack.

Figure 6.3 shows the wavelet transforms (ócoif4ô at scale 32 and the polynomial padding method with $\beta_1 = \beta_2 = 0.5$ and $\tilde{\beta}_1 = \tilde{\beta}_2 = 0.667$ are used) of the static *non-normalized* deflections of two cracked cantilevers (see Section 3.3.1.3) of unit length, subjected to P = 10 kN, with EI/L equal to 5Ã10^5 Nm. A beam has a crack of rotational stiffness k_c = 9000 kNm at x_c/L = 0.1 (Fig. 6.3a) while the other one has a crack of rotational stiffness k_c = 1000 kNm at x_c/L = 0.9 (Fig. 6.3b) (note that the crack relative rotation φ_c induced by the load P is equal to 0.001 rad in both the beams). The beam deflections are sampled at dx/L = 0.001 and SNR = 100 dB is added.

The results in Fig. 6.3 highlight that, if the value of the normalized CWT coefficient at the crack location is significantly greater than the others along the beam, this latter does not depend on the crack location (h_a = h_b = 0.0131). Furthermore, the value of the normalized coefficient at x_c depends on the analyzing scale (e.g. h_a = 0.0131 Í $h_{nc,2}$ = 0.00163).

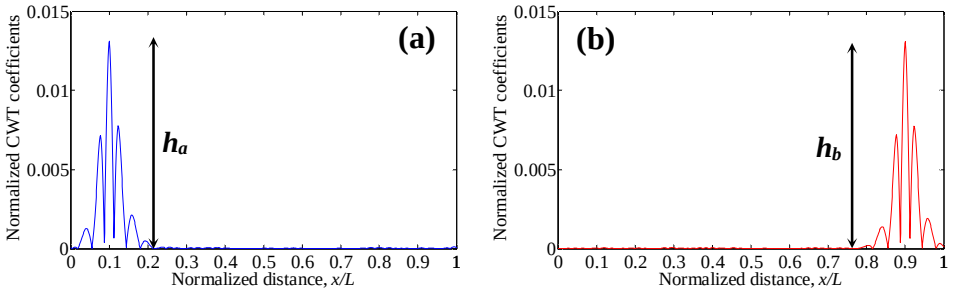

Fig. 6.3 ï Absolute value of the normalized CWT coefficients at s = 32 obtained by analyzing the static *non-normalized* deflections of cantilever beams, having length L = 1 m and, flexural stiffness EI/L = 5Ã10^5 Nm and crack of rotational stiffness k_c dependent on the crack location x_c. The signals are sampled at dx/L = 0.001 and SNR = 100 dB. (a) k_c = 9000 kNm and x_c/L = 0.1; (b) k_c = 1000 kNm and x_c/L = 0.9.

In the light of the above discussion, we can conclude that, when the coefficients of the wavelet transform attain negligible values in the undamaged parts of the beam in comparison with those close to the crack location (this happens when the crack discontinuity due to relative rotation alters significantly the beam curvature), the value of the normalized CWT coefficient at the crack location depends, with good approximation, on the value of the crack relative rotation and on the analyzing wavelet scale.

The bilogarithmic graph of Fig. 6.4 shows that the relative rotations due to the crack, φ_c, and the normalized CWT coefficients at the crack location x_c, $\overline{W}(x_c, s)$ (when $\overline{W}(x \neq x_c, s) << \overline{W}(x_c, s)$) are linearly dependent and function of the scale s. Plotting the curves of Fig. 6.4 in bilinear graphs (Fig. 6.5) we

obtain approximately straight lines, passing through the axis origin and characterized by different values of the angular coefficient, Θ̄(*s*), function of the wavelet scale *s*, that is:

$$\overline{W}(x_c, s) = \Theta(s)\,\Delta\vartheta_c \,. \qquad 6.1$$

In Appendix A tabular values of Θ̄(*s*) related to óCoif4ô are reported. In Fig. 6.6 the trend of Θ̄(*s*) against the wavelet scale is illustrated.

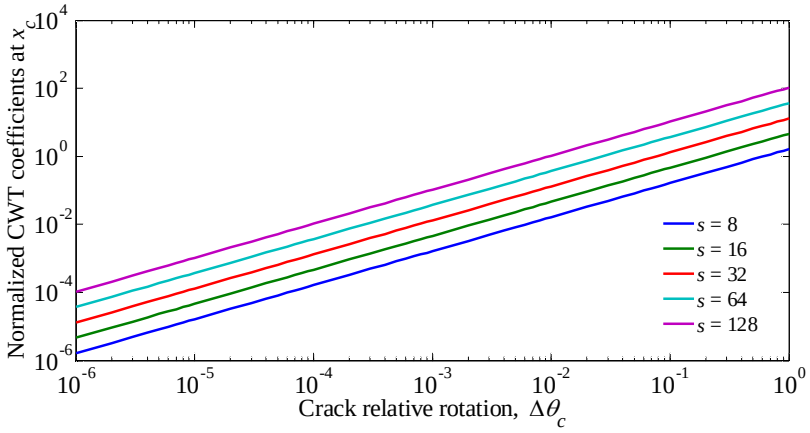

Fig. 6.4 ï Relation between the normalized CWT coefficients at the crack location x_c and the relative rotation due to the crack. Different scales *s* are considered.

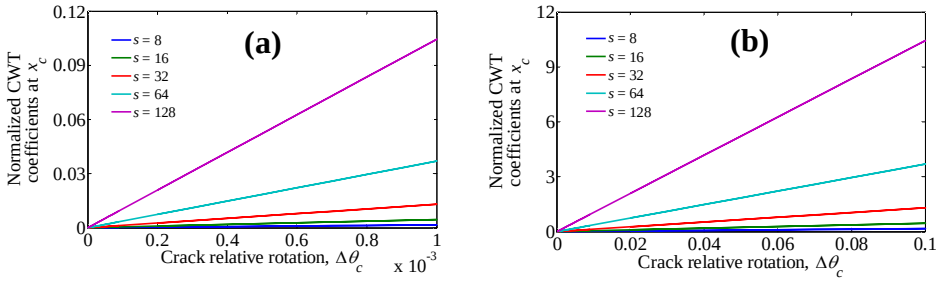

Fig. 6.5 ï The curves of Fig. 6.4 are plotted in bilinear graphs assuming different ranges of crack relative rotation: (a) qp' $_c$ = [0 ï 0.001] rad; (b) qp' $_c$ = [0 ï 0.1] rad.

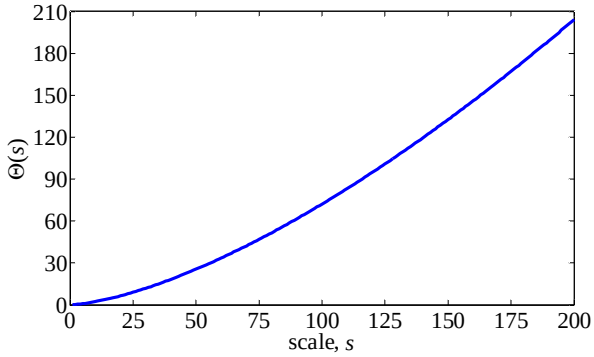

Fig. 6.6 ï Trend of the function Ū(*s*).

6.3 Identification method of the nonlinear crack behaviour

The proposed time-space wavelet-based damage identification method allows the description of the nonlinear crack behaviour in terms of relative rotation of the crack. The technique requires the availability of the beam response both in time and in space at rather dense intervals. Furthermore, the crack discontinuity has to be such that the wavelet transform can locate it by means of a peak of its coefficients markedly higher than the coefficient values along the undamaged parts of the beam. The proposed method operates as following, at each time step:

(i) the beam deflection, opportunely extended to avoid edge effects, is analysed through CWT;
(ii) the wavelet coefficient value at the crack location (which has to be known a priori) is normalized with respect to the square of the spatial interval;
(iii) the crack relative rotation φ'_c is determined through Eq. 6.1, knowing the value of Ū(*s*).

Once the time history of the crack relative rotation is extracted, the evolution of damage can be determined through an appropriate mechanical model.

The reliability of the method depends particularly on the crack size and on the accuracy of the response data in terms of precision and noise cleaning. An opportune pre-processing (e.g. data denoising) of the time-space input data and a post-processing (e.g. data smoothing) of the output data of the crack relative rotation can enhance the effectiveness of the damage quantification.

6.4 Numerical examples

The damage calibration method is applied to numerical data which simulate both the static and the dynamic responses of a cracked fiber-reinforced composite beam subjected to a point load $P(t)$ at the free end (see Fig. 3.5). The FE model presented in Section 3.3.2. is used. A cracked beam reinforced with long unidirectional fibers equally distributed in the matrix with a volume fraction ζ_f of 10% is assumed. The beam is long L = 2 m with height h = 0.2 m and width b = 0.15 m. The matrix has density ρ_m, Youngôs modulus E_m and Poisson coefficient ζ_m, respectively, equal to 2400 kg/m^3, 30 GPa and 0.15. The fibers are characterized by diameter of 30 ε m, density ρ_f of 2500 kg/m^3, Youngós modulus E_f of 80 GPa and tensile/compression yield stress of 2000 MPa. The density and Youngôs modulus of the composite are, respectively, equal to $\rho_{eq} = (1 - \zeta_f)\rho_m + \zeta_f \rho_f$ = 2410 kg/m^3 and $E_{eq} = (1 - \zeta_f)E_m + \zeta_f E_f$ = 35 GPa. The crack has a relative depth α = 10% and its position is varied in the simulations (i.e. x_c/L = 0.05, 0.1). The damping ratio of the first two modes of the beam is assumed to be equal to 3%.

The beam deflection shapes are sampled considering different sampling intervals (i.e. dx = 0.01 m, 0.001 m) and to simulate real measurement data, synthetic Gaussian white noise is added (different SNR values are imposed). The deflections of the static analysis are sampled at each variation φP = ± 2000 N of the acting load $P(t)$. For the dynamic analysis an integration time step dt of 0.0002 sec is assumed.

In the static analysis Timoshenkoôs finite element formulation, exposed in Section 3.3.2.1, is used. In the dynamic analysis instead, Euler-Bernoulliôs formulation is preferred (the shear deformation parameter $\tilde{u}$ = 0 is imposed in Eqs 3.34 to 3.43 and in the formulations related to the uncracked elements; Friedman & Kosmatka, 1993) in order to avoid the discontinuity between the elements of first derivative of the transversal displacements due to nodal inertial forces.

Two different finite element discretizations of the beam are adopted for the static problem and for the dynamic one. Since the shape functions of the finite element model are cubic and the static deflection due to a point load is also described by a cubic function, only the cracked finite element and the two adjacent solid finite elements are needed to obtain the theoretical exact solution of the static problem. On the other hand, in the dynamic analysis a more refined FE model is required. In fact the shapes of dynamic beam deflection are described by trigonometric functions. Since the finite element model adopts cubic shape functions, in order to obtain accurate results and to minimize the inter-element curvature discontinuities, which can be detected by wavelet transform, a very dense finite element discretization is used in the dynamic

analysis. For instance, after a convergence study, when the crack is at $x_c/L = 0.05$ and $dx = 0.001$, a cracked finite element of 0.04 m length and 2 and 47 uncracked finite elements, respectively before and after the crack, are considered.

The CWT is executed using óCoif4ô wavelet and the polynomial padding method is adopted to reduce border distortions (if $dx = 0.001$m, $\beta_1 = \beta_2 = \tilde{\beta}_1 = \tilde{\beta}_2 = 0.5$; if $dx = 0.01$m, $\beta_1 = \beta_2 = \tilde{\beta}_1 = \tilde{\beta}_2 = 1$).

The analysis results are discussed in respect to the analysing scale s of the wavelet, the spatial sampling interval dx/L and the noise level. Different load time histories are considered.

6.4.1 Nonlinear static analysis

The illustrative examples presented in the following are related to the load histories of Fig. 6.7.

Firstly the wavelet scale providing the best estimation of the crack relative rotation is determined. Different scale values are investigated, i.e. s = 10, 30, 60, 90 and 120. The load path (a) is imposed to the beam, and the crack position x_c/L, the spatial sampling interval dx and the noise level are assumed, respectively, equal to 0.1, 0.001 m, SNR = 120 dB. Figures 6.8a and 6.8b display respectively the histories of the beam displacement at the free and of the rotational stiffness of the crack section.

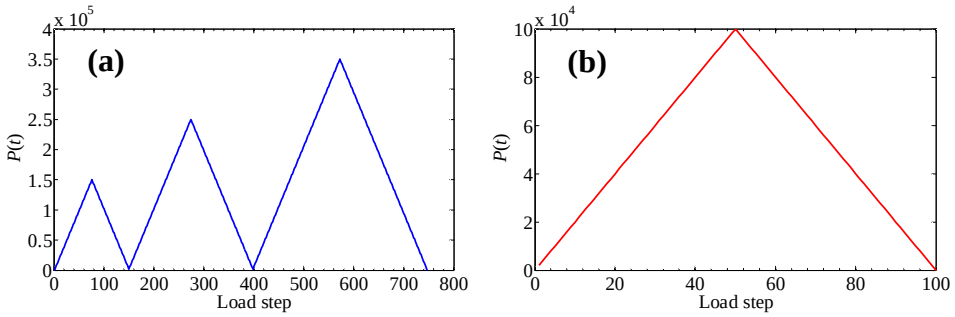

Fig. 6.7 ï Load histories considered in the nonlinear static analysis.

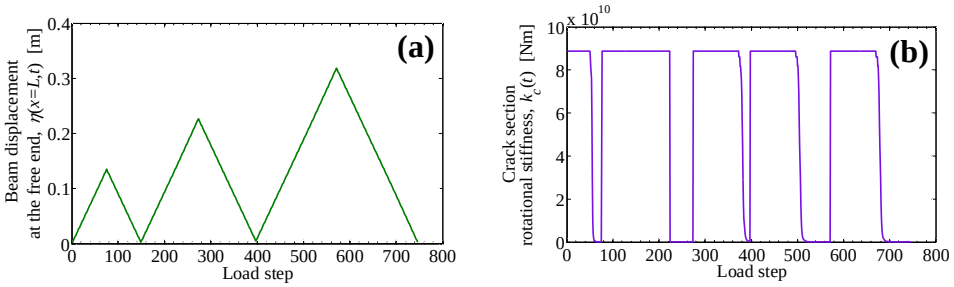

Fig. 6.8 ï (a) History of the beam displacement at the free end; (b) history of the rotational stiffness of the crack section.

In Fig. 6.9 the history of the crack relative rotation φ_c estimated by the wavelet-based calibration method at the scales *s* equal to 10, 30, 60, 90 and 120, is displayed. Figure 6.10 reports the normalized CWT coefficients at a position far from the crack location (say, $x/L = 0.7$) divided by $\bar{U}(s)$ for different wavelet scales. By juxtaposing the results of Fig. 6.10 with those of Fig. 6.9, one can verify that the proposed calibration method is applicable. In fact, at each load step the value of the CWT coefficient at a beam point far away from the crack location is at least one order of magnitude smaller than that at the crack section for every considered scales.

It can be noted that in Fig. 6.11, the distributions of the normalized CWT coefficients along the beam length for a certain load level at different wavelet scales are reported. Scale 120, in comparison with the other scales, identifies higher values of φ_c, due to the influence of the edge effects (Fig. 6.11d). On the contrary, Figs 6.11(a-c) show that using the scales 30, 60 and 90 the edge effects do not influence the peak value of the CWT coefficients.

Among the scales 10, 30, 60 and 90, scale 60 is chosen to estimate φ_c as it averages the estimations of the other scales. Figure 6.12a highlights that the wavelet-based calibration method using $s = 60$ describes accurately the history of the crack relative rotation simulated by the FE model. Furthermore, calculating from static equilibrium the bending moment at the crack location, the moment versus relative rotation curve estimated with the wavelet analysis can be compared with that of the FE model (Fig. 6.12b).

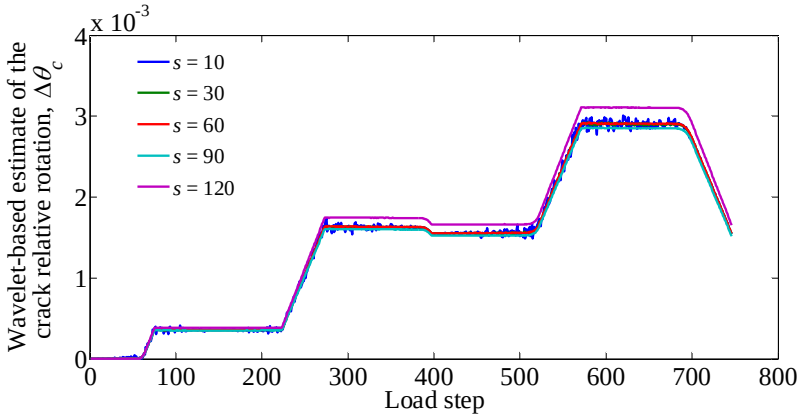

Fig. 6.9 ï Histories of the crack relative rotation φ_c estimated by the wavelet-based calibration method at different scale s of the wavelet (SNR = 120 dB).

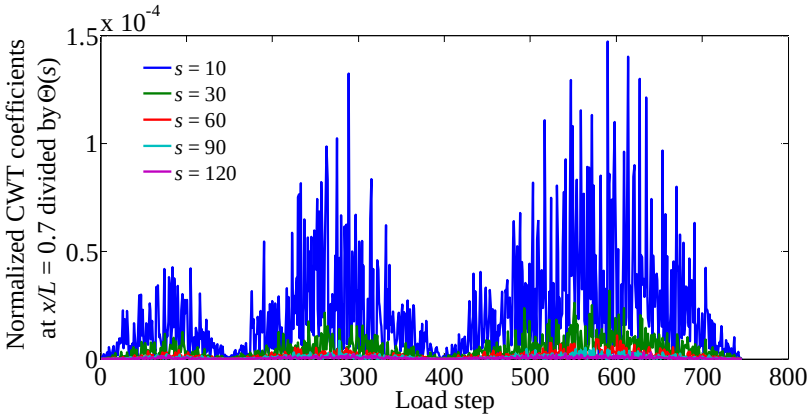

Fig. 6.10 ï Normalized CWT coefficients at x/L = 0.7 divided by $\bar{U}(s)$ at different wavelet scale s (SNR = 120 dB).

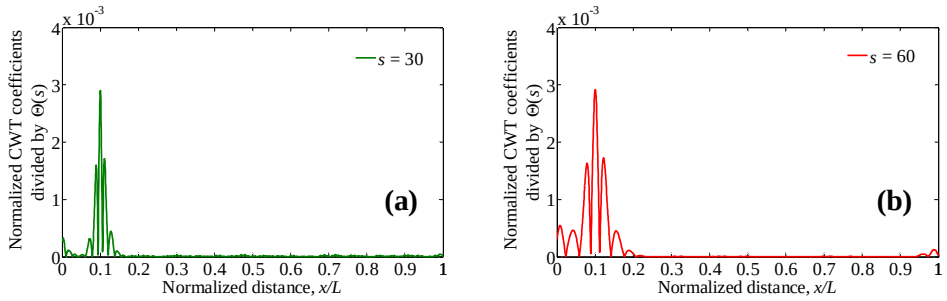

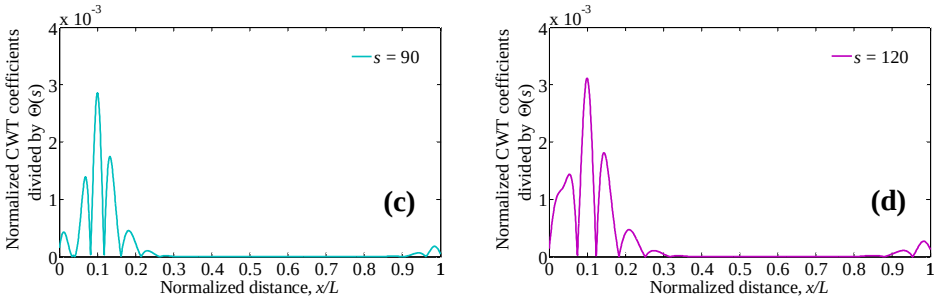

Fig. 6.11 ï Normalized CWT coefficients divided by Ū(*s*) along the beam at different wavelet scale *s* when *P*(*t*) = 3.5Ã10^5 N (SNR = 120 dB). (a) *s* = 30; (b) *s* = 60; (c) *s* = 90; (d) *s* = 120.

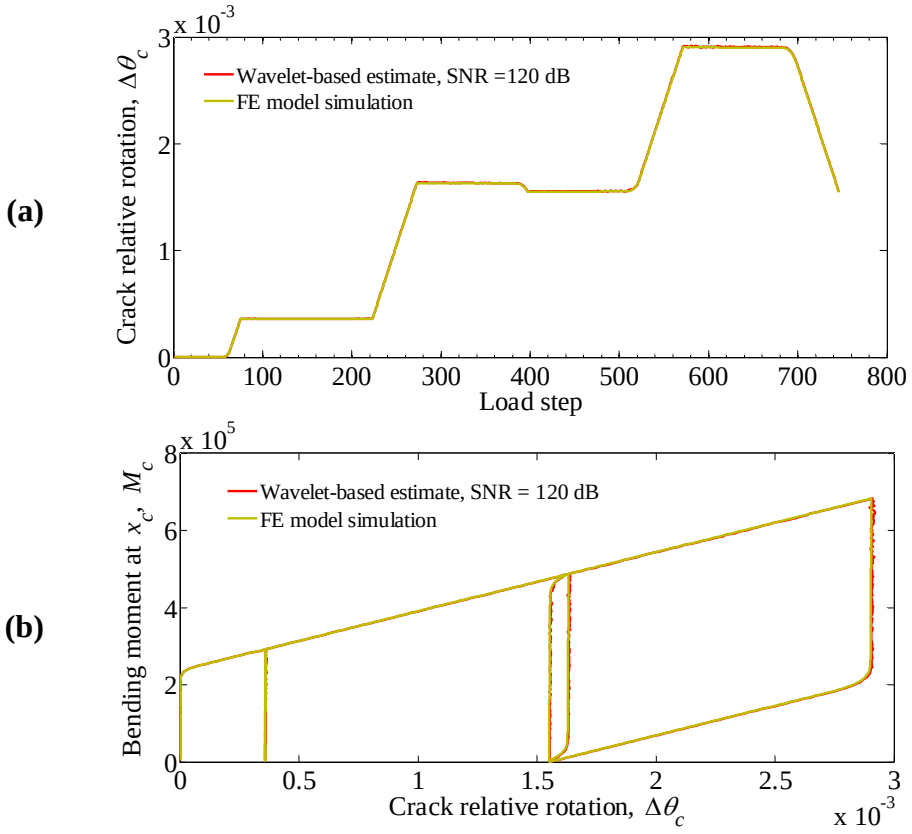

Fig. 6.12 ï Comparison of the estimate of the wavelet-based calibration method at *s* = 60 (SNR = 120 dB) and the simulation of the FE model: (a) history of the crack relative rotation; (b) bending moment at x_c against the crack relative rotation.

Let us now consider the same problem but with an increasing noise level (SNR equal to 100 and 80 dB is imposed). Figure 6.13 shows that the calibration method at SNR = 100 dB provides still a good description of the history of the crack relative rotation. At SNR = 80 dB, the history of φ'_c is sensibly influenced by the presence of noise, but an approximate quantification of the values of φ'_c can be carried out (a smoothing post-processing of the data could be helpful).

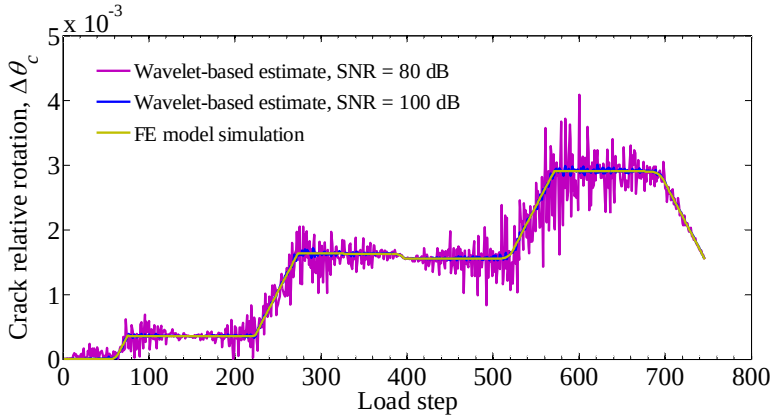

Fig. 6.13 ï Comparison of the history of the crack relative rotation φ'_c estimated by the wavelet-based calibration method at s = 60 with SNR = 80 dB and 100 dB and that obtained by the FE model.

Consider now to apply the load history of Fig. 6.7b to the beam. The crack is located near the clamped end at x_c/L = 0.05 and dx and SNR are assumed to be equal to 0.001 m and 120 dB. Figures 6.14a and 6.14b show respectively the histories of the beam displacement at the free end and of the rotational stiffness of the crack section. In this load case, the beam is significantly less stressed than in the load case of Fig. 6.7a, so that, as comparing Fig. 6.14b with Fig. 6.8b, the rotational stiffness at the crack section is higher due to the fact that most of the fibers are not yielded.

Figure 6.15 shows that, using the wavelet scales 40, 60 or 80, the orders of magnitude of the normalized CWT coefficients divided by $\bar{U}(s)$ at the crack section and at x/L = 0.7 is the same. This means that at these scales the wavelet analysis is significantly affected by noise and, hence, higher scales have to be used in order to reduce the influence of noise.

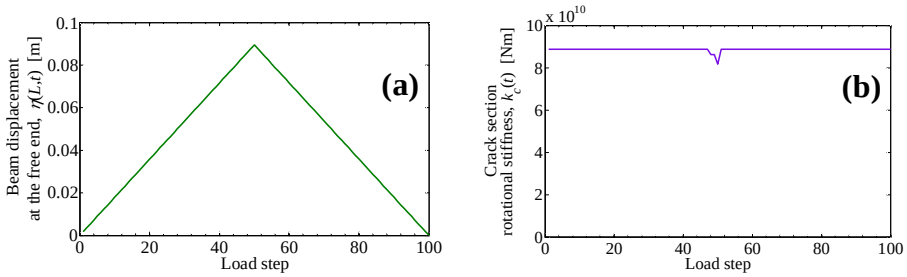

Fig. 6.14 ï (a) History of the beam displacement at the free end; (b) history of the rotational stiffness at the crack section.

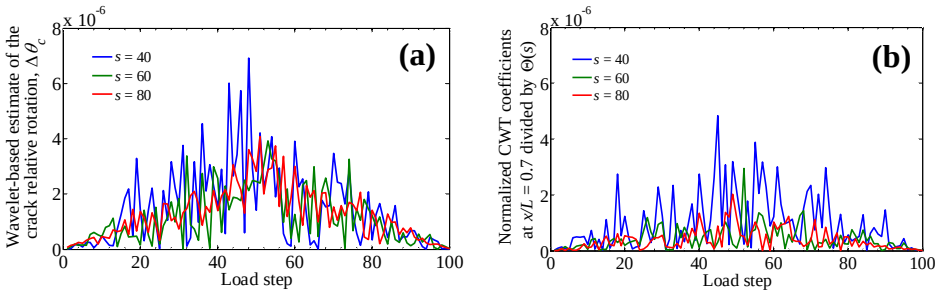

Fig. 6.15 ï Histories of the normalized CWT coefficients divided by $\bar{U}(s)$ at the scales 40, 60 and 80 at: (a) the crack section; (b) x/L = 0.7. SNR = 120 dB.

Figure 6.16 highlights that using higher scales, such as s = 100, 120 or 140, the difference between the values of the CWT coefficients at the crack section (Fig. 6.16a) and those at x/L = 0.7 (Fig. 6.16b) is greater than before. Scale 120 is chosen and the comparison between the wavelet-based results and those obtained by the FE model simulation are shown in Fig. 6.17.

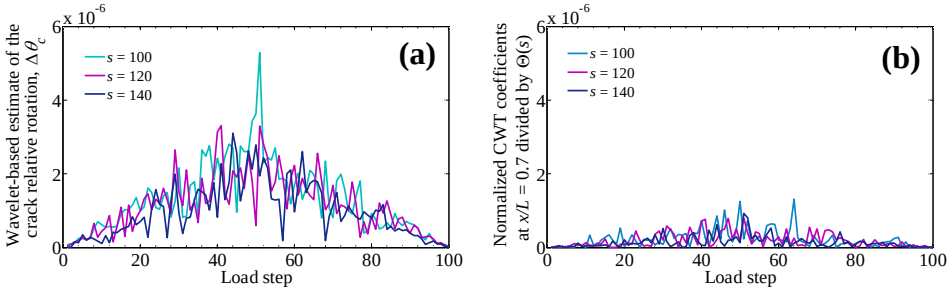

Fig. 6.16 ï Histories of the normalized CWT coefficients divided by $\bar{U}(s)$ at the scales 100, 120 and 140 at: (a) the crack section; (b) x/L = 0.7. SNR = 120 dB.

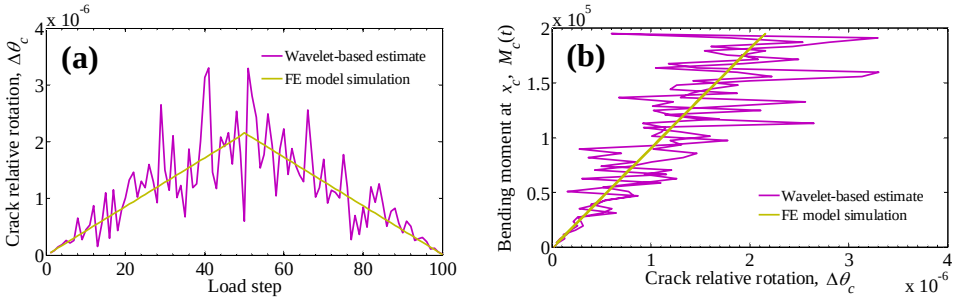

Fig. 6.17 ï Comparison of the estimate of the wavelet-based calibration method at s = 120 (SNR = 120 dB) and the simulation of the FE model: (a) history of the crack relative rotation; (b) bending moment at x_c against the crack relative rotation.

6.4.2 Nonlinear dynamic analysis

The time histories of the point loads at the free end of the cantilever beam (Fig. 3.5) are described by the following harmonic functions (Fig. 6.18):

$$P_a(t) = 5 \cdot 10^4 + 10^5 \, sen(\Omega_a t) \quad \text{N} \qquad 6.2$$

and

$$P_b(t) = 10^5 \, sen(\Omega_b t) \quad \text{N}, \qquad 6.3$$

where $\Omega_a = 0.5\omega_1$ and $\Omega_b = 2\omega_1$ being ω_1 the first natural pulsation of the uncracked beam equal to 192.45 rad/sec.

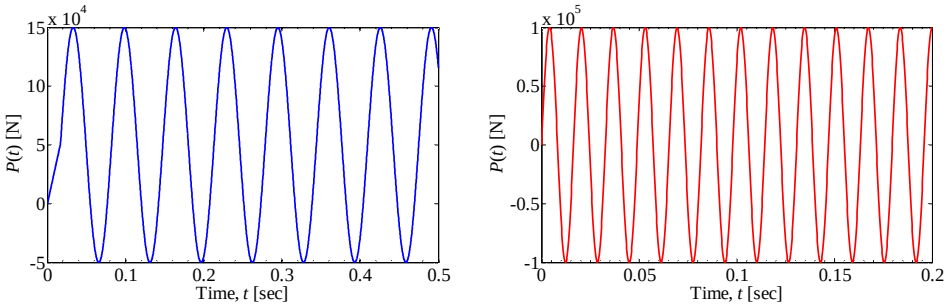

(a) **(b)**

Fig. 6.18 ï Time histories of the harmonic loads being considered in the nonlinear dynamic analysis.

As a first example, consider the beam subjected to the load (a) at Fig. 6.18 with crack at x_c/L = 0.1. Its response is sampled either at dx = 0.001m or dx = 0.01m and two SNR values equal to 100 and 80 dB are imposed. Figure 6.19 displays the time histories of beam displacement at the free end (Fig. 6.19a), of

bending moment at the crack section (Fig. 6.19b), of rotational stiffness at the crack section (Fig. 6.19c), as well as the diagram of the bending moment against crack relative rotation (Fig. 6.19d). Figure 6.19d highlights that all the fibers yield in tension and compression during the loading cycles.

Figure 6.20 shows that the wavelet-based calibration method allows a good estimation of the time history of the crack relative rotation when the beam deflection is sampled at dx = 0.001 m and dx = 0.01 m with SNR equal to 100 dB and 80 dB. Note that the results related to the higher sampling interval are more corrupted by the presence of noise (Fig. 6.20b).

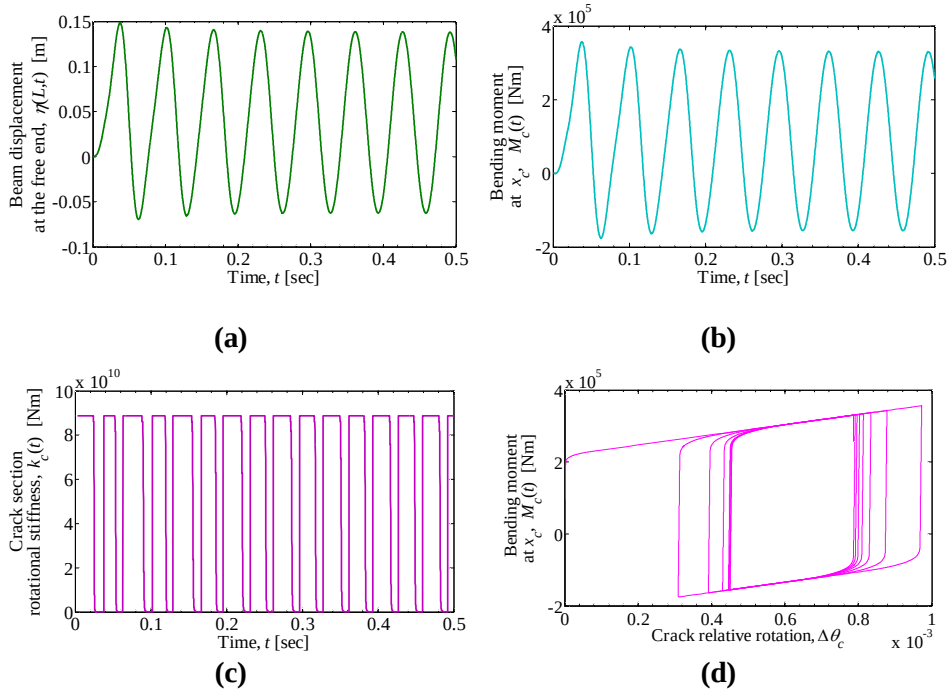

Fig. 6.19 ï (a) Time history of the beam displacement at the free end; (b) Time history of the bending moment at the crack section; (c) Time history of the rotational stiffness at the crack section; (d) Diagram of the bending moment against crack relative rotation at the crack section.

(a)

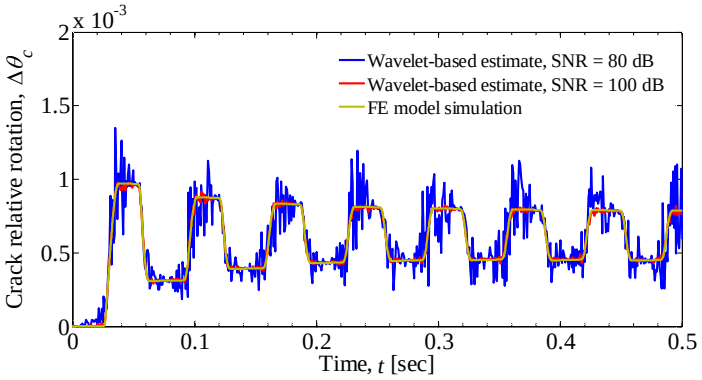

(b)

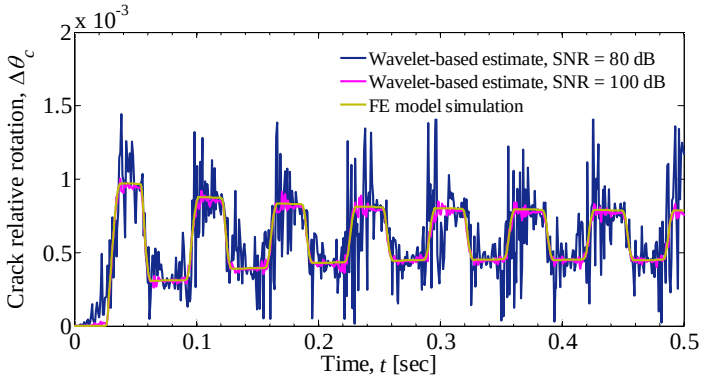

Fig. 6.20 ï Comparison between the time histories of the crack relative rotation obtained by FE model simulation and that evaluated by the wavelet-based calibration method considering: (a) s = 60 and dx = 0.001 m; (b) s = 8 and dx = 0.01 m. SNR values equal to 100 and 80 dB are imposed.

In the second numerical example, the harmonic load (b) of Fig. 6.18 is imposed so that the beam, with crack at x_c/L = 0.05, is less stressed than in the previous example. Figure 6.21 shows the beam response in terms of beam displacement at the free end (Fig. 6.21a), bending moment at the crack section (Fig. 6.21b), rotational stiffness at the crack section (Fig. 6.21c) and bending moment against crack relative rotation at the crack section (Fig. 6.21d).

The beam deflection is sampled at dx = 0.001m and dx = 0.01m and a noise level of 120 dB is imposed. Figure 6.22 highlights again that a denser discretization of the beam shape helps the wavelet-based method to quantify more accurately the damage.

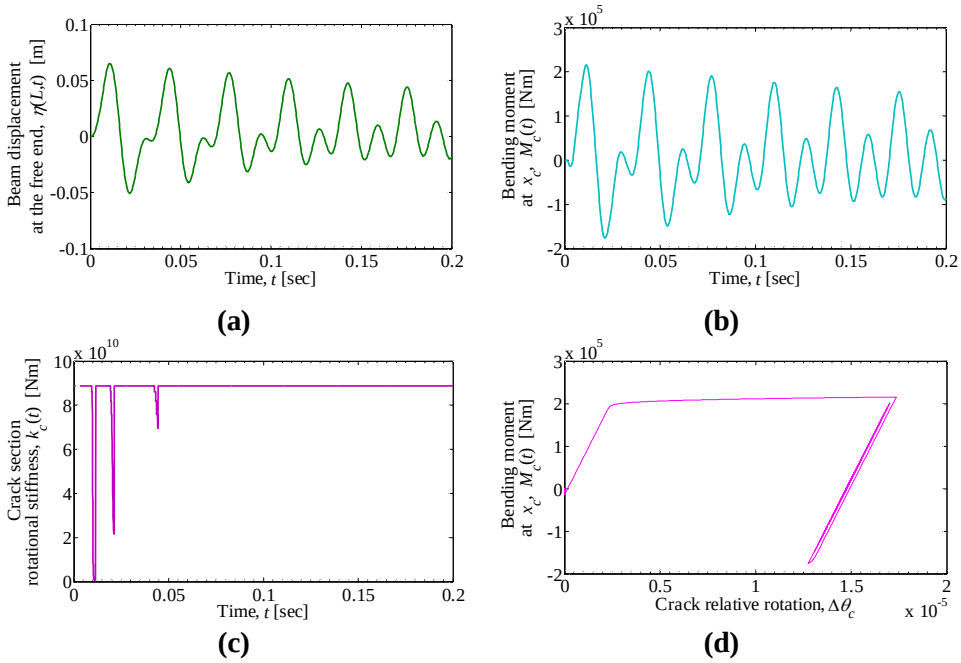

Fig. 6.21 ï (a) Time history of the beam displacement at the free end; (b) Time history of the bending moment at the crack section; (c) Time history of the rotational stiffness at the crack section; (d) Diagram of the bending moment against crack relative rotation at the crack section.

(a)

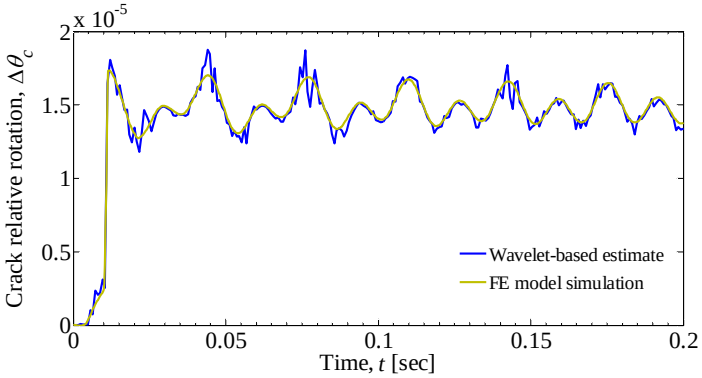

(b)

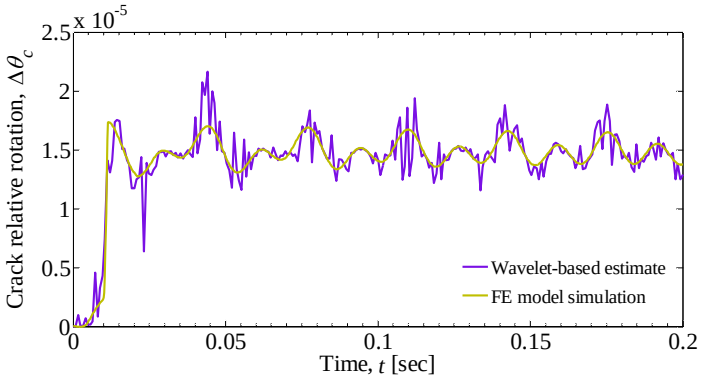

Fig. 6.22 ï (a) Comparison between the time history of the crack relative rotation obtained by the FE model simulation and that evaluated by the wavelet-based calibration method considering: (a) s = 55 and dx = 0.001 m; (b) s = 6 and dx = 0.01 m. SNR = 120 dB.

Conclusions

The present thesis deals with the vibration-based damage identification in beam structures through wavelet analysis. Three main problems of damage identification through continuous wavelet transform are studied: the minimization of border distortions, the effect of the spatial sampling in damage detection and the assessment of the nonlinear behaviour of damage for structural health monitoring and control.

A new effective and computational efficient signal extension method to reduce CWT edge effects of beam deflections is presented. The method is based on the approach of padding the original signal using two functions that satisfy continuity conditions and extend the average trend of the noisy signal and its derivatives. Two high-order degree polynomial functions are determined through a fitting procedure of the noisy signal and by imposing signal and first derivative continuity conditions in the beam extrema. The capability of the polynomial method is compared with that of the most effective padding methods available in the literature, such as the linear padding method and, Messinaôs isomorphism methods. The analytical free vibration and static deflection responses of cantilever and simply supported cracked beams are analysed. Crack depth ratio and position are varied, and different levels of synthetic Gaussian white noise are introduced to the signal to emulate real measured data. The comparison between the considered padding methods highlights a great effectiveness and versatility of the proposed method.

A thorough parametric investigation of the effect of spatial sampling interval in damage detection by CWT is carried out to answer to the following key questions: can the cost of damage detection be reduced by down-sampling? What is the minimum number of sampling intervals performing the optimal damage detection? With reference to the results obtained using the proposed polynomial padding method and ócoif4ô wavelet, the optimal performance of the CWT damage detection in terms of the minimum detectable crack size is shown to be dependent only on a particular value of the pseudo-frequency, which is a function of the length and the shape of the beam and of the crack location. Since the sampling interval is strictly related to the pseudo-frequency, general charts are produced in order to provide with good approximation the minimum optimal number of sampling intervals required to perform the optimal damage detection.

Finally, a new health structural monitoring method based on time-space wavelet analysis is presented to control the static and dynamic, nonlinear

behaviour of a cracked fiber-reinforced beam. The method is based on a linear relation between the normalized CWT coefficients and the relative rotation due to the crack, which holds true on particular conditions related to the CWT beam deflection and the features of the wavelet (such as óCoif4ô). The effectiveness of the method in describing the nonlinear structural response due to a small crack is discussed in relation to the wavelet scale, the noise level and the spatial sampling interval.

References

Abraham, O. N. L., & Brandon, J. A., 1995. *The modelling of the opening and closure of a crack*. Journal of vibration and acoustics, 117(3) 370-377.

Adams, R. D., Cawley, P., Pye, C. J., and Stone, B. J., 1978. *A vibration technique for non-destructively assessing the integrity of structures*. Journal of Mechanical Engineering Science, 20(2) 93-100.

Adeli, H., 2001. *Neural networks in civil engineering: 1989-2000*. Computer-Aided Civil and Infrastructure Engineering, 16(2) 126-142.

Adeli, H. & Park, H. S., *Neurocomputing in Design Automation*, CRC Press, Boca Raton, FL, 1998.

Adewuyi, A. P., Wu, Z., & Serker, N. K., 2009. *Assessment of vibration-based damage identification methods using displacement and distributed strain measurements*. Structural Health Monitoring, 8(6) 443-461.

Allemang, R.J. & Brown, D.L., 1982. *Correlation coefficient for modal vector analysis*. In: Proceedings of the 1st International Modal Analysis Conference, Orlando, Florida, USA, 110-116.

American Society for Metals, Metals Handbook, 9th edition. Volume 17, *Nondestructive Evaluation and Quality Control*. ASM International. USA, 1989.

Anderson, J. A., & Davis, J., *An introduction to neural networks* (Vol. 1). MIT press, Cambridge, MA, 1995.

Andreaus, U., & Baragatti, P., 2011. *Cracked beam identification by numerically analysing the nonlinear behaviour of the harmonically forced response*. Journal of Sound and Vibration, 330(4), 721-742.

Andreaus, U., & Baragatti, P., 2012. *Experimental damage detection of cracked beams by using nonlinear characteristics of forced response*. Mechanical Systems and Signal Processing, 31 382-404.

Araújo dos Santos, J. V., Soares, C. M., Mota Soares, C. A., and Pina, H. L. G., 2000. *A damage identification numerical model based on the sensitivity of orthogonality conditions and least squares techniques*. Computers & Structures, 78(1) 283-291.

Atkinson, K., *An introduction to numerical analysis*, 2nd edition. John Wiley & Sons, New York, 1989.

Baruch, M., 1978. *Optimization procedure to correct stiffness and flexibility matrices using vibration tests.* AIAA journal, 16(11) 1208-1210.

Baruch, M., 1997. *Modal data are insufficient for identification of both mass and stiffness matrices*. AIAA Journal, 35(11) 1797-1798.

Basu, B., & Gupta, V. K., 1998. Seismic response of SDOF systems by wavelet modeling of nonstationary processes. Journal of engineering mechanics, 124(10), 1142-1150.

Basu, B., Nagarajaiah, S., and Chakraborty, A., 2008. *Online identification of linear time-varying stiffness of structural systems by wavelet analysis*. Structural Health Monitoring, 7(1), 21-36.

Ben-Haim, Y., & Prells, U., 1993. *Selective sensitivity in the frequency domain, Part I: Theory*. Mechanical Systems and Signal Processing, 7(5) 461-475.

Bently, D. E. & Hatch, C. T. *Fundamentals of rotating machinery diagnostics*. ASME Press, New York, 2003

Berman, A., 1979. *Mass matrix correction using an incomplete set of measured modes*. AIAA Journal, 17(10) 1147-1148.

Bishop, C. M., *Neural networks for pattern recognition*. Oxford university press, 1995.

Boller, C., & Buderath, M., 2007. *Fatigue in aerostructures-where structural health monitoring can contribute to a complex subject*. Philosophical Transactions of the Royal Society A: Mathematical, Physical and Engineering Sciences, 365(1851) 561-587.

Bovsunovsky, A. P., & Surace, C., 2005. *Considerations regarding superharmonic vibrations of a cracked beam and the variation in damping caused by the presence of the crack.* Journal of Sound and Vibration, 288(4), 865-886.

Bracewell, R. N., *The Fourier transform and its applications*. McGraw-Hill. New York, 1986.

Brock, J. E., 1968. *Optimal matrices describing linear systems*. AIAA Journal, 6(7) 1292-1296.

Broek, D., *Elementary engineering fracture mechanics*. Springer, 1986.

Brownjohn, J. M., 2007. *Structural health monitoring of civil infrastructure*. Philosophical Transactions of the Royal Society A: Mathematical, Physical and Engineering Sciences, 365(1851) 589-622.

Bunke, H., & Sanfeliu, A., *Syntactic and Structural Pattern Recognition: Theory and Applicationss (Vol. 7)*. World Scientific, 1990.

BŤrmen, Á., Puhan, J., & Tuma, T., 2006. *Grid restrained nelder-mead algorithm*. Computational Optimization and Applications, 34(3), 359-375.

Cao, M., & Qiao, P., 2008. *Integrated wavelet transform and its application to vibration mode shapes for the damage detection of beam-type structures*. Smart materials and structures, 17(5), 055014.

Carden, E. P., & Fanning, P., 2004. *Vibration based condition monitoring: a review*. Structural Health Monitoring, 3(4) 355-377.

Carlson, R. L., 1974. *An experimental study of the parametric excitation of a tensioned sheet with a cracklike opening*. Experimental Mechanics, 14(11) 452-458.

Carpinteri Al., & Massabò, R., 1996. *Bridged versus cohesive crack in the flexural behaviour of brittle-matrix composites*. International Journal of Fracture 81, 125-145.

Carpinteri, Al., & Massabò, R., 1997. *Continuous vs discontinuous bridged-crack model for fiber-reinforced materials in flexure*. International Journal of Solids and Structures, 34(18) 2321-2338.

Carpinteri, An., Spagnoli, A. and Vantadori, S., 2004. *A fracture mechanics model for a composite beam with multiple reinforcements under cyclic bending*. International Journal of Solids and Structures, 41 5499-5515.

Carvalho, J., Datta, B. N., Gupta, A., and Lagadapati, M., 2007. *A direct method for model updating with incomplete measured data and without spurious modes*. Mechanical Systems and Signal Processing, 21(7) 2715-2731.

Casas, J. R., & Aparicio, A. C., 1994. *Structural damage identification from dynamic-test data*. Journal of Structural Engineering, 120(8) 2437-2450.

Casciati, F., & Fuggini, C., 2009. *Engineering vibration monitoring by GPS: long duration records*. Earthquake Engineering and Engineering Vibration, 8(3) 459-467.

Casciati, F., & Wu, L., 2010. *Investigating the potential of LPS in structural health monitoring*. In: Proceedings of the 6th International Conference on Wireless Communications Networking and Mobile Computing (WiCOM), IEEE, 1-4.

Casciati, F., & Wu, L. J., 2012. *Positioning Systems: Global Versus Local*. In: Advanced Dynamics and Model-Based Control of Structures and Machines, pp. 43-52. Springer, Vienna.

Cawley, P., & Adams, R. D., 1979. *A vibration technique for non-destructive testing of fibre composite structures*. Journal of Composite Materials, 13(2) 161-175.

Chen, H. L., Spyrakos, C. C., and Venkatesh, G., 1995. *Evaluating structural deterioration by dynamic response*. Journal of Structural Engineering, 121(8) 1197-1204.

Chen, J. C., & Garba, J. A., 1988. *On-orbit damage assessment for large space structures*. AIAA Journal, 26(9) 1119-1126.

Chen, Q., Chan, Y. W., and Worden, K., 2003. *Structural fault diagnosis and isolation using neural networks based on response-only data*. Computers & structures, 81(22) 2165-2172.

Cheng, S. M., Swamidas, A. S. J., Wu, X. J., and Wallace, W., 1999. *Vibrational response of a beam with a breathing crack*. Journal of Sound and Vibration, 225(1) 201-208.

Cheng, J., Yu, D. and Yang, Y., 2007. *Application of support vector regression machines to the processing of end effects of Hilbertï Huang transform*. Mechanical Systems and Signal Processing, 21(3) 1197-1211.

Chinchalkar, S., 2001. *Determination of crack location in beams using natural frequencies*. Journal of Sound and vibration, 247(3) 417-429.

Chopra A. K., Dynamics of Structures. *Theory and Applications to Earthquake Engineering*. Prentice Hall, edition, 1995.

Chou, J. H., & Ghaboussi, J., 2001. *Genetic algorithm in structural damage detection*. Computers & Structures, 79(14) 1335-1353.

Clark, R., Dover, W. D., and Bond, L. J., 1987. *The effect of crack closure on the reliability of NDT predictions of crack size*. NDT International, 20(5) 269-275.

Cochocki, A., & Unbehauen, R., *Neural networks for optimization and signal processing*. John Wiley & Sons, Inc., 1993.

Cohen, L., *Time-frequency analysis*. Prentice-Hall, Englewood Cliffs, New Jersey, 1995.

DôAmbrogio, W. and Zobel, P.B., 1994. *Damage detection in truss structures using a direct updating technique*. In: Proceedings of the 19th Int. Seminar for Modal Analysis on Tools for Noise and Vibration Analysis, Katholieke Universiteit, Leuven, Belgium, Vol. 2, 657-667.

Daubechies I., *Ten lectures on wavelets*. Society for Industrial and Applied Mathematics, 1992.

Deng, Y., Wang, W., Qian, C., Wang, Z. and Dai, D., 2001. *Boundary-processing-technique in EMD method and Hilbert transform*. Chinese Science Bulletin, 46(11) 954-960.

Doherty, J.E. *Nondestructive Evaluation*, Chapter 12. In: Kobayashi, A.S. (Edt.), Handbook on Experimental Mechanics, 527-555. VCH Publishers, Inc., New York, 1991.

Doebling, S. W., 1996. *Minimum-rank optimal update of elemental stiffness parameters for structural damage identification*. AIAA Journal, 34(12) 2615-2621.

Doebling, S. W., Farrar, C. R., Prime, M. B., & Shevitz, D. W.,1996. *Damage identification and health monitoring of structural and mechanical systems from changes in their vibration characteristics: a literature review* (No. LA-13070-MS). Los Alamos National Laboratory, NM, USA.

Doebling, S. W., Farrar, C. R., and Goodman, R. S., 1997. *Effects of Measurement Statistics on the Detection of Damage in the Alamosa Canyon Bridge*. In: Proceedings of the 15th International Modal Analysis Conference, Orlando, FL, 919-929.

Douka, E., & Hadjileontiadis, L. J., 2005. *Time-frequency analysis of the free vibration response of a beam with a breathing crack*. NDT & E International, 38(1) 3-10.

Douka, E., Loutridis, S., and Trochidis, A., 2003. *Crack identification in beams using wavelet analysis*. International Journal of Solids and Structures, 40(13) 3557-3569.

Dunn, S. A., 1998. *The use of genetic algorithms and stochastic hill-climbing in dynamic finite element model identification*. Computers & Structures, 66(4) 489-497.

Ewins, D. J. *Modal testing: theory, practice and application (Vol. 2)*. Baldock: Research studies press, 2000.

Fanning, P. J., & Carden, E. P., 2003. *Damage detection based on single-input-single-output measurements*. Journal of engineering mechanics, 129(2) 202-209.

Fanning, P. J., & Carden, E. P., 2004. *Experimentally validated added mass identification algorithm based on frequency response functions*. Journal of engineering mechanics, 130(9) 1045-1051.

Farhat, C., & Hemez, F. M., 1993. *Updating finite element dynamic models using an element-by-element sensitivity methodology.* AIAA Journal, 31(9) 1702-1711.

Farrar, C. R., Baker, W. E., Bell, T. M., Cone, K. M., Darling, T. W., Duffey, T. A., Eklund, A. and Migliori, A., 1994. *Dynamic characterization and damage detection in the I-40 bridge over the Rio Grande* (No. LA-12767-MS). Los Alamos National Laboratory, NM, USA.

Farrar, C. R., Doebling, S. W., Cornwell, P. J., and Straser, E. G., 1997. *Variability of Modal Parameters Measured on the Alamosa Canyon Bridge*. In: Proceedings of the 15th International Modal Analysis Conf., Orlando, FL, 257-263.

Farrar, C. R., & Doebling, S. W. *Damage detection and evaluation II*. In: Modal analysis and testing, 345-378. Springer Netherlands, 1999.

Farrar, C. R., Doebling, S. W., and Nix, D. A., 2001. *Vibration-based structural damage identification.* Philosophical Transactions of the Royal Society of London. Series A: Mathematical, Physical and Engineering Sciences, 359(1778) 131-149.

Farrar, C. R., & Worden, K., 2007. *An introduction to structural health monitoring.* Philosophical Transactions of the Royal Society A: Mathematical, Physical and Engineering Sciences, 365(1851) 303-315.

Farrar, C. R., Worden, K., Todd, M. D., Park, G., Nichols, J., Adams, D. E., Matthew T. Bement, M. T. and Farinholt, K., 2007. *Nonlinear system identification for damage detection* (No. LA-14353-MS). Los Alamos National Laboratory, NM, USA.

Feldman, M., 2011. *Hilbert transform in vibration analysis*. Mechanical systems and signal processing, 25(3) 735-802.

Fitzgerald, B., Arrigan, J., & Basu, B., 2010. *Damage detection in wind turbine blades using time-frequency analysis of vibration signals.* In: The 2010 International Joint Conference on Neural Networks (IJCNN), IEEE, 1-5.

Francis, T. S., Yin, S. and Ruffin, P. B., *Fiber optic sensors*. CRC press, 2010.

Friedman, Z. & Kosmatka, J. B., 1993. *An improved two-node Timoshenko beam finite element*. Computers & structures, 47(3) 473-481.

Friswell, M. I., & Mottershead, J. E., *Finite Element Model Updating in Structural Dynamics*, Kluwer Academic Publishers, 1995.

Friswell, M. I., & Penny, J. E. T., 1992. *A simple nonlinear model of a cracked beam*. In: proceedings of the 10th international modal analysis conference, 516-516.

Friswell, M. I., 2007. *Damage identification using inverse methods.* Philosophical Transactions of the Royal Society A: Mathematical, Physical and Engineering Sciences, 365(1851) 393-410.

Fritzen, C. P., Jennewein, D., and Kiefer, T., 1998. *Damage detection based on model updating methods.* Mechanical Systems and Signal Processing, 12(1) 163-186.

Frýba, L., & Pirner, M., 2001. *Load tests and modal analysis of bridges*. Engineering Structures, 23(1) 102-109.

Furukawa, A., Otsuka, H., and Kiyono, J., 2006. *Structural damage detection method using uncertain frequency response functions*. Computer-Aided Civil and Infrastructure Engineering, 21(4) 292-305.

Gentile, A., & Messina, A., 2003. *On the continuous wavelet transforms applied to discrete vibrational data for detecting open cracks in damaged beams*. International Journal of Solids and Structures, 40(2), 295-315.

Giannini, O., Casini, P., and Vestroni, F., 2013. *Nonlinear harmonic identification of breathing cracks in beams*. Computers & Structures, 129, 166-177.

Giannoccaro, N. I., Messina, A. and Rollo, G., 2009. *A damage detection based on the processing of multiple dynamic shapes through CWTs*. In: Proceedings of the Sixth International Conference on Condition Monitoring and Machinery Failure Prevention Technologies, Dublin.

Gökdaĵ, H., & Kopmaz, O., 2009. *A new damage detection approach for beam-type structures based on the combination of continuous and discrete wavelet transforms.* Journal of Sound and Vibration, 324(3), 1158-1180.

Goldberg D. E., Genetic *Algorithms in Search, Optimization, and Machine Learning*. Addison-Wesley: Reading, MA, 1989.

Grafe, H., 1998. *Model updating of large structural dynamics models using measured response functions*. Ph.D. Dissertation, Imperial College of Science, Technology and Medicine, University of London, UK.

Guan, H., & Karbhari, V. M., 2008. *Improved damage detection method based on element modal strain damage index using sparse measurement*. Journal of Sound and Vibration, 309(3) 465-494.

Gudmundson, P., 1983. *The dynamic behaviour of slender structures with cross-sectional cracks*. Journal of the Mechanics and Physics of Solids, 31(4) 329-345.

Hamming R. W., *Digital filters*, 3rd edition. Prentice-Hall International Editions, Emglewood Cliffs, New Jersey, 1989.

Han, J. G., Ren, W. X., and Sun, Z. S., 2005. *Wavelet packet based damage identification of beam structures*. International Journal of Solids and Structures, 42(26), 6610-6627.

Hao, H., & Xia, Y., 2002. *Vibration-based damage detection of structures by genetic algorithm*. Journal of computing in civil engineering, 16(3) 222-229.

Haykin, S., *Neural Networks: A Comprehensive Foundation*, 2nd edition, Prentice-Hall, Englewood Cliffs, New Jersey, 1999.

Hecht-Nielsen, R., 1989. *Theory of the backpropagation neural network*, In: Proceedings of the International Joint Conference In Neural Networks, 593-605.

Hegazy, T., Fazio, P., and Moselhi, O., 1994. *Developing Practical Neural Network Applications Using Back-Propagation*. Computer-Aided Civil and Infrastructure Engineering, 9(2) 145-159.

Hemez, F. M., *Theoretical and experimental correlation between finite element models and modal tests in the context of large flexible space structures*, Ph.D Dissertation, Dept. of Aerospace Engineering Sciences, University of Colorado, Boulder, CO., 1993.

Heng, A., Zhang, S., Tan, A. C., & Mathew, J., 2009. *Rotating machinery prognostics: State of the art, challenges and opportunities*. Mechanical Systems and Signal Processing, 23(3) 724-739.

Henry, M. P., & Clarke, D. W., 1993. *The self-validating sensor: rationale, definitions and examples*. Control Engineering Practice, 1(4) 585-610.

Hera, A., & Hou, Z., 2003. *Application of wavelet approach for ASCE structural health monitoring benchmark studies*. Journal of Engineering Mechanics, 130(1), 96-104.

Heylen, W., Lammens, S., and Sas, P., *Modal analysis theory and testing*. Leuven, KUL Press, 1997.

Hou, Z., Noori, M., and Amand, R. S., 2000. *Wavelet-based approach for structural damage detection*. Journal of Engineering Mechanics, 126(7), 677-683.

Hsu, W. K., Chiou, D. J., Chen, C. W., Liu, M. Y., Chiang, W. L., and Huang, P. C., 2013. *Sensitivity of initial damage detection for steel structures using the Hilbert-Huang transform method*. Journal of Vibration and Control, 19(6) 857-878.

Hong, J. C., Kim, Y. Y., Lee, H. C., and Lee, Y. W., 2002. *Damage detection using the Lipschitz exponent estimated by the wavelet transform: applications to*

vibration modes of a beam. International Journal of Solids and Structures, 39(7), 1803-1816.

Huang, N. E., Shen, Z., Long, S. R., Wu, M. C., Shih, H. H., Zheng, Q., Yen, N.-C., Tung, C. C. and Liu, H. H., 1998. *The empirical mode decomposition and the Hilbert spectrum for nonlinear and non-stationary time series analysis*. Proceedings of the Royal Society of London. Series A: Mathematical, Physical and Engineering Sciences, 454(1971) 903-995.

Huang, N. E., & Shen, S. S., *Hilbert-Huang transform and its applications* (Vol. 5). World Scientific, 2005.

Huang, Y., Meyer, D., & Nemat-Nasser, S., 2009. *Damage detection with spatially distributed 2D continuous wavelet transform.* Mechanics of Materials, 41(10), 1096-1107.

Jain, A. K., Duin, R. P. W., and Mao, J., 2000. *Statistical pattern recognition: A review. Pattern Analysis and Machine Intelligence*, IEEE Transactions on, 22(1) 4-37.

Janter, T., & Sas, P., 1990. *Uniqueness aspects of model-updating procedures*. AIAA journal, 28(3) 538-543.

Jung, D. S., & Kim, C. Y., 2009. *FE model updating based on hybrid genetic algorithm and its verification on numerical bridge model*. Structural Engineering and Mechanics, 32(5), 667-683.

Kammer, D. C., 1988. *Optimum approximation for residual stiffness in linear system identification.* AIAA Journal, 26(1) 104-112.

Kaouk, M. & Zimmerman, D. C., 1994. *Assessment of damage affecting all structural properties.* In: Proceedings of the 9th VPI&SU Symposium on Dynamics and Control of Large Structures, 445-455.

Kaouk, M. & Zimmerman, D. C., 1995. *Structural health assessment using a partition model update technique*. In: Proceedings of the 13th International Modal Analysis Conf., 1673-1679.

Kennedy, J., 2010. *Particle swarm optimization*. In Encyclopedia of Machine Learning, pp. 760-766. Springer US.

Kessler, S. S., Spearing, S. M., Atalla, M. J., Cesnik, C. E., and Soutis, C., 2002. *Damage detection in composite materials using frequency response methods*. Composites Part B: Engineering, 33(1) 87-95.

Khan, A. Z., Stanbridge, A. B., and Ewins, D. J., 2000. Detecting damage in vibrating structures with a scanning LDV. Optics and Lasers in Engineering, 32(6) 583-592.

Kijewski, T. & Kareem, A., 2002. *On the presence of end effects and their melioration in wavelet-based analysis*. Journal of Sound and Vibration, 256(5) 980-988.

Kim, H., & Melhem, H., 2004. *Damage detection of structures by wavelet analysis*. Engineering Structures, 26(3), 347-362.

Kim, J.-T. & Stubbs, N., 1995. *Model-uncertainty impact and damage-detection accuracy in plate girder*. Journal of Structural Engineering, 121(10) 1409-1417.

Kim, J.-T. & Stubbs, N., 2002. *Improved damage identification method based on modal information*. Journal of Sound and Vibration, 252(2) 223-238.

Kim, J. T., Ryu, Y. S., Cho, H. M., & Stubbs, N., 2003. *Damage identification in beam-type structures: frequency-based method vs mode-shape-based method*. Engineering structures, 25(1), 57-67.

King, F. W., *Hilbert transforms* (Vol. 2). Cambridge University Press. Cambridge, UK, 2009.

Kisa, M., & Brandon, J., 2000. *The effects of closure of cracks on the dynamics of a cracked cantilever beam*. Journal of Sound and Vibration, 238(1) 1-18.

Kosmatka, J. B. & Ricles, J.M., 1999. *Damage detection in structures by modal vibration characterization*. Journal of Structural Engineering, 125(12) 1384-1392.

Kramer, M. A., 1991. *Nonlinear principal component analysis using autoassociative neural networks*. AIChE journal, 37(2) 233-243.

Kramers, M. A., 1992. *Autoassociative neural networks*. Computers in Chemical Engineering, 16 313-328.

Krawczuk, M. & Ostachowicz, W. M., 1994. *Forced Vibrations of a Cantilever Timoshenko Beam with a Closing Crack*. In: Proceedings of ISMA 19, Leuven, Belgium, 3 1067-1078.

Lang, Z. Q., & Billings, S. A., 1996. *Output frequency characteristics of nonlinear systems*. International Journal of Control, 64(6), 1049-1067.

Lang, Z. Q., & Billings, S. A., 2005. *Energy transfer properties of non-linear systems in the frequency domain*. International Journal of Control, 78(5), 345-362.

Lang, Z. Q., Park, G., Farrar, C. R., Todd, M. D., Mao, Z., Zhao, L., and Worden, K., 2011. *Transmissibility of non-linear output frequency response functions with application in detection and location of damage in MDOF structural systems*. International Journal of Non-Linear Mechanics, 46(6), 841-853.

Larson, C. B., & Zimmerman, D. C., 1993. *Structural model refinement using a genetic algorithm approach.* In: Proceedings-spie the international society for optical engineering, 1095-1095.

Law, S. S., Shi, Z. Y., and Zhang, L. M., 1998. *Structural damage detection from incomplete and noisy modal test data*. Journal of Engineering Mechanics, 124(11) 1280-1288.

Law, S. S., Chan, T. H., & Wu, D., 2001. *Efficient numerical model for the damage detection of large scale structure*. Engineering Structures, 23(5) 436-451.

Lee, U., & Shin, J., 2002. *A frequency response function-based structural damage identification method*. Computers & Structures, 80(2) 117-132.

Lee, Y. S., & Chung, M. J., 2000. *A study on crack detection using eigenfrequency test data*. Computers & structures, 77(3) 327-342.

Levin, R. I., & Lieven, N. A. J., 1998. *Dynamic finite element model updating using neural networks*. Journal of Sound and Vibration, 210(5) 593-607.

Li, H., Deng, X., and Dai, H., 2007. *Structural damage detection using the combination method of EMD and wavelet analysis*. Mechanical Systems and Signal Processing, 21(1), 298-306.

Li, H. N., Li, D. S. and Song, G. B., 2004. *Recent applications of fiber optic sensors to health monitoring in civil engineering.* Engineering structures, 26(11) 1647-1657.

Lieven, N. A. J. & Ewins, D. J., 1988. *Spatial correlation of modespaces: the coordinate modal assurance criterion (COMAC).* In: Proceedings of the 6th International Modal Analysis Conference, Kissimmee, Florida, USA, 1063-1070.

Liew, K. M., & Wang, Q., 1998. *Application of wavelet theory for crack identification in structures*. Journal of Engineering Mechanics, 124, 152ï 157.

Lim, T. W., & Kashangaki, T. A., 1994. *Structural damage detection of space truss structures using best achievable eigenvectors*. AIAA Journal, 32(5) 1049-1057.

Lim, T. W., 1995. *Structural damage detection using constrained eigenstructure assignment*. Journal of Guidance, Control, and Dynamics, 18(3) 411-418.

Lin, R. M., Du, H., and Ong, J. H., 1993. *Sensitivity based method for structural dynamic model improvement*. Computers & structures, 47(3) 349-369.

Lin, R. M., Lim, M. K., & Du, H., 1995. *Improved inverse eigensensitivity method for structural analytical model updating.* Journal of vibration and acoustics, 117(2) 192-198.

Lin, T. W. & Ewins, D. J., 1990. *Model updating using FRF data*. In: Proceedings of the 15th International Seminar on Modal Analysis, Leuven, Belgium, 141-162.

Liu, P.-L., 1995. *Identification and damage detection of trusses using modal data*. Journal of Structural Engineering, 121(4) 599-608.

Loutridis, S., Douka, E., and Trochidis, A., 2004. *Crack identification in double-cracked beams using wavelet analysis*. Journal of Sound and Vibration, 277(4), 1025-1039.

Loutridis, S., Douka, E., and Hadjileontiadis, L. J., 2005. *Forced vibration behaviour and crack detection of cracked beams using instantaneous frequency*. Ndt & E International, 38(5) 411-419.

Lowe, D., 2000. *Feature extraction, data visualisation, classification and fusion for damage assessment*. In: Oral Presentation at EPSRC SIDANet Meeting, Derby, UK.

Lynch, J. P., 2007. *An overview of wireless structural health monitoring for civil structures*. Philosophical Transactions of the Royal Society A: Mathematical, Physical and Engineering Sciences, 365(1851) 345-372.

Malhotra, V. M., & Carino, N. J., *Handbook on nondestructive testing of concrete*, 2nd edition. CRC press, New York, 2004.

Mallat S., *A wavelet tour on signal processing*. Academic Press, New York, 2001.

Mallat, S., & Hwang, W. L.,1992. *Singularity detection and processing with wavelets*. Information Theory, IEEE Transactions on, 38(2), 617-643.

Mares, C., & Surace, C., 1996. *An application of genetic algorithms to identify damage in elastic structures*. Journal of Sound and Vibration, 195(2) 195-215.

Marwala, T., 2005. *Finite Element Model Updating Using Particle Swarm Optimization*. International Journal of Engineering Simulation, 6:25-30.

Marwala, T., *Finite Element Model Updating Using Computational Intelligence Techniques: Applications to Structural Dynamics*, Springer, 2010.

McCulloch, W. S., & Pitts, W., 1943. *A logical calculus of the ideas immanent in nervous activity*. The Bulletin of Mathematical Biophysics, 5(4) 115-133.

Melhem, H., & Kim, H., 2003. *Damage detection in concrete by Fourier and wavelet analyses*. Journal of Engineering Mechanics, 129(5), 571-577.

Mertins, A., Signal Analysis: *Wavelet, Filter Banks, Time-Frequency, Transforms and Applications*, Wiley, Chichester, 1999.

Messina, A., 2004. *Detecting damage in beams through digital differentiator filters and continuous wavelet transforms*. Journal of Sound and Vibration, 272(1), 385-412.

Messina, A., 2008. *Refinements of damage detection methods based on wavelet analysis of dynamical shapes*. International Journal of Solids and Structures, 45(14) 4068-4097.

Messina A., Jones A. I. and Williams E. J., 1996. *Damage detection and localisation using natural frequency changes*. In: Proceedings of Conference on Identification in Engineering Systems, Swansea, U. K., 56-65.

Messina, A., Williams, E. J., and Contursi, T., 1998. *Structural damage detection by a sensitivity and statistical-based method*. Journal of Sound and Vibration, 216(5) 791-808.

Misiti, M., Misiti, Y., Oppenheim, G. and Poggi, J., *Wavelet Toolbox*. The MathWorks Inc, 2000.

Möller, P. W. & Friberg, O., 1998. *Updating large finite element models in structural dynamics*. AIAA Journal, 36(10) 1861-1868.

Montanari, L., Basu, B., Spagnoli, A., & Broderick, B. M., 2013. *Damage Assessment in a Cracked Fiber-Reinforced Cantilever Beam Using Wavelet-Kurtosis Techniques*. Key Engineering Materials, 569, 1226-1233.

Montanari, L., Basu, B., Spagnoli, A., and Broderick, B. M., *A padding method to reduce edge effects for enhanced damage identification using wavelet analysis*. Submitted to International Journal of Mechanical Systems and Signal Processing, 2014.

Montgomery D. C., *Introduction to Statistical Quality Control*, 4th edition. John Wiley & Sons, Inc. New York, 2001.

Morassi, A., & Rovere, N., 1997. *Localizing a notch in a steel frame from frequency measurements*. Journal of engineering mechanics, 123(5) 422-432.

Mottershead, J. E., & Friswell, M. I., 1993. *Model updating in structural dynamics: a survey*. Journal of sound and vibration, 167(2) 347-375.

Nagarajaiah, S., & Basu, B., 2009. *Output only modal identification and structural damage detection using time frequency & wavelet techniques*. Earthquake Engineering and Engineering Vibration, 8(4) 583-605.

Narkis, Y., 1994. *Identification of crack location in vibrating simply supported beams*. Journal of Sound and Vibration, 172(4) 549-558.

Nickitopoulou, A., Protopsalti, K., and Stiros, S., 2006. *Monitoring dynamic and quasi-static deformations of large flexible engineering structures with GPS: Accuracy, limitations and promises*. Engineering Structures, 28(10) 1471-1482.

Nikolakopoulos, P. G., Katsareas, D. E., and Papadopoulos, C. A., 1997. *Crack identification in frame structures*. Computers & structures, 64(1) 389-406.

Orteu, J. J., 2009. *3-D computer vision in experimental mechanics*. Optics and Lasers in Engineering, 47(3) 282-291.

Ozbek, M., Rixen, D. J., Erne, O., and Sanow, G., 2010. *Feasibility of monitoring large wind turbines using photogrammetry*. Energy, 35(12) 4802-4811.

Pai, P. F., & Young, L. G., 2001. *Damage detection of beams using operational deflection shapes*. International Journal of Solids and Structures, 38(18) 3161-3192.

Pakrashi, V., Basu, B., and OôConnor, A., 2007. *Structural damage detection and calibration using a waveletï kurtosis technique*. Engineering Structures, 29(9) 2097-2108.

Pakrashi, V., Basu, B., and OôConnor, A., 2009. *A statistical measure for wavelet based singularity detection*. Journal of vibration and acoustics, 131(4).

Palacz, M., & Krawczuk, M., 2002. *Vibration parameters for damage detection in structures*. Journal of Sound and Vibration, 249(5) 999-1010.

Pandey, A. K., Biswas, M., and Samman, M. M., 1991. *Damage detection from changes in curvature mode shapes*. Journal of sound and vibration, 145(2) 321-332.

Pandey, A. K., & Biswas, M., 1994. *Damage detection in structures using changes in flexibility*. Journal of sound and vibration, 169(1) 3-17.

Pandey, P. C., & Barai, S. V., 1995. *Multilayer perceptron in damage detection of bridge structures*. Computers & Structures, 54(4) 597-608.

Paola, J. D., & Schowengerdt, R. A., 1995. *A review and analysis of backpropagation neural networks for classification of remotely-sensed multi-spectral imagery*. International Journal of remote sensing, 16(16) 3033-3058.

Park, N. G., & Park, Y. S., 2005. *Identification of damage on a substructure with measured frequency response functions*. Journal of mechanical science and technology, 19(10) 1891-1901.

Paya, B. A., Esat, I. I., and Badi, M. N. M., 1997. *Artificial neural network based fault diagnostics of rotating machinery using wavelet transforms as a preprocessor*. Mechanical systems and signal processing, 11(5) 751-765.

Paya-Zaforteza, I., Yepes, V., Hospitaler, A., Gonzalez-Vidosa, F., 2009. *CO2-Optimization of Reinforced Concrete Frames by Simulated Annealing*. Engineering Structures, 31 1501ï 1508.

Peng, Z. K., & Chu, F. L., 2004. *Application of the wavelet transform in machine condition monitoring and fault diagnostics: a review with bibliography*. Mechanical systems and signal processing, 18(2) 199-221.

Peng, Z. K., Chu, F. L., and Tse, P. W., 2007. *Singularity analysis of the vibration signals by means of wavelet modulus maximal method*. Mechanical Systems and Signal Processing, 21(2) 780-794.

Peng, Z. K., Lang, Z. Q., and Chu, F. L., 2008. *Numerical analysis of cracked beams using nonlinear output frequency response functions*. Computers & Structures, 86(17), 1809-1818.

Peng, Z. K., Lang, Z. Q., Wolters, C., Billings, S. A., and Worden, K., 2011. *Feasibility study of structural damage detection using NARMAX modelling and Nonlinear Output Frequency Response Function based analysis*. Mechanical Systems and Signal Processing, 25(3), 1045-1061.

Polikar, R., 1999. *The story of wavelets*. Physics and modern topics in mechanical and electrical engineering, 192-197.

Pugno, N., Surace, C., and Ruotolo, R., 2000. *Evaluation of the non-linear dynamic response to harmonic excitation of a beam with several breathing cracks*. Journal of sound and vibration, 235(5) 749-762.

Qian, G. L., Gu, S. N., & Jiang, J. S., 1990. *The dynamic behaviour and crack detection of a beam with a crack*. Journal of Sound and Vibration, 138(2) 233-243.

Raich, A. M., & Ghaboussi, J., 1997. *Implicit representation in genetic algorithms using redundancy*. Evolutionary Computation, 5(3) 277-302.

Randall, R. B., 2004a. *State of the art in monitoring rotating machinery-part 1*. Sound and Vibration, 38(3) 14-21.

Randall, R. B., 2004b. *State of the art in monitoring rotating machinery-part 2*. Sound and Vibration, 38(5) 10-17.

Rastogi, P. K., *Optical measurement techniques and applications*. Artech House, Boston, 1997.

Rathcliffe, C. P. & Bagaria, W.J., 1998. *Vibration technique for locating delamination in a composite beam*. AIAA Journal, 36(6) 1074-1077.

Ren, W.-X. & De Roeck, G., 2002a. *Structural damage identification using modal data. I: Simulation verification*. Journal of Structural Engineering, 128(1) 87-95.

Ren, W.-X. & De Roeck, G., 2002b. *Structural damage identification using modal data. II: Test verification*. Journal of Structural Engineering, 128(1) 96-104.

Ren, W.-X., & Sun, Z. S., 2008. *Structural damage identification by using wavelet entropy*. Engineering Structures, 30(10), 2840-2849.

Ricles, J. M., & Kosmatka, J. B., 1992. *Damage detection in elastic structures using vibratory residual forces and weighted sensitivity*. AIAA Journal, 30(9) 2310-2316.

Rilling, G., Flandrin, P., and Gonçalvés, P., 2003. *On empirical mode decomposition and its algorithms*. In: IEEE-EURASIP Workshop on Nonlinear Signal and Image Processing NSIP, Volume 3, pp. 8-11.

Ripley, B. D., *Pattern recognition and neural networks*. Cambridge university press, 2007.

Rosenblatt, F., *Principles of Neurodynamics*. Spartan, New York, 1962.

Rucka, M., & Wilde, K., 2006a. *Crack identification using wavelets on experimental static deflection profiles*. Engineering structures, 28(2) 279-288.

Rucka, M., & Wilde, K., 2006b. *Application of continuous wavelet transform in vibration based damage detection method for beams and plates*. Journal of Sound and Vibration, 297(3) 536-550.

Rucka, M., 2011. *Damage detection in beams using wavelet transform on higher vibration modes*. Journal of Theoretical and Applied Mechanics, 49, 399-417.

Rumelhart, D. E., Hinton G. E. and Williams, R. J., *Learning internal representations by error propagation.* In Parallel Distributed Processing: Explorations in the Microstructure of Cognition, Vol. 1: Foundations (Edited by D. E. Rumelhart and J. L. McClelland). MIT Press, Cambridge, MA (1986).

Ruotolo, R., Surace, C., Crespo, P., and Storer, D., 1996. *Harmonic analysis of the vibrations of a cantilevered beam with a closing crack.* Computers & structures, 61(6) 1057-1074.

Rytter, A., *Vibration based inspection of Civil Engineering structures*. PhD Thesis, Department of Building Technology and Structural Engineering, University of Aalborg, Denmark, 1993.

Salawu, O.S. & Williams, C., 1995. *Bridge assessment using forced-vibration testing*. Journal of Structural Engineering, 121(2) 161-173.

Salawu, O. S., 1997. *Detection of structural damage through changes in frequency: a review.* Engineering structures, 19(9) 718-723.

Sampaio, R. P. C., Maia, N. M. M., & Silva, J. M. M., 1999. *Damage detection using the frequency-response-function curvature method*. Journal of Sound and Vibration, 226(5) 1029-1042.

Sazonov, E., & Klinkhachorn, P., 2005. *Optimal spatial sampling interval for damage detection by curvature or strain energy mode shapes*. Journal of sound and vibration, 285(4) 783-801.

Schalkoff, R. J., *Pattern recognition.* John Wiley & Sons, Inc. New York, 1992.

Schwarz, B. J., & Richardson, M. H., 1999. *Introduction to operating deflection shapes*. CSI Reliability Week, 10 121-126.

Schulz, M. J., Pai, P. F., and Abdelnaser, A. S., 1996. *Frequency response function assignment technique for structural damage identification*. In Proceedings-spie the international society for optical engineering, 105-111.

Shi, Z. Y., Law, S. S., and Zhang, L., 2000. *Structural damage detection from modal strain energy change*. Journal of engineering mechanics, 126(12) 1216-1223.

Shull, P. J., *Nondestructive evaluation theory, techniques, and applications*. Marcel Dekker, Inc. New York, 2002.

Smith, S. W. & Beattie, C. A., 1991. *Secant-Method Adjustment for Structural Models*, AIAA Journal, 29(1) 119-126.

Sohn, H., Farrar, C. R., Hemez, F. M., Shunk, D. D., Stinemates, D. W., Nadler, B. R., & Czarnecki, J. J., 2004. *A review of structural health monitoring literature: 1996-2001* (LA-13976-MS). Los Alamos National Laboratory, NM, USA.

Sohn, H., 2007. *Effects of environmental and operational variability on structural health monitoring*. Philosophical Transactions of the Royal Society A: Mathematical, Physical and Engineering Sciences, 365(1851) 539-560.

Spagnoli, A., Carpinteri, An., & Montanari, L., 2014. *Application of the Shakedown Theory to Brittle-Matrix Fiber-Reinforced Cracked Composite*

Beams Under Combined Traction and Flexure. Journal of Applied Mechanics, 81(3), 031012.

Spanos, P. D., Failla, G., Santini, A. and Pappatico, M., 2006. *Damage detection in Euleri Bernoulli beams via spatial wavelet analysis*. Structural Control and Health Monitoring, 13(1) 472-487.

Stanbridge, A. B., & Ewins, D. J., 1999. *Modal testing using a scanning laser Doppler vibrometer*. Mechanical Systems and Signal Processing, 13(2) 255-270.

Staszewski, W. J., 2002. *Intelligent signal processing for damage detection in composite materials*. Composites science and technology, 62(7) 941-950.

Staszewski, W. J., Worden, K., Wardle, R., and Tomlinson, G. R., 2000. *Fail-safe sensor distributions for impact detection in composite materials*. Smart Materials and Structures, 9(3) 298.

Staszewski, W. J., & Robertson, A. N., 2007. *Time-frequency and time-scale analyses for structural health monitoring*. Philosophical Transactions of the Royal Society A: Mathematical, Physical and Engineering Sciences, 365(1851) 449-477.

Su, H., Liu, Q. and Li, J., 2011. *Alleviating Border Effects in Wavelet Transforms for Nonlinear Time-varying Signal Analysis*. Advances in Electrical and Computer Engineering, 11(3) 55-60.

Sun, Z., & Chang, C. C., 2004. *Statistical wavelet-based method for structural health monitoring*. Journal of structural engineering, 130(7), 1055-1062.

Surace, C., & Ruotolo, R., 1994. *Crack detection of a beam using the wavelet transform*. In: In: Proceedings of the 12th International Modal Analysis Conference. Honolulu, Hawaii, 1141ï 1147.

Surace, C., Yanb, G., Archibaldc, R., Saxenad, R., and Fenge, R., 2012. *Structural Damage Detection using the Polynomial Annihilation Edge Detection Method*. http://info.ornl.gov/sites/publications/Files/Pub39615.pdf.

Surace, C., Archibald, R., and Saxena, R., 2013. *On the use of the polynomial annihilation edge detection for locating cracks in beam-like structures*. Computers & Structures, 114, 72-83.

Tada, H., Paris, P. C. and Irwin, G. R., *The stress analysis of cracks Handbook*, 3rd edition, ASME press, New York, 2000.

Tang, J. P., Chiou, D. J., Chen, C. W., Chiang, W. L., Hsu, W. K., Chen, C. Y., and Liu, T. Y., 2011. *A case study of damage detection in benchmark buildings using a Hilbert-Huang Transform-based method*. Journal of Vibration and Control, 17(4) 623-636.

Tsyfansky, S. L., & Beresnevich, V. I., 2000. *Non-linear vibration method for detection of fatigue cracks in aircraft wings*. Journal of sound and vibration, 236(1), 49-60.

Umesha, P. K., Ravichandran, R., and Sivasubramanian, K., 2009. *Crack detection and quantification in beams using wavelets*. Computer-Aided Civil and Infrastructure Engineering, 24(8), 593-607.

Viola, E., Nobile, L., and Federici, L., 2002. *Formulation of cracked beam element for structural analysis*. Journal of engineering mechanics, 128(2) 220-230.

Wahab, M.M.A. & De Roeck, G., 1999. *Damage detection in bridges using modal curvatures: applications to a real damage scenario*. Journal of Sound and Vibration, 226(2) 217-235.

Waldron, K., Ghoshal, A., Schulz, M. J., Sundaresan, M. J., Ferguson, F., Pai, P. F., & Chung, J. H., 2002. *Damage detection using finite element and laser operational deflection shapes*. Finite Elements in Analysis and Design, 38(3) 193-226.

Wang, Q., & Deng, X., 1999. *Damage detection with spatial wavelets*. International Journal of Solids and Structures, 36, 3443ï 3468.

Wang, Q., & Wu, N., 2011. *Detecting the delamination location of a beam with a wavelet transform: an experimental study*. Smart Materials and Structures, 20(1), 012002.

Wang, S., Ren, Q., and Qiao, P., 2006. *Structural damage detection using local damage factor*. Journal of Vibration and Control, 12(9), 955-973.

Wang, Z., Lin, R. M., and Lim, M. K., 1997. *Structural damage detection using measured FRF data*. Computer Methods in Applied Mechanics and Engineering, 147(1) 187-197.

Werbos, P. J., 1990. *Backpropagation through time: what it does and how to do it*. Proceedings of the IEEE, 78(10) 1550-1560.

Williams, J. R. & Amaratunga, K., 1997. *A discrete wavelet transform without edge effects using wavelet extrapolation*. Journal of Fourier Analysis and Applications, 3(4) 435-449.

Worden, K., 1997. *Structural fault detection using a novelty measure*. Journal of Sound and vibration, 201(1) 85-101.

Worden, K., & Dulieu-Barton, J. M., 2004. *An overview of intelligent fault detection in systems and structures*. Structural Health Monitoring, 3(1) 85-98.

Worden, K., Farrar, C. R., Haywood, J., and Todd, M., 2008. *A review of nonlinear dynamics applications to structural health monitoring.* Structural Control and Health Monitoring, 15(4), 540-567.

Worden, K., Manson, G., & Fieller, N. R. J., 2000. *Damage detection using outlier analysis.* Journal of Sound and Vibration, 229(3) 647-667.

Wu, X., Ghaboussi, J., and Garrett, J. H., 1992. *Use of neural networks in detection of structural damage*. Computers & Structures, 42(4) 649-659.

Yam, L. H., Yan, Y. J., and Jiang, J. S., 2003. *Vibration-based damage detection for composite structures using wavelet transform and neural network identification*. Composite Structures, 60(4) 403-412.

Yan, A., & Golinval, J. C., 2005. *Structural damage localization by combining flexibility and stiffness methods.* Engineering Structures, 27(12) 1752-1761.

Yan, Y. J., Cheng, L., Wu, Z. Y., and Yam, L. H., 2007. *Development in vibration-based structural damage detection technique*. Mechanical Systems and Signal Processing, 21(5) 2198-2211.

Yang, J. N., Lei, Y., Lin, S., and Huang, N., 2003. *Hilbert-Huang based approach for structural damage detection*. Journal of engineering mechanics, 130(1) 85-95.

Yang, S., & Allen, M. S., 2011. *Output-only modal analysis using continuous-scan laser Doppler vibrometry and application to a 20kW wind turbine*. In: Modal Analysis Topics, Volume 3, pp. 47-64. Springer, New York.

Yun, C. B., & Bahng, E. Y., 2000. *Substructural identification using neural networks*. Computers & Structures, 77(1) 41-52.

Zastrau, B., 1985. *Vibration of cracked structures.* Archive of Mechanics, 37(6) 731-743.

Zhang, G., Eddy Patuwo, B., and Y Hu, M., 1998. *Forecasting with artificial neural networks: The state of the art*. International journal of forecasting, 14(1) 35-62.

Zhao, J., & DeWolf, J. T., 1999. *Sensitivity study for vibrational parameters used in damage detection.* Journal of structural engineering, 125(4) 410-416.

Zheng, D., Chao, B. F., Zhou, Y. and Yu, N., 2000. *Improvement of edge effect of the wavelet timeï frequency spectrum: application to the length-of-day series*. Journal of Geodesy, 74(2) 249-254.

Zhong, S., & Oyadiji, S. O., 2011a. *Crack detection in simply supported beams using stationary wavelet transform of modal data.* Structural Control and Health Monitoring, 18(2), 169-190.

Zhong, S., & Oyadiji, S. O., 2011b. *Detection of cracks in simply-supported beams by continuous wavelet transform of reconstructed modal data*. Computers & structures, 89(1) 127-148.

Zhong, S., & Oyadiji, S. O., 2013. *Sampling interval sensitivity analysis for crack detection by stationary wavelet transform*. Structural Control and Health Monitoring, 20(1) 45-69.

Zhou, G., & Sim, L. M., 2002. *Damage detection and assessment in fibre-reinforced composite structures with embedded fibre optic sensors-review.* Smart Materials and Structures, 11(6) 925.

Zimmerman, D. C., & Kaouk, M., 1992. *Eigenstructure assignment approach for structural damage detection.* AIAA Journal, 30(7) 1848-1855.

Zimmerman, D. C. & Kaouk, M., 1994. *Structural damage detection using a minimum rank update theory*. Journal of Vibration and Acoustics, 116 222-230.

Zimmerman, D. C., Kaouk, M. and Simmermacher T., 1995. *On the role of engineering insight and judgement structural damage detection*. In: Proceedings of the 13th International Modal Analysis Conf., 414-420.

Appendix A

Values of the function Ū(*s*) related to ócoif4ô (see Section 6.2):

Scale *s*	Ū(*s*)
1	0.0721748817892021
2	0.204141393377929
3	0.375031686867526
4	0.57739905431362
5	0.806939709743333
6	1.06074979577544
7	1.33669751683799
8	1.63313114702344
9	1.94872180830845
10	2.28237016307287
11	2.63314702401343
12	3.00025349494022
13	3.38299308218976
14	3.78075151420547
15	4.19298172776103
16	4.61919243450894
17	5.05893923926692
18	5.51181762120409
19	5.9774573036414
20	6.45551767794671
21	6.94568404054367
22	7.44766446616427
23	7.96118718534858
24	8.48599836620349
25	9.02186022365025
26	9.56854939649426
27	10.1258555454232
28	10.693580134704
29	11.2715353677388
30	11.8595432523644
31	12.4574347762391

Scale *s*	Ū(*s*)
33	13.6822332881701
34	14.3088409667854
35	14.9447325650247
36	15.5897744664677
37	16.2438386633143
38	16.9068023746316
39	17.5785477000201
40	18.258961304583
41	18.9479341316499
42	19.6453611401905
43	20.3511410642526
44	21.0651761921074
45	21.7873721630702
46	22.5176377802217
47	23.2558848374626
48	24.0020279595218
49	24.7559844536963
50	25.5176741722411
51	26.2870193844425
52	27.0639446575182
53	27.8483767455748
54	28.6402444859367
55	29.4394787022265
56	30.2460121136437
57	31.0597792499417
58	31.8807163716486
59	32.7087613951251
60	33.5438538220883
61	34.3859346732658
62	35.234946425871
63	36.0908329546259

32	13.0650491761875
65	37.8230124959393
66	38.6991997593657
67	39.5820502037585
68	40.4715139141355
69	41.36754208077
70	42.2700869589934
71	43.1791018310152
72	44.094540969633
73	45.01635960371
74	45.9445138853192
75	46.878960858441
76	47.8196584291314
77	48.7665653370654
78	49.7196411283817
79	50.6788461297467
80	51.6441414235738
81	52.6154888243285
82	53.5928508558629
83	54.5761907297188
84	55.5654723243495
85	56.5606601652096
86	57.5617194056684
87	58.5686158086995
88	59.5813157293141
89	60.5997860976895
90	61.6239944029676
91	62.6539086776822
92	63.6894974827885
93	64.7307298932644
94	65.7775754842529
95	66.8300043177241
96	67.8879869296279
97	68.9514943175194
98	70.0204979286298
99	71.0949696483623
100	72.1748817892022
101	73.2602070800089
102	74.3509186556861
103	75.4469900472019

64	36.9535394760715
108	81.006844363386
109	82.1345398054755
110	83.2674200997646
111	84.4054616244367
112	85.5486410776315
113	86.6969354702797
114	87.8503221191639
115	89.0087786401979
116	90.172282941911
117	91.3408132191235
118	92.5143479468223
119	93.6928658742058
120	94.8763460189154
121	96.0647676614279
122	97.2581103396152
123	98.4563538434583
124	99.6594782099124
125	100.867463717917
126	102.080290883548
127	103.297940455298
128	104.5203934095
129	105.74763094586
130	106.979634483129
131	108.21638565487
132	109.457866305361
133	110.704058485593
134	111.954944449376
135	113.210506649548
136	114.470727734283
137	115.735590543495
138	117.005078105329
139	118.279173632746
140	119.557860520197
141	120.841122340367
142	122.128942841021
143	123.421305941905
144	124.718195731741
145	126.019596465285
146	127.325492560461

104	76.5483951719537
105	77.6551083244553
106	78.7671041673342
107	79.8843577226333
151	133.921869162734
152	135.25441899705
153	136.591359460205
154	137.93267618006
155	139.2783549247
156	140.628381600158
157	141.982742248212
158	143.34142304421
159	144.704410294962
160	146.07169043666
161	147.443250032861
162	148.819075772504
163	150.199154467972
164	151.583473053192
165	152.972018581786
166	154.36477822525
167	155.761739271175
168	157.162889121513
169	158.568215290866
170	159.977705404818
171	161.391347198304
172	162.809128514006
173	164.231037300786
174	165.657061612146
175	167.08718960473

147	128.635868595561
148	129.950709306513
149	131.269999584215
150	132.593724471928
176	168.521409536838
177	169.959709766989
178	171.402078752497
179	172.848505048088
180	174.298977304531
181	175.753484267306
182	177.212014775291
183	178.674557759483
184	180.141102241732
185	181.611637333505
186	183.08615223468
187	184.564636232346
188	186.047078699645
189	187.533469094618
190	189.02379695909
191	190.518051917554
192	192.016223676098
193	193.518302021337
194	195.024276819368
195	196.534138014744
196	198.04787562947
197	199.565479762011
198	201.086940586321
199	202.612248350888
200	204.141393377798